PROTEIN-PROTEIN INTERACTIONS OF HUMAN SOMATIC ANGIOTENSIN-CONVERTING ENZYME

Kerry Gordon

Thesis presented for the degree of
DOCTOR OF PHILOSOPHY
in the Division of Medical Biochemistry
UNIVERSITY OF CAPE TOWN
March 2011

Supervisors: Prof E.D. Sturrock, S.L.U. Schwager

DECLARATION

I, **Kerry Gordon,** declare that this thesis is my own unaided work, both in concept and in execution (except where the acknowledgements indicate otherwise). Neither the whole work nor any part thereof has been submitted in the past, or is being, or is to be submitted for a degree at this University or at any other University.

I grant the University of Cape Town free licence to reproduce the above thesis in whole or in part, for the purpose of research

_____

Signature of applicant

Signed on this the _____ day of _____ , 2011

ABSTRACT

Angiotensin-converting enzyme (ACE) is a zinc metalloprotease that has been classically defined as a key regulator of blood homeostasis. Novel insights into its function demonstrate its broader role in other physiological systems. Pivotal to these roles are the specific protein-protein interactions that allows cross-talk between different pathways. The development of domain-specific ACE inhibitors calls for better understanding of the interaction of the two ectodomains of ACE and the role of specific interactions in processing events. These include ACE-ACE interaction in homodimerisation and recognition and binding of the ACE secretase(s) responsible for proteolytic processing. There is also increasing evidence for inter-domain interaction and movement in sACE that may be involved in shedding, dimerisation and domain cooperativity with respect to catalysis.

The crystal structures of the individual domains of sACE, the N and C domains, have been solved whereas the full-length structure has not. Growth of viable crystals is thought to be impaired by the presence of extensive glycosylation and flexibility of movement between the two domains. In this study, novel disulphide bridges were engineered into the linker region of ACE in an attempt to limit inter-domain movement, thereby producing a candidate for crystallisation and to determine the effect of these bridges on inter-domain movement. The use of the native unbound N domain cysteine to form a disulphide bridge with residues in the linker region appeared to be an effective approach.

Protein-protein interactions were explored using site-directed mutagenesis and a panel of domain-specific monoclonal antibodies (mAbs) to ACE to better understand their role in ACE expression and processing. Fine epitope mapping of the mAbs to ACE has elucidated regions involved in shedding, dimerisation and inter-domain interaction. In this study, fine epitope mapping of two mAbs, known to influence shedding and dimerisation, was performed in order to isolate a region of the N domain of ACE that may be involved. Three residues were identified in the overlapping region of the two mAb epitopes that alter sACE shedding, mAb binding and increase dimerisation on the cell surface highlighting the importance of this region in post-translational processing.

The role of the unbound cysteine residues in each domain in dimerisation and shedding was investigated. Dimerisation appears to involve both non-covalent interactions in the N domain and disulphide-mediated interactions in the C domain. The latter has an effect on shedding and may be involved in intracellular signalling.

Finally, a novel ACE mutation that results in increased plasma ACE was described. The increased soluble ACE is the result of significantly increased rate of shedding that follows a similar mechanism to wild-type ACE and implicates the N domain in ACE secretase interaction. Thus, we have gained some insight into regions and residues of ACE that are important in the protein-protein interactions involved in processes such as shedding, dimerisation and domain cooperativity.

ACKNOWLEDGMENTS

I would like to thank the following people for their support and assistance in the undertaking of this work:

Prof. Sergei Danilov (University of Illinois at Chicago, USA), who performed the plate precipitation assays. I would also like to thank for him for his generous supply of monoclonal antibodies, helpful advice and assistance with experimental setup.

Ronnie Dreyer (Flow Cytometry Core Facility, Division of Immunology, UCT) for performing the FACS analysis and Nasiema Allie (Experimental Tuberculosis and Immunology Research Group, Division of Immunology, UCT) for kindly donating FITC-labelled secondary antibody for FACS.

Diane James (Department of Molecular and Cell Biology, UCT), who conducted the nucleotide sequencing.

Maré Vlok and Busiswa Kekana at the Centre for Proteomic and Genomic Research, Cape Town for performing the MALDI MS/MS analysis.

Pierre Redelinghuys, for the generation of the pcDNA-NdomD629, solsACE and sACENJ constructs and Gannie Tzoneva, who designed and generated the N domain mutants H600C and EY/CC.

Ross Douglas for his guidance in designing the fluorogenic assays and with kinetic analysis.

A special thanks to Sylva Schwager for her assistance with HPLC and MALDI MS/MS, transfection of the free thiol mutants and shedding experiments and her initial work with NdomH600C.

Jean Watermeyer for her assistance with the structural work.

A special mention must be made to my fellow lab members, past and present, who have instilled a great deal of fun into the day-to-day. To Ayesha, Chris, Colin, Nailah, Kate, Ross, Raymond, Riyad, Tony, Trudi and Wendy thank you for making this an enjoyable experience.

I owe an enormous debt of gratitude to my supervisors, Edward Sturrock and Sylva Schwager. To Ed, I am grateful for your support, encouragement and gentle critique, which has moulded me into the researcher I am today. To Sylva, for always having time to solve a crisis, for your unwavering enthusiasm, endless assistance and poolside chats.
You have created a wonderful and inspiring place to work and I feel privileged to have been part of it.

I would like to acknowledge the support and encouragement from my family and friends. I'm eternally grateful to you for patiently putting things into perspective in my moments of crisis and for creating wonderfully safe spaces to seek sustenance.

This work was conducted with the financial support of the National Research Foundation, the Medical Research Council, the German Academic Exchange Service and the University of Cape Town. I am truly grateful for their support, without which this degree would not have been possible.

ABBREVIATIONS

3D	three-dimensional
β-ME	β-mercaptoethanol
Å	angstrom
Aβ	amyloid β peptide 1-42
ACE	angiotensin-converting enzyme
ACE2	angiotensin-converting enzyme 2
ACN	acetonitrile
Ac-SDKP	acetyl-SDKP
AEBSF	4-(2-Aminoethyl) benzenesulfonyl fluoride hydrochloride
AnCE	*Drosophila melanogaster* angiotensin-converting enzyme homologue
angI	angiotensin I
angII	angiotensin II
APMA	4-aminophenylmercuric acetate
APP	amyloid precursor protein
BK	bradykinin
B2K-R	bradykinin 2 receptor
BiP	immunoglobulin binding protein
BRET	bioluminescence resonance energy transfer
BS^3	bis[sulfosuccinimidyl] suberate
BSA	bovine serum albumin
CaM	calmodulin
CARD15	caspase recruitment domain family, member 15
CHO	Chinese hamster ovary
CK2	casein kinase
COS-7	African green monkey fibroblast-like kidney cells
COX-2	cyclooxygenase-2
CnBr	cyanogen bromide
CPM	carboxypeptidase M
CRD	carbohydrate recognition domain
DCI	3,4-dichloroisocoumarin
dH_2O	double distilled deionised water
DMEM	Dulbecco's Modified Eagle Medium
DNA	deoxyribonucleic acid
DRB	5,6-Dichloro-1-β-D-ribofuranosylbenzimidazole
DTT	dithiothreitol

E.coli	*Escherischia coli*
EDTA	ethylenediaminetetraacetic acid
ECE-1	endothelin converting enzyme 1
EGF-R	endothelial growth factor receptor
ELISA	enzyme-linked immunosorbent assay
EM	electron microscopy
ER	endoplasmic reticulum
FACS	fluorescence-activated cell sorting
FCS	foetal calf serum
FITC	fluorescein isothiocyanate
FRET	fluorescence resonance energy transfer
G3PDH	glyceraldehyde-3-phosphate dehydrogenase
$GalNac_2$	N-acetylgalactosamine dissacharide
$GlcNac_2Man_3$	N-acetylglucosamine and three mannose residues
GPCR	G-protein coupled receptor
GPI	glycosylphosphatidylinisotol
GPVI	glycoprotein VI
HEK	human embryonic kidney
HEPES	4-(2-hydroxyethyl)-1-piperazineethanesulfonic acid
HIV	human immunodeficiency virus
HL	His-Leu
HHL	hippuryl-L-His-L-Leu
HMEC	human microvascular endothelial cell line
HPLC	high performance liquid chromatography
HRP	horseradish peroxidase
HUVEC	human umbilical vein endothelial cells
JNK	c-Jun N-terminal kinase
KKS	kallikrein-kinin system
LHRH	luteinising hormone-releasing hormone
mAb	monoclonal antibody
MAM domain	meprin/A5-protein/PTPmu domain
MAP	mitogen-activated protein
MDCK	Madin-Darby canine kidney
MDP	membrane dipeptidase
MKK7	MAP kinase kinase 7
MMP	matrix metalloprotease

NB-DNJ	N-butyldeoxy-nojirimycin
NCAM	neural cell adhesion molecule
NEP	neprilysin
nf	nuclease free
NOD2	nucleotide-binding oligomerization domain containing 2
PAGE	polyacrylamide gel electrophoresis
PBS	phosphate-buffered saline
PCR	polymerase chain reaction
PDB	protein database
PDBu	phorbol 12,13-dibutyrate
PfCP	*Pyrococcus furiosis* carboxypeptidase
PKA	protein kinase A
PKC	protein kinase C
PMA	phorbol-12-myristate-13-acetate
PMSF	phenylmethylsulfonyl fluoride
RAAS	renin-aldosterone-angiotensin system
RE	restriction enzyme
RNA	ribonucleic acid
RT-PCR	reverse transcriptase polymerase chain reaction
RTK	receptor tyrosine kinases
sACE	somatic ACE
SAXS	small-angle x-ray scattering
SD	standard deviation
SDS	sodium dodecyl sulphate
subsP	substanceP
tACE	testis ACE
TACE	TNF-α converting enzyme
TAPI	tumour necrosis factor-α protease inhibitor
TCEP	Tris (2-carboxyethyl) phosphine
TFA	trifluoroacetic acid
TMB	tetramethylbenzidine
TNF-α	tumour necrosis factor-α
TOP	thimet oligopeptidase
VEGF-R	vascular endothelial growth factor
wt	wild-type
ZFHL	benzyloxycarbonyl-Phe-L-His-Leu

TABLE OF CONTENTS

CHAPTER 1: Introduction

Angiotensin-converting enzyme (ACE) has been classically described with respects to its cardiovascular roles in the renin- angiotensin-aldosterone (RAAS) and the kallikrein-kinin (KKS) systems that maintain blood homeostasis. ACE mediates its effects by hydrolysing angiotensin I (angI) to form the potent vasoconstrictor, angiotensin II (angII), in the RAAS and inactivates the vasoconstrictor, bradykinin (BK), in the KKS. In recent years other substrates of ACE have been identified, implicating this enzyme in other physiological systems. These include cleavage of the amyloid β protein 1-42 (Aβ) associated with amyloid plaque formation in Alzheimer's disease (Oba *et al*, 2005); its action on N-acetyl-seryl-aspartyl-lysyl-proline (Ac-SDKP), a peptide involved in haematopoietic stem cell regulation (Azizi *et al*, 1996) and increased ACE expression in macrophages associated with resistance to melanoma (Shen *et al*, 2007).

A better understanding of the role ACE plays in these systems is particularly relevant considering that ACE inhibitors are a front-line therapy for hypertension and myocardial infarction. Common side effects of treatment with ACE inhibitors are a persistent dry cough and angioedema, sufficiently acute to induce patients to terminate treatment. These effects are thought to be the result of a build-up of BK due to wholesale inhibition of ACE (reviewed by Dykewicz, 2004). A new approach towards the development of ACE inhibitors is directed towards targeting its primary function of ang I hydrolysis, minimising the effect on other functions. In order to pursue this line of investigation, a thorough understanding of the structure-function of ACE as well as its regulation and expression are required. Common to all these functions are the specific protein-protein interactions involved.

Cross-talk between proteins and peptides is key at almost every level of cell function; in enzyme-substrate interaction; intracellular signalling; for protein expression and membrane targeting; for proteolysis and cell-to-cell adhesion. These interactions range from relatively transient ones, such as the binding of enzyme and substrate to long-term associations that are required for activity, such a homo- or hetero-dimer formation and enzyme complex formation. To understand the regulation and expression of a protein in the broader context, it is important to look at what interactions take place. With ACE in particular, its extended role beyond the RAAS necessitates an understanding of the cellular processes and regulatory pathways involved.

This chapter will encompass what is known regarding the structure-function relationship of ACE with respect to specific protein-protein interactions involved in processes such as ectodomain shedding, glycosylation, dimerisation and inter-domain interaction.

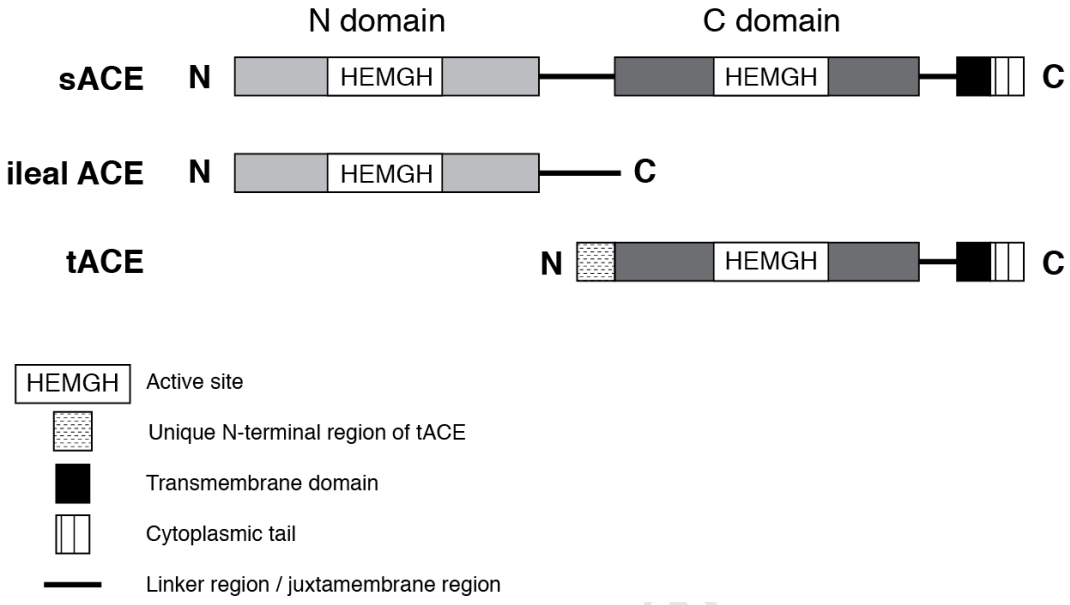

Figure 1.1. Isoforms of ACE.

1.1 BIOCHEMICAL PROPERTIES OF ACE

1.1.1 Physical characteristics of ACE

Human somatic ACE (sACE) is encoded by 26 exons from a single gene locus on chromosome 17 (mouse ACE chromosome 11) (Hubert *et al*, 1991). The inferred amino acid sequence is 1306 residues, giving rise to a 170kDa protein. It consists of a 29-residue signal sequence; two ectodomains: the N and C domains, each of approximately 600 residues joined by an 11-residue linker region; a juxtamembrane region; a 17-residue hydrophobic transmembrane domain and terminates in a 30-residue cytoplasmic tail (Soubrier *et al*, 1988; Wei *et al*, 1991a; Wei *et al*, 1991b) (Figure 1.1). There is approximately 60% amino acid sequence identity between the two domains thought to be the result of an ancient gene duplication event (Hubert *et al*, 1991). Each domain contains a conserved zinc-binding motif, HEMGH, present in the active sites of zinc metalloproteases, including thermolysin, neutral endopeptidase, neurolysin and collagenase (Soubrier *et al*, 1988). There are 7 cysteine residues in each domain, 6 of which form three intramolecular disulphide bridges in an *aabbcc* configuration (Sturrock *et al*, 1996; Natesh *et al*, 2003; Corradi *et al*, 2006).

The smaller isoform, testis ACE (tACE), is expressed solely in male germinal cells as a single 110kDa ectodomain protein (Strittmatter & Snyder, 1984; Yotsumoto *et al*, 1984; Brentjens *et al*, 1986). It is transcribed from an intronic promoter (Howard *et al*, 1990; Kumar *et al*, 1989; Lattion *et al*, 1989) in the 12th intron from the same gene as sACE (Bernstein *et al*, 1988; Soubrier *et al*, 1988; Howard *et al*, 1990). Full-length human tACE cDNA was cloned by screening a testicular library with anti-bovine lung ACE antibodies and ACE cDNA probes (Ehlers *et al*, 1989). This recombinant form was expressed in Chinese hamster ovary (CHO) cells and generated a protein that was structurally, catalytically and immunologically identical to its physiological counterpart (Ehlers *et al*, 1991). tACE is structurally and catalytically identical to the C domain of sACE, except for a unique 36-residue N terminal region downstream of the signal sequence that is rich in serine and threonine residues (El-Dorry *et al*, 1982) [*].

A third isoform that is identical to the N domain has been isolated from human ileal fluid (Deddish *et al*, 1994) and has been found in urine of hypertensive patients (Casarini *et al*, 2001). Unlike, tACE this isoform seems to arise from limited proteolysis of sACE, rather than direct gene expression.

1.1.2 Catalytic properties of ACE

ACE exhibits dipeptidyl carboxypeptidase activity (Soffer & Sonnenblick, 1978) and endopeptidase activity (Jaspard *et al*, 1993). The zinc-binding motif in each domain is critical for enzyme function (Wei *et al*, 1991a). ACE cleaves a variety of peptides including angI, BK, Ac-SDKP, substance P (subsP), Aβ-peptide and luteinising hormone-releasing hormone (LHRH) (Bünning *et al*, 1983; Ehlers & Riordan, 1991a; Wei *et al*, 1991a). Both domains can hydrolyse substrates independently, as evidenced from activity of the individual domains through active site knockout mutants (Wei *et al*, 1992) and generated by limited proteolysis of sACE (Sturrock *et al*, 1997).

ACE falls into a small group of enzymes containing two catalytic domains, which includes sucrase-isomaltase (Hunziker *et al*, 1986), lactase-phlorizin hydrolase (Mantei *et al*, 1988), protein disulphide isomerase (Ellgaard & Ruddock, 2005) and adenylyl transferase (Jaggi *et al*, 1997). Each domain has distinct and complementary functions in these proteins

[*] Residue numbers of tACE are referred to with sACE numbering throughout this document (there is a 576 residue difference between the numbering)

as a result of minor differences in their active sites. Despite the approximately 89% structural homology between the N and C domain active sites of sACE (Corradi *et al*, 2006), the two ectodomains display different profiles for substrate hydrolysis and chloride activation (Wei *et al*, 1991a; Wei *et al*, 1992). While both domains cleave BK at relatively the same rate, angI hydrolysis by the C domain is approximately three times more efficient (Wei *et al*, 1991a; Georgiadis *et al*, 2003). It appears that the C domain active site maintains the dipeptidyl carboxypeptidase function whereas the N domain active site catalyses other substrates through endopeptidase activity (Ehlers & Riordan, 1991a; Wei *et al*, 1991b; Jaspard *et al*, 1993). There has been some discussion in the literature regarding the interaction of the two domains in sACE with respect to their activity. Since the turnover (k_{cat}) of sACE was not higher than that of the C domain (Sturrock *et al*, 1997; Woodman *et al*, 2005; Skirgello *et al*, 2005), it has been speculated that there is some degree of negative cooperativity between the domains. This is supported by active site titration of inhibitors and isothermal titration calorimetry (Binevski *et al*, 2003; Anjudar-Sanchez *et al*, 2004; Skirgello *et al*, 2005). It is thought that binding of substrate or inhibitors to the active site in one domain results in a conformational change that prevents access of compounds to the second active site. There is evidence of domain interaction, both with shedding and monoclonal antibody (mAb) binding (discussed later in Section 1.4) and most likely extends to enzyme activity as well.

1.2 THREE-DIMENSIONAL STRUCTURE OF ACE

1.2.1 Three-dimensional structure determination of ACE

Until recently, characterisation of ACE with respect to substrate and inhibitor specificity, function and post-translational processing was hampered by the lack of a three-dimensional (3D) structure. This was largely due to the difficulty in obtaining reproducible crystals for x-ray crystallography. The major obstacle in obtaining crystals was due to the microheterogeneity of glycan chains and the hydrophobicity of the transmembrane region, which affected the packing of the crystal lattice. Both tACE and the N domain are heavily glycosylated and the presence of these oligosaccharides is required for correct folding and protein stability (detailed in Section 1.3.2). The first crystal structures of human tACE and the N domain in complex with the inhibitor lisinopril were obtained by expressing soluble constructs lacking the transmembrane domain in the presence of N-butyldeoxy-nojirimycin (NB-DNJ). This α-glucosidase-I inhibitor restricts oligosaccharides to the high mannose form

sufficient to allow for the proper folding and expression of ACE while limiting the heterogeneity of the oligosaccharide chain (Natesh *et al*, 2003, Corradi *et al*, 2006). However, the prohibitive cost of NB-DNJ and the potential loss of expression (Butters *et al*, 1999) necessitated an alternate expression system. The *Drosophila melanogaster* ACE homologue (AnCE) was successfully expressed in Hi5 insect cells, resulting in glycans composed of simple oligomannosidic chains (Tomiya *et al*, 2004; Harrison & Jarvis *et al*, 2006) and was used for x-ray crystallography where the presence of sugars did not seem to obstruct crystal packing (Kim *et al*, 2003). Similarly, another ACE homologue, ACE2, was expressed in a baculovirus system and the crystal structure successfully resolved (Towler *et al*, 2004). A minimally glycosylated tACE variant, containing glycans at Asn^{648} and Asn^{685} (tACE-g13) was developed by site-directed mutagenesis in order to develop a high through-put and cost-effective method for crystallisation and a number of structures co-crystallised with different inhibitors have been solved in this way (Gordon *et al*, 2003; Watermeyer *et al*, 2006; Watermeyer *et al*, 2008; Watermeyer *et al*, 2010). A similar approach has recently been successful for the N domain (Anthony *et al*, 2010).

1.2.2 Three-dimensional structure of single domain ACE isoforms

1.2.2.1 N domain structures

Two human N domain structures have been resolved. The first, using protein purified from NB-DNJ-treated cells, was co-crystallised with lisinopril (Corradi *et al*, 2006). The second is a minimally glycosylated mutant, Ndom389 (only containing glycans at Asn^{45}, Asn^{416} and Asn^{480}) (Anthony *et al*, 2010), co-crystallised with the N-domain-specific inhibitor RXP407. These two approaches formed different space groups but had similar overall structures (Figure 1.2). Interestingly, both the NB-DNJ treated protein and Ndom389 packed as two molecules per asymmetrical unit. In the first structure residues L1-D612 were modelled with high definition, which included the linker region (P602-D612) that connects the domains in sACE (Corradi *et al*, 2006). The first part of the linker region (P602-Y607) is rigid due to hydrogen bonding between Y607 and E161, whereas the last four residues (E609-D612) are considered highly flexible since the side chains were not defined.

1.2.2.2 C domain structures

Human tACE structures, which include the NB-DNJ treated protein co-crystallised with lisinopril (Natesh *et al*, 2003) and several structures using the minimally glycosylated mutant

tACE-g13, co-crystallised with lisinopril and its novel derivatives as well as the C-domain-specific inhibitor RXPA380 (Watermeyer *et al*, 2006; Watermeyer *et al*, 2008; Watermeyer *et al*, 2010; Corradi *et al*, 2007). These structures resolve in the same space group as a single molecule per asymmetrical unit. Residues D616-Q1194 comprising the tACE ectodomain, were consistently resolved in these structures whereas the N terminus and flexible juxtamembrane stalk were not.

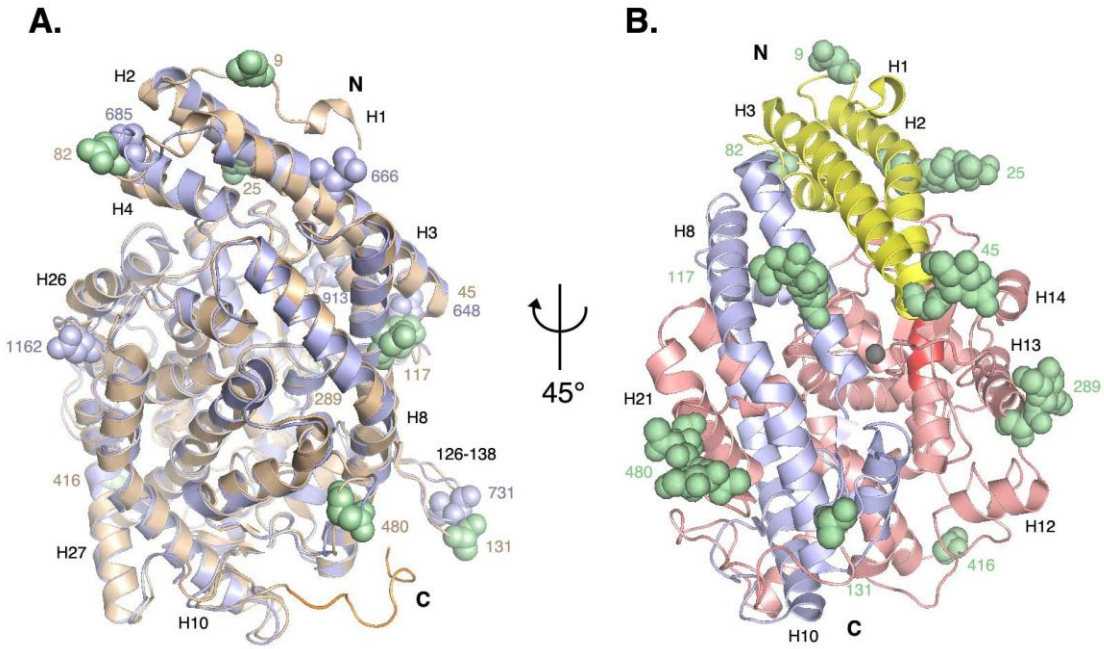

Figure 1.2. Three-dimensional structure of ACE. A. Overlay of the N domain (*light orange*) and tACE (*blue*) crystal structures (PDB accession numbers: 2C6F and 1O86, respectively). B. Organisation of domains, represented with N domain structure: lid helices (*yellow*), subdomain I (*blue*) and subdomain II (*pink*). In A and B, helices and residues of interest are shown (*black type*), glycans resolved in structures are shown as spheres (N domain: *green* and tACE: *blue*) and linker region shown in *orange*.

The ~60% sequence identity of the two domains is reflected in the high homology between the structures. The most marked difference being the extension of the N domain structure at the N and C termini compared to tACE (Figure 1.2A).

Both domains are dominated by α-helices, contain 6 β-sheets and a number of flexible loops with similar positioning in the domains. The overall topology of the domains is ellipsoid in shape, with a deep central groove positioned laterally, dividing the structure into two subdomains, I and II (Natesh *et al*, 2003; Corradi *et al*, 2006) (Figure 1.2B). The zinc binding motif, HEMGH is positioned on helix α15 at a point midway along the groove where the cleft is slightly pinched. Three N-terminal helices, α1-3, form a lid subdomain over the active site cleft, which is thought to restrict access of peptides. In both structures, the lid subdomain has

higher *B* factors, a measurement of the predicted mobility of residues, than the rest of the molecule suggesting some degree of flexibility. In the N domain structure the N-terminal region is well defined and packs tightly against helix α3 (Natesh *et al*, 2003). There are also differences between the active sites of the two domains, which could explain substrate specificity. These differences have been exploited to develop domain selective inhibitors (Nchinda *et al*, 2006a; Nchinda *et al*, 2006b; Kröger *et al*, 2009; Watermeyer *et al*, 2010). The N-linked glycosylation sequons of both domains are situated on the surface, except for the last sites (N domain: N494, C domain N1196). This N domain site is situated within the active site cleft and the C domain counterpart was not resolved, but is in the juxtamembrane stalk. In the N domain structure, the proposed hinge region on the lid subdomain is flanked by the 1st and 2nd sites (N9 and N25), where the latter has been shown to be important for thermal stability (Anthony *et al*, 2010). With tACE-g13, the glycans at N648 are within hydrogen bonding contact of E625 at the N-terminal end of helix α3 (2.5Å) and the oligosaccharide at N685 are in close proximity (3.2-4.5Å) to the side chains of T651 and E653 at the C terminal end of helix α1. These glycans may play a role in stabilising the lid subdomain with respect to the rest of the molecule (Watermeyer *et al*, 2006). This data supports the minimal glycosylation requirements determined by site-directed mutagenesis (Gordon *et al*, 2003) (refer to Section 1.3.2).

1.2.3 Dimer interfaces of the N domain three-dimensional structures

Both the native structure and the minimally glycosylated structure resolved as two molecules per asymmetric unit (Corradi *et al*, 2006; Anthony *et al*, 2010). This is intriguing as it suggests that regions on the surface might be involved in dimer interactions or other protein-protein interactions. The N domain is more extensively glycosylated than the C domain (refer to Section 1.3.2) and a series of mAbs raised against sACE predominantly recognised the N domain indicating that it is more likely involved in interactions (Danilov *et al*, 1994) (refer to Section 1.4). Moreover, oligosaccharides on the N domain have been implicated in ACE homodimerisation in a proposed carbohydrate recognition domain (CRD) (Kost *et al*, 2000; Kost *et al*, 2003) (refer to Section 1.3.4). The dimer interfaces, apparent from the two asymmetrical units, involve different orientations of the two molecules relative to each other. In the first, molecule B mirrors molecule A and is almost completely inverted in a "head to tail" arrangement (Figure 1.3) (Corradi *et al*, 2006). N416 in both molecules lies at the edge of the interface.

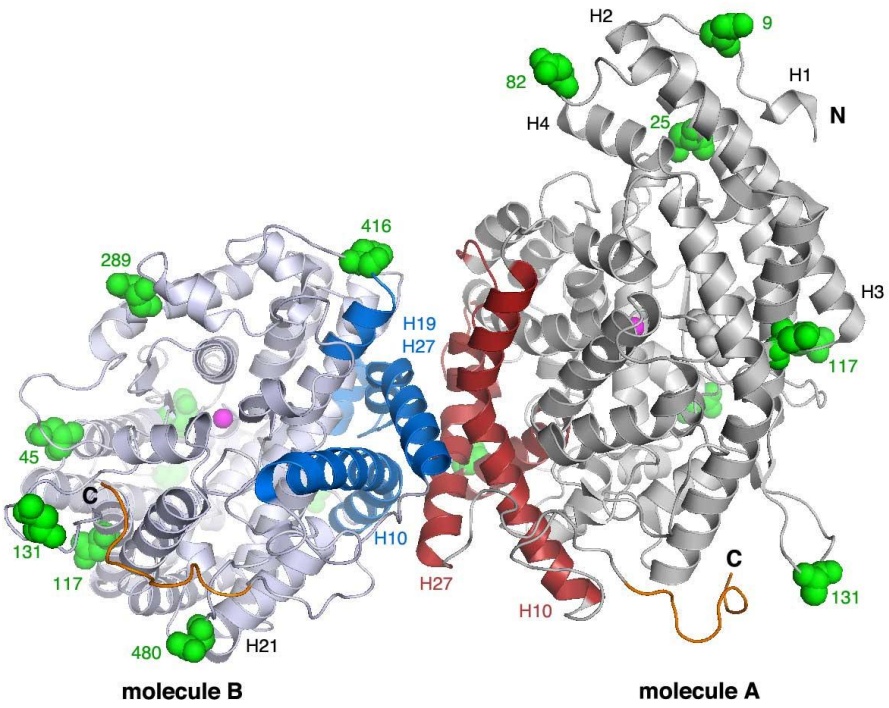

Figure 1.3. Dimer interface of wild-type N domain. Molecule A (*grey*) is orientated as in figure 1.2A with the dimer interface centred (molecule A: *red*, molecule B: *blue*) and molecule B (*blue-grey*) on the left. Helices are numbered (eg H1), glycans resolved in structures (*green spheres*) and linker region in each molecule (*orange*), zinc ion (*magenta*) are shown. (PDB accession number: 2C6F).

In the most recent structure, the two molecules are once again arranged as mirror images and molecule B is rotated approximately 45° (Figure 1.4) (Anthony *et al*, 2010). In this way, the linker region of both molecules, particularly that of molecule A lies within the interface. N480 in both molecules lies within this region, suggesting that it might play a role in interaction (Anthony *et al*, 2010). The unbound cysteine (C474) on both molecules lies within the interface.

The dimer interfaces partially overlap the epitope of mAb 3A5 (refer to Section 1.4), identified as region involved in shedding of sACE (Balyasnikova *et al*, 2002; Balyasnikova *et al*, 2005a). The proposed CRD, which encompasses the epitopes of mAbs 9B9 and 3G8 are not concomitant with these dimer interfaces (Kost *et al*, 2000; Kost *et al*, 2003). However the CRD was shown to involve oligosaccharide groups and considering the degree of flexibility and extension of these modifications, it is possible that groups proximal to these interfaces may be involved. In particular, N480 lies on the boundary of the second interface described, the 4th site (N82) and the 6th site (N131) are also in close proximity.

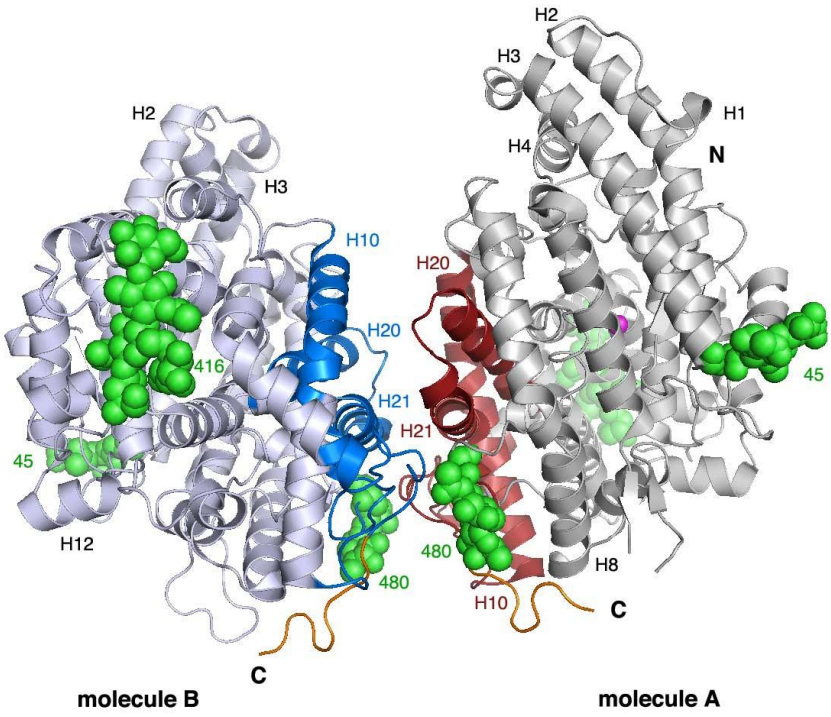

Figure 1.4. Dimer interface of Ndom389. Molecule A (*grey*) is orientated as in figure 1.2A with the dimer interface centred (molecule A: *red*, molecule B: *blue*) and molecule B (*blue-grey*) on the left. Helices are numbered (eg H1), glycans resolved in structures (*green spheres*) and linker region in each molecule (*orange*), zinc ion (*magenta*) are shown. (PDB accession number: 3NXQ).

It is important to note that the inter-chain interactions observed in the crystal structures do not necessarily infer interactions *in vivo*, particularly as there is scant evidence to indicate which regions are involved in protein-protein interactions of ACE.

1.2.4 Homology to other structures and evidence for hinge movement

Based on sequence homology and kinetic properties, ACE was classed in the MA clan of metalloproteases, closely related to carboxypeptidase A and thermolysin (Cushman *et al*, 1977; Rawlings & Barrett *et al*, 1993). However the crystal structures of both the N domain and tACE show structural homology to the metalloproteases neurolysin (Brown *et al*, 2001), thimet oligopeptidase (TOP) (Ray *et al*, 2004) and *Pyrococcus furiosis* carboxypeptidase (PfCP) (Arndt *et al*, 2002) despite little sequence homology. Common to all these structures is the ellipsoid shape, a predominance of α-helices and a deep active site channel that contains the zinc-binding motif (HExxH) that further divides the molecule into two subdomains. The structures of two ACE homologues; ACE2, similar to the N domain (Towler *et al*, 2004), and AnCE, similar to the C domain (Kim *et al*, 2003), revealed the same basic topology. Interestingly, these structures contained a similar lid arrangement to ACE, which presumably

limits access of larger peptides. It has been proposed that some form of hinge mechanism occurs upon substrate binding, which is supported by the high *B* factor of residues in the lid helices suggesting a degree of flexibility. Solving the crystal structures of tACE in both the unbound and inhibitor bound forms did not show any major differences in the position of these helices. However, insights into the closely related structures allows for some inference of the hinge mechanism in ACE. The structure of ACE2 in particular was solved in both forms and adopts an "open" and "closed" conformation (Towler *et al*, 2004). Modelling of the tACEg13 structure based on the "open" conformation of ACE2 revealed how the lid helices move relative to the two subdomains to open the active site cleft (Watermeyer *et al*, 2006). This mechanism was observed in TOP, neurolysin and AnCE (Brown *et al*, 2001; Kim *et al*, 2003; Ray *et al*, 2004). Moreover, the recent structure of the minimally glycosylated N domain mutant, Ndom389, bound to RXP407, while detected only in the "closed" conformation, hinted at hinge movement due to a slight twist in molecule A compared to molecule B in the asymmetrical unit. It appears that the molecule undergoes a twisting motion between the N and C termini with the lid helices moving away from the active site cleft (Anthony *et al*, 2010). Epitope mapping of the N domain-specific anti-ACE mAbs i2H5 and 5F1, which showed anti-catalytic activity towards ACE, also revealed evidence of this hinge mechanism (Skirgello *et al*, 2006; Danilov *et al*, 2007) (refer to Section 1.4).

1.2.5 Model of sACE and proposed domain interaction

Despite successful 3D structure determination of the individual domains of sACE, the crystal structure of the full-length isoform has not been resolved due to the difficulty in obtaining reproducible, high quality crystals. In addition to the microheterogeneity imposed by the oligosaccharides, the high degree of flexibility conferred by the linker region, allowing movement of the two domains relative to each other, is proposed to influence crystal lattice formation. The high-resolution structures of the individual domains, particularly of the linker region, allowed for the development of a model of sACE (Corradi *et al*, 2006) (Figure 1.5). However, the lack of data for the N-terminal helices of the C domain and the side chains of the linker region and flexible loop limit the accuracy of the model. The N domain has been shown to negatively regulate both kinetic activity of the C domain (Andujar-Sanchez *et al*, 2004) and ectodomain shedding (Woodman *et al*, 2005) and this may be the result of shielding of the C domain lid helices or a sheddase recognition motif by the N domain (refer

to Section 1.3.3). The last four residues of the linker region have a high degree of flexibility and form a prominent patch with the flexible loop (K126-S138) held in place by the disulphide bridge C128-C136 that may interact with the C domain, having sufficient flexibility to mould itself to fit against the C domain (Corradi *et al*, 2006). N-glycosylation sequons in the flexible loop (N480) and on the lid subdomain of the C domain (N648 and N666) may be involved in inter-domain interaction. Corradi *et al* (2006) proposed two models of sACE representing two extremes of interaction between the domains, based on the fact that only 4-7 residues showed sufficient flexibly to allow movement, namely "extended" and "compact" models. In the latter, there is a greater interaction surface between the domains and this "compact" model is consistent with the occlusion of the C domain by the N domain.

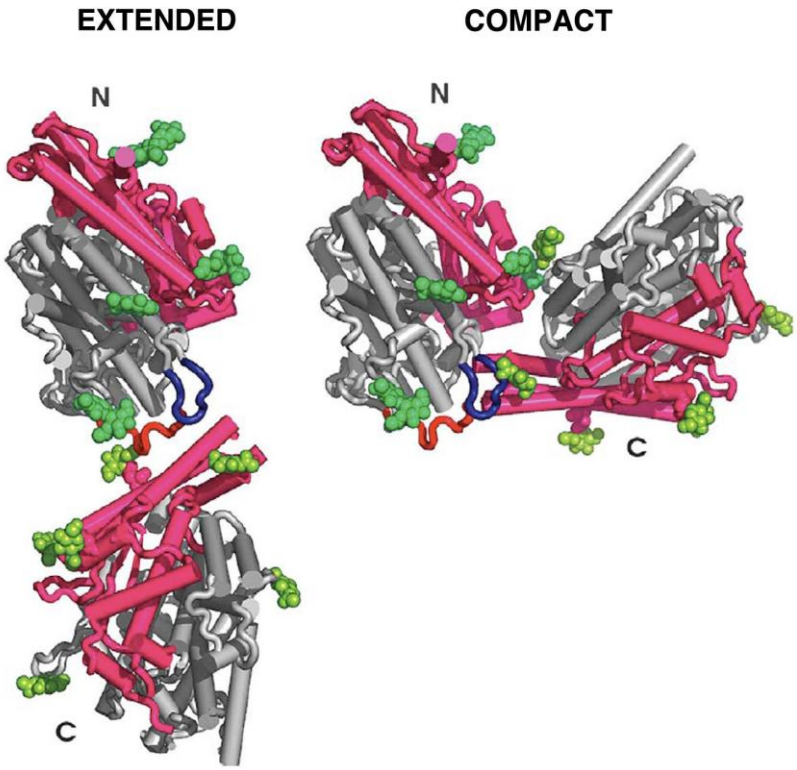

Figure 1.5. Proposed model of sACE in extended (*left*) and compact (*right*) orientations. Lid helices (*pink*), glycans (*green*), the linker region (*red*) and the flexible loop (*blue*) mentioned in the text are shown. (Figure from Corradi *et al* , 2006)

Recently, the electron microscopy (EM) structure of porcine pulmonary ACE, homologous to human sACE, was described (Chen *et al*, 2010). Despite being at comparatively low resolution, it gives some indication of the positioning of the two domains relative to each

other. The structure refined was similar to the "extended" model proposed by Corradi *et al* (2006), although the domains are positioned further apart than proposed. The linker region connecting the two domains was observed in this structure, separating the two domains by between 20-25Å. Distinct characteristics of each domain observed in the individual EM structures were used to identify each domain in the full-length structure. Interestingly, a large central cavity was observed for the C domain, consistent with the "open" unbound conformation of ACE2 (Towler *et al*, 2004). The N domain was assumed to be in the "closed" conformation since this deep pore was not observed. The crystal structures of the N domain and the "open" structure of ACE2 were modelled into the assumed analogous domains to determine their relative positioning. The position of the C domain is similar to that described by Corradi *et al* (2006) where the lid subdomain is orientated towards the N domain and could potentially be obstructed, which supports the proposed negative cooperativity of the C domain by the N domain. The linker region and flexible loop (K126-S138) in the N domain, modelled as a tight fit in the sACE model, are orientated away from the C domain at the C-terminal end of the active site cleft. Interestingly, this is consistent with one of the dimer interfaces of the N domain crystal structures (Figure 1.3) (refer to Section 1.2.3).

1.3 CELLULAR PROCESSING OF ACE AND PROTEIN-PROTEIN INTERACTIONS INVOLVED

Extensive study of the expression of ACE in mammalian cell culture systems; including transformed cell lines such as CHO, human endothelial kidney (HEK) and primary cultures including human umbilical vein endothelial cells (HUVEC); have identified the following cellular events: ACE is glycosylated during processing (Section 1.3.2), undergoes ectodomain shedding (Section 1.3.3), has been shown to form homodimers on the cell surface (Section 1.3.4), and acts as an initiator of an intracellular signalling pathway (Section 1.3.5). Each of these functions requires specific, regulated protein-protein interactions in order to take place. What is currently understood about these processes and the interactions involved will be discussed in the following sections.

1.3.1 Protein-Protein Interactions

Biological processes require the co-ordinated interactions of different proteins and peptides. These range from transient to permanent associations and can involve both homo- or hetero-oligomeric interactions (reviewed in Nooren & Thornton, 2003). The obligate formation of enzyme complexes required for function or the non-obligate protein-ligand, enzyme-inhibitor or antibody-antigen associations are some examples. There is a continuous equilibrium between these types of interactions depending on physiological conditions, the cellular environment and the likelihood of different components encountering each other. Protein-protein interactions involve specific interaction surfaces that require the coordination of a number of residues. The characterisation of these interaction surfaces as a means to define types of protein-protein interactions, considering the diversity of these associations, has led to the development of a number of databases and online services (Janin *et al*, 2008).

These interaction surfaces consist of hydrophobic interactions or polar interactions between groups in the amino acid side chain, and the protein backbone to some extent. Transient interactions in particular comprise either weak non-covalent interactions or strong interactions that require a molecular trigger to disrupt. The interaction surfaces of tighter associations, such as dimers, seem to contain a greater percentage of hydrophobic residues (Nooren & Thornton, 2003; Janin *et al*, 2008; Ma *et al*, 2003). Interestingly, interaction surfaces contain binding hotspots, which encompass highly conserved residues (Ma *et al*, 2003).

1.3.2 Glycosylation of ACE and its involvement in protein-protein interactions

1.3.2.1 Structure and function of glycosylation

Membrane proteins undergo either N-linked or O-linked glycosylation in the rough endoplasmic reticulum (ER) and Golgi apparatus, where oligosaccharide synthesis and chain elongation occur, respectively (reviewed by Lis & Sharon, 1993; Gahmberg & Tolvanen, 1996; Wyss & Wagner, 1996; Sears & Wong, 1998). N-linked polysaccharide chains are synthesised from the pentasaccharide core consisting of two N-acetylglucosamine and three mannose residues ($GlcNac_2Man_3$). This is attached to an asparagine residue in the sequon Asn-X-Ser/Thr -Y (Ronin *et al*, 1981) with a preference for sequons containing a threonine (Kasturi *et al*, 1997), where X or Y are not proline residues (Bause, 1983; Roitsch & Lehle, 1989; Mellquist *et al*, 1998). O-linked polysaccharide chains are attached to serine or

threonine residues, by an N-acetylgalactosamine dissacharide ($GalNac_2$), where these residues appear in clusters (Wilson *et al*, 1991).

Oligosaccharide chains play important roles in two key aspects, namely they ensure correct folding and processing of proteins in the ER and, through the sequence variety introduced in the Golgi during chain elongation, confer greater heterogeneity to proteins, introducing a greater potential for interactions. Oligosaccharides can extend some distance from the peptide backbone and thus act as individual domains. The oligosaccharide sequence of N-linked chains is determined by the expression of particular enzymes in the Golgi and is thus specific to cell type and cellular conditions (reviewed by Kobata, 1992; Sears & Wong *et al*,1998; Helenius & Aebi, 2001).

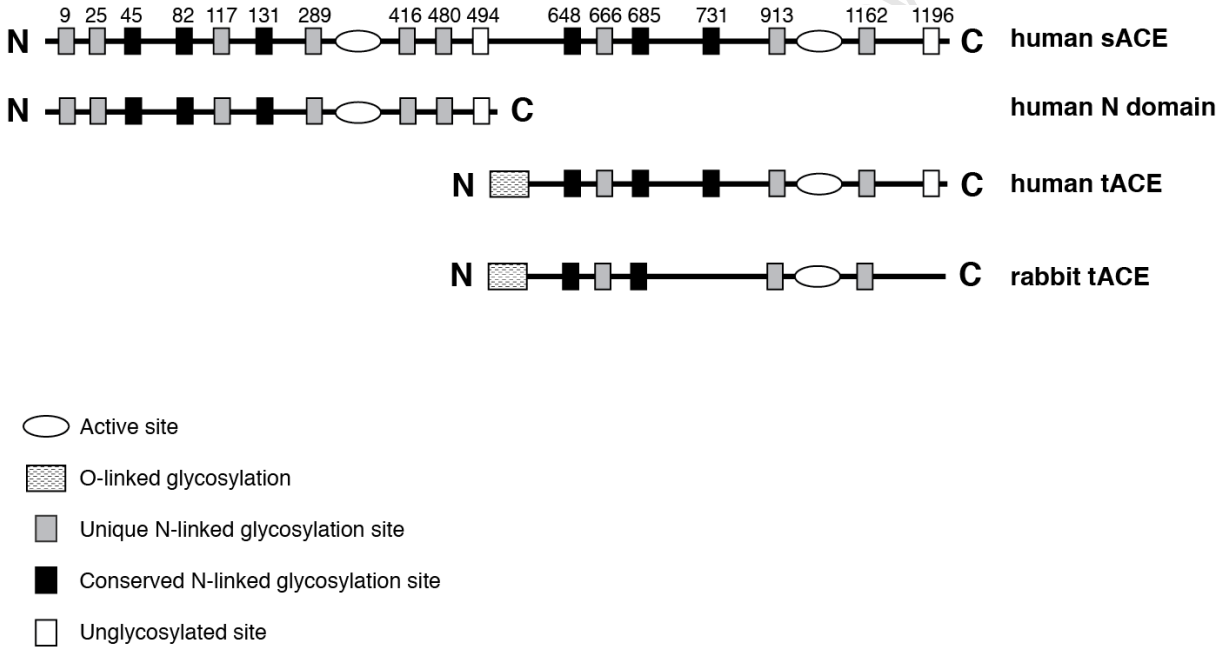

Figure 1.6. Glycosylation of ACE.

1.3.2.2 Glycosylation patterns of ACE isoforms

In human somatic ACE, there are 10 potential N-linked glycosylation sequons in the N domain and 7 in the C domain, three of which are conserved between the domains (sites N45/N648, N82/N685 and N131/N731) (Figure 1.6). Five of the sites in tACE are complementary to the sites in rabbit tACE (Yu *et al*, 1997; Kasturi *et al*, 1994). Across four species (human, rat, rabbit and guinea pig) 7-8 sites are known to be glycosylated (Ripka *et al*, 1993), but thorough analysis of the glycosylation of full-length sACE has not been

performed. The extent of glycosylation of tACE and a soluble N domain counterpart has been well defined. Enzymatic deglycosylation, limited proteolysis and mass spectrometry showed that 6 of the potential sites of human tACE are glycosylated, with three sites (N731, N913 and N1162) present in both unglycosylated and glycosylated forms (Yu *et al*, 1997). Using a similar approach, eight of the ten potential N-linked glycosylation sites in the N domain were shown to be glycosylated (N9, N25, N45, N82, N117, N131, N416 and N480) (Anthony *et al*, 2010). The C-terminal site (N domain: N494, C domain: N1196) is unglycosylated in both the N and C domains. In tACE, this was proposed to be due to the presence of a tryptophan at position X (NWT) that prevents formation of the Asx-turn (Gordon *et al*, 2003), which is necessary for chain elongation (Imperiali & O'Connor, 1999). The juxtamembrane mutant, tACE-Δ6, generated a novel sequon at N620 (NRSE) that was glycosylated, which appears to corroborate this suggestion (Schwager *et al*, 1999). However, both unglycosylated sites in the N and C domains contain a proline at position Y (N domain: NVTP, C domain: NWTP) that would prevent formation of the Asx-turn and subsequent glycosylation (Bause *et al*, 1983; Roitsch *et al*, 1989). This was confirmed by the recent finding that the tACE P1199L mutant, in which the proline is removed, is glycosylated at N1196 (Sturrock *et al*, unpublished results) and further explains why this same site in tACE-Δ6 is glycosylated since this site also lacks a proline at position Y.

1.3.2.3 Role of glycosylation in ACE folding and expression

The unique 36-residue N-terminal region of tACE, rich in serine and threonine residues, is heavily O-glycosylated (Ehlers *et al*, 1992). O-glycosylation of tACE was not required for the expression of active enzyme since a human tACE construct lacking the unique N-terminal region was expressed and enzymatically active (Ehlers *et al*, 1992) as was rabbit tACE expressed in *ldl*D cells, which are unable to produce O-linked and complex N-linked sugars (Kasturi *et al*, 1994). Since tACE has been shown to play a role in fertility, binding spermatozoa to the zona pellucida (Hagaman *et al*, 1998), it is possible that the O-linked sugars are involved, however the specific role of these modifications has not been established. Rabbit tACE expressed in *E.coli* (Sadhukhan & Sen, 1996) or in HeLa cells in the presence of tunicamycin (Kasturi *et al*, 1994) was degraded intracellularly implicating N-linked glycosylation in correct folding and expression of tACE. Furthermore, a null mutant lacking all five N-linked glycan sequons showed the same results (Sadhukhan & Sen, 1996). A soluble human tACE mutant lacking the 36-residue O-glycosylated region was successfully

expressed in the presence of the α-glucosidase-I inhibitor NB-DNJ (Yu *et al*, 1997) and was used for 3D structure determination of ACE (Natesh *et al*, 2003) (refer to Section 1.2).

Determination of the minimal glycosylation requirements for the expression of correctly folded, enzymatically active ACE using site-directed mutagenesis has been conducted for both the N domain and tACE (Sadhukhan & Sen, 1996; Gordon *et al*, 2003; Anthony *et al*, 2010). In both human and rabbit tACE, there is a preference for intact glycosylation sequons at the N-terminus for expression of active protein (Sadhukhan & Sen, 1996; Gordon *et al*, 2003) and the presence of glycans is not site specific. Intact glycosylation sequons at either the first and second sites was sufficient for rabbit tACE expressed in HeLa cells whereas the third site was not (Sadhukhan & Sen, 1996). Similarly, the first and third sites (N648 and N685) in human tACE expressed in CHO cells were sufficient but the second (N666) was not (Gordon *et al*, 2003). The site preferences between the two studies suggest that glycosylation requirements differ between species and between cell types. The requirements of glycosylation for the expression of active N domain were surprisingly different to tACE (Anthony *et al*, 2010). First, three C-terminal sites were preferred (the 7^{th}: N289, 8^{th}: N416 and 9^{th}: N480 sites) and mutants lacking all but the N terminal sites were inactive. Second, the expression of an active protein, demonstrated by the mutant Ndom389 having intact sites at positions N45, N416 and N480, required the presence of at least three sites. Two of these were required to be the 7^{th}, 8^{th} or 9^{th} sites, but there was some redundancy (Anthony *et al*, 2010).

1.3.2.4 Role of glycosylation in thermal stability of ACE

The N domain has a higher melting temperature than the C domain (T_m = 70°C versus 55°C respectively), thus it is more thermostable (Voronov *et al*, 2002; O'Neill *et al*, 2008; Anthony *et al*, 2010). This has been attributed to the higher proportion of α-helices, increased proline content and extent of glycosylation of the N domain (Voronov *et al*, 2002). Recent studies with minimally glycosylated N domain and tACE mutants demonstrate that thermostability does indeed depend on the presence of glycosylation with a preference for sugars at particular positions (O'Neill *et al*, 2008; Anthony *et al*, 2010). In tACE, the presence of glycosylation at the 5^{th} (N913) and 6^{th} (N1162) sites confers greater thermostability (O'Neill *et al*, 2008) whereas in the N domain it is the N-terminal sites 2 (N25) and 3 (N45) (Anthony *et al*, 2010).

1.3.2.5 Role of ACE glycosylation in protein-protein interactions

Oligosaccharides within each domain of ACE are proximal to key interfaces. Sites N9, N25, N45 and N82 in the N domain and N648, N666 and N685 in the C domain lie within or are proximal to the hinge region thought to be involved in substrate access. Moreover, certain sites resolved in tACE are sufficiently close to residues to form an interaction (Watermeyer *et al*, 2006) (refer to Section 1.2.2). The dimer interfaces observed with the N domain crystal structures also have glycans within sufficient contact (Corradi *et al*, 2006; Anthony *et al*, 2010) (refer to Section 1.2.3) and glycans are implicated in inter-domain interaction in the model of sACE (Corradi *et al*, 2006). Furthermore, fine epitope mapping of domain-specific mAbs to ACE implicated glycans in these interactions (Danilov *et al*, 2007; Gordon *et al*, 2010; Balyasnikova *et al*, 2005a; Balyasnikova *et al*, 2007; Balyasnikova *et al*, 2008) (refer to Section 1.4.2) and ACE homodimerisation involved sialic acid or galactose residues (Kost *et al*, 2003) (refer to Section 1.3.4). Since glycosylation is cell and tissue specific, the pattern of glycosylation of sACE may be an important regulator in cell associated and plasma ACE, as has been implicated in a recent investigation using anti-ACE mAbs to investigate sarcoidosis (Danilov *et al*, 2010a). Moreover, a very recent study has shown that removal of galactose residues from ACE can modulate its activity (Batista *et al*, 2011).

1.3.3 Interaction of ACE and its cognate sheddase in ectodomain shedding

Although ACE is expressed as an integral membrane protein, soluble forms are found in plasma and other fluids (Hooper, 1991). This is the result of regulated cleavage secretion of ACE (Ehlers *et al*, 1991; Wei *et al*, 1991b; Oppong & Hooper *et al*, 1993; Parvathy *et al*, 1997) at the plasma membrane (Beldent *et al*, 1995) through the action of an unidentified sheddase (Ehlers & Riordan, 1991b). Thus, ACE falls into a class of membrane proteins that are proteolytically processed from the cell surface, which include integral membrane proteins such as the amyloid precursor protein (APP) (Palmert *et al*, 1989; Weidemann *et al*, 1989); ectoenzymes such as neprilysin (NEP) (Erdös *et al*, 1985); adhesion molecules such as L-selection and neural cell adhesion molecule (NCAM) (Nybroe *et al*, 1989) and receptors such as tumour necrosis factor-α (TNF-α) (Porteu *et al*, 1991) (reviewed in Ehlers & Riordan, 1991b; Garton *et al*, 2006; Edwards *et al*, 2008; Hayashida *et al*, 2010). The cleavage secretion of ACE in endogenously expressed cells is mirrored in cells overexpressing recombinant ACE, such as CHO cells (Ehlers *et al*, 1991) and epithelial cell lines

(Ramchandran *et al*, 1994), indicating a common machinery amongst mammalian cells and thus these cell lines are a model system to study the mechanism of shedding.

The search for the ACE secretase is on going. Sheddases include metalloproteases, serine proteases and aspartate proteases, which tend to be distinguished by their inhibitor profile (Hooper *et al*, 1997). ACE shedding is stimulated in the presence of phorbol esters such as phorbol 12,13-dibutyrate (PDBu) or phorbol-12-myristate-13-acetate (PMA) (Ramchandran *et al*, 1994; Ehlers *et al*, 1995). This mechanism of membrane protein proteolysis is the result of protein kinase C (PKC) activation of the secretase most likely by direct phosphorylation (Bosenberg *et al*, 1992; Caporaso *et al*, 1992; Pandiella *et al*, 1992). Both basal and phorbol ester stimulated shedding are inhibited by hydroxamate-based matrix metalloprotease (MMP) inhibitors, including TNF-α protease inhibitors (TAPIs), compound 3 (TAPI-II) (Ramchandran & Sen, 1995) and batimastat, which suggests that the ACE secretase involved is a zinc metalloprotease (Parvathy *et al*, 1997; Schwager *et al*, 1998). Interestingly, shedding is stimulated in the presence of the serine protease inhibitor 3,4-dichloroisocoumarin (DCI) (Ehlers *et al*, 1995; Schwager *et al*, 1999), a phenomenon uniquely described for the proteolysis of APP by α-secretase and ACE by its unknown sheddase (Parkin *et al*, 2002). DCI-activated shedding is also inhibited by TAPI-1, suggesting that it is an activator for the sheddase involved in ACE shedding (Schwager *et al*, 1999).

It is known that the sheddase is a metalloprotease and a requirement for shedding is that ACE is inserted into the membrane (Ramchandran & Sen, 1995; Beldent *et al*, 1995). Cleavage secretion of membrane proteins such as the amyloid precursor protein (APP) has been shown to occur in lipid rafts or caveolae on the membrane. However, this does not seem to be a requirement for ACE shedding since introduction of a glycosylphosphatidylinisotol (GPI) anchor that targets proteins to caveolae had no effect on shedding (Parkin *et al*, 2003). ADAM 17, or TNF-α converting enzyme (TACE or ADAM17), a common protease involved in shedding of many proteins, has been ruled out as the cognate ACE sheddase since TACE does not cleave ACE efficiently (Parvathy *et al*, 1998a) and ACE is still released from the membrane in TACE negative cell lines (Sadhukhan *et al*, 1999). Knockdown of two metalloproteases, TACE and ADAM10, in human SH-SY5Y cells expressing either ACE or APP demonstrated that neither of these sheddases are involved in ACE shedding, but does reduce α-secretase release of APP (Allinson *et al*, 2004). The ACE sheddase has a highly similar profile to the α-secretase that cleaves APP (Parvathy *et al*, 1997; Parvathy *et al*, 1998b; Parkin *et al*, 2002) including its activation by DCI. These sheddases can be

distinguished by the action of 4-aminophenylmercuric acetate (APMA), which stimulates shedding of ACE but not APP (Allinson *et al*, 2004).

Pinpointing the major ACE sheddase has involved identifying regions or residues of ACE required for sheddase interaction. This has been performed through two approaches, firstly, identification of the cleavage site and sequence/structural requirements in the stalk region for sheddase recognition and secondly, the identification of recognition motifs in the juxtamembrane region or ectodomain.

Cleavage occurs within the juxtamembrane stalk between R1203 and S1204, in both the sACE (Woodman *et al*, 2000) and tACE (numbering of scissile bond residues in tACE - R627-S628) (Ehlers *et al*, 1996) isoforms. The corresponding site in rabbit tACE is between R663 and S664 (Ramchandran *et al*, 1994). Deletion mutants of the stalk region have demonstrated a weak specificity of the secretase for ACE, where despite removal of a number of residues and extended regions of the juxtamembrane stalk, ACE is still shed (Ehlers *et al*, 1996; Schwager *et al*, 1998; Schwager *et al*, 1999). From these investigations, it appears that the sequence around the cleavage site is not pivotal for cleavage to occur, but requires an unfolded stalk of 10-15 residues. Furthermore, the secretase positions itself according to the ectodomain and requires a minimum distance from the membrane. Two investigations showed that mutations in the stalk region can induce ACE shedding by alternate sheddases. In the first, an Asn to Gln mutation at position 1196 in tACE altered the cleavage site resulting in shedding of ACE resistant to DCI stimulation (Alfalah *et al*, 2001). The same was observed when a serine/threonine rich sequence was introduced into the stalk region with the mutant ACE-JGL (Schwager *et al*, 1999). Recently, substitutions in rabbit tACE of 5 amino acids on the boundary of the ectodomain and flexible juxtamembrane showed that these residues were important for secretase recognition and corroborate the specific interaction of a sheddase (Chattopadhyay *et al*, 2008).

1.3.3.1 Recognition of ACE by the sheddase

The relaxed specificity of the cleavage site as demonstrated by numerous stalk mutations of ACE indicates that this is not the most significant region for sheddase recognition, which leaves the cytoplasmic tail and ectodomain. Removal of the cytoplasmic tail results in increased basal shedding (Sadhukhan *et al*, 1998; Chubb *et al*, 2004) and therefore does not appear to contain a recognition motif. Chimeras of ACE and CD4, a protein that is not shed, showed that the presence of the ACE ectodomain is sufficient to induce shedding and suggests the existence of a recognition motif in this domain (Sadhukhan *et al*, 1998).

However, these results are controversial in light of a similar study conducted with the ectodomain of another unshed protein, porcine membrane dipeptidase (MDP) where the presence of the juxtamembrane stalk, the transmembrane domain and cytoplasmic tail of ACE was sufficient to induce shedding (Pang *et al*, 2001). It was proposed that the lack of shedding of the ACE/CD4 chimera was as a result of insufficient folding of the ACE portion, which included some of the ectodomain. However, an ACE mutant lacking the C domain and thus with the N domain adjacent to the stalk region, ACEΔC, was not shed, corroborating the presence of a specific recognition motif in the C domain (Pang *et al*, 2001). A conclusion of this study was that shedding might be the result of the action of two classes of sheddases, where the first has a strong affinity for residues in the juxtamembrane stalk and the second interacts with ACE via a specific recognition motif in the ectodomain.

Although shedding occurs at the same cleavage site in the two ACE isoforms, sACE is shed less efficiently than tACE (Beldent *et al*, 1995; Woodman *et al*, 2000), suggesting different regulation and ACE-secretase interaction. It was initially proposed that sACE was cleaved at a different site to tACE and this was the result of alteration of shedding by the N domain, which directs the secretase to an alternative site (Beldent *et al*, 1995). However, it was shown that sACE is cleaved at the same site as tACE, which supports the hypothesis that cleavage is regulated by the N domain, possibly via occlusion of a C-domain recognition motif (Woodman *et al*, 2000). Moreover, a region of the N domain has been implicated in the regulation of sACE shedding through the investigation of domain-specific mAbs to ACE. Three N-domain-specific mAbs, 9B9, 3A5 and 3G, were shown to alter shedding efficiency (Balyasnikova *et al*, 2002) (refer to Section 1.4). This was proposed to be the result of conformational changes induced by mAb binding that would alter the access of the sheddase to the stalk region. The secretase involved in mAb-induced shedding appeared to be distinct from that responsible for basal shedding and phorbol ester induced shedding. ACE domain chimeras, where the two domain positions were swopped or the N domain as replaced with a second C domain, indicated that a recognition motif exists in the C domain and that the N domain negatively regulates shedding by occluding the C domain recognition motif (Woodman *et al*, 2005). The crystal structure of tACE (Natesh *et al*, 2003) and homology modelling of the N domain allowed for identification of surface regions that could be implicated and, harnessing the high degree of sequence homology between the domains, homologous substitution of the C domain with N domain counterparts was used in an attempt

to delineate the recognition motif (Woodman *et al*, 2006). This either disrupted ACE expression or altered its enzyme activity but did not alter shedding.

Unlike other secreted proteins, such as aberrant release of APP in Alzheimer's disease (Haass & Selkoe, 2007) and release of TNF-α in the inflammatory response (Kriegler *et al*, 1988; Gearing *et al*, 1994), the biological significance of secreted or plasma ACE is unknown. It is possible that release of ACE from certain tissues allows for its action at distal sites. Alternatively, tethering the enzyme to the membrane could concentrate its effects, which could be regulated by ectodomain shedding. It has been shown that membrane-bound sACE is critical for AngII production in the vascular endothelium since soluble ACE is not sufficient to restore blood pressure in null ACE mice (Kessler *et al*, 2007), suggesting a requirement for localised action.

1.3.3.2 Regulation of ACE shedding

In order to understand the physiological role of soluble ACE, the regulatory processes involved have been investigated by probing protein-protein interactions. Immunoprecipitation of ACE from ACE89 cells, a mouse epithelial cell line stably transfected with ACE, revealed an interaction with immunoglobulin binding protein (BiP) and PKC (Santhamma *et al*, 2000). BiP is a chaperone expressed in the ER that facilitates protein folding (Munro & Pelham, 1987; Gething, 1999). Interaction of BiP with ACE prolonged cell surface expression, but had no effect on shedding. The same study found that distinct isoforms of PKC interact directly with ACE and that these interactions are disrupted in the presence of phorbol esters. However, there is scant evidence to link this interaction and shedding and it is more likely that the phorbol induced shedding response is mediated by PKC activation of the sheddase rather than ACE directly. Moreover, PKC may be involved in regulation of ACE phosphorylation by CK2 (Fleming, 2006) (detailed in Section 1.3.5).

Interestingly, tyrosine phosphorylation of the ACE ectodomain appears to regulate shedding where treatment of cells with pervanadate, a tyrosine phosphatase inhibitor, increased shedding of tACE (Santhamma *et al*, 2004). Both ACE and BiP were phosphorylated indicating a regulation of shedding at the expression level. This appeared to be independent of the PKC dependent pathway and involved p38 mitogen-activated protein (MAP) kinase.

Investigations into ACE signalling have shown that phosphorylation by CK2 modulates ACE shedding (refer to Section 1.3.5) through serine phosphorylation. Increased basal shedding in the absence of the cytoplasmic tail (Sadhukhan *et al*, 1998; Chubb *et al*, 2004) is indicative of negative modulation of shedding by residues in the cytoplasmic tail. Furthermore, it was

shown that interaction of calmodulin (CaM) with the cytoplasmic tail of rabbit tACE reduces shedding and that ACE is phosphorylated by CaM at S1270 (Chattopadhyay *et al*, 2005). In this case, phosphorylation does not appear to have an effect on shedding, but may be the result of cell and species differentiation. It may be that regulated shedding requires activation by PKC and is therefore independent of phosphorylation of the cytoplasmic tail whereas basal shedding is regulated by CK2 phosphorylation.

Thus, it is apparent from the extensive investigation into cleavage secretion of ACE that it is a regulated process that involves specific protein-protein interactions and several potential regulatory pathways. A deeper understanding of the key components of these pathways could help to elucidate the role of ACE shedding. Furthermore, identifying regions or residues of ACE that are important for regulation of shedding and for interaction with secretases, co-factors or other key components would greatly enhance our understanding of these pathways.

1.3.4 Dimerisation of ACE

1.3.4.1 Importance of dimerisation

Dimerisation on the cell surface is an important regulatory mechanism for many receptors; including those involved in cardiovascular regulation; such as the angII receptors, type 1 and type 2 (reviewed in Mogi *et al*, 2009) and BK 2 receptor (B2K-R) (AbdAlla *et al*, 1999). Dimerisation is initiated upon ligand binding and activates intracellular signalling cascades. Homo- and hetero-dimerisation of enzymes is also a common phenomenon, with more than two-thirds of described enzymes existing in dimeric or multimeric forms (reviewed in Marianayagam *et al*, 2004). This increases enzyme stability, enables enzyme activation and creates binding sites for co-factors to improve enzyme function. The endothelin converting enzyme 1 (ECE-1), which is structurally homologous to ACE, forms homodimers that increase catalytic efficiency (Shimada *et al*, 1996) whereas the closely related protein, NEP, does not.

1.3.4.2 Homodimerisation of ACE

Higher molecular weight (MW) forms of ACE have been observed during gel electrophoresis of purified samples (Naim *et al*, 1992; Kohlstedt *et al*, 2006) and have been attributed to aggregates of ACE. Two recent studies have described ACE dimerisation in a reverse micelle

system (Kost *et al*, 1998; Kost *et al*, 2000 Kost *et al*, 2003) and in primary cell culture, HUVEC and porcine aortic endothelial cells (Kohlstedt *et al*, 2006).

It was demonstrated that sACE has the ability to form a homodimer using a split-ubiquitin assay in *Saccharomyces cerevisiae* (Kohlstedt *et al*, 2006). In the reverse micelle system purified full-length sACE was detected as both a monomer and higher MW variants consistent with dimeric and oligomeric forms (Kost *et al*, 2003). An N-domain isoform, generated by limited proteolysis of human sACE by trypsin, formed both monomer and dimer in the same system and the bovine N domain counterpart formed multiple higher MW forms (Kost *et al*, 2000; Kost *et al*, 2003). Purified tACE was detected solely as a monomer. Dimers observed with sACE and the N domain were inhibited in the presence of galactose (Kost *et al*, 2000; Kost *et al*, 2003), indicating that carbohydrate residues were likely involved in dimer formation and a carbohydrate recognition domain in the N domain was proposed (Kost *et al*, 2000; Kost *et al*, 2003). A putative region of the N domain involved in dimerisation was identified using two mAbs to ACE (described in more detail in Chapter 4). These two mAbs, 9B9 and 3G8, shown to affect shedding of ACE from CHO cells, inhibited dimerisation in reverse micelles.

Formation of ACE dimers on the surface of porcine aortic endothelial cells was induced by ACE inhibitors and initiated the intracellular signalling cascade (detailed in Section 1.3.5) (Kohlstedt *et al*, 2006). The presence of either sugars such as galactose and glucose and the mAbs mentioned previously had no effect on this process (Kohlstedt *et al*, 2006). Active site knockout mutants demonstrated that an active C domain was required for this inhibitor-associated dimerisation to occur. These two studies are the first indication of self-association of ACE and implicate this process in other important cellular events such as shedding and intracellular signalling.

The mechanism of ACE homodimerisation is unclear. In work by Kost *et al*, carbohydrate residues and a carbohydrate recognition domain in the N domain are implicated suggesting a non-covalent interaction (Kost *et al*, 1998; Kost *et al*, 2000; Kost *et al*, 2003) and more detailed mapping of the epitopes of the mAbs that inhibit dimerisation would be useful in understanding this further. The C domain dependent dimerisation described by Kohlstedt *et al* (2006) was detected by chemical cross-linking of cell lysate and thus it is unclear what mechanism is involved.

1.3.4.3 Heterodimeric interactions of ACE

The substrate promiscuity of ACE and its increasing role in physiological pathways, implicates a number of protein-protein interactions in communication and regulation of these processes. What is known regarding protein-protein interactions of ACE and components of other systems is detailed here.

There is a degree of cross-talk between components of the RAAS and KKS. The B2K-R is resensitised, namely it is able to re-couple with G-protein for signal transduction, in the presence of ACE inhibitors (Minshall *et al*, 1997; Marcic *et al*, 1999; Marcic *et al*, 2000) and this was found to be dependent on direct interaction of ACE, through the formation of heterodimers on the cell surface (Chen *et al*, 2006). Binding of ACE inhibitors is thought to stabilise the heterodimer and prevent homodimer formation of B2K-R, which would otherwise lead to internalisation (Marcic *et al*, 2000).

Recently, heterodimerisation of ACE and the GPI-anchored protein carboxypeptidase M (CPM) has been described (Sun *et al*, 2008). This corroborated the finding that ACE has GPI-ase activity, cleaving proteins such as CPM from the membrane, which was linked to male fertility (Kondoh *et al*, 2005). However, this novel function of ACE was not substantiated in a follow-up study using various GPI-anchored proteins (Leisle *et al*, 2005) and remains controversial.

1.3.5 Intracellular Signalling of ACE

Kohlstedt *et al* (2002, 2004, 2005, 2006) have shown in both primary HUVEC endogenously expressing ACE and ACE overexpressed in porcine aortic endothelial cells that ACE can act as a signalling molecule initiating an intracellular cascade to regulate gene expression. The same signalling pathway has been demonstrated in CHO cells overexpressing murine sACE (Sun *et al*, 2010). There is also preliminary evidence to suggest that the same occurs in a mouse model (Fleming, 2006). Recently, this was also described in preadipocytes and adipocytes (Böttcher *et al*, 2006; Kohlstedt *et al*, 2009; Kohlstedt *et al*, 2010), demonstrating a link in the ACE inhibitor effects on the development of type-2 diabetes.

There are 5 serine residues in the short cytoplasmic tail of human ACE and 1 tyrosine and 3 serines in murine ACE, potential sites for phosphorylation and the initiation of a signalling cascade. Three serines of human ACE lie within consensus binding sites for PKC (S1253), protein kinase A (PKA) (S1263) and casein kinase (CK2) (S1270) (Kohlstedt *et al*, 2002). A PKC inhibitor, RO 31-8220, did not prevent ACE phosphorylation whereas 5,6-Dichloro-1-β-

D-ribofuranosylbenzimidazole (DRB), a CK2 inhibitor, did. Further investigation showed that ACE is phosphorylated by CK2 (Kohlstedt *et al*, 2002) at S1270 resulting in association of MAP kinase kinase 7 (MKK7) and the activation of c-Jun N-terminal kinase (JNK) leading to phosphorylation of c-Jun (Kohlstedt *et al*, 2004). c-Jun then translocates to the nucleus and activates gene expression of ACE and cyclooxygenase-2 (COX-2), which is involved in pain and inflammation (Kohlstedt *et al*, 2004; Kohlstedt *et al*, 2005) (Figure 1.7).

This signalling cascade is initiated by binding of ACE inhibitors and, to some extent, BK (Kohlstedt *et al*, 2004). However, angI, the major substrate for ACE, does not initiate this cascade in porcine aortic endothelial cells overexpressing human ACE. Interestingly, angI and BK, as well as angII, were shown to increase JNK activity in CHO cells overexpressing murine ACE (Sun *et al*, 2010), suggesting species specificity in this pathway.

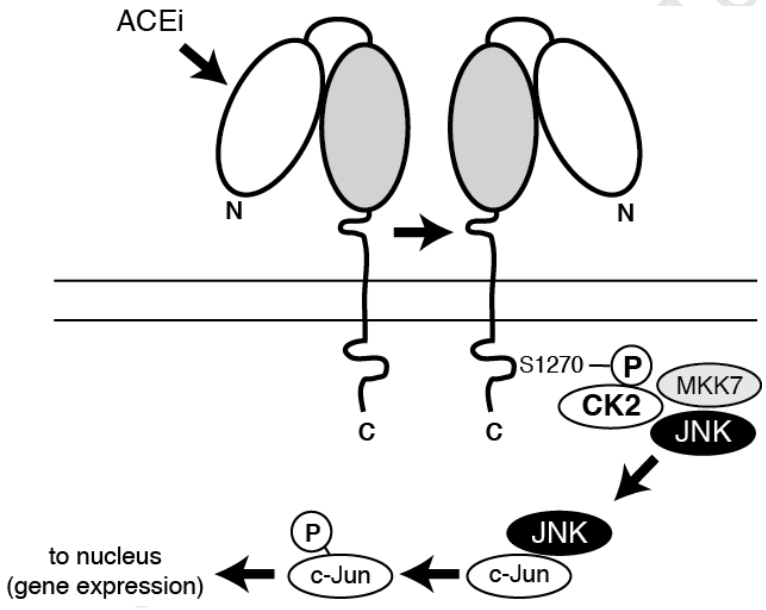

Figure 1.7. ACE signalling pathway. Binding of ACE inhibitors (ACEi) induces dimer formation, which activates CK2, phosphorylating ACE at S1270 leading to association of MKK7. JNK is then activated and phosphorylates c-Jun, which translocates to the nucleus and activates gene expression.

The mechanism involved in ACE inhibitor initiation of signalling is unclear, although it is most likely induced by conformational changes upon binding. ACE homodimerisation has been shown to mediate signalling upon inhibitor binding (Kohlstedt *et al*, 2006). This requires an active C domain, demonstrated by active site knockouts. Once again there appears to be some degree of species selectivity since murine ACE active site knockouts showed some preference for signalling via the C domain, although the N domain alone demonstrated the ability to activate JNK (Sun *et al*, 2010). Moreover there appeared to be

some degree of negative cooperativity between domains with regards to JNK activation upon substrate binding.

CK2 phosphorylation of ACE appears to regulate basal shedding of ACE (Kohlstedt *et al*, 2002). Soluble ACE is not phosphorylated and the S1270A mutant, which lacks the ability to be phosphorylated, was shed more efficiently. Once phosphorylated by CK2, ACE is retained in the plasma membrane. Phorbol ester stimulated shedding was independent of this process, indicating that this results in activation of a metalloprotease by PKC whereas basal shedding is regulated by CK2 phosphorylation.

1.4 PROBING PROTEIN-PROTEIN INTERACTIONS WITH ANTI-ACE MONOCLONAL ANTIBODIES

1.4.1 Use of monoclonal antibodies for protein structure-function analysis

MAbs being targeted to specific regions of a protein are valuable tools in structure-function studies. Fine-epitope mapping of mAbs to a particular protein, in combination with site-directed mutagenesis, can facilitate the identification of regions or hotspots on the surface involved in protein-protein interactions, particular functions or facilitate structure determination.

1.4.2 Epitopes of domain-specific anti-ACE monoclonal antibodies

The 3D structures of both domains has facilitated fine-epitope mapping of domain-specific anti-ACE mAbs. The epitopes of these mAbs have been defined using a combination of site-directed mutagenesis, cross-species reactivity and reactivity towards different ACE isoforms and deletion constructs or chimeras. Residues that affect mAb-ACE interaction were used to delineate regions of 700-800Å^2, encompassing the mAb epitopes. The epitopes of eight N domain-specific mAbs (9B9, 3G8, 3A5, i1A8, 6A12, 1G12, 5F1 and i2H5) and eight C domain-specific mAbs (1B3, 1B8, 3F10, 1E10, 4E3, 2H9, 3F11 and 2B11) have been mapped to regions of each domain (Danilov *et al*, 1994; Balyasnikova *et al*, 2005b; Skirgello *et al*, 2006; Danilov *et al*, 2007; Balyasnikova *et al*, 2007; Balyasnikova *et al*, 2008; Naperova *et al*, 2008a; Gordon *et al*, 2010). The binding of these mAbs to different ACE chimeras has allowed for the identification of regions that may be involved in protein-protein interactions that affect dimerisation, shedding and catalysis. Moreover, analysis of binding to

different ACE isoforms has given an indication of the interaction surface between the two domains.

1.4.2.1 N domain-specific monoclonal antibodies

The epitopes of the eight N domain-specific mAbs were classed into three antigenic regions, based on competitive binding assays (Danilov *et al*, 1994) (Figure 1.8). The first consists of mAb 5F1, the second of mAbs i2H5, 1G12 and 6A12 and the third of mAbs 3A5, i1A8, 9B9 and 3G8. Interestingly, mAb 3A5 competitively inhibited binding of all other mAbs despite having different epitopes, which could be explained by a gross conformational change in the N domain upon binding of mAb 3A5 that alters the epitopes of the other mAbs.

The first antigenic region contains the epitope of mAb 5F1 and is localised on the distal side of the molecule compared to the other N domain-specific mAbs (Danilov *et al*, 1994; Danilov *et al*, 2007). It is proximal to the linker region and spans the active site cleft (Danilov *et al*, 2007). N-linked glycosylation sites N45 and N117 lie within the epitope of mAb 5F1 and sites N133 and N480 are proximal to this epitope. The second antigenic region (mAbs i2H5, 1G12 and 6A12) is localised on the C terminal portion of the N domain on subdomain II. N-linked glycosylation site N416 lies within this region and site N289 lies within the epitope of mAb 6A12. The epitopes of mAbs i2H5, 6A12 and 1G12 overlap to an extent, encompassing the flexible loops between helices α18 and α19 and between helices α23 and α24 (Skirgello *et al*, 2006; Balyasnikova *et al*, 2007). The epitope of mAb i2H5 lies below this overlap at the C terminal edge of the active site cleft, with mAb 6A12 above it and mAb 1G12 to the anterior portion, distal to the active site cleft. The third antigenic region encompasses four epitopes (mAbs 3A5, i1A8, 9B9 and 3G8) with varying degrees of overlap in the N terminal protein of subdomain II, distal to the active site cleft. The epitope of i1A8 is positioned proximal to the epitope of mAb 1G12 albeit slightly closer to the N terminal portion. The epitope of mAb i1A8 overlaps with those of mAb 3G8 and 9B9, which themselves overlap and are positioned within the lid subdomain (Danilov *et al*, 1994; Gordon *et al*, 2010). N-linked glycosylation sites N9, N25, N82 lie within this overlapping region. The epitope of mAb 3A5, overlaps that of mAbs i1A8, 1G12 and i2H5.

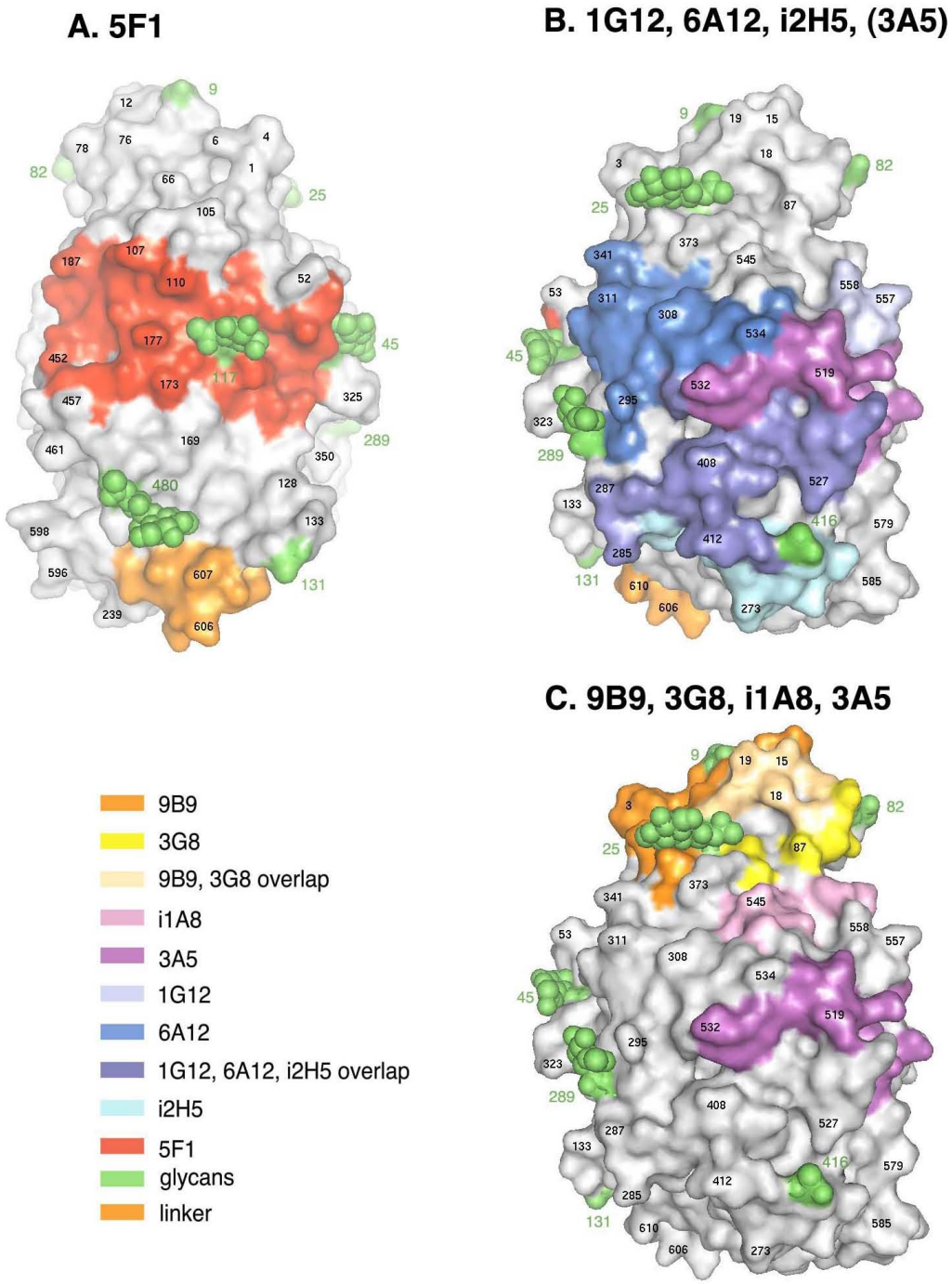

Figure 1.8. Epitopes of N domain-specific mAbs. Surface structure of wild-type N domain depicting the epitopes of 8 mAbs, divided into three regions (*A, B and C*) (PDB accession no 2C6F).

1.4.2.2 C domain-specific monoclonal antibodies

The C domain-specific mAbs have not been as extensively investigated as their N domain counterparts. However, some preliminary epitope mapping has allowed for the localisation of their epitopes and implicated particular regions in ACE function and inter-domain interaction (Naperova *et al*, 2008a; Naperova *et al*, 2008b; Balyasnikova *et al*, 2008). Competitive binding assays placed the eight C domain-specific epitopes into three antigenic regions (Naperova *et al*, 2008b) (Figure 1.9). The first comprises mAbs 1B8 and 3F10, the second mAb 1B3 and the third mAbs 2H9, 1E10, 4E3, 2B11 and 3F11 (Naperova *et al*, 2008a).

The first region lies towards the C-terminus of the C domain on the edge of the active site cleft. It encompasses the flexible loop (T726-E738), which forms a large protrusion from the surface. This loop is homologous to the flexible loop in the N domain (K126-S138) proposed to create a large reaction surface for domain interaction (Corradi *et al*, 2006). Epitope mapping showed that the epitope of mAb 1B3 overlaps the epitopes of mAbs 1B8 and 3F10.

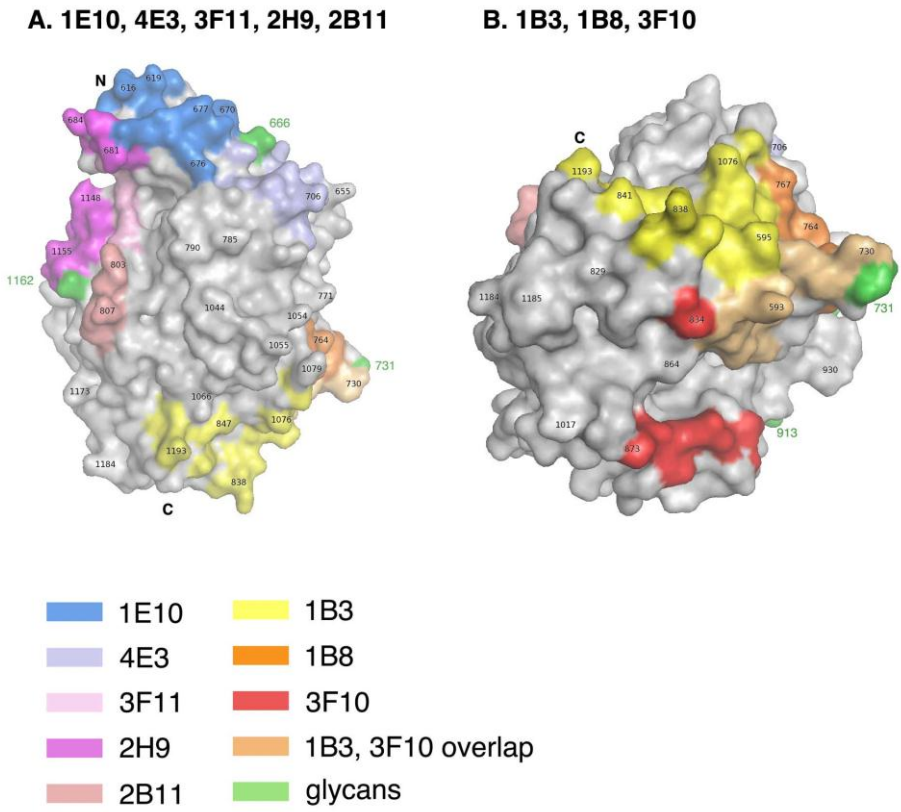

Figure 1.9. Epitopes of C domain-specific mAbs. Surface structure of wild-type C domain depicting the epitopes of 8 mAbs, divided into two regions (*A and B*) (PDB accession no 1O86).

The mAb 1B3 epitope lies on the C-terminal end of the C domain, recognising the juxtamembrane stalk in particular (Balyasnikova *et al*, 2005b). Epitopes within the third antigenic region (mAbs2H9, 1E10, 4E3, 2B11 and 3F11) lie on the N-terminal portion of the C domain (Naperova *et al*, 2008a). mAbs 1E10 and 4E3 bind to overlapping epitopes, encompassing the lid helices α2 and α3. The epitopes of mAbs 2H9, 3F11 and 2B11 lie in an overlapping region distal to the active site cleft. Interestingly, the unique 36-residue region of tACE did not alter binding of the C domain-specific mAbs and does not appear to confer immunogenicity.

1.4.3 Anti-catalytic activity of domain-specific anti-ACE monoclonal antibodies

The N domain-specific mAbs 3A5 and i2H5, which each lie in different antigenic regions, show anti-catalytic properties towards ACE (Danilov *et al*, 1994; Danilov *et al*, 2007; Skigello *et al*, 2006,). Similarly, mAb 5F1 was shown to have an inhibitory effect on ACE activity, observed at only high concentrations due to the weak binding of the mAb to ACE (Danilov *et al*, 2007). MAbs 3A5 and i2H5 bind the enzyme-substrate complex more readily in kinetic analysis using the synthetic substrates benzyloxycarbonyl-Phe-L-His-Leu (ZFHL) and hippuryl-L-His-L-Leu (HHL) and bind ACE more efficiently in the presence of the ACE inhibitor lisinopril (Skirgello *et al*, 2006). This not only demonstrates that ACE undergoes a conformational change upon substrate binding, corroborating the proposed hinge mechanism, but also explains the anti-catalytic effect. Since the mAb i2H5 epitope is proximal to the active site cleft, it can be argued that binding locks ACE into the "closed" position hampering access of substrates. Comparably, the epitope of mAb 5F1 spans the active site cleft and its inhibitory effect can be explained in the same way (Danilov *et al*, 2007). Binding of mAb 3A5, which is positioned distal to the active site, appears to confer a gross conformational change on the N domain that subsequently alters substrate access. A similar anti-catalytic effect was observed towards the C domain with mAbs 4E3 and 1E10 (Naperova *et al*, 2008a). In this case the ratio of conversion of ZFHL to HHL (Danilov *et al*, 2008) was used to assess the activity of each domain in the presence of mAbs. Since the epitopes of these mAbs lie in the lid subdomain, it is possible that their interaction with ACE prevents the proposed hinge movement of the lid helices.

1.4.4 Effect of domain-specific anti-ACE monoclonal antibodies on shedding

The N domain-specific mAbs 9B9 and 3A5 have been demonstrated to stimulate shedding of ACE (by 3- and 4-fold respectively) whereas mAb 3G8 inhibited shedding by 30% (Balyasnikova *et al*, 2002; Balyasnikova *et al*, 2005). The inhibitor profile of mAb-induced shedding was altered compared to basal and phorbol ester induced shedding. The DCI induction of shedding was much stronger in the presence of mAbs and the presence of the PKC inhibitor, staurosporine, unexpectedly stimulated mAb shedding further. This implicates an alternate shedding mechanism. It has been proposed that binding of these antibodies results in conformational change that allows better access of the secretase, most likely due to rearrangement of the two domains. This could either result in exposure of the C domain recognition motif or the juxtamembrane stalk containing the cleavage site.

Binding of the C domain-specific mAbs 1B3, 1B8 and 3F10 depend on the presence of the juxtamembrane region (Naperova *et al*, 2008a) and are thus valuable in probing the conformation of the stalk region and the effect of changes in this region on ACE cleavage secretion (Balyasnikova *et al*, 2005b; Naperova *et al*, 2008a). In particular, mAb 1B3 was used to define the effect of the P1199L mutation on shedding and has been developed in conjunction with mAb 9B9 in an immunoassay to detect P1199L and other ACE mutants in plasma (Danilov *et al*, 2005).

1.4.5 Effect of N domain-specific anti-ACE monoclonal antibodies on dimerisation

As has been mentioned in Section 1.3.4, sACE forms dimers in reverse micelles that appear to be mediated by a carbohydrate recognition motif in the N domain (Kost *et al*, 2000; Kost *et al*, 2003). A potential dimer interface was identified using the panel of N domain-specific mAbs. Both mAbs 9B9 and 3G8 in overlapping epitopes of the same antigenic region inhibited dimer formation in the reverse micelle system (Kost *et al*, 2003). Interestingly, these two mAbs have opposite effects on shedding (Section 1.4.4), suggesting a link between these two processes. Fine epitope mapping identified residues that play an important role in mAb binding and the role of this region in dimerisation and shedding is detailed in Chapter 4 (Gordon *et al*, 2010).

1.4.6 Use of monoclonal antibody binding to determine domain interactions

The N domain-specific mAbs 1G12 and 6A12, and mAb i2H5 to some extent, were more reactive towards the N domain than full-length sACE, indicating that the epitopes of these mAbs are occluded by the C domain (Balyasnikova *et al*, 2007) (Figure 1.10). Interestingly,

binding of mAbs 1G12 and 6A12 to plasma ACE, but not the N domain alone, was increased in the presence of ACE inhibitors and EDTA. The latter chelates the active site zinc, rendering ACE inactive. This suggests that upon inhibitor binding there is rearrangement of the domains, reducing the degree to which the N domain is occluded by the C domain, thereby exposing the epitopes of these two mAbs. The use of domain-specific inhibitors and active site knockouts could not distinguish a particular domain, which implies that both domains are involved in this rearrangement. Similarly, the epitopes of the C domain-specific mAbs 1E10 and 4E3 appear to be occluded by the N domain, since they bound tACE more efficiently that sACE (Naperova *et al*, 2008a).

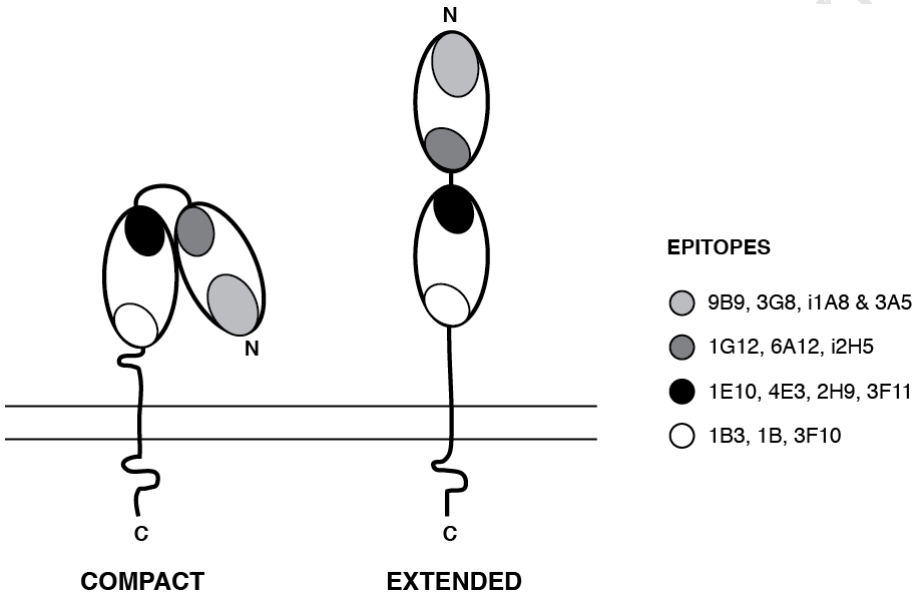

Figure 1.10. sACE domain interaction. The "compact" and "extended" models of membrane-bound sACE are depicted with the position of the mAb epitopes shown as circles. The potential masking of the epitopes by each domain in the "compact" model can be seen.

The position of the antigenic region in the N domain containing the epitopes of mAbs 1G12, 6A12 and i2H5 is consistent with the model proposed by Corradi *et al* (2006). The authors indicated there is a range within the proposed model wherein the two domains could interact. With a slight rotation of the C domain around the N domain in the "compact" model, the C domain comes into close proximity to the antigenic region containing the epitopes for mAbs 1G12, 6A12 and i2H5. The C domain lid subdomain, wherein the epitopes of mAbs 1E10 and 4E3 are located, is in contact with the N domain in both the "extended" and "compact" models and was modelled in a similar orientation in the EM structure (Chen *et al*, 2010) (Figure 1.10).

1.5 AIMS OF RESEARCH

As has been laid out in this chapter, cellular ACE expression and function is regulated by specific protein-protein interactions; from correct folding in the ER, to cell surface expression, ectodomain shedding, enzyme function including substrate binding and domain interaction and intracellular signalling. However, there are many aspects of these events that are not clearly understood. Identifying surface regions or residues of ACE that may be involved in these processes may give insight into regulatory pathways of ACE expression. In this way, the structure-function of ACE with respect to shedding and dimerisation and the interaction of the two domains may be explored.

The objectives of this study were:

1. To investigate the effect of introducing a novel disulphide bridge on stabilising inter-domain movement of sACE.
2. To identify region/residues involved in dimerisation and shedding using fine-epitope mapping.
3. To determine the role of the free cysteines in each domain in dimerisation and shedding.
4. To determine the biochemical mechanism of increased plasma ACE observed with a familial mutation, Y465D, in the N domain.

CHAPTER 2: Materials And Methods

2.1 MUTAGENESIS AND SUBCLONING

2.1.1 ACE constructs

Recombinant full length human somatic ACE cloned into the sequencing vector pBluescript KS II (pBS-sACE) was used as a template for site-directed mutagenesis. This sequence encodes the entire ACE coding region including the signal sequence, N-terminal and C-terminal catalytic domains, the transmembrane region and the cytoplasmic tail (Figure 2.1). A soluble N-domain form of ACE in the plasmid pBluescript SK II (pBS-Ndom) was also used as a template. This construct was generated by Pierre Redelinghuys as part of his doctoral work from the pECE-ACED629 plasmid, a generous gift from Prof. S Danilov (University of Illinois at Chicago, USA) (Balyasnikova *et al*, 2003). This sequence is a truncated form of sACE that contains the catalytic N domain, 11 residues of the linker region and 17 residues of the C domain, terminated at D628 by a stop codon introduced via an engineered *XbaI* site.

The generation of each mutant by site-directed mutagenesis is described in the relevant chapter. Briefly, pBS-Ndom was used to generate Ndom-H600C, Ndom-EY/CC (Chapter 3), and mutants for epitope mapping (Chapter 4). pBS-sACE was used to generate sACE-H600C (Chapter 3), sACE-Q22A (Chapter 4), sACE-C474S, sACE-C1072S and sACE-CC/SS (Chapter 5).

For expression of protein in CHO cells, genes were cloned into the mammalian expression vector pcDNA3.1 (Invitrogen, USA), which contains a neomycin resistance gene for selection of stable cell lines. Full-length sACE was generated by excising the entire coding region from pBS-sACE with *Xba*I and *Hind*III and cloning it into pcDNA3.1(+). Wild-type soluble N domain was generated by cloning the coding region via *Eco*RI/*Xba*I into pcDNA3.1(-).

Constructs pcDNA-Ndom-H600C and pcDNA-Ndom-EY/CC (Chapter 3) were generated by Gannie Tzoneva using the approach described above. Briefly, site-directed mutagenesis was performed using pBS-Ndom as a template to introduce cysteine residues at either position H600 or positions E161 and Y607. These constructs, NdomH600C and NdomEY/CC, were then cloned into pcDNA3.1(+) for expression in CHO cells.

Soluble sACE constructs were generated by introducing a fragment containing the mutation into pcDNA-sACE-NJ. This construct is a truncated form of sACE that lacks the transmembrane region and cytoplasmic tail (Figure 2.1). It was generated by cloning the

N-terminal portion of sACE into pcDNA-tACE-Δ36NJ via *Xba*I/*Sfi*I. The tACE-Δ36NJ construct is a fully N-glycosylated soluble form of tACE, which lacks the unique N-terminal O-glycosylated region and was created by introducing two stop codons and an *EcoRI* site at S1201 (Yu *et al*, 1997).

Another soluble sACE isoform (pcDNA-solsACE), transfected into CHO cells, available in our laboratory was used as a source of wild-type sACE for protein purification. This protein also lacks the transmembrane domain and cytoplasmic tail and is truncated at S1211, downstream of the endogenous cleavage site.

tACE-Δ36-NJ and CCdom-AC were used in western blotting experiments (refer to Chapter 5, Section 5.2.2). CCdom-ACE is a two-domain construct where the N domain has been replaced by a second C domain (Woodman *et al*, 2005).

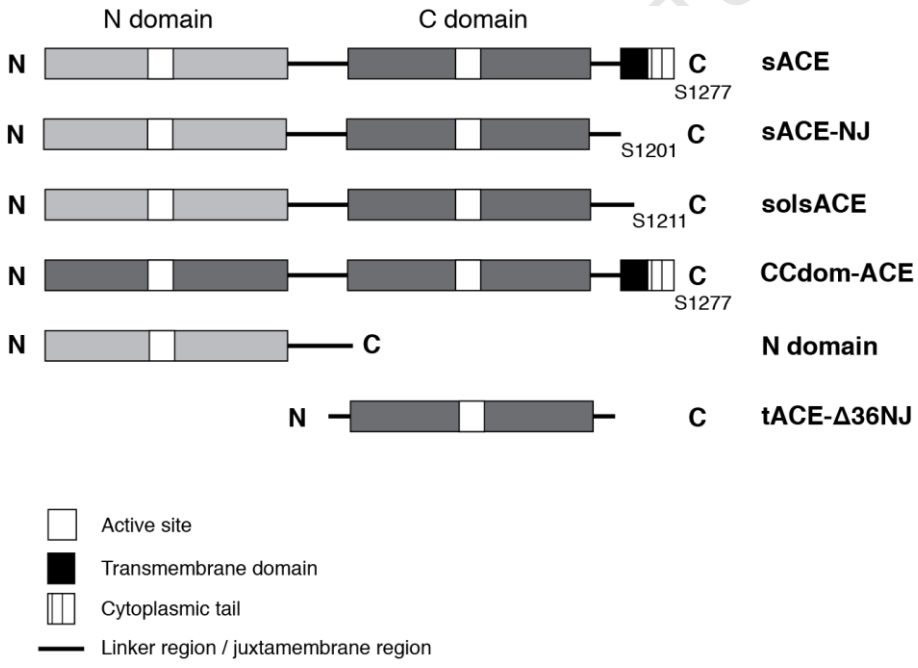

Figure 2.1 Schematic representation of ACE constructs.

2.1.2 Site-directed mutagenesis

Mutagenesis was performed using a PCR-based method adapted from the Quickchange® Site-Directed Mutagenesis protocol (Stratagene La Jolla, CA, USA). Complementary primers containing the desired mutation were designed with WATCUT (http://watcut.uwaterloo.ca/watcut, designed by Michael Palmer, University of Waterloo, Canada.), using the restriction analysis and silent mutation analysis software, and purchased from Inqaba Biotechnical Industries (South Africa) (refer to Appendix A.1.1 for sequences).

Restriction enzyme sites were introduced through silent mutations to facilitate screening. Mutagenesis was performed with either *Pfu* Turbo polymerase (Promega, USA) or High Fidelity *Taq* polymerase (Kapa Biosystems, South Africa) on a Hybaid Express thermocycler (Hybaid Ltd, UK) (refer to Appendix A.1.8). Aliquots of the PCR products were visualised by agarose gel electrophoresis, while the remainder was *Dpn*I digested overnight, transformed into E.*coli* JM109 competent cells and plated on Luria agar plates with 100µg/ml ampicillin (refer to Appendix A.1.3). DNA was isolated from overnight cultures of picked colonies and screened by restriction enzyme digestion (refer to Appendix A.1.4 & A.1.5). Mutations were confirmed by DNA sequencing analysis using primers flanking the multiple cloning site (T7 and T3) and internal primers complementary to ACE cDNA (refer to Appendix A.1.2). Sequencing reactions were performed by Di James (Molecular and Cell Biology DNA Sequencing Service, UCT, South Africa) using Big Dye® Terminator v3.1 Cycle Sequencing kit (Applied Biosystems, USA) and Half-dye Mix (Bioline, UK). Electrophoresis was performed by Macrogen Inc. (Korea) using a 3730XL DNA sequencer (Applied Biosystems, USA).

sACE-Y465D was a gift from Prof S. Danilov and comprises sACE cDNA containing the Y465D mutation in the pcDNA-Hyg vector.

2.1.3 Introduction into a mammalian expression vector

pBS-sACE or pBS-Ndom constructs containing the desired mutation were introduced into the mammalian expression vector pcDNA3.1 (- or + depending on the desired orientation of the multiple cloning site). Details of the subcloning of each mutant into pcDNA are described in the relevant chapters, following the same general protocol described below.

DNA was digested with the relevant restriction enzymes to excise the vector (pcDNA) and insert DNA (pBS-sACE or pBS-Ndom mutants) and separated by agarose gel electrophoresis refer to Appendix A.1.5). The bands of interest were excised and gel purified using the Wizard SV Gel and PCR Clean-up System (Promega, USA) as per the manufacturer's instructions. DNA ligation was performed using T4 DNA Ligase (Fermentas, USA) at 4°C for 48 hours and transformed into competent *E.coli* JM109 cells and plated on Luria agar plates with 100µg/ml ampicillin (refer to Appendix A.1.6). DNA was isolated from overnight cultures of colonies, digested with restriction enzymes and separated by agarose gel electrophoresis to confirm the presence of the mutation. Sufficient DNA for transfection was prepared using the Plasmid Midi kit (QIAGEN, USA) and DNA concentration was

determined spectrophotometrically using a Nanodrop 2000 (Thermo Scientific, USA). The correct orientation and size of the ACE construct and the desired mutation were confirmed by restriction enzyme digestion and agarose gel electrophoresis.

2.1.4 RNA isolation and RT-PCR

CHO cells grown to confluency in enriched medium were lysed in Trizol® reagent (Invitrogen, USA) and separated into an organic and aqueous phase by the addition of chloroform. RNA was precipitated from the aqueous phase with isopropanol and washed with 70% ethanol. RNA was resuspended in 50µl nuclease-free double distilled deionised water (dH_2O), quantitated by nanodrop and visualised by agarose gel electrophoresis. RNA from cell lines expressing the mutants, untransfected CHO cells, and total human placental RNA (included as a positive control) was used to synthesise cDNA with the Advantage® RT-for-PCR kit (Clonetech Laboratories, USA) (refer to Appendix A.1.7). ACE DNA was amplified by PCR from total cDNA using internal primers to ACE DNA (1R and 3F) (refer to Appendix A1.1). Human glyceraldehyde-3-phosphate dehydrogenase (G3PDH) cDNA was amplified as a positive control using the supplied primers. PCR was performed with Hi-Fi *Taq* polymerase (Kapa Biotech, South Africa) on a Hybaid Express thermocycler (Hybaid Ltd, UK) (refer to Appendix A.1.8.3). PCR products were visualised by agarose gel electrophoresis.

2.2 PROTEIN EXPRESSION AND CHARACTERISATION

2.2.1 Expression of recombinant ACE in mammalian cells

2.2.1.1 Transfection into mammalian cells

DNA was introduced into CHO cells using the calcium phosphate method according to the manufacturer's instructions (Profection Mammalian Transfection System, Promega, USA). After transfection, cells were grown to confluency in enriched medium [50% Dulbecco's Modified Eagle Medium (DMEM) (Sigma, USA), 50% HAMS-F12 (Sigma, USA) supplemented with 10% foetal calf serum (FCS)(Sigma, USA) and 20M HEPES buffer] containing 0.8mg/ml geneticin G418 (Sigma, USA) for pcDNA3.1 constructs or 400µg/ml hygromycin (Sigma, USA) for pcDNAHyg-Y465D to select for positive clones. Cells were grown in the presence of selective medium until all cells in the negative control plates (no vector DNA added) had died off and colonies were observed in the transfected plates. In the case of the full-length sACE mutants (sACE-Q18H, sACE-L19E, sACE-Q22A, sACE-

C474S, sACE-C1072S, sACE-CC/SS, sACE-H600C and sACE-Y465D), cells were then lifted and seeded for fluorescence-activated cell sorting (FACS). For the soluble isoforms (sACE-NJ and sACE-H600C), individual clones were picked and grown to confluency. Cells were then serum starved overnight in minimal medium [50% DMEM, 50% HAMS-F12 supplemented with 2% FCS, 20M HEPES buffer, 100U/ml penicillin and 100µg/ml streptomycin], and the medium assayed for ACE activity. Colonies that produced the highest ACE activity were used in our experiments. Soluble N domain mutants were used without clonal selection.

2.2.1.2 Selection of high expressing cells lines

For selection of high expressing cell lines by FACS, approximately $5x10^6$ cells were lifted from confluent flasks and washed twice in phosphate-buffered saline (PBS). They were then labelled for an hour with 10µg/ml mAb 5C5 (an N domain-specific anti-ACE monoclonal antibody), followed by extensive washing in PBS. Cells were then incubated for an hour with a goat anti-mouse IgG FITC-conjugated $F(ab')_2$ fragment (Dako, Denmark), followed again by extensive washing in PBS. FACS was performed on labelled cells by Ronnie Dreyer at the Flow Cytometry Core Facility (Department of Immunology, UCT, South Africa) on a FACS Vantage^{TM} SE cytometer (BD Biosciences, USA). Cells were gated according to highest fluorescence into enriched medium with 100U/ml penicillin and 100µg/ml streptomycin. Cells were grown to confluency and then assayed for ACE activity.

For experiments described below, medium was harvested and cells lysed in 1% triton lysis buffer (0.05M HEPES, 0.5M NaCl, 1% triton X-100, 1mM PMSF) containing Protease Inhibitor Cocktail (Set III, Calbiochem, USA - 0.2mM AEBSF, 0.16µM Aprotinin, 0.01mM Bestatin, 3µM E-64, 4µM Leupeptin and 2µM Pepstatin A). Samples were centrifuged at 10000xg for 5 minutes and the supernatant extracted. For plate precipitation assays and western blotting, medium was concentrated using Amicon or Micron centrifuge columns (Millipore, USA) to between 80 and 100mU/ml ACE.

2.2.2 Determination of ACE activity

Cell lysate, medium or purified protein was assayed for ACE activity using the synthetic peptide ZFHL (for preparation refer to Appendix A.2.5.1) as a substrate and the fluorescent adduct o-phthaldialdehyde for detection using a fluorescent assay (Friedland *et al*, 1976) adapted for a microtitre plate as described previously (Schwager *et al*, 2006). Assays were performed in a 96-well plate in duplicate. 3µl cell lysate (diluted 1 in 10) or culture fluid was

incubated with 30µl 1mM ZFHL in 1X potassium phosphate buffer (100mM $KHPO_4/KH_2PO_4$, pH 8.3) at 37°C for 15 minutes, 1 hour or 4 hours, depending on expression levels of ACE in cells. Enzyme activity was stopped by addition of 120µl 0.4M NaOH. The HL moiety was derivitised with o-phthaldialdehyde (24mg/ml in methanol) at room temperature for 10 minutes. This reaction was stopped with 30µl 3M HCl. Fluorescence intensity was measured using a fluorescence spectrophotometer (Varian Inc., USA) at $\lambda_{excitation}$ = 360nm and $\lambda_{emission}$ = 485nm. 1 milliunit (mU) of ACE activity was calculated as nmol His-Leu (HL) formed/minute from a standard curve of fluorescent units (FU) versus HL concentration (refer to Appendix A.2.2).

2.2.3 Protein purification

Soluble N domain and sACE cell lines were seeded into four 150cm^2 flasks and grown to confluency in enriched medium. Cells were then incubated in minimal medium, with medium being harvested and frozen after 48-72 hours for four harvests. Medium was thawed at 4°C overnight and protein was purified by lisinopril sepharose affinity chromatography (Bull *et al*, 1985). For N domain constructs, 0.8M NaCl was added to the medium to facilitate purification. Medium was applied to a sepharose-28-lisinopril column and washed thoroughly (0.5M NaCl, 20mM HEPES, pH 7.5) to remove unbound protein. ACE was eluted from the column with 50mM Borate (pH 9.5) followed by overnight dialysis against 50mM HEPES. Protein concentration determined by Bradford protein assay (BIO-RAD Bradford reagent, USA) (Appendix A.2.1) or by A_{280} absorbance on a nanodrop. Protein was then concentrated on Amicon centrifuge columns to approximately 1mg/ml. Sodium dodecyl sulphate (SDS)-polyacrylamide gel electrophoresis (PAGE) (Section 2.2.7) and Coomassie staining was performed to visualise the purity and integrity of the purified protein.

2.2.4 Determination of ACE shedding

Cells were grown until confluency in enriched medium. Confluent cells were then grown in the presence of minimal medium or serum-free medium (Gibco Opti-MEM, Invitrogen, USA) for 4 hours (high ACE expressing cell lines) or for 16 or 24 hours (low ACE expressing cell lines). Medium was harvested and cells were lysed in 1% triton lysis buffer and assayed for ACE activity as described above. The percentage ACE shed was calculated as the ratio of total ACE activity in the medium to total ACE activity in the medium and cell lysate.

2.2.4.1 Effect of phorbol ester and DCI stimulation or TAPI inhibition on ACE shedding

To determine the effects of stimulation or inhibition of the ACE secretase cells were grown to confluency overnight in enriched medium. They were then incubated for 4 hours in minimal medium containing 1μM PDBu (Sigma, USA), 10μM TAPI-1 (Sigma, USA) or 200μM 3,4-DCI (Sigma, USA). Medium and cell samples were collected and shedding was determined as described (Section 2.2.4).

2.2.4.2 Antibody-induced shedding

Similarly, 10μg/ml purified (or 1:50 dilution of culture fluid) anti-ACE monoclonal antibodies in minimal medium was added to confluent cells for 4 hours (high ACE expressing cell lines) or 24 hours (low ACE expressing cell lines). Samples were collected and shedding was determined as described (Section 2.2.4).

2.2.4.3 Effect of substance P on ACE shedding

Cells were grown in the presence of 10μM substance P in minimal medium for 4 hours and shedding determined as described (Section 2.2.4).

2.2.5 Plate precipitation assay

Total cell lysate and concentrated cell culture medium were sent to our collaborator Prof. S. Danilov, who performed the plate precipitation assays. Microtiter plates bound with goat-anti-mouse IgG were coated with different anti-ACE mAbs and were incubated with serum-free culture medium or cell lysates. In some experiments, mAbs were adsorbed to the wells of microtiter plates directly, without the goat-anti-mouse bridge. In all experiments anti-mouse IgG wells were included to control for non-specific antibody binding.

The amount of ACE precipitated by a given mAb reflects the binding affinity and was quantified by two methods:

i) Precipitated ACE activity in the wells was estimated using substrates Hip-His-Leu or Z-Phe-His-Leu, as described previously (Danilov *et al*, 1994).

ii) The amount of precipitated ACE protein was quantified by incubation with sheep anti-ACE polyclonal antibodies conjugated with horseradish peroxidase (HRP) from an ACE ELISA kit (Chemicon Int, USA), followed by a spectrophotometric assay with tetramethylbenzidine (TMB) as a substrate (Danilov *et al*, 1996).

The percentage of binding was calculated as the percentage of binding to the IgG control.

2.2.6 Cell ELISA

sACE cell lines were grown to confluency overnight in microtitre plates in enriched medium. Once confluent, cells were incubated on ice with blocking buffer (PBS with 2% skim milk) to minimise non-specific binding and then in the presence of 10μg/ml anti-ACE mAbs in the same buffer before fixing to minimise the loss of epitopes on membrane bound ACE. Cells were fixed with 4% para-formaldehyde and incubated in blocking buffer containing a goat anti-mouse IgG HRP-conjugated antibody, which was used to detect the amount of mAb bound to ACE spectrophotometrically using a TMB substrate. In all experiments, control wells containing untransfected cells and wells with anti-mouse IgG added to CHO-sACE cells were used to determine the non-specific binding of anti-ACE mAbs and antibodies in general, respectively. The percentage binding of anti-ACE mAbs was calculated as the percentage of binding to the IgG control.

2.2.7 Polyacrylamide gel electrophoresis

Purified protein, medium or cell lysates were mixed with sample buffer (20% glycerol, 6% SDS, 125mM Tris, Bromophenol blue, pH 6.8) either with or without reducing agent [5% β-mercaptoethanol (β-ME) or 50mM dithiothreitol (DTT)] and boiled for 5 minutes. Samples were separated by SDS-PAGE using the Mini PROTEAN^{TM} III system (BIO-RAD, USA) with 7% resolving (0.1% SDS, 375mM Tris buffer, pH 8.8) and 3% stacking (0.1% SDS, 125mM Tris buffer, pH 6.8) gels in a Tris-glycine tank buffer (pH 8.3) at 25mA/gel. Gels were either stained with Coomassie dye or used for western blotting as described below.

2.2.7.1 Two-dimensional gel electrophoresis

Purified sACE was separated by SDS-PAGE under non-reducing conditions. This lane was then excised and placed perpendicularly along a 7% resolving gel and a 3% stacking gel was set above the gel slice. The gel was run under reducing conditions by adding sample buffer containing 5% β-ME. The gel was then stained with Coomassie dye to visualise protein.

2.2.7.2 Native PAGE

Samples were mixed with sample buffer (without SDS). Non-denaturing PAGE was performed in the same way as SDS-PAGE, except SDS was excluded from the resolving gel, stacking gel and tank buffer. Gels were run at 4°C at 25mA/gel.

2.2.8 Western blotting to detect ACE and cross-linking of proteins

After SDS-PAGE, protein was transferred to Hybond ECL nitrocellulose membrane (GE Healthcare LifeSciences, UK) in transfer buffer (20mM Tris-base, 150mM glycine, 20% methanol) at 100V for 1 hour using the Mini PROTEAN^{TM} III system. For detection of protein, membranes were incubated in blocking buffer (Tris-buffered saline, 0.1% tween-20, 5% skim-milk) containing culture fluid of the anti-ACE mAbs 4G6 and 1D8, specific to the N domain and C domain respectively. Binding of mAb was detected using either goat anti-rat (to detect 4G6) or goat anti-mouse (to detect 1D8) HRP-conjugated antibody using the ECL^{+} detection system (GE Healthcare LifeSciences, UK) or the Immun-star WesternC^{TM} detection system (BIO-RAD, USA). Chemiluminescence was detected by autoradiography or with a chemiluminescence detector (G:BOX Chemi, Syngene, USA). Densitometry of detected protein was performed using GeneTools software (Syngene, USA).

For dimerisation studies, confluent cells were serum starved overnight in minimal medium or Opti-MEM and then cross-linked for 1 hour on ice with 1mM bis[sulfosuccinimidyl] suberate (BS^3) in PBS. Excess crosslinker was quenched with 20mM Tris (pH 7.5) for 15 minutes at ambient temperature. Cells were then lysed in 1% triton lysis buffer with protease inhibitor cocktail and resolved by SDS-PAGE and ACE detected by western blotting.

2.2.9 CnBr digestion and MALDI MS/MS

Approximately 500µg of purified Ndom-H600C, wild-type sACE and sACE-H600C in 70% formic acid were cleaved overnight with cyanogen bromide (CnBr) and then freeze-dried. Protein was resuspended in dH_2O to a final concentration of 5mg/ml. 50µg of cleaved protein was separated by SDS-PAGE in the presence or absence of 5% β-ME and peptides detected by Coomassie stain.

Bands of interest were excised, cut into 1mm^2 pieces and destained with 200mM NH_4CO_3:acetonitrile (ACN) (50:50) until clear. Samples were dehydrated with 100% ACN and dried on a Savant SpeedyVac (ThermoScientific, USA). Samples were sent to the Centre for Proteomic and Genomic Research (CPGR, Cape Town, South Africa) for further analysis. Briefly, samples were reduced with 5mM Tris (2-carboxyethyl) phosphine (TCEP) (Fluka, USA) in 100mM NH_4CO_3 in the dark for 30 minutes at room temperature. Excess TCEP was removed and the gel slices dehydrated. Cysteine protection was performed by carbamidomethylation with 100mM iodoacetamide (Sigma, USA) in 100mM NH_4CO_3 for 30 minutes at room temperature in the dark. The gel slices were then dehydrated, washed

with 50mM NH_4CO_3 and dehydrated. An in-gel tryptic digest was performed by rehydrating the gel slices in trypsin solution (Promega, USA) to a 20ng/µl final concentration and incubating at 37°C overnight. Peptides were extracted from the gel slices with 50µl 0.1% trifluoroacetic acid (TFA) (Sigma, USA). Samples were dried down, resuspended in 50µl dH_2O and further dried down to 20µl to remove residual NH_4CO_3.

Peptides were spotted onto a 10mg/ml α-cyano-4-hydroxycinmanic acid matrix (Fluka, USA) in 80% ACN, 0.2% TFA for a final concentration of 5mg/ml matrix in 40% ACN, 0.1% TFA, 10mM $NH_4H_2PO_4$. Mass spectrometry was performed with a 4800 MALDI TOF/TOF (Applied Biosytems) with all spectra recorded in positive reflector mode. Spectra were generated with 400 laser shots/spectrum at a laser intensity of 3800 (arbitrary units) with a grid voltage of 16kV. Peptides spots were internally calibrated with trypsin autolytic fragments.

2.2.10 Cleavage site determination

Purified sACE-Y465D was resolved by SDS-PAGE and protein detected by Coomassie stain. The sACE band was excised and an in-gel tryptic digest and MALDI-MS/MS was performed as described above.

2.2.11 Thermal stability determination

10nM purified wt sACE or sACE-H600C in 50mM HEPES buffer was incubated in 0.2mm tubes at 55°C for 2.5, 5, 10, 15, 30, 60, or 90 minutes on a thermocycler plate and then placed on ice. A zero time control was placed on ice throughout the incubation. ACE activity was determined for each time point using ZFHL as a substrate (Section 2.2.2). The percentage residual activity was determined according to the zero time sample.

2.2.12 Substrate hydrolysis

2.2.12.1 HPLC

HPLC was performed using a sephadex C18 Jupiter column. 37nM wild-type sACE or sACE-Y465D and 50µM substrate [angI or subsP (for preparation refer to Appendix A.2.6.1)] in 50mM HEPES buffer (containing 300mM NaCl, 10µM $ZnSO_4$) were incubated for 1 hour at 37°C. Sample was separated by HPLC over a 14-70% ACN in 0.1% TFA gradient. Sample runs were compared to those with buffer only and substrate only. Absorbance was read at λ = 215nm for ang I and subsP.

2.2.12.2 Fluorogenic assay

Hydrolysis of angI was performed using acetyl-angI (Bachem, Switzerland) to decrease background fluorescence caused by interaction of the primary amine with the derivitising agent. 5nM ACE was incubated with increasing concentrations of angI in the μM range, from 0-1000μM, for 15 minutes at 37°C in the same 50mM HEPES used for HPLC. The same procedure for the ZFHL plate assay was followed, using o-phthaldialdehyde to detect product (refer to Section 2.2.2). A Michealis-Menton curve was determined by plotting the nmol HL/minute formed versus the change in substrate concentration in Graphpad Prism (GraphPad Software Inc, USA).

The rate of hydrolysis of subsP was determined using fluorescamine to derivitise the product. 0-500μM subsP were incubated with 5nM sACE at 37°C for 15 minutes. The reaction was stopped with 1M HCl and then neutralised with 1M NaOH. The pH was increased by the addition of 5X potassium phosphate buffer (500mM $KHPO_4/KH_2PO_4$, pH 8.3). Hydrolysis products were then derivitised by the addition of 2mg/ml fluorescamine (in acetone). The fluorescence intensity was measured at $\lambda_{excitation}$ = of 390nm and $\lambda_{emission}$ = 475nm. Baseline fluorescence was determined at a range of concentrations using subsP alone (refer to Appendix A.2.3). These values were used to normalise the experimental values. The rate of hydrolysis was plotted as the nmol/min product determined from complete overnight hydrolysis of subsP by ACE vs the substrate concentration (refer to Appendix A.2.4).

2.3 STATISTICAL ANALYSIS

Data was entered into GraphPad PRISM 4.0 software (GraphPad software Inc, USA) and analysed using in-built statistical software. One-way and two-way ANOVAs with Bonferri/Tukey post tests were performed. Results were viewed as statistically significant when $p < 0.05$. Statistically significant data in figures of Chapters 3, 4, 5, and 6 are indicated as follows: * $p < 0.05$; ** $p < 0.01$; *** $p < 0.001$.

CHAPTER 3: Towards limiting inter-domain movement in somatic ACE: the introduction of additional cysteine residues in the linker region

3.1 INTRODUCTION

The elucidation of the crystal structures of the N and C domains (Corradi *et al*, 2006, Natesh *et al*, 2003) has allowed for deeper insight into the structure-function relationship of ACE by furthering the understanding of substrate binding (Watermeyer *et al*, 2010), domain selectivity and inhibitor design (Watermeyer *et al*, 2008), post-translational processes such as shedding and dimerisation (Chattopadhyay *et al*, 2008; Kost *et al*, 2003) and has facilitated epitope mapping of ACE mAbs (Danilov *et al*, 2007; Naperova *et al*, 2008a).

However, little is known regarding the interaction between the two domains of sACE and the nature of their interactions with respect to substrate binding and domain cooperativity, as well as protein-protein interactions relating to shedding and dimerisation. This is largely due to the lack of detailed structural knowledge of full-length sACE. The crystal structure of sACE has not as yet been determined. A model of sACE has been extrapolated from the N and C domain crystal structures, but is limited due to parts of the structures that could not be resolved (Corradi *et al*, 2006) (refer to Chapter 1, Section 1.2.5). These include three N-terminal residues of the tACE structure and several side chains on the linker of the N domain (Corradi *et al*, 2006). The recently described EM structure of full-length sACE was consistent with the "extended" model proposed by Corradi *et al* (2006) (Chen *et al*, 2010), indicating that the linker region is capable of a large degree of movement. However, this structure did little to elucidate the interaction of the two domains proposed in the "compact" model.

To date, attempts at obtaining crystals of sACE have been unsuccessful. This is thought to be the result of two limitations. The first is the presence of post-translational glycosylation, which hampers the formation of a uniform crystal lattice due to the sequence heterogeneity and flexibility within the glycan chains (McPherson *et al*, 1982; Butters *et al*, 1999). The second is thought to be due to the flexibility afforded by the inter-domain linker region. By removing either one or both of these limitations, it may be possible to generate candidates for crystallisation.

The minimal glycosylation requirements for the expression of active N domain and tACE have been investigated and have facilitated reproducible crystallisation and determination of a number of structures (Gordon *et al*, 2003; Watermeyer *et al*, 2006; Watermeyer *et al*, 2008;

Anthony *et al*, 2010). The application of this approach to full-length sACE may be a viable means to generate a candidate for crystallisation.

The proposed model of sACE (Corradi *et al*, 2006) indicates that there is a range of conformations wherein the two domains can interact. This range of movement is governed by the flexibility of the linker region, which would allow rotation and movement of the domains relative to one other. Engineering a disulphide bridge into the linker region may limit the range of movement and restrict the overall conformational flexibility.

The introduction of covalent linkages through an engineered disulphide bridge has been a successful approach in improving protein stability and to enable structure determination. *De novo* disulphide bridges were used to determine the role of subunit interactions in the formation of f-actin filaments by cryo-EM (Kim *et al*, 2000; Orlova *et al*, 2001). In addition, these novel disulphides bridges can be useful tools for limiting movement to further understand the role of certain regions in conformational changes, an analysis that was performed with the coil-coiled region of *E.coli* RNA polymerase (Anthony *et al*, 2002). The introduction of disulphide bonds successfully facilitated X-ray crystallography of thioredoxin multimers (Das *et al*, 2007), an active conformation of methionine synthase (Datta *et al*, 2008) and the HIV-1 hexameric capsomer (Pornillos *et al*, 2010). The stability of *Drosophila melanogaster* acetlycholinesterase was improved by the introduction of novel disulphide bonds without affecting enzyme activity (Siadat *et al*, 2006). It is evident from the literature that engineered disulphide bonds are a useful tool in furthering our understanding of the structure-function relationship of enzymes. An important consideration in this approach is that the *de novo* bonds should not alter the native protein conformation or enzyme activity.

The introduction of a disulphide bond in the linker region of sACE, relative to the N domain may limit inter-domain movement. The 11-residue linker region (P602-D612) between the N and C domains was well defined in the recently solved crystal structure of the N domain (Corradi *et al*, 2006). The first part of the linker was rigid, despite predictions that this region is highly flexible. This is due to the constraint imposed by a hydrogen bond between residues E161 and Y607. A flexible loop proximal to this region is held in place by the C128-C136 disulphide bond and is proposed as a possible surface for domain interaction (Figure 3.1). Thus, by limiting movement in this region, the overall structure of sACE could potentially be restricted and thus allow for crystal formation.

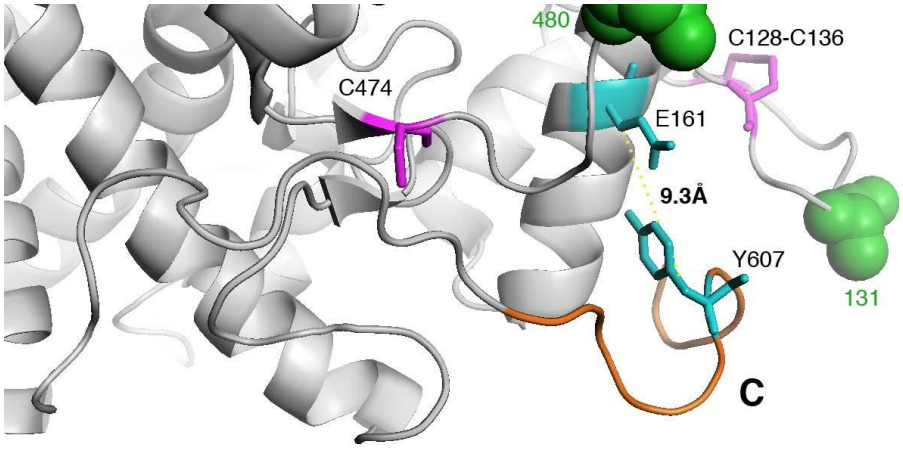

Figure 3.1. C-terminal region of the N domain. The flexible linker region (*orange*) from residues P602-D612 (*from left to right*) is indicated. The side chains of the C474 free thiol and native C128-C136 bridge (*magenta*), residues E161 and Y607 (*cyan*) are indicated as stick models and glycans as spheres (*green*). The straight-line measurement between the Cβ atoms of E161 and Y607 was 9.3Å (*yellow dashed line*).

The aim of this study was to limit the inter-domain movement of human sACE towards generating a sACE candidate for crystallisation and investigating domain cooperativity.

This included the following objectives:

1. To engineer a disulphide bridge in the linker region of N domain ACE as proof of concept.
2. To introduce a successful N domain mutant into full-length sACE and soluble sACE.
3. To determine the effect of the novel disulphide on ACE expression, stability and conformation.

3.2 RESULTS

3.2.1 *In silico* design of de novo disulphide bridges in ACE

The recently solved structure of the N domain included the well-defined linker region between the N and C domains (PDB accession number 2C6F) (Corradi *et al*, 2006). This facilitated the design of novel disulphide bridges to limit inter-domain movement using the N domain structure in PYMOL v0.99 (DeLano Scientific LLC).

The free thiol C474 is positioned in the short β-sheet 6 before a flexible loop, proximal to the linker region, and could potentially form a disulphide bridge with cysteine residues introduced into this region (Figure 3.2). Three sites within range of C474, with Cβ atoms between 5-7Å apart, were identified by straight-line measurements: W599, H600 and P601. These comply with the criterion that theoretical cysteine residues should be within 6Å of each other to form a disulphide bridge (Orlova *et al*, 2001; Kim *et al*, 2000). In addition, the degree of flexibility afforded by the position of these residues in the linker region could theoretically allow for movement of an introduced cysteine 2Å towards C474 to favour the formation of a novel disulphide bridge.

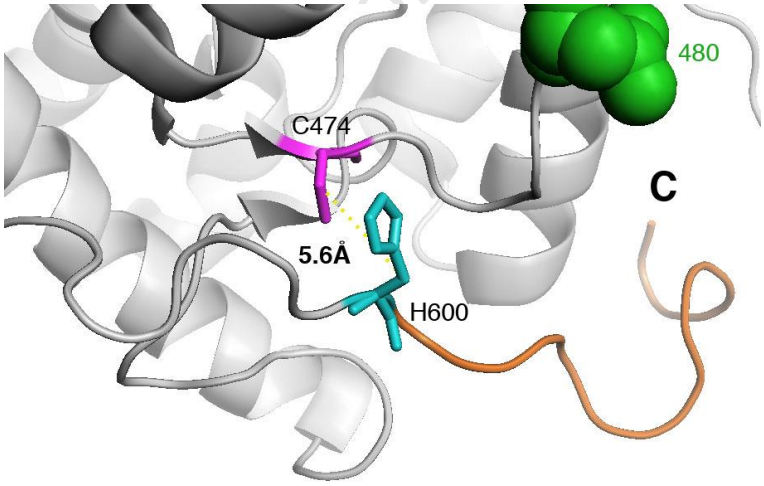

Figure 3.2. C474 and H600. The flexible linker region (*orange*) from residues P602-D612 (*from left to right*). The side chains of the C474 free thiol (*magenta*) and H600 (*cyan*) are shown as stick models. The straight-line measurement between the Cβ atoms of C474 and H600 was 5.6Å (*yellow dashed line*).

The position of the free thiol limited the range of potential sites for the introduction of cysteine residues to the upper portion of the linker region. Thus, the position of a novel disulphide formed may not greatly limit the movement of this region or interaction of the two domains. In order to impose greater constraint on movement, the lower portion of the linker

region closer to the C domain was examined for potential sites. The hydrogen bond between Y607 in the linker region and E161 in helix α8 was identified as a potential target for conversion to a disulphide bond (Figure 3.1). The distance between the Cβ atoms was less than 10Å, well within range for formation of a disulphide considering the flexibility of the linker region.

As a proof of principle, mutagenesis was initially performed on the soluble N domain construct pcDNA-Ndom, which contains 11 residues of the linker region and the first 17 residues of the C domain. A single cysteine residue was introduced at site H600 to generate a disulphide bridge with the free cysteine (C474). The double mutant E161C/Y607C was designed to form a novel disulphide bridge at a more preferable site. The presence of the *de novo* disulphide bridge was determined by proteolysis, SDS-PAGE and MALDI-MS/MS. Successful mutants were cloned into full-length sACE to determine their effect on protein expression, processing, thermal stability and inter-domain interaction.

3.2.2 Site-directed mutagenesis and cloning into a mammalian expression vector

3.2.2.1 N domain constructs: Ndom-H600C and Ndom-EY/CC

Two constructs, NdomH600C and NdomEY/CC, in pcDNA3.1(+) were previously generated in our laboratory (refer to Methods in Chapter 2, Section 2.1.1).

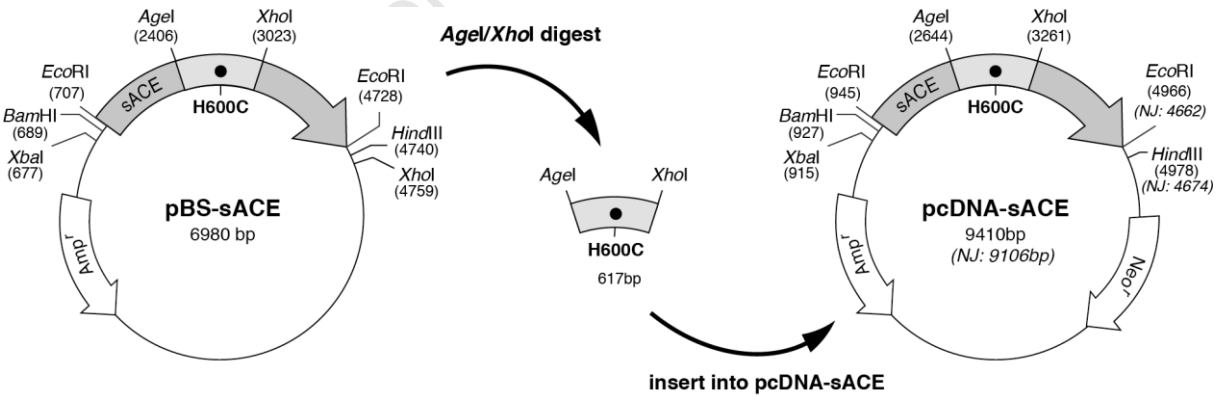

Figure 3.3. Subcloning of H600C into pcDNA-sACE. A 617bp fragment was excised from pBS-sACE-H600C via *Age*I/*Xho*I and inserted into pcDNA-sACE and pcDNA-sACE-NJ to generate full length and soluble constructs respectively. The positions of common restriction enzymes are indicated (positions that differ in sACE-NJ are indicated in italics).

3.2.2.2 Full-length sACE construct: sACE-H600C

A full-length sACE construct of H600C was generated. Since there were no compatible cloning sites to allow for the subcloning of a fragment containing H600C from the N domain into sACE, site-directed mutagenesis was repeated using pBS-sACE as a template (for Methods refer to Chapter 2, Section 2.1.2). A region flanking the mutation was sequenced using two internal primers complementary to ACE, 3R and 5R (refer to Appendix A.1.2 for details), which confirmed the presence of the mutation and that the remaining sequence was unchanged. A 617bp fragment of this region, containing the mutation, was subcloned into full-length sACE in pcDNA3.1(-) (pcDNA-sACE) via *Age*I/*Xho*I sites (Figure 3.3) (Methods in Chapter 2, Section 2.1.3). Restriction enzyme digestion verified the correct size and orientation of the ACE cDNA and the presence of the mutation (Figure 3.4).

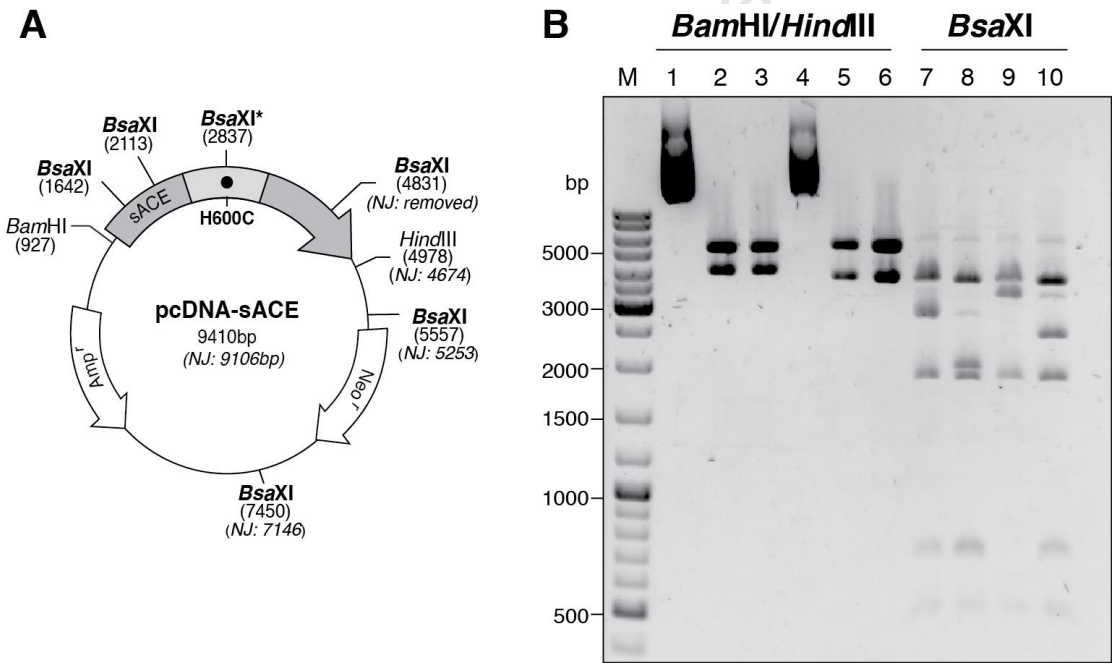

Figure 3.4. Full-length and soluble sACE-H600C constructs in pcDNA. A. Restriction map of pDNA-sACE-H600C depicting sites used to verify the correct size of the sACE insert (*Bam*HI/*Hind*III) and to confirm the presence of the mutation (*Bsa*XI). The novel *Bsa*XI site introduced during site-directed mutagenesis (position 2837) is indicated with an asterisk. The positions of restriction enzyme sites of pcDNA-sACE-NJ are indicated in italics. B. Gel electrophoresis of restriction enzyme digests. Lanes 1, 4 are undigested full-length and soluble pcDNA-sACE respectively. *Bam*HI/*Hind*III digestion: sACE and sACE-H600C, full-length (lanes 2 and 3 respectively) and soluble (NJ, lanes 5 and 6 respectively). *Bsa*XI digestion: sACE and sACE-H600C, full-length (lanes 7 and 8 respectively) and soluble (lanes 9 and 10 respectively).

3.2.2.3 Soluble sACE constructs for ACE protein purification: wt and sACEH600C-NJ

Soluble wt sACE used for purification and protein analysis was derived from a construct that was available in our laboratory. It contains the sACE sequence truncated at S1211 (pcDNA-sACE-sol), 8 residues downstream of the endogenous cleavage site (R1203) (Woodman *et al*, 2000), stably expressed in CHO cells (Methods in Chapter 2, Section 2.1.1). Soluble sACE-H600C was generated by subcloning the 617bp *Age*I/*Xho*I fragment bearing the mutation from pBS-sACE-H600C into pcDNA-sACE-NJ (Figures 3.3 and 3.4). This construct contains the sACE coding region truncated at S1201. Sufficient protein yields for purification was obtained from a high expressing cell line generated by clonal selection.

3.2.3 Determination of the formation of novel disulphide bridges in N domain mutants

3.2.3.1 Expression and purification of a single cysteine N domain mutant in CHO cells

High expressing cell lines were generated by clonal selection of stably transfected CHO cells (refer to Chapter 2, Section 2.2.1 for Methods). Sufficient quantities of soluble ACE were detected in culture fluid by an ACE activity assay to allow for the preparation of bulk cultures for protein purification (for Methods refer to Chapter 2, Section 2.2.2). Protein was purified by lisinopril-sepharose affinity chromatography with sufficient yields for further experiments (NdomH600C: 4mg/L) (Methods in Chapter 2, Section 2.2.3). Purified protein was separated by SDS-PAGE to assess purity (Figure 3.5) (refer to Chapter 2, Section 2.2.7 for Methods). A clear band resolved at approximately 95kDa, the expected size for fully glycosylated N domain ACE (Corradi *et al*, 2006).

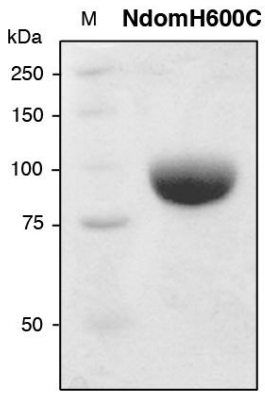

Figure 3.5. SDS-PAGE of purified Ndom-H600C. 10µg of purified protein was separated by 10% SDS-PAGE and visualised by Coomassie Blue staining.

3.2.3.2 Investigation of disulphide bridge formation between C474 and H600C

3.2.3.2.1 Cyanogen bromide cleavage and SDS-PAGE

Approximately 500μg of purified Ndom-H600C was cleaved with cyanogen bromide (CnBr) and peptide fragments separated by SDS-PAGE under non-reducing and reducing conditions to detect the formation of a disulphide bridge between residues C474 and H600C (Figure 3.6) (for Methods refer to Chapter 2, Section 2.2.9). A band of approximately 18kDa (S2) corresponding to the free thiol fragment (FT) was detected under reducing conditions. A band (S3) was detected in the range corresponding to the 8kDa novel thiol fragment (NT) under reducing conditions. Moreover, a band of approximately 25kDa (S1) was detected under non-reducing conditions. The discrepancy in size between the expected and observed with S1 and S3 is due to glycosylation at position N480 (Anthony *et al*, 2010).

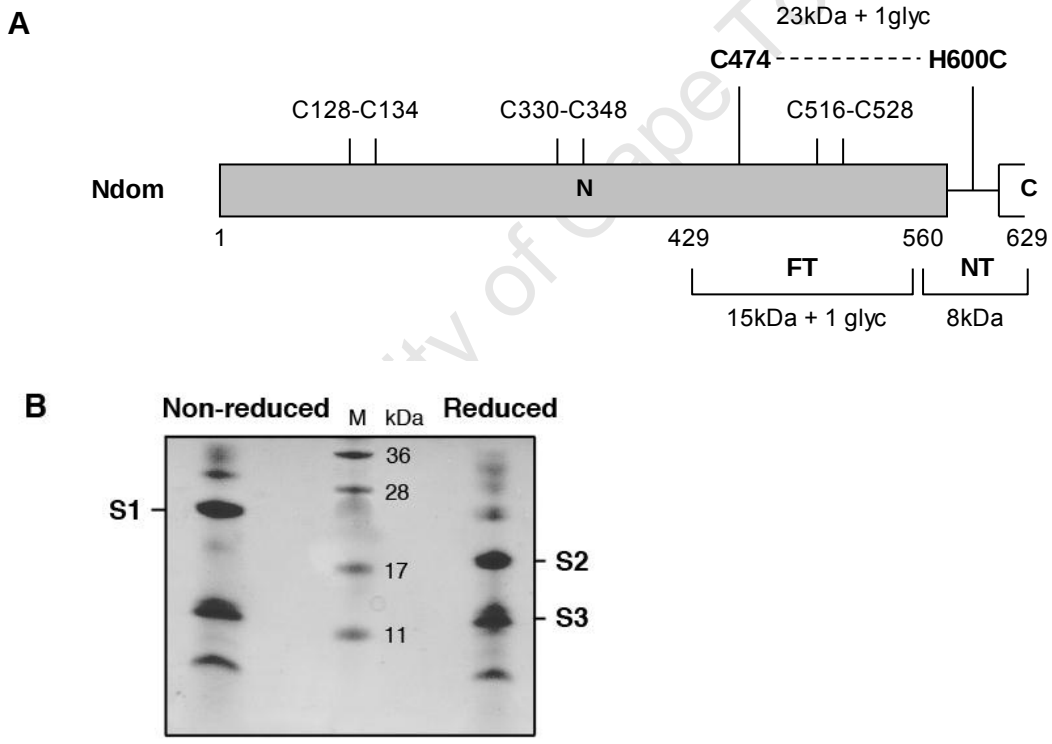

Figure 3.6. CnBr cleavage of Ndom-H600C. A. Schematic representation of Ndom-H600C. Ndom comprises the N domain (*grey box*), linker region (*solid line*) and N-terminal region of the C domain (*white box*). The cysteine residues with the three inter-chain disulphide bridges are shown. The free thiol C474 and the mutation H600C are indicated (*bold*). The C-terminal CnBr fragments of interest are shown as the free thiol containing fragment (FT) and the novel thiol containing fragment (NT) with their predicted sizes (glyc: N-linked glycosylation). The predicted novel disulphide bridge C474-H600C is indicated as a dashed line with the expected size of the disulphide-linked FT and NT fragments shown. B. CnBr digestion of purified Ndom-H600C and 16% SDS-PAGE in the absence or presence of β-ME.

The striking size difference observed between the non-reduced and reduced samples was consistent with the formation of a cysteine bridge between the free cysteine (C474) and the

introduced cysteine (H600C). The three native intra-chain disulphide bonds each lie on the same CnBr peptide, thus reduction of these bonds would not account for the size shift observed. The three bands (S1, S2, and S3) from Ndom-H600C were excised; and in-gel tryptic digests performed before the peptides were subjected to MALDI MS/MS.

3.2.3.2.2 MALDI-MS/MS of Ndom-H600C

MALDI-TOF/TOF analysis was performed on tryptic digests of the non-reduced S1 and reduced S2 and S3 fragments (Figure 3.7 and Table 3.1) (Methods in Chapter 2, Section 2.2.9). Masses could be assigned to FT in S2 and to both FT and NT in S1. The latter was confirmed by MS/MS fragmentation of four tryptic peptides. The tryptic peptide containing H600C could not be identified in S1 or S2. C474 was identified in peptides from S1 and S2 (*m/z* 1190.59 and *m/z* 1190.60 respectively). The mass profile of S3 did not correspond to NT, but matched a number of masses within the N domain, including the 15kDa fragment. This suggests that S3 is not NT and most likely contains a mixture of CnBr digested fragments since a number of fragments were predicted to be of similar size. Identification of both FT and NT peptides in the non-reduced S1 and the lack of any NT peptides in the reduced S2 strongly suggests the formation of the additional disulphide bridge. Since the formation of the novel C474-C600 disulphide appeared to be successful, the H600C mutation was introduced into full-length sACE (Section 3.2.4).

Table 3.1. Observed masses of Ndom-H600C fragments after CnBr and tryptic digest. MALDI TOF/TOF was performed on CnBR fragments S1, S2 and S3 after digestion with trypsin. MS/MS was performed on four peptides of S1. Tryptic peptides containing C474 (in FT) and H600C (in NT) are indicated in bold.

CnBr fragment analysed:		**S1**			**S2**	**S3**
	Residue no	**Calculated mass** [MH]+	**Observed mass** [MH]+	**Peptide sequence** (determined by MS/MS)	**Observed mass** [MH]+	**Observed mass** [MH]+
	188-199	1416.61			1416.61	1416.64
	241-245	678.38			678.38	678.39
	433-446	1724.92	1724.92	IAFLPFGYLVDQWR	1724.93	
	447-453	808.41	808.41		808.41	808.41
	459-467	1362.62	1362.62	YNFDWWYLR	1362.63	
FT	**470-479**	**1190.66**	**1190.59**		**1190.60**	
	490-500	1342.71	1342.73	FHVPNVTPYIR	1342.73	
	518-532	1807.81	1807.81		1807.83	
	546-577	1357.72	1357.72		1357.73	
	560-572	1352.77	1352.77	VGLDALDAQPLLK		
NT	**573-622**	**5922.75**				
	623-629	914.41	914.41			

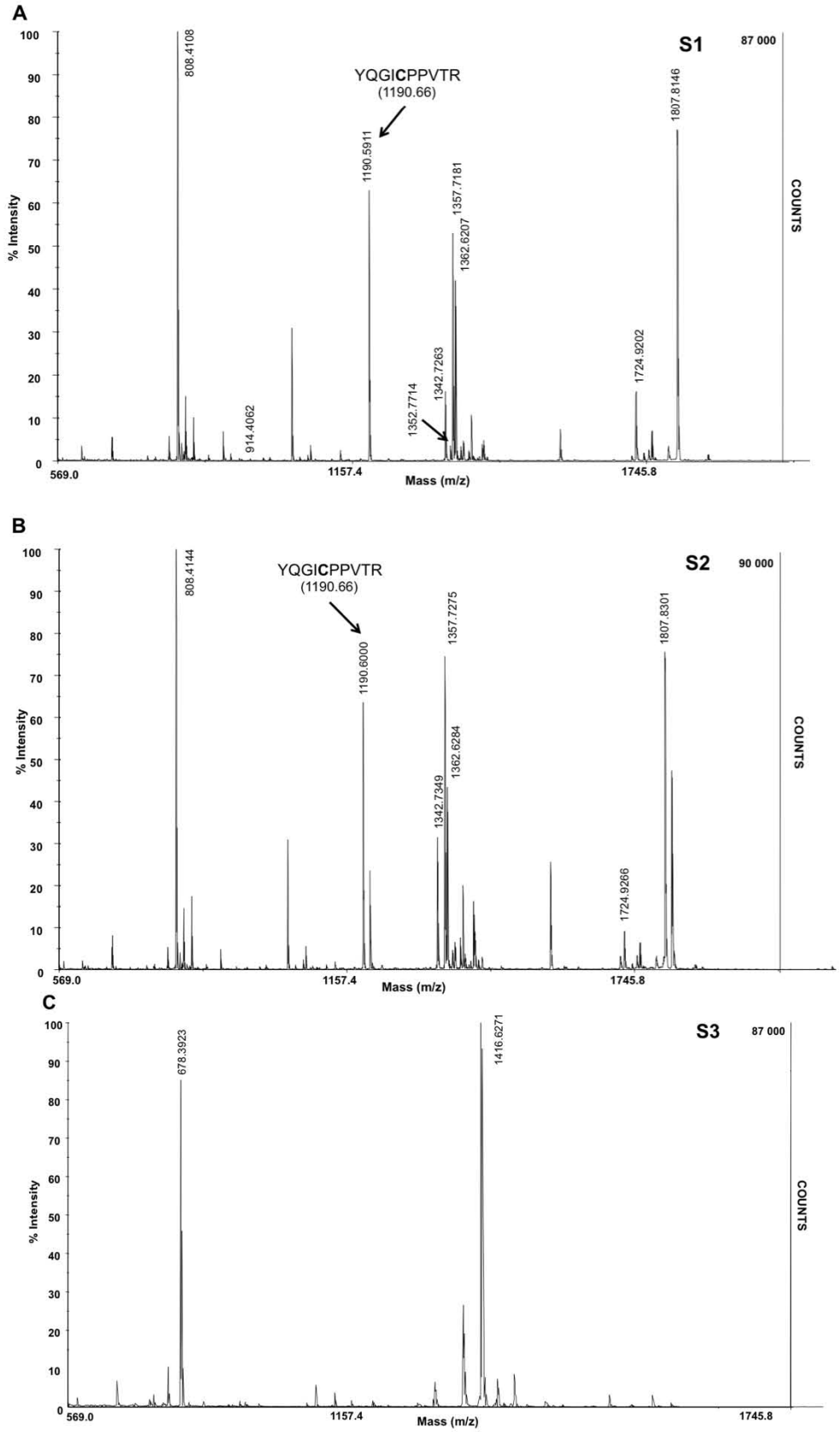

Figure 3.7. MALDI TOF/TOF spectra of Ndom-H600C CnBr fragments after tryptic digest. Three bands were excised from an SDS-PAGE and subjected to in-gel tryptic digest and MALDI-TOF/TOF, namely the non-reduced S1 (*A*), reduced S2 (*B*) and the reduced S3 (*C*) fragments. The tryptic peptide containing H600C is indicated with the expected mass in brackets.

3.2.3.3 Expression of a double cysteine N domain mutant in CHO cells

pcDNA-Ndom-EY/CC was stably transfected into CHO cells for expression and protein purification (for Methods refer to Chapter 2, Section 2.2.1). No significant ACE activity was detected in medium compared to wt and untransfected controls in repeat transfections (Table 3.2) (Methods in Chapter 2, Section 2.2.2). This seemed to indicate that the mutant was not being expressed, either due to low mRNA expression levels from an inefficient transfection or through targeted degradation during processing. To investigate the expression of Ndom-EY/CC, the presence of ACE mRNA was determined by RT-PCR and protein levels detected by Western blot analysis.

Table 3.2. ACE activity in cell lysate and medium from CHO cells. ACE activity was determined using ZFHL as a substrate. Data is the mean of one experiment performed in triplicate. Protein concentration in total cell lysates was determined using Bradford reagent.

	CELLS		**MEDIUM**
	ACE activity mU/ml	**Total protein** mg/ml	**ACE activity** mU/ml
CHO	0.04 ± 0.00	1.62 ± 0.03	0.51 ± 0.13
wt Ndom	3.14 ± 0.08	1.98 ± 0.13	13.78 ± 0.21
Ndom-EYCC	0.75 ± 0.06	1.57 ± 0.15	2.42 ± 0.06

3.2.3.4 Determination of expression of Ndom-EY/CC

3.2.3.4.1 Detection of mRNA levels in transfected CHO cells

Total RNA was extracted from CHO cells stably transfected with pcDNA-Ndom-EY/CC. As controls, total RNA was extracted from untransfected CHO cells and cells transfected with pcDNA-Ndom (wt soluble N domain) (Figure 3.8A) (refer to Chapter 2, Section 2.1.4 for Methods).

Equivalent amounts of total RNA were used to synthesise cDNA from these three cells lines as well as from the control, namely total human placental RNA. An 860bp portion of the N domain was amplified by RT-PCR as well as a 983bp portion of G3PDH, included as a positive control (Figure 3.8B). The 983bp G3PDH amplicon was visible in all three cells lines and the positive control upon gel electrophoresis, as expected. From visual inspection, the levels of G3PDH mRNA appear to be lower in the wt N domain and Ndom-EY/CC (wt > EY/CC) transfected cells compared to untransfected cells. Since G3PDH mRNA levels are expected to be consistent, the differences observed are likely due to three factors. First, inconsistent cDNA synthesis across the total RNA samples used and second, inconsistent amplification of cDNA across samples or finally, incorrect quantification of RNA.

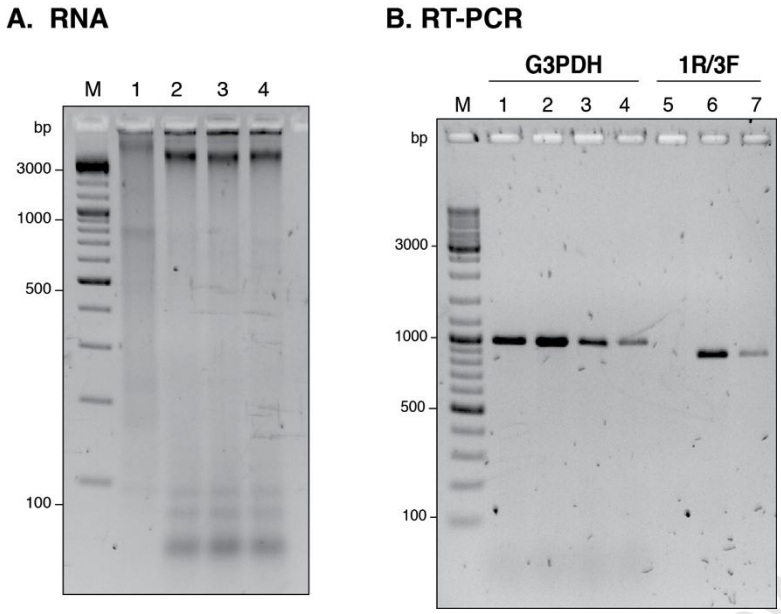

Figure 3.8. Expression of Ndom-EY/CC mRNA. A. Control RNA (human total placental RNA, lane 1) and RNA extracted from untransfected CHO cells (lane 2) and CHO cells expressing either wt Ndom (lane 3) or Ndom-EYCC (lane 4) were separated by agarose gel eletrophoresis. B. RT-PCR was performed on extracted RNA and control RNA using a control primer (G3PDH, lanes 1-4) and ACE specific primers 1R and 3F (lanes 5-7). Lane 1 control RNA, lanes 2 & 5 untransfected CHO cells, lanes 3 & 6 wt Ndom and lanes 4 & 7 Ndom-EYCC.

The 860bp ACE amplicon was detected in both the wt N domain and Ndom-EY/CC cell lines, but not the untransfected CHO cells. Similar to G3PDH, there are decreased levels of the Ndom-EY/CC amplicon compared to wt. This serves to confirm that the lower ACE and G3PDH levels observed for Ndom-EY/CC transfected cells are due to decreased amounts of cDNA available, compared to the other samples. Hence, if the levels of mRNA are adjusted according to the G3PDH, there is expression of Ndom-EY/CC, albeit to a lower degree than wt. This indicates that Ndom-EY/CC DNA was introduced into CHO cells at sufficient levels for mRNA expression. Thus, the lack of ACE activity in Ndom-EY/CC transfected cells was mostly likely due to aberrant processing of protein.

3.2.3.4.2 Determination of protein expression of Ndom-EY/CC

Total cell lysate and cell culture medium from untransfected CHO cells and CHO cells expressing either wt N domain and Ndom-EY/CC were collected in parallel with total RNA extraction (Table 3.2). Equivalent amounts of cell lysate and medium were separated by SDS-PAGE and N domain ACE visualised by Western blot analysis (Figure 3.9) (Methods in Chapter 2, Section 2.2.8). As expected, a band resolving at 90kDa was observed in the lysate of cells expressing wt N domain, corresponding to immature protein and a roughly 95kDa band in the medium, corresponding to properly processed soluble protein. The size shift

observed is the result of the addition of glycans during processing. The mature form is not observed in the cell lysate as this a soluble construct that is released into the extracellular milieu upon processing.

A band of similar size as wt N domain was observed in the lysate of cells expressing Ndom-EY/CC. A similarly sized band in the medium could be faintly detected by visual inspection. The levels of Ndom-EY/CC in cells appear to be higher than that of wt. It appears that there is improper processing of this mutant, where protein is retained in cells and is not processed to the mature form. This is most likely the due to improper folding, resulting in targeted degradation of the protein

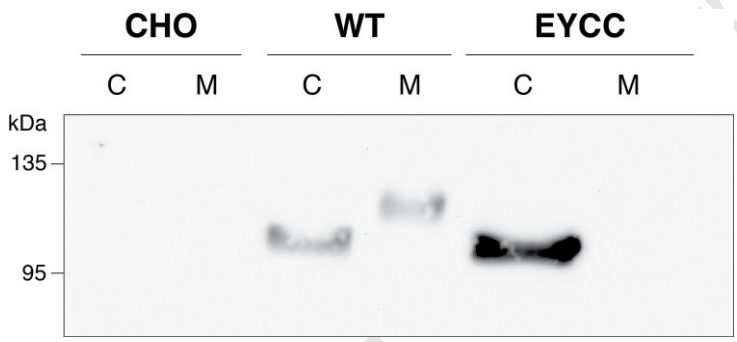

Figure 3.9. Western blot analysis of transfected CHO cells. Total cell lysate (C) and medium (M) from untransfected CHO cells (CHO) and CHO cells transfected with wt Ndom (WT) and Ndom-EYCC (EYCC) were separated by 10% SDS-PAGE. Western blot analysis was performed and ACE detected using the N domain-specific mAb 4G6.

3.2.4 Characterisation of a novel disulphide bridge in sACE-H600C

3.2.4.1 Expression of a single cysteine somatic ACE mutant in CHO cells

Full-length and soluble sACE-H600C constructs were transfected into CHO cells (Methods in Chapter 2, Section 2.2.1). High expression levels of the full-length protein were obtained by FACS, yielding sufficient levels of ACE for further experiments, determined by an ACE activity assay of the total cell lysate and cell culture medium (450-500mU/ml in cell lysate and 10-15mU/ml in medium) (for Methods refer to Chapter 2, Section 2.2.2). The full-length protein was used to characterise the effect of H600C on ACE expression, shedding and conformation (Section 3.2.4.4).

A cell line expressing soluble sACE-H600C (pcDNA-sACE-H600C-NJ) with sufficient ACE activity (30mU/ml) in cell culture medium for protein purification was isolated by clonal selection. Protein was purified from the soluble sACE-H600C cell line and used to determine

the formation of the engineered disulphide and the effect of the mutation on enzyme stability (Section 3.2.4.3).

3.2.4.2 Purification of soluble wt sACE and sACE-H600C

Lisinopril-sepharose affinity chromatography (Methods in Chapter 2, Section 2.2.3) of harvested cell culture medium yielded 1.2 mg/L medium sACE and 8.3 mg/L sACE-H600C. Both samples resolved as a single band of approximately 190 kDa by SDS-PAGE equivalent to fully glycosylated sACE (Figure 3.10). Both wt sACE and sACE-H600C migrated as diffuse bands characteristic for glycoproteins.

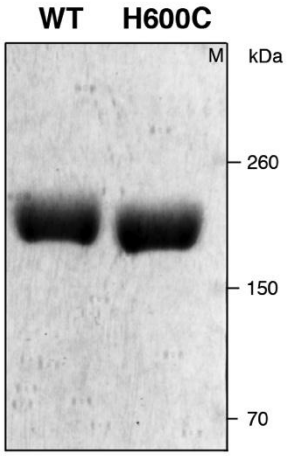

Figure 3.10. SDS-PAGE of purified wt sACE and sACE-H600C. 5µg-10µg of purified wt sACE (*wt*) and sACE-H600C (*H600C*) protein were separated by 6% SDS-PAGE and visualised by Coomassie Blue staining.

3.2.4.3 Determination of C474-H600C disulphide bridge formation

3.2.4.3.1 Cyanogen bromide digestion and SDS-PAGE

As with Ndom-H600C, purified wt sACE and sACE-H600C were cleaved with CnBr and the resultant fragments separated by SDS-PAGE under non-reducing and reducing conditions (Figure 3.11) (for Methods refer to Chapter 2, Section 2.2.9). A prominent band of approximately 18kDa (S2) corresponding to FT was observed in both wt and sACE-H600C under reducing conditions. The disappearance of this band and the appearance of a prominent band of approximately 37kDa (S1) in sACE-H600C under non-reducing conditions are consistent with the formation of a disulphide bridge between FT and NT fragments. Once again, the discrepancy between the expected and observed sizes of S1 and S2 can be attributed to glycosylation at position N480.

The non-reduced sACEH600C S1 fragment was excised and used for MALDI MS/MS analysis to confirm the presence of the disulphide bridge.

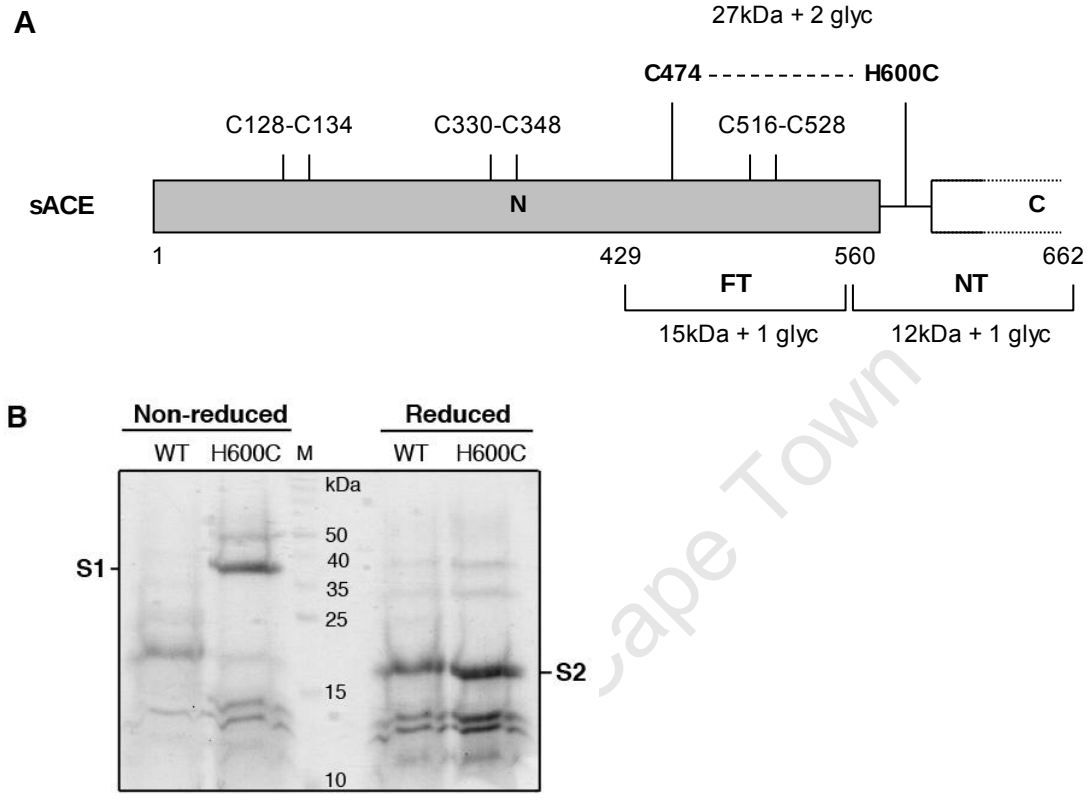

Figure 3.11. CnBr cleavage of sACEH600C. A. Schematic representation of sACE. The N domain (*grey box*), linker region (*solid line*) and N-terminal region of the C domain (*white dashed box*) are indicated. The cysteine residues, disulphide bridges and CnBr fragments are depicted as in Figure 3.6. B. 16% SDS-PAGE of CNBr peptides of wt sACE and sACE-H600C in the absence or presence of β-ME.

3.2.4.3.2 MALDI MS/MS of sACE-H600C

An in-gel tryptic digest was performed on S1 and the peptides analysed by MALDI-TOF/TOF (Figure 3.12 & Table 3.3) (Methods in Chapter 2, Section 2.2.9). Masses were assigned to both the FT and NT peptides and three masses were confirmed by MS/MS fragmentation. A fragment corresponding to the C474 peptide was identified (*m/z* 1190.60), however the tryptic peptide containing H600C was not. These results strongly suggest that a disulphide bridge was formed between C474 and H600C in sACE.

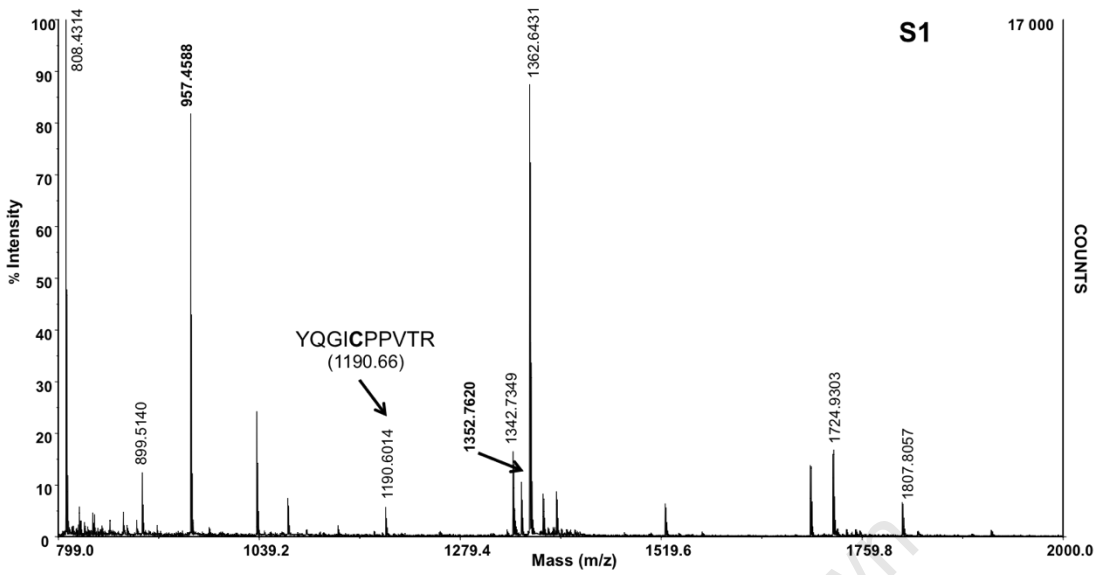

Figure 3.12. MALDI TOF/TOF spectrum of sACE-H600C CnBr fragments after tryptic digest. The tryptic peptide containing H600C is indicated with the expected mass in brackets. NT peptides are indicated in bold.

Table 3.3. Observed masses of sACE-H600C S1 CnBr fragment after tryptic digest. The peptides containing C474 (FT) and H600C (NT) are indicated in bold.

CnBr fragment analysed:		**S1**		
	Residue no	**Calculated mass** $[MH]^+$	**Observed mass** [MH]+	**Peptide sequence** (determined by MS/MS)
	433-446	1724.92	1724.93	
	447-453	808.41	808.43	WGVFSGR
	459-467	1362.62	1362.64	YNFDWWYLR
FT	**470-479**	**1190.66**	**1190.60**	
	490-500	1342.71	1342.73	
	518-532	1807.81	1807.81	
	551-557	899.50	899.51	
	560-572	1352.77	1352.76	
NT	**573-622**	**5905.71**		
	623-629	957.43	957.46	FVEEYDR

3.2.4.4 Characterisation of sACE-H600C

3.2.4.4.1 Constitutive shedding of sACE-H600C

The amount of ACE shed from the cell surface of CHO cells expressing wt sACE and sACE-H600C was determined from an activity assay of total cell lysate and cell culture medium after incubation in minimal medium for four hours (Figure 3.13) (for Methods refer to Chapter 2, Section 2.2.4). sACE is shed inefficiently from the cell surface (3-6% of total after four hours) as found previously (Woodman *et al*, 2000). There was a slight but significant

increase in shedding of sACE-H600C compared to wt. This may be the result of subtle conformational changes induced by the presence of the disulphide bridge.

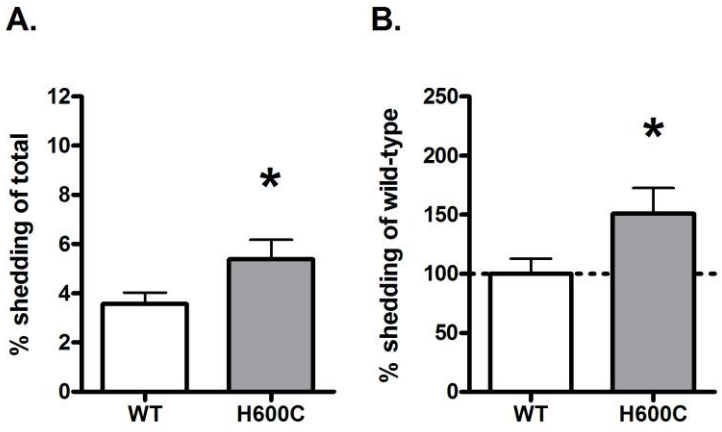

Figure 3.13. Shedding of sACE-H600C. Shedding was calculated as the percentage ACE activity in medium of total activity in medium and cell lysate from CHO cells expressing sACE and sACE-H600C. Data is the mean±SD of three experiments (sACE) or two experiments (sACE-H600C) performed in triplicate. A. Percentage shed of total activity, B. Percentage shed of wt sACE.

3.2.4.4.2 Effect of the H600C mutation on ACE conformation

A panel of domain-specific monoclonal antibodies (mAbs) to ACE were used to determine the effect of the H600C mutation on the conformation of ACE and to detect any change in domain interaction (Figure 3.14). The conformation of membrane-bound ACE was determined with a cell-based ELISA assay (for Methods refer to Chapter 2, Section 2.2.6). N domain-specific mAbs showed a similar trend in binding of sACE-H600C compared to wt with the exception of mAbs 3A5, 1G12 and i2H5. Noticeably higher levels of bound mAb were detected for sACE-H600C for each of these three mAbs (149.45% ± 4.91%, $p < 0.001$; 123.74% ± 8.17%, $p < 0.05$ and 156.37% ± 16.63%, $p < 0.01$ binding of wt, respectively). No remarkable difference in binding of C domain-specific mAbs to sACE-H600C compared to wt was observed, besides a significant increase in affinity for mAb 4E3 (130.96% ± 5.87%, $p < 0.001$ binding of wt).

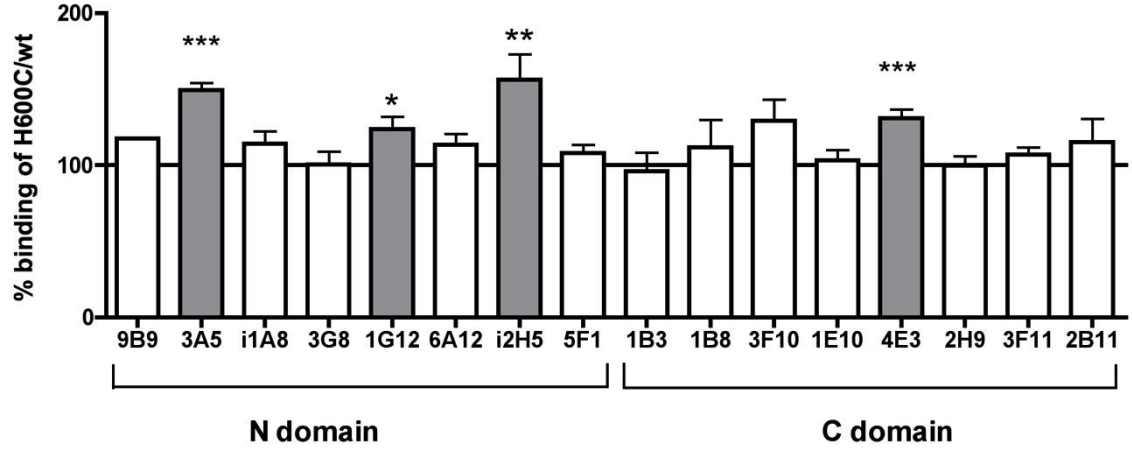

Figure 3.14. Cell ELISA of sACE-H600C. A cell based ELISA assay was performed on CHO cells expressing sACE and sACE-H600C using the panel of domain-specific mAbs. Data is shown as the % binding of wt, normalised as the ratio of binding to control (IgG) and is the mean±SD of two experimenrts performed in triplicate.

3.2.4.4.3 Thermal stability of sACE-H600C

The effect of the *de novo* disulphide bridge formed between C474 and H600C on sACE thermal stability was determined (Figure 3.15) (Methods in Chapter 2, Section 2.2.11). The loss of activity over time after incubation at 55°C showed similar trends for wt, as previously reported (O'Neill *et al*, 2008) where rapid loss and apparent destabilisation of sACE occurs after 5 minutes (23% residual activity). A similar trend was observed for sACE-H600C, which appears to indicate that the novel disulphide has not improved sACE thermal stability.

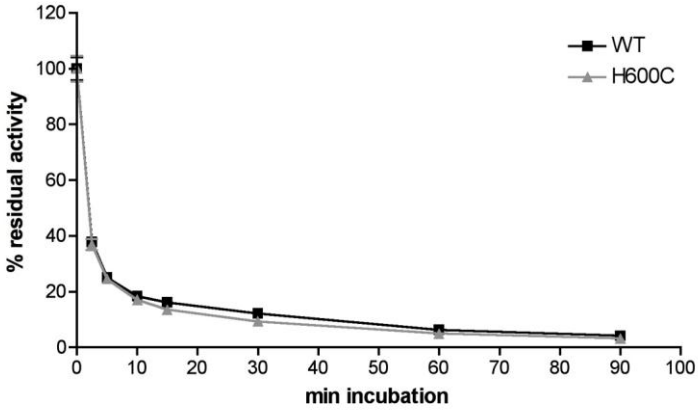

Figure 3.15. Thermal stability of wt (*black*) and sACE-H600C (*grey*) was determined by incubation at 55°C over 90 minutes. Data is represented as the percent residual activity remaining compared to control (sample left on ice) and is the mean±SD of three experiments performed in triplicate.

3.3 DISCUSSION

The crystal structures of both the N (Corradi *et al*, 2006) and C domains (Natesh *et al*, 2003) of ACE have been solved individually, but the solution of the full-length 3D structure of ACE remains elusive. The presence of heterogeneous glycosylation on both domains and the degree of inter-domain flexibility afforded by the linker region have been suggested as possible reasons for the difficulty in obtaining sACE crystals. As discussed in Chapter 1, minimally glycosylated variants of the N and C domains have facilitated reproducible crystal formation (Gordon *et al*, 2003; Watermeyer *et al*, 2006; Anthony *et al*, 2010) and may be a viable approach for solving the 3D structure of sACE.

A second and possibly parallel approach would be to limit the flexibility of the linker region and thereby constrain the two domains through the introduction of an intra-molecular disulphide bridge. The use of *de novo* disulphide bridges has been a successful approach in stabilising proteins for molecular studies. These include the subtilisins (Bryan *et al*, 2000), RNaseA (Pecher *et al*, 2009) and F-actin filaments (Kim *et al*, 2000).

In this study, novel disulphide bridges were designed *in silico* between residues in the N domain and the linker region (Figures 3.1 & 3.2). To ascertain the position at which a novel disulphide bridge would limit inter-domain movement, two strategies were employed: 1) to utilise the free thiol (C474) to interact with a novel cysteine at position 600 in the linker region, and 2) to modify the stabilising hydrogen bond between residues E161 and Y607 in the lower portion of the linker region by creating a *de novo* disulphide bridge. Cysteine residues were introduced by site-directed mutagenesis and mutant protein stably expressed in CHO cells. The presence of the novel disulphide bridge was verified by limited proteolysis of purified protein and SDS-PAGE and MALDI MS/MS of the resulting peptides. These mutations were initially introduced into a soluble N domain construct as proof of concept. Utilisation of the free thiol in the N domain appeared to be a successful strategy to introduce a *de novo* disulphide bridge. The introduction of H600C into the N domain resulted in the formation of C474-C600 disulphide linkage confirmed by CnBr cleavage, SDS-PAGE and MALDI MS/MS (Table 3.1, Figures 3.6 & 3.7).

The double cysteine mutant Ndom-EY/CC, designed to impose greater restriction of movement of the linker region, was not properly processed - as determined by RT-PCR and western blotting analysis (Table 3.2, Figures 3.8 & 3.9). Despite detectable levels of mRNA and protein in the cell lysate, negligible amounts of mature, active soluble protein were observed. This is indicative of incorrect processing of the protein. In general terms, lack of

protein expression is the result of misfolding or insufficient glycosylation (Helenius & Aebi, 2001). Two glycosylation sequons lie in close proximity to E161C and Y607C at sites N131 and N480. However, the conversion of E161 and Y607 to cysteine residues is unlikely to affect the attachment of glycans at these sites. A native intra-molecular disulphide bridge, C128-C136, lies within 12Å of E161 and 16Å of Y607 on a flexible loop that is exposed on the surface (Figure 3.1). Furthermore, the free thiol of C474 lies within 14Å of E161 and 17Å of Y607. Considering the flexibility of the linker region and the loop wherein the C128-C136 bridge lies, it is possible that the presence of additional cysteine residues in close proximity to this region may have a detrimental effect on protein folding by interfering with the formation of the C128-C136 bridge and allowing formation of non-native disulphide bonds. A similar observation was made when introduction of novel cysteine residues resulted in loss of expression of acetylcholinesterase (Siadat *et al*, 2006).

Thus, data from the two mutants Ndom-H600C and Ndom-EY/CC indicate that the strategy of utilising the free thiol is a less disruptive means of introducing a novel disulphide bridge.

The effect of this novel disulphide linkage on ACE expression, processing and inter-domain interaction was assessed in the sACE isoform. The introduction of H600C into full-length sACE resulted in the successful formation of the novel C474-C600 linkage, detected by limited proteolysis and MALDI MS/MS (Table 3.3, Figures 3.11 & 3.12). The *de novo* disulphide linkage had no adverse effect on protein expression since membrane-bound sACE-H600C was expressed as a catalytically active protein that was proteolytically processed from the membrane and the soluble version was also expressed as an active protein (Figures 3.10 & 3.13).

In order to assess the potential of any mutants containing engineered disulphides as crystallisation candidates, it was important to determine the effect of the novel disulphide bridge on sACE stability and inter-domain interaction. This was investigated using thermal stability assays and cell ELISA with the panel of domain-specific ACE mAbs.

The mutation had no effect on thermal stability, contrary to our expectations (Figure 3.15). This was based on previous observations that interactions between the N and C domains may have a stabilising effect on sACE (O'Neill *et al*, 2008). This could be due to the following factors: first, the *de novo* disulphide linkage, while present, is insufficient to constrain the linker region in such a way as to improve stability and second, the formation of the C474-C600 linkage is not energetically favourable, resulting in a mixed population of both disulphide-bonded and non-bonded protein. However, the disulphide linked CnBr fragment

observed by SDS-PAGE was of a greater intensity than the wt or non-linked peptide indicating that the majority of the protein exists in the disulphide-bridged form.

To evaluate the effect of H600C on inter-domain interaction, changes in the conformation of the two domains were determined using the domain-specfic monoclonal antibodies to ACE (Figure 3.14). The epitopes of eight N domain-specfic mAbs (9B9, 3G8, i1A8, 6A12, 1G12, 5F1 and i2H5) and eight C domain-specfic mAbs (1B3, 1B8, 3F10, 1E10, 4E3, 2H9, 3F11 and 2B11) have been mapped to 700-800Å^2 regions of each domain (Danilov *et al*, 1994; Balyasnikova *et al*, 2005a; Balyasnikova *et al*, 2007; Balyasnikova *et al*, 2008; Danilov *et al*, 2007; Naperova *et al*, 2008a; Gordon *et al*, 2010) (Chapter 1, Section 1.4). The binding of these mAbs to different ACE chimeras has allowed for the identification of regions where the two domains may be in close proximity. Most noticeably the epitopes of the N domain-specfic mAbs 1G12 and 6A12 appear to be occluded by the C domain (Balyasnikova *et al*, 2007). Similarly, the epitopes of the C domain-specfic mAbs 1E10 and 4E3 appear to be partly occluded by the N domain and it has been proposed that a point of contact between the two domains may lie within these epitopes (Naperova *et al*, 2008a). This point of contact on the N domain is proximal to the overlapping epitopes of mAbs 3A5, 1G12 and i2H5, which is distal to the linker region and C474-C600 disulphide bridge. All three of these mAbs showed increased affinity for sACE-H600C. Moreover, the same effect was observed for the C domain-specfic mAb 4E3. This suggests that the novel disulphide has had some effect on inter-domain interaction..

Determining the effects of the novel C474-C600 disulphide bridge on inter-domain interaction and protein stability by thermal denaturation and cell ELISA were inconclusive. There appeared to be some localised effect on the interaction of the two domains, evidenced by the increased affinity for certain mAbs, but there was no effect on thermal stability. The engineering of disulphide bonds successfully improved the stability of acetylcholinesterase (Siadat *et al*, 2006) and *Rhizomucor miehei* lipase (Han *et al*, 2009), where changes in thermal stability were measured in a similar manner. This suggests that the failure to detect an effect of the C474-H600C disulphide bridge on thermal stability was more likely the result of the bridge not being favourably positioned than the methods used.

This study was limited by the lack of information regarding the interaction of the two domains. Inter-domain movement has been hypothesised based on the negative cooperativity of the two domains with regards to substrate hydrolysis (Binevski *et al*, 2003; Andujar-Sanchez *et al*, 2004) and shedding (Woodman *et al*, 2005), from the crystal structures of the

two domains (Corradi *et al*, 2006) and from mAb binding (Balyasnikova *et al*, 2007; Naperova *et al*, 2008a). However, a means to directly determine inter-domain interaction and movement has not been established. It was hoped that the determination of the effect of the *de novo* bridge on thermal stability and protein conformation would be sufficient to detect changes in this respect. At this stage, the reasons for no significant effect on conformation and enzyme stability have not been established and there remains the possibility that the position of the C474-C600 linkage is not ideal to produce an effect.

In summary, the introduction of *de novo* disulphide bonds in the linker region between the two domains may still be an effective approach towards limiting inter-domain movement and developing a candidate for crystallisation. However, the positioning of the bridge is critical in eliciting the desired effect. While the use of the free thiol to form the *de novo* C474-C600 bridge was successful, results suggest that this is not in an optimal position to elicit a strong stabilising effect. The crystal structure of the N domain indicates that the flexible linker region is held in position by a hydrogen bond between the side chains of residues E161 and Y607 (Corradi *et al*, 2006). To effectively limit inter-domain movement, this position seemed optimal, however introduction of cysteines at these positions led to protein misfolding. It may be useful to determine the role of the C128-C136 bridge in protein expression and stability and whether these sites could be removed or altered.

Finally, the question remains as to whether the introduction of *de novo* disulphides into sACE is a viable approach for obtaining crystal for 3D structure determination. Particularly since the difficulty in obtaining crystals has also been attributed to the presence of a high degree of heterogeneous glycosylation. An additional approach would be to introduce any *de novo* disulphide bridges into a minimally glycosylated version of sACE, thereby reducing both problems thought to hamper crystallisation of sACE. With this in mind, sACE-H600C was expression in CHO cells in the presence of the α-glucosidase inhibitor N-butyl-deoxynojirimycin (NB-DNJ) to limit the heterogeneity of glycan residues (Butters *et al*, 1999). Sufficient protein was obtained for purification and has been sent for crystallisation trials (performed in the laboratory of Prof. K. Ravi Acharya, University of Bath, UK), the results of which are forthcoming.

CHAPTER 4: Dimerisation and shedding: Fine epitope mapping of N domain-specific ACE monoclonal antibodies 9B9, 3G8 and i1A8[†]

4.1 INTRODUCTION

Monoclonal antibodies are valuable tools in biology, due to their high degree of specificity (reviewed in Ladner *et al*, 2007). Epitope mapping of target regions has enhanced a number of molecular techniques including ELISA (He *et al*, 2010) and flow cytometry (Danilov *et al*, 2003; Nikolaeva *et al*, 2006); as well as in therapeutics including targeted immunotherapy, for diagnostic tools, identification of cell and serum markers and vaccine development (Baloria *et al*, 2011). Moreover, the understanding of the structure-function relationship of a number of proteins has been enhanced through epitope mapping. Some examples include the characterisation of human mAbs to the hepatitis C virus envelope 2 protein (Iacob *et al*, 2008); epitope mapping of three mAbs to adenovirus type 2 E3/19K protein used to investigate the immune response to infection (Menz *et al*, 2008) as well as the investigation of the multiple drug resistant P-glycoprotein and its role in chemotherapy (Cianfriglia *et al*, 2002)

Defining the epitope of a mAb identifies distinct regions of a protein. In combination with site-directed mutagenesis, epitope mapping can be used to define particular residues involved in protein-protein interactions.

4.1.1 Monoclonal antibodies to ACE and their effect on processing and function

Extensive mapping of the epitopes of a panel of eight N domain-specific (Balyasnikova *et al*, 2005a; Balyasnikova *et al*, 2007; Skirgello *et al*, 2006; Danilov *et al*, 2007; Gordon *et al*, 2010) and eight C domain-specific (Balyasnikova *et al*, 2008, Naperova *et al*, 2008a) monoclonal antibodies to ACE has been performed (refer to Chapter 1, Section 1.4). Binding of these antibodies affects ACE activity (Skirgello *et al*, 2006), proteolytic cleavage (Balyasnikova *et al*, 2002, Balyasnikova *et al*, 2005a) and dimerisation (Kost *et al*, 2003, Gordon *et al*, 2010). Recently epitope mapping of the N domain-specfic antibody 5F1 has been used to shed light on hinge movement upon substrate binding (Danilov *et al*, 2007).

[†] The work described in this chapter was part of a larger study conducted in collaboration with Prof S. Danilov (University of Illinois at Chicago, USA) and was recently published (Gordon *et al*, 2010). This chapter focuses on our contribution to this work, detailed in Section 4.2.

Two of these mAbs, 9B9 and 3G8, which bind overlapping regions of the N domain (Danilov *et al*, 1994), were shown to have a significant effect on ACE shedding (Balyasnikova *et al*, 2002) and homodimerisation (Kost *et al*, 2003). The presence of mAb 9B9 increased ACE shedding from the surface of CHO cells and inhibited dimerisation in reverse micelles (Balyasnikova *et al*, 2002; Kost *et al*, 2003). Conversely, mAb 3G8 had an inhibitory effect on both shedding and dimerisation in the same experiments. In order to identify regions or residues that may be involved in these processes, fine epitope mapping of mAbs 9B9, 3G8 and i1A8 was performed. mAb i1A8 was included since the proposed epitope of this antibody overlaps those of mAbs 9B9 and 3G8 to a large extent (Danilov *et al*, 1994) but its binding has no effect on dimerisation (Kost *et al*, 2003) or shedding (Balyasnikova *et al*, 2002). Thus, it was used to eliminate residues within the overlapping regions of these epitopes.

4.1.2 The N domain epitopes of anti-ACE mAbs 9B9, 3G8 and i1A8

The proposed epitope of mAb 9B9 was localised to the N-terminal portion of the N domain, based on precipitation of different ACE isoforms, cross-species reactivity and sequence homology (Balyasnikova *et al*, 2005a; Gordon *et al*, 2010). This epitope is localised around a four-amino acid motif, 9NFSA12, which is conserved amongst the mammalian ACE species that mAb 9B9 recognises (Gordon *et al*, 2010). The degree of binding of mAb 9B9 is thought to be affected by glycan residues since ACE from human umbilical vein endothelial cells (HUVEC) and macrophages is precipitated by mAb 9B9 to a much smaller extent than that from CHO cells.

The proposed epitope of mAb 3G8 overlaps that of mAb 9B9 (Danilov *et al*, 1994) and lies within a region that is partially occluded by the C domain since mAb 3G8 bound sACE significantly less than the N domain, similar to what was observed for mAbs 1G12 and 6A12 (Balyasnikova *et al*, 2007). This epitope contains residues within the first 141 amino acids because mAb 3G8 bound the ACE chimera N-del-ACE/*Bgl*II, which has the first 141 residues of the C domain replaced by the N domain (Balyasnikova *et al* 2005a; Gordon *et al*, 2010). As with mAb 9B9, binding of mAb 3G8 is affected by the type and extent of glycosylation, evident by the increased binding of mAb 3G8 observed with CHO cells compared to COS and human embryonic kidney (HEK) cells. Furthermore, NB-DNJ treatment of CHO cells led to increased precipitation of sACE by mAb 3G8 as well as that of purified ACE from seminal fluid and plasma after neuraminidase treatment (Gordon *et al*, 2010).

The putative epitope for mAb i1A8 overlaps both the mAb 9B9 and 3G8 epitopes (Danilov *et al*, 1994). It does not seem to be occluded by the C domain since sACE and the N domain are precipitated equally by this antibody (Gordon *et al*, 2010). The binding of mAb i1A8 appears to be influenced by glycans, as with mAbs 9B9 and 3G8. Changes in binding were observed for ACE from different sources and sACE was precipitated more efficiently from the culture fluid of NB-DNJ treated cells. Neuraminidase treatment of purified plasma and seminal fluid ACE had the same effect.

Based on previous cross-species comparisons, Q22, Q87, R90 and R96 were identified as possible residues within the epitopes of mAbs 9B9 and 3G8 (Balyasnikova *et al*, 2005a, Gordon *et al*, 2010). These formed a basis for fine epitope mapping using site directed mutagenesis to target specific residues.

Thus, the aim of this study was to perform fine epitope mapping of mAb 9B9, 3G8 and i1A8. This involved the following objectives:

1. To perform fine epitope mapping of mAbs 9B9, 3G8 and i1A8 by site-directed mutagenesis.
2. To identify residues in the overlapping region of the epitopes of mAbs 9B9 and 3G8 that may be involved in ACE dimerisation and shedding.
3. To characterise the effect of these residues on ACE shedding, dimerisation and mAb binding in CHO cells.

4.2 RESULTS

4.2.1 Site-directed mutagenesis and construction of mutants in a mammalian expression vector

4.2.1.1 N domain mutants for fine epitope mapping

To further define the epitopes of the three monoclonal antibodies 9B9, 3G8 and i1A8, key residues were identified within these epitopes through site-directed mutagenesis.

Using the crystal structure of the ACE N domain (PDB accession number 2C6F) (Corradi *et al*, 2006), the surface residues within the proposed epitopes were examined to identify those that were exposed or caused protuberances from the structure, and thus would more likely to be involved in ACE-mAb interactions.

Mutations of 10 amino acids (indicated in bold below) were generated, which formed part of a larger panel of mutations produced in collaboration with Prof. S. Danilov (University of Illinois at Chicago, USA).

In order to disrupt interactions between ACE and mAbs 9B9, 3G8 and i1A8, surface residues were altered to the corresponding amino acid of a different species (**Q18H**, **Q30V**, **I79V**, R90K, R96G, N203E, EG315-316AE, L562S) or of the C domain (R541A, K542T, K557Q, D558L). Alternatively, residues were converted to amino acids with small sides chains to drastically alter the local extended surface conformation (**P3A**, **Q6A**, D13A, Q22A, Q87G, **R340A**, **D374A**, R550A) or to alter the properties of the side chain without having a large effect on the surface structure (**G4E**, **L19E**). Furthermore, three glycosylation sequons were disrupted to determine the role of glycan chains in antibody binding (N9Q, **N25Q**, N82Q).

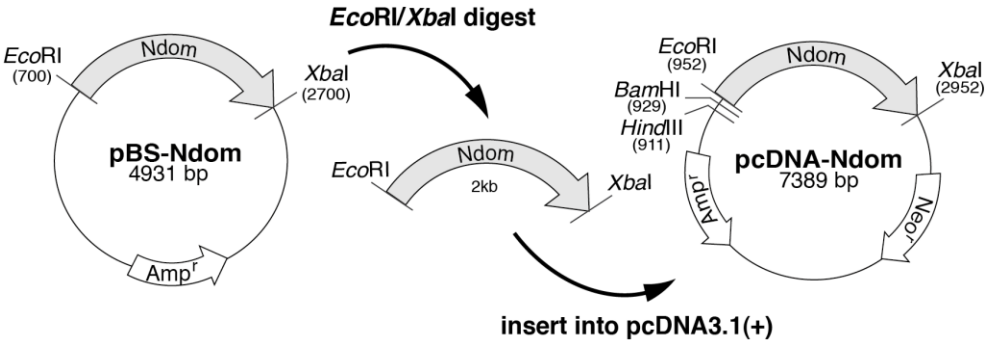

Figure 4.1. Cloning of N domain mutants into pcDNA3.1(+). The ACE N domain containing mutations generated by site-directed mutagenesis was excised from pBS-Ndom via *Eco*RI/*Xba*I. This 2kb fragment was cloned into pCDNA3.1(+).

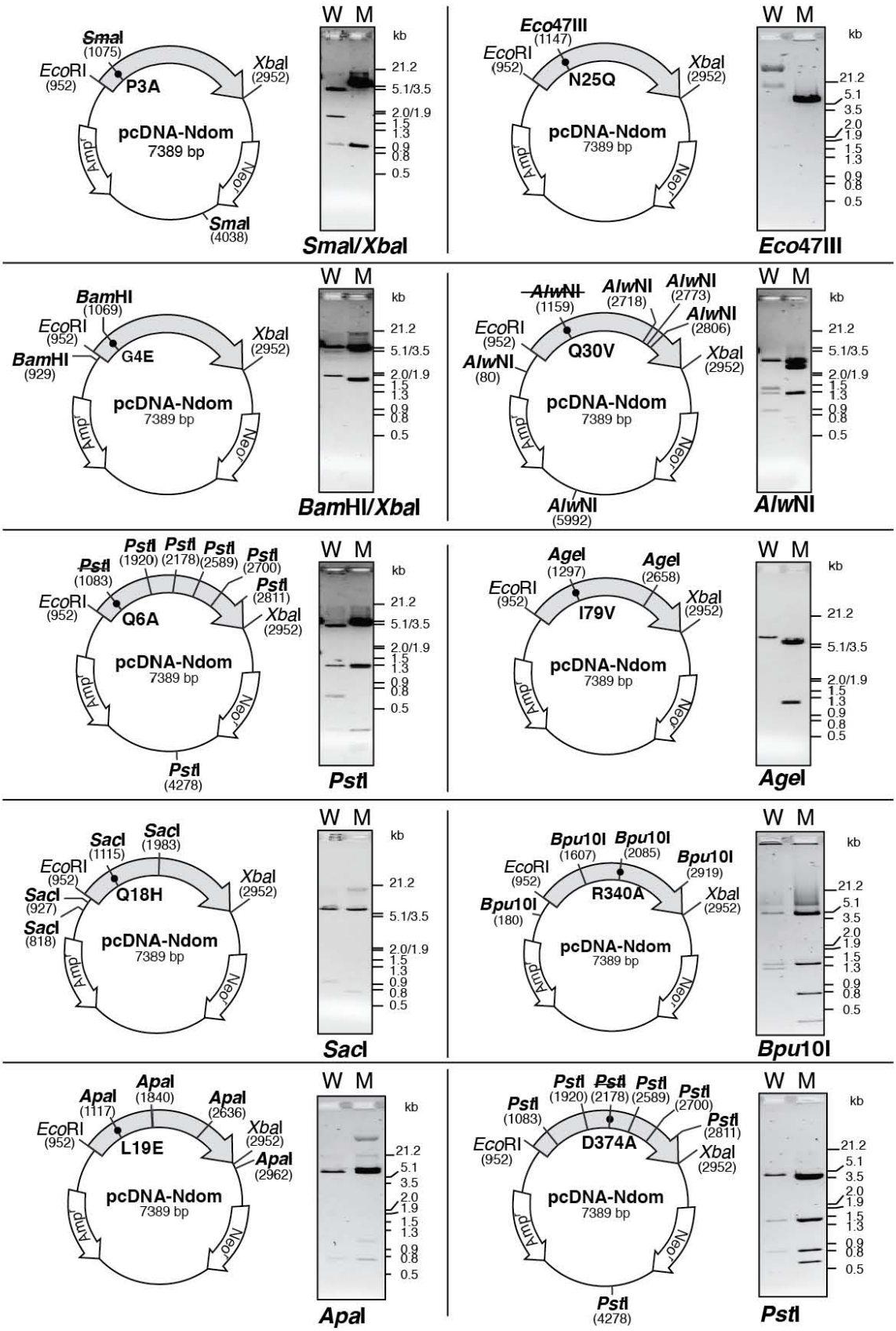

Figure 4.2. Restriction enzyme digestion of pcDNA-Ndom mutants. Each box contains a schematic map of pcDNA-Ndom mutant construct (*left*) and agarose gel electrophoresis of wild-type pcDNA-Ndom (W) and mutant (M) (*right*). The restriction enzyme used for detection of the mutation is indicated (*bold*). The molecular weight marker included in each gel was *Hind*III/*Eco*RI digested lambda DNA.

Site-directed mutagenesis was performed to generate the 10 mutants (highlighted in bold above) using pBS-Ndom as a template (refer to Methods in Chapter 2, Section 2.1.2). Sequencing of the entire N domain insert confirmed the presence of the desired mutations and the lack of any spurious mutations that may have been introduced during mutagenesis. Complete N domain genes containing each of these ten mutants were excised as a 2kb fragment via the restriction sites *Eco*RI and *Xba*I and introduced into pcDNA3.1(+) (Figure 4.1) (Methods in Chapter 2, Section 2.1.3). The correct size and orientation of the insert and the presence of the mutated ACE cDNA was confirmed by restriction enzyme digestion (Figure 4.2).

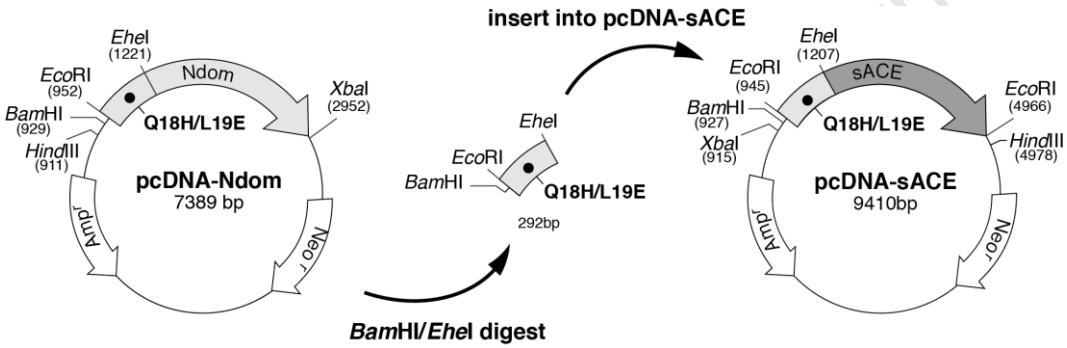

Figure 4.3. Cloning of Q18H and L19E into pcDNA-sACE. A 292bp fragment containing either Q18H or L19E was generated by *Bam*HI/*Ehe*I digestion of pcDNA-Ndom-Q18H and pcDNA-Ndom-L19E respectively and introduced into pcDNA-sACE.

4.2.1.2 Introduction of mutants into full length sACE

Three mutations within the overlapping region of the mAbs 9B9 and 3G8 epitopes - Q18H, L19E and Q22A - were introduced into somatic ACE for further characterisation (refer to Methods in Chapter 2, Section 2.1.3). pcDNA-sACE-Q18H and pcDNA-sACE-L19E were generated using the constructs pcDNA-Ndom-Q18H and pcDNA-Ndom-L19E respectively (Figure 4.3). *Bam*HI/*Ehe*I fragments containing the N-terminal region of Ndom-Q18H and Ndom-L19E were cloned into pcDNA-sACE. sACE-Q22A was generated by site directed mutagenesis of pBS-sACE and the entire sACE cDNA was sequenced using internal primers to the ACE gene, confirming both the presence of the mutation and the lack of any undesired mutations (Methods in Chapter 2, Section 2.1.2). sACE-Q22A was introduced into pcDNA3.1(-) via *Xba*I/*Hind*III sites (Figure 4.4) (Methods in Chapter 2, Section 2.1.3).

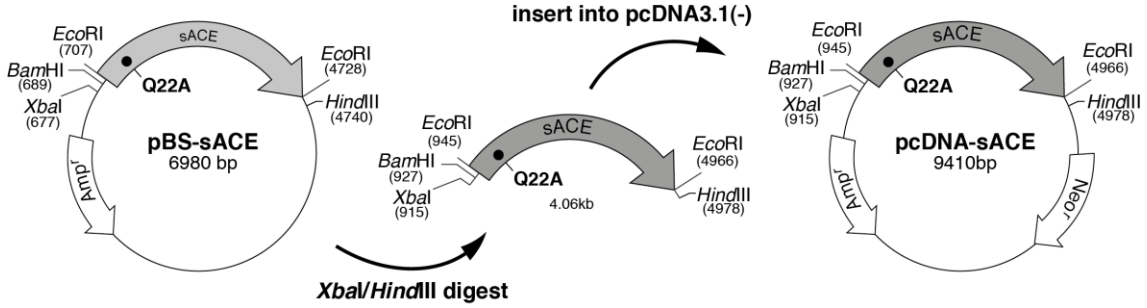

Figure 4.4. Cloning of sACE-Q22A into pcDNA3.1(-). sACE containing Q22A was excised from pBS-sACE-Q22A via *Xba*I/*Hind*III, and the 4.06kb fragment and introduced into pcDNA3.1(-).

Restriction enzyme analysis was performed on the pcDNA-sACE constructs (Figure 4.5). Additional bands observed with *Sac*I, *Apa*I and *Psi*I digestion of pcDNA-sACE-Q18H, pcDNA-sACE-L19E and pcDNA-sACE-Q22A respectively, confirmed the presence of the mutations and the correct size and orientation of the sACE insert.

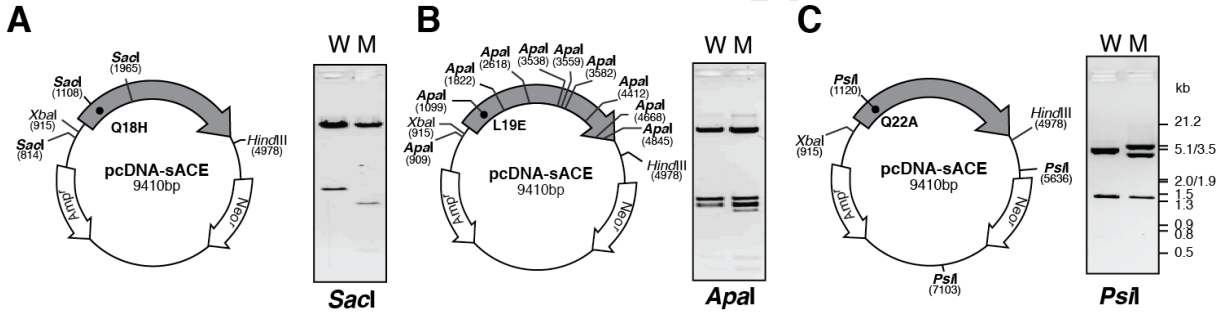

Figure 4.5. Restriction enzyme digestion of pcDNA-sACE mutant constructs. Schematic representation of pcDNA-sACE constructs (*left*) with restriction enzyme used in digestion indicated (*bold*), and agarose gel electrophoresis of wt (W) and mutant (M) pcDNA-sACE contructs (*right*). A. pcDNA-sACE-Q18H, B. pcDNA-sACE-L19E and C. pcDNA-sACE-Q22A.

4.2.2 Expression of N domain mutations in CHO cells

Soluble wt Ndom and the 10 Ndom mutations were stably transfected in CHO cells (refer to Methods in Chapter 2, Section 2.2.1) and ACE detected by activity assay of culture fluid (Methods in Chapter 2, Section 2.2.2). All mutants were active and had comparable activity to wt, indicating that there was no detrimental effect on enzyme expression or function. Sufficient activity was obtained to conduct experiments and these cell lines were expanded (Figure 4.6).

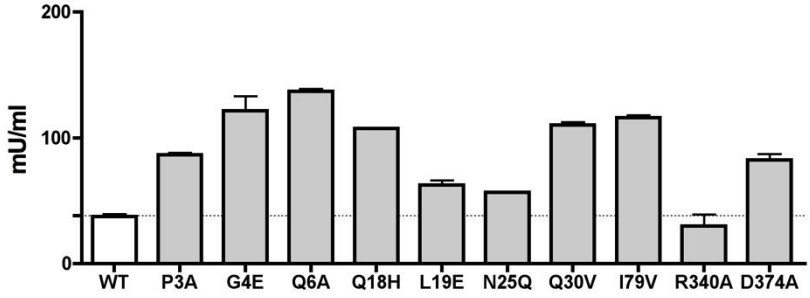

Figure 4.6. ACE activity of Ndom mutants stably expressed in CHO cells. An ACE activity was assay performed on culture fluid harvested from CHO cells after 24 hour incubation. Data is the mean±SD of one experiment performed in triplicate.

4.2.3 Effect of mutations on monoclonal antibody binding to the N domain

Soluble N domain mutants were precipitated from culture fluid by mAbs 9B9, 3G8 and i1A8 to quantitate the effect of these mutations on mAb binding (Figure 4.7) (refer to Methods in Chapter 2, Section 2.2.5).

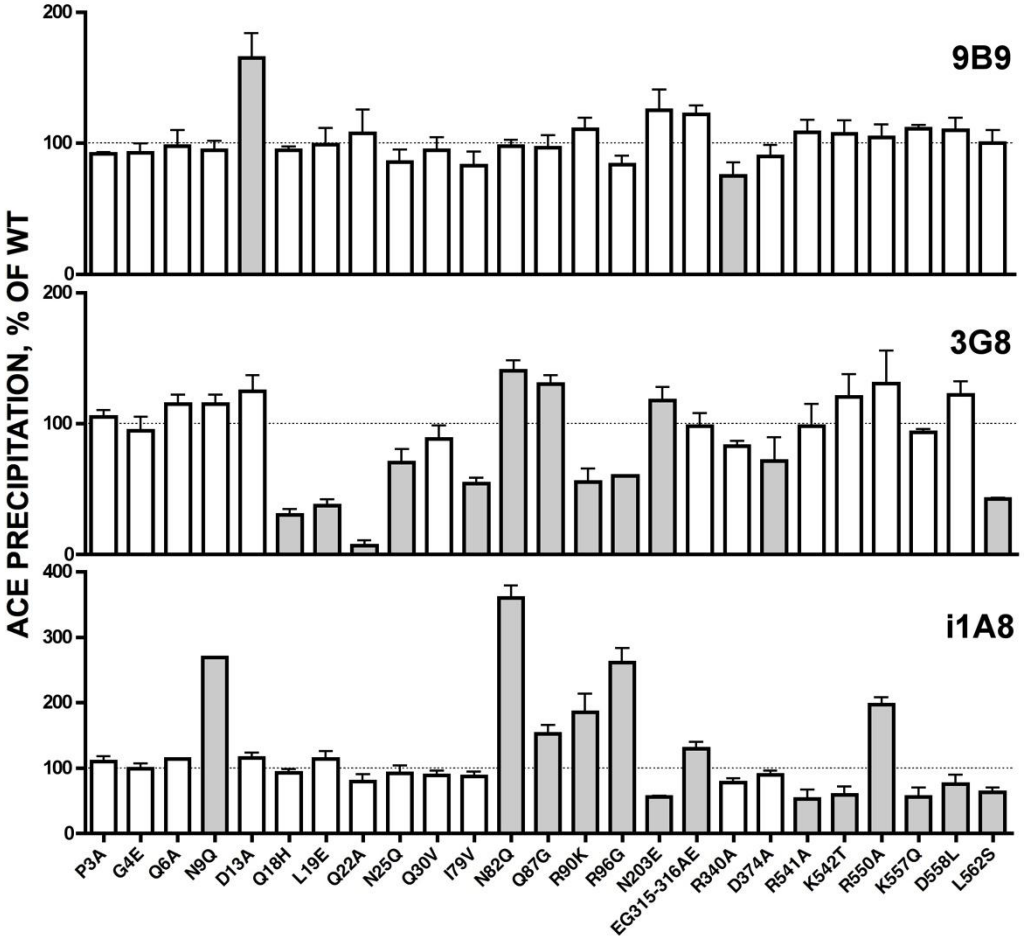

Figure 4.7. The effect of mutations on the precipitation of Ndom ACE by mAbs. Results are expressed as a percentage of precipitated ACE activity from each mutant to that of wt Ndom and shown as mean±SD of 4 to 6 independent experiments, each performed in duplicate or triplicate, changes from wt are indicated (*grey bars*).

Of these mutations, only two had an effect on binding of mAb 9B9; D13A increased binding 1.5-fold and R340A decreased binding by 25%. Both of these residues are conserved across all the mammalian ACE proteins that are recognised by mAb 9B9. Three residues, Q18H, L19E and Q22A had the most marked effect on mAb 3G8 binding (30%, 37% and 7% of wt, respectively). While the removal of glycans at position N25 and N82 either increased or decreased binding respectively, the same mutation at position N9 had no effect. Cross-species reactivity and sequence homology indicated that sites Q22, Q87, R90 and R96 were important residues for mAb 9B9 and 3G8 binding (Gordon *et al*, 2010). Interestingly mutations at all four residues affected binding of mAb 3G8, but had no effect on mAb 9B9 binding. Mutations within the C-terminal region of the N domain altered binding of mAb i1A8, most notably R90K, R96G and L562S (185%, 260% and 60% of wt, respectively). In addition, increased binding of ACE to mAb i1A8 was observed after removal of glycans at sites N9 and N82 (2.5- and 3.5-fold, respectively).

4.2.4 Fine epitope mapping of mAbs 9B9, 3G8 and i1A8 epitopes

Results obtained from cross-species reactivity and sequence homology, immunoblotting of ACE chimeras (Gordon *et al*, 2010) as well as anti-ACE antibody precipitation of N domain mutations generated by site-directed mutagenesis (Figure 4.7) were used for fine epitope mapping of the epitopes of mAbs 9B9, 3G8 and i1A8. The surface structure of the N domain was used to define a 700-800Å^2 area for each epitope, delineated by residues whose mutations altered mAb binding (Figure 4.8).

9B9 Epitope. The epitope for mAb 9B9 was delineated by the 9NFSA12 motif (Gordon *et al*, 2010). The removal of a bulky side chain at residue 13, allowing for better access of the antibody to this motif, would explain the increased precipitation observed with D13A compared to wt. Therefore, this epitope was drawn to include the 9NFSA12 motif and residue R340 (since mutation of this residue decreased binding), but not residues I79, Q87, R90 and D374 because mutation of these sites had no effect on mAb binding.

3G8 Epitope. The mutations that had the greatest effect on mAb 3G8 binding - namely Q18H, L19E, Q22A, I79V, Q87G, R90K, R96G and D374A – defined the area of this epitope where the proposed epitope was drawn to include these residues and exclude D13 and R340, which had no effect. This epitope also includes the glycosylation sequons at sites N25 and N82 that play a role in mAb 3G8 binding based on the site-directed mutagenesis. This

epitope also contains residues within the first 141 amino acids in agreement previous findings (Balyasnikova *et al*, 2005a; Gordon *et al*, 2010).

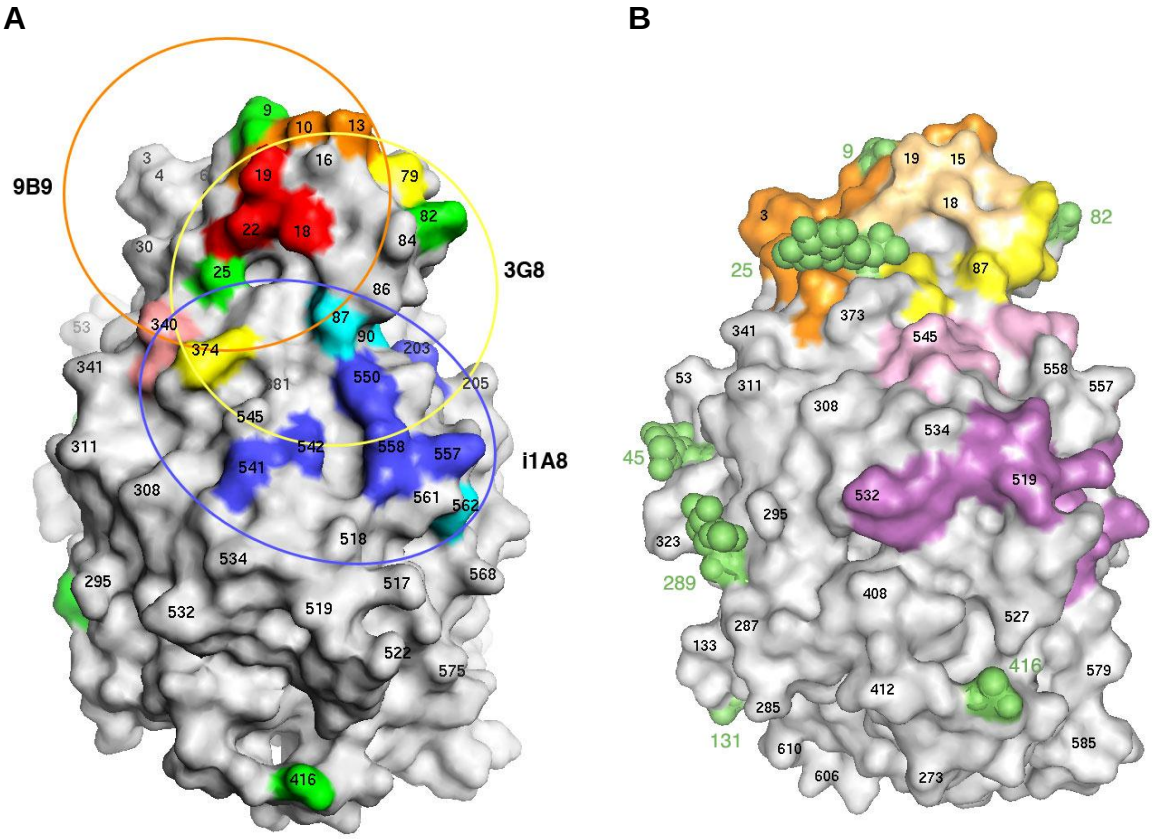

Figure 4.8. Fine epitope mapping of mAbs 9B9, 3G8, and i1A8. Surface representations of Ndom ACE from the crystal structure (PDB accession code 2C6F). A. Amino acid residues whose substitution altered mAb 9B9, 3G8, and i1A8 binding are indicated as follows: mAb 9B9 (*orange*), mAb 3G8 (*yellow*), mAb i1A8 (*blue*), both mAbs 9B9 and i1A8 (*pink*) and both mAbs 3G8 and i1A8 (*cyan*). Residues Q18, L19, and Q22 are highlighted (*red*). The proposed epitopes for mAbs 9B9 (*orange circle*), 3G8 (*yellow circle*), and i1A8 (*blue circle*) are defined. B. Epitope depicted on surface with residues that lie within the epitopes of mAb 9B9 (*orange*), 3G8 (*yellow*), i1A8 (*pink*) and within the overlapping region of mAbs 9B9 and 3G8 (*light orange*). The epitope of mAb 3A5 is indicated for reference (*purple*). Glycosylation sites (*green*) are indicated in both structures.

i1A8 Epitope. The epitope for mAb i1A8 lies closer to the C terminus than the epitopes for mAb 9B9 and 3G8 since mutagenesis of residues in this region affected binding. The limits of this epitope were defined by the residues that had the greatest effect, from N203 to R541 and R340 to L562.

The epitopes of mAbs 9B9, 3G8 and ilA8 overlap to some extent. mAb i1A8 overlaps largely with the epitope of mAb 3A5 (Skirgello *et al*, 2006) (refer to Chapter 1, Section 1.4). Residues Q18, L19, Q22 and N25 lie within the region where epitopes of mAb 9B9 and 3G8, but not mAb i1A8, overlap.

Thus, through fine epitope mapping of mAbs 9B9, 3G8 and i1A8 a region containing residues Q18, L19, Q22 and N25 was identified. Three mutants, Q18H, L19E and Q22A were introduced into full-length sACE to determine their effect on mAb binding, ACE shedding, and dimerisation.

4.2.5 Expression of full-length sACE mutations in CHO cells

Wt full-length sACE, sACE-Q18H, sACE-L19E and sACE-Q22A were stably transfected in CHO cells and clones picked from the transfection dish to elicit high-expressing clones (refer to Methods in Chapter 2, Section 2.2.1). ACE protein was detected by activity assay of culture fluid and cell lysate (Methods in Chapter 2, Section 2.2.2). Sufficient activity was obtained to conduct experiments, albeit low levels of activity were detected in medium. There was a slight increase in ACE activity in the cell lysates of sACE-L19E and sACE-Q22A compared to wt (Table 4.1). This could be due to differences in transfection efficiency or increased ACE expression as the result of the mutation.

Table 4.1. ACE activity of sACE mutants transfected into CHO cells. ACE activity was determined after incubation in 2% FCS for 24 hours. Data is the mean of one experiment performed in triplicate.

	CELLS mU/ml	**MEDIUM** mU/ml
wt sACE	25.06 ± 1.58	0.14 ± 0.02
sACE-Q18H	26.52 ± 3.08	0.23 ± 0.04
sACE-L19E	50.22 ± 8.69	0.51 ± 0.02
sACE-Q22A	51.63 ± 6.29	0.56 ± 0.04

4.2.6 Effect of Q18H, L19E and Q22A on shedding of sACE

Basal shedding of the mutant cell lines was determined by calculating the ratio of ACE activity in the medium versus the total in medium and cell lysate, after a prolonged incubation in minimal medium (Figure 4.9) (refer to Methods in Chapter 2, Section 2.2.4). Shedding of wt sACE was low, with 3-6% activity detected in medium, as reported previously (Woodman *et al*, 2000).

Basal shedding of sACE-Q18H, sACE-L19E and sACE-Q22A was significantly higher than that of wt (181% ± 25%, 203% ± 41% and 197% ± 28%, respectively). This indicates that the three single mutations have increased the efficiency of shedding.

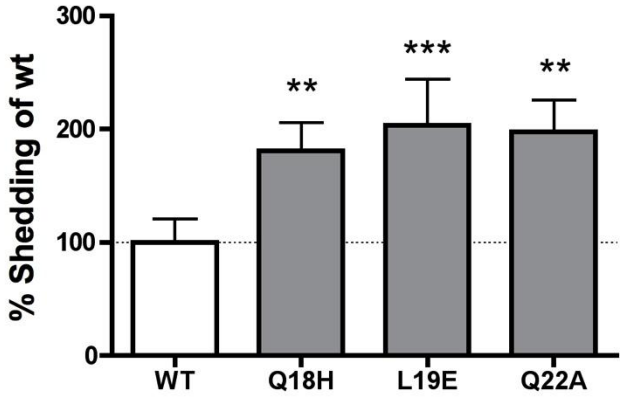

Figure 4.9. Basal shedding of wild-type sACE, sACE-Q18H, sACE-L19E, and sACE-Q22A. Shedding was calculated as the percentage ACE activity in harvested medium of total activity in cell lysate and medium. Results are mean±SD of three experiments performed in triplicate, presented as percentage total ACE shed of wild-type.

4.2.7 Effect of Q18H, L19E and Q22A on mAb binding to membrane bound sACE

Changes in mAb 9B9 and 3G8 binding to full-length sACE constructs was determined with an ELISA assay on live cells (refer to Methods in Chapter 2, Section 2.2.6). mAb 3A5 was included as a positive control for ACE-mAb interaction as it binds strongly to the N domain of sACE (Figure 4.10) (Balyasnikova *et al*, 2002). Increased mAb 9B9, 3G8 and 3A5 binding was observed for sACE-Q18H, sACE-L19E and sACE-Q22A compared to wt (Figure 4.10A), which agrees with the higher ACE activity detected in cell lysate and further confirms the increased levels of ACE expression in these cell lines. However, no significant difference in mAb binding to sACE-Q18H, sACE-L19E and sACE-Q22A was observed for ACE mAb, when normalised for increases in cell surface expression (Figure 4.10B). This suggests that none of these residues is responsible for mAb binding alone. However, significant differences were observed when single N domain mutants were precipitated from culture fluid by the same ACE mAbs (Figure 4.7). Since the single N domain was used for precipitation and full-length sACE was used in the ELISA experiment, different criteria for mAb binding would be involved which could include changes in surface structure, glycosylation patterns and in the case of sACE inter-domain interaction(s). Furthermore the differences in experimental setup could explain the change in binding observed.

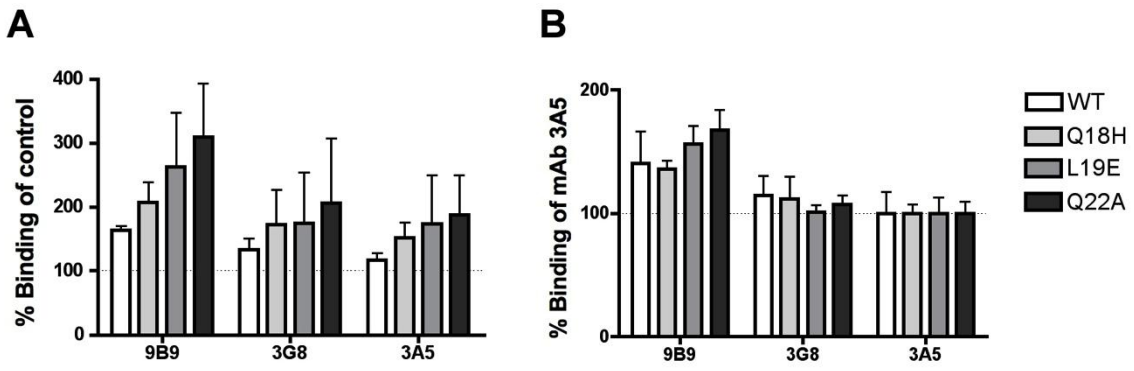

Figure 4.10. Cell ELISA of sACE constructs. A. Results are shown as percentage binding of control antibody, IgG, and B. % percentage binding of mAb 3A5, mean±SD of three separate experiments performed in triplicate

4.2.8 Effect of mutations on ACE shedding in the presence of mAbs

The presence of certain ACE mAbs in culture fluid has been shown to have an effect on ACE shedding from the surface of CHO cells (Balyasnikova *et al*, 2002; Kost *et al*, 2003; Skirgello *et al*, 2006). Both mAb 9B9 and 3A5 significantly increase the amount of somatic ACE shed from the cell surface (2.7 and 4.1-fold, respectively) (Balyasnikova *et al*, 2002), whereas mAb 3G8 has been shown to have an inhibitory effect (36% decrease in shedding) (Balyasnikova *et al*, 2002). The effect of the Q18H, L19E and Q22A mutations on mAb-induced shedding of sACE from CHO cells was determined (Figure 4.11) (refer to Methods in Chapter 2, Section 2.2.4.2). Wt sACE, sACE-Q18H, sACE-L19E and sACE-Q22A were incubated in the presence of mAbs 9B9 and 3G8 and with mAb 3A5, a positive control for shedding, and with IgG and mAb i2H5, negative controls for antibody binding and shedding respectively. As expected, shedding of wt, sACE-Q18H, sACE-L19E and sACE-Q22A was increased in the presence of mAbs 3A5 (2.4 to 3-fold), but not with IgG and i2H5. Shedding of wt sACE was increased in the presence of mAb 9B9 (1.2-fold) as previously shown (Balyasnikova *et al*, 2002) and no significant change in shedding occurred in the presence of mAb 3G8. There was no significant change in shedding of mutant sACE compared to wt. Thus, it seems that these single mutations have no effect on mAb 9B9-induced shedding of ACE and that Q18, L19 and Q22 alone are not involved in this mechanism. It was surprising that Q18H, L19E and Q22A had no effect on mAb 3G8-induced shedding since the noticeable effect these mutations had on binding of the N domain (Figure 4.7) suggested that they may be involved. As with mAb 9B9, this may be due to synergistic effects by more than one residue in the overlapping region of the two epitopes. Also, mAb 3G8 binds sACE poorly

compared to other antibodies such as mAbs 9B9 and 3A5, which could explain why the inhibitory effect of this antibody was not observed in any of the cell lines.

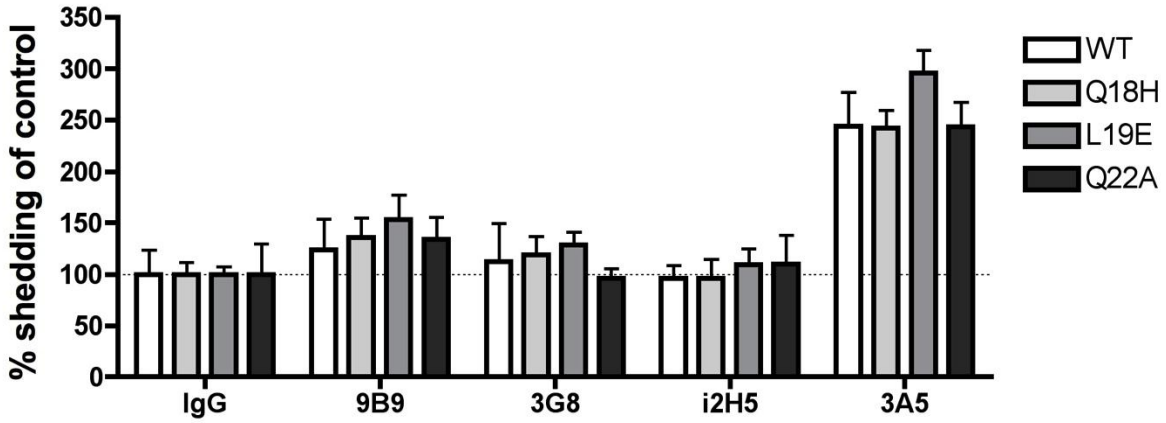

Figure 4.11. mAb-induced shedding performed on sACE cell lines. Results are a mean±SD of three experiments performed in triplicate and expressed as the percentage shedding of IgG control.

The low expression levels of these cell lines resulted in minimal ACE activity in culture fluid (Table 4.1). Thus, the shedding assay and ACE activity assay were optimised to allow for reproducibility in these experiments. The incubation time of the cell lines was increased from 4 hours to 24 hours to allow for sufficient accumulation of ACE in culture fluid to be detected by the activity assay. Incubation times in the activity assay were also extended to obtain sufficient values above background. Since these conditions were not optimal, this may explain the large degree of error observed in the experiments.

4.2.9 Effect of mutations on ACE dimerisation

Since it was shown in reverse micelles that mAbs 9B9 and 3G8 inhibit homodimerisation of both sACE and the N domain (Kost *et al*, 2003), the effect of Q18H, L19E and Q22A on dimerisation of sACE in CHO cells was investigated (Figure 4.12). CHO cells expressing wt sACE, sACE-Q18H, sACE-L19E and sACE-Q22A were incubated either in the presence or absence of the membrane-impermeable crosslinker bis[sulfosuccinimidyl] suberate (BS^3) and immunoblotting performed on cell lysate under both non-reducing and reducing conditions (refer to Methods in Chapter 2, Section 2.2.8). Under non-reducing conditions in the absence of crosslinker, sACE resolved as three distinct bands of approximately 190, 350 and >400kDa which are equivalent in size to an ACE monomer (M), dimer (D1) and oligomer (O). There

was no significant difference between the wt and mutants with respect to D1 (Figure 4.12A, -BS^3 lanes). With the addition of the reducing agent, DTT, the oligomer disappears and the dimer is visibly reduced (Figure 4.12B, -BS^3 lanes). The dimer population that is still present could be formed through non-covalent interactions, although these would most likely be disrupted during sample preparation. An alternative is that these are covalently-mediated and that there was incomplete reduction of the dimeric species. These observations seem to indicate the involvement of intermolecular disulphide bridges in ACE dimerisation/oligomerisation.

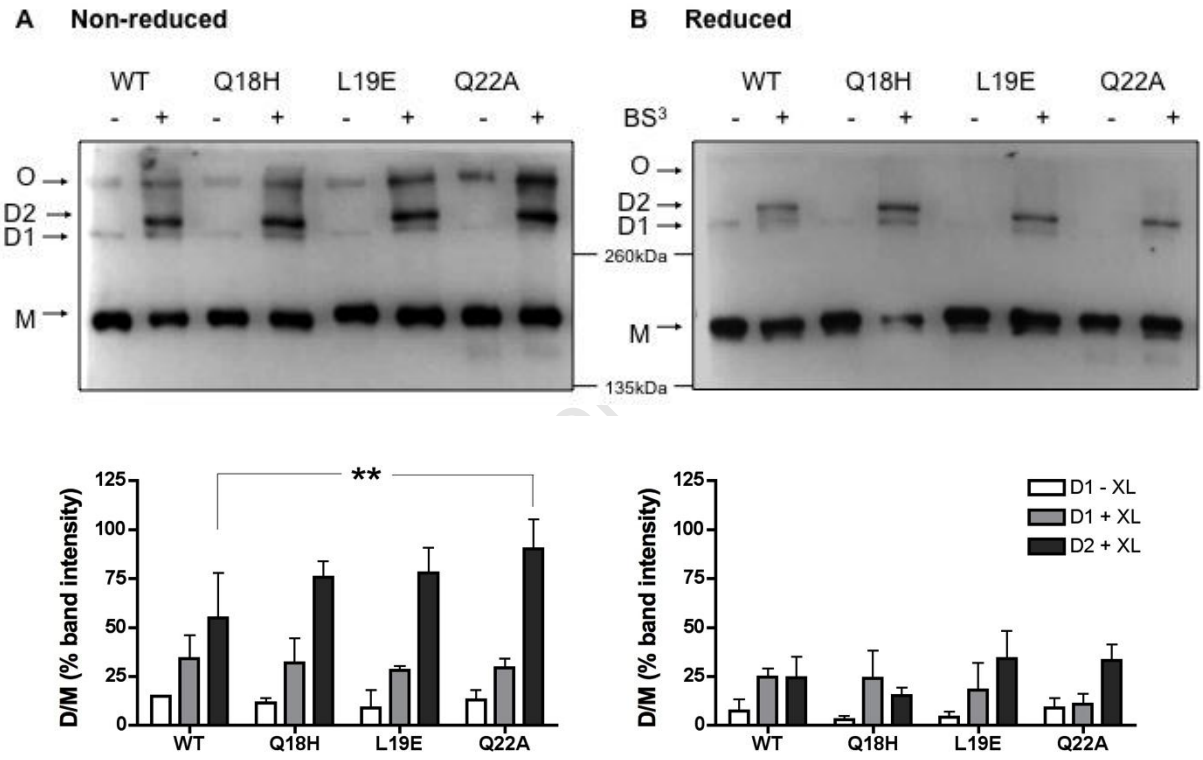

Figure 4.12. Crosslinking and western blot analysis of sACE constructs. A and B. Representative blots of three separate experiments is shown (*top*), ACE was detected with the C domain-specific mAb 1D8. Densitometry was performed to determine the relative intensity of each band to the monomer (*bottom*). In each panel, values are mean ± SD. O: oligomer; D1: dimer; D2: crosslinked dimer; M: monomer; XL: crosslinker.

In the presence of BS^3, an additional, slightly larger dimeric form of ACE (D2) appears that has greater intensity than the dimeric form observed in the absence of crosslinker (D1) (Figure 4.12, +BS^3 lanes). In the absence of reducing agent, this form is significantly increased with sACE-Q22A compared to wt, but not sACE-Q18H and sACE-L19E (Figure 4.12A, + BS^3 lanes). Under reducing conditions, the higher molecular weight forms of both unmodified and crosslinked samples lose intensity with all cell lines (Figure 4.12B).

This could be the result of a mixed population of susceptible disulphide-mediated and insufficiently crosslinked dimers. The appearance of an additional dimer in the presence of crosslinker can be explained as follows: first, dimers formed by the action of BS^3 may have decreased mobility and would thus resolve as larger forms compared to the non-cross linked dimers. Second, crosslinking may have resulted in an ACE heteromer, as has been shown with carboxypeptidase M (CPM) (Sun *et al*, 2008). It must be noted that the latter study was conducted using Madin-Darby canine kidney (MDCK) cells transfected with ACE, which have high endogenous expression of CPM. Third, the crosslinked dimer (D2) may be a fully glycosylated form whereas the non-crosslinked form is a disulphide-mediated form of immature ACE glycoforms. The two glycoforms are routinely observed by immunoblotting of cell lysates from ACE expressing cells under reducing conditions (Ehlers *et al*, 1992, Kasturi *et al*, 1994).

Crosslinking of ACE on the cell surface facilitated the visualisation of ACE dimers that are most likely mediated by non-covalent interactions. The overlapping region of the mAbs 9B9 and 3G8 epitopes is implicated given that increased formation of D2 was observed for sACEQ22A.

4.3 DISCUSSION

MAbs to ACE are valuable tools in western blotting (Balyasnikova *et al*, 2008), ELISA (Danilov *et al*, 1996), immunohistochemistry (Danilov *et al*, 1987) and flow cytometry (Danilov *et al*, 2003). Furthermore, our understanding of the structural and functional aspects of ACE shedding (Balyasnikova *et al*, 2002; Balyasnikova *et al*, 2005a), dimerisation (Kost *et al*, 2003; Gordon *et al*, 2010), binding and the detection of inhibitors (Balyasnikova *et al*, 2005b) and mutations (Kramers *et al*, 2001; Nesterovitch *et al*, 2009; Danilov *et al*, 2010b) has been improved by the use of mAbs to ACE. Fine epitope mapping of mAbs defines regions that may be involved in these functions and in this study the epitopes of the mAbs 9B9, 3G8 and i1A8 were scrutinised in order to define a region that may be involved in shedding and dimerisation.

Both mAbs 9B9 and 3G8 have been shown to inhibit N domain dimerisation in reverse micelles (Kost *et al*, 2003). Furthermore, shedding of sACE from CHO cells is induced by mAb 9B9 whereas mAb 3G8 was shown to have an inhibitory effect (Balyasnikova *et al*, 2002). The third mAb, i1A8, has no effect on dimerisation or shedding despite the proximity of its epitope to those of mAbs 9B9 and 3G8 (Danilov *et al*, 1994) and was therefore useful in ruling out candidate regions.

Site-directed mutagenesis was performed on the N domain to identify residues involved in mAb binding. Together with findings from cross-species reactivity and comparison of the N domain secondary structure (Gordon *et al*, 2010), fine epitope mapping of these three mAbs was performed (Figure 4.8). mAbs 9B9 and 3G8 were mapped to the N-terminal region and mAb i1A8 to the region overlapping the epitope of mAb 3A5 (Danilov *et al*, 1994). Interestingly, mAb 3A5 has anti-catalytic effects and induces shedding whereas binding of mAb i1A8 does not (Balyasnikova *et al*, 2002, Skirgello *et al*, 2006). An overlapping region of the epitopes of mAb 9B9 and 3G8, but not i1A8, contained residues important for binding of mAb 3G8, namely Q18, L19, Q22 and N25.

Full-length sACE variants of Q18H, L19E and Q22A were stably expressed in CHO cells to determine the effects of these mutations on mAb binding, shedding and dimerisation.

There was noticeable increase in surface expression, detected by both activity assays of cell lysate and by cell ELISA (Table 4.1 & Figure 4.10A). In addition, the mutations led to a significant increase in shedding (Figure 4.9). This implicates these residues and the overlapping region of the epitopes of mAbs 9B9 and 3G8 in ACE processing, particularly its cleavage secretion.

The recognition motif for the cognate ACE secretase has yet to be identified and it is possible that regions in the N domain may be involved in interaction with the secretase, particularly since some sheddases have been shown to require interaction with regions distal to the cleavage site for proteolysis (Takeda *et al*, 2006). Tyrosine phosphorylation in the ectodomain was shown to increase ACE shedding, further implicating the distal domains in ACE cleavage secretion (Santhamma *et al*, 2004).

This region may be involved in dimerisation and have an effect on shedding. The orientation of the N domain with respect to the C domain is likely to have an effect on cleavage secretion (Woodman *et al*, 2000; Woodman *et al*, 2005) and it may be this alone that is responsible. This is reinforced by the proposal that binding of mAbs 9B9 and 3G8 position sACE in such a way as to respectively allow or obstruct access of the secretase (Balyasnikova *et al*, 2005a; Kost *et al*, 2003). Residues within the overlapping region of mAbs 9B9 and 3G8 may be involved in domain interaction, evidenced by the fact that the mAb 3G8 epitope may be partly occluded by the C domain (Gordon *et al*, 2010). Mutations of Q18, L19 and Q22 that enhance shedding may alter the orientation of the two domains, improving the interaction of the C domain with the secretase. However, these mutations had no effect on shedding in the presence of mAbs suggesting a synergistic effect involving a number of residues.

The role of the overlapping region of the two epitopes of mAbs 9B9 and 3G8 in dimerisation was investigated by western blotting (Figure 4.12). Both mAbs inhibit dimerisation of the N domain and sACE in reverse micelles (Kost *et al*, 2003), implicating this domain in dimer formation. Furthermore, competitive inhibition of dimerisation in the same system by carbohydrates such as Neu5Ac- and Gal-terminated saccharides suggests that this may involve a carbohydrate recognition domain. This is reinforced by the appearance of dimers after crosslinking, most likely mediated by non-covalent interactions. The increased formation of crosslinker dimer upon mutation of Q22 points towards the involvement of this overlapping region. Glycan sequons N9 and N82 are proximal and N25 lies within this region, all three sites are glycosylated in the N domain (Anthony *et al*, 2010) and could potentially be involved in dimer formation. Kohlstedt *et al* (2006) found that sACE overexpressed in porcine aortic endothelial cells and endogenous ACE in primary HUVEC is present in both monomeric and dimeric forms. These dimers are significantly increased in the presence of ACE inhibitors and require an active C domain. The addition of mAbs 9B9 and 3G8 as well as saccharides had no effect on ACE inhibitor induced dimerisation in porcine aortic endothelial cells. There is no reason to accept that this mechanism and that observed in

reverse micelles are one and the same. It is possible that ACE dimerisation is mediated by both non-covalent, via glycans, and covalent interactions, via disulphide-bridges, as has been seen with the human bradykinin B2 receptor (Michineau *et al*, 2006). Furthermore, the presence of dimers in the absence of crosslinking and their susceptibility to reducing agents suggests that covalent interactions may be involved. The role of disulphide-bridge formation in ACE dimerisation is explored further in Chapter 5.

The role of dimerisation in ACE processing is unclear. The inhibition of dimerisation by mAbs 9B9 and 3G8 implicates this process in shedding since both these mAbs have been shown to affect cleavage secretion of ACE expressed in CHO cells (Balyasnikova *et al*, 2005a; Kost *et al*, 2003). Furthermore, mutations in the overlapping regions of the epitopes of these mAbs have a significant effect on shedding from CHO cells. Mutation of Q22 significantly increases dimerisation, compounding the link between dimerisation and shedding. ACE inhibitor induced dimerisation mediated via the C domain initiated the ACE signalling cascade (Kohlstedt *et al*, 2006). It seems that these two mechanisms involve distinct regions on both domains and it will be useful to determine the relationship between non-covalent and covalent mechanisms of ACE dimerisation and what role they play in ACE processing.

CHAPTER 5: The role of free thiols in dimerisation and shedding

5.1 INTRODUCTION

The cellular control of ACE expression and cleavage secretion is not clearly understood. It has been shown that ACE inhibitor binding can initiate an intracellular signalling cascade via the c-Jun/Fos pathway that leads to increased ACE expression (Kohlstedt *et al*, 2002; Kohlstedt *et al*, 2004) (refer to Chapter 1, Section 1.3.5). The relationship between this signalling process and the cleavage secretion of ACE are unclear as are the mechanisms which control ACE shedding. Recent insights into the dimerisation of ACE may shed light on these processes. Dimerisation is an important event for the function of membrane proteins. Hetero- and homo-dimerisation of receptor tyrosine kinases (RTK's) such as vascular endothelial growth factor (VEGF-R) (Claffey *et al*, 1995), the epidermal growth factor receptor (EGF-R) (Ferguson *et al*, 2003) occurs upon substrate binding and initiates intracellular signalling cascades. The cleavage secretion of the Aβ peptide from amyloid precursor protein (APP), a type I membrane protein, appears to be dependent on homodimer formation (Scheuermann *et al*, 2001).

ACE can form a homodimer and this process initiates ACE inhibitor induced signalling (Kohlstedt *et al*, 2006). Furthermore, an overlapping region of the epitopes of N domain-specific mAbs 9B9 and 3G8 has been implicated in dimerisation and shedding (Kost *et al*, 2003). Of interest in these two studies are the proposed interactions involved in dimerisation. Kost *et al* (2003) showed that dimerisation of human sACE and the N domain alone in reverse micelles could be inhibited in the presence of galactose and propose that a carbohydrate recognition domain in the N domain mediates dimerisation (Kost *et al*, 2003). Alternatively, sACE active mutants overexpressed in porcine aortic endothelial cells showed that a catalytically active C domain was required for dimerisation and initiation of signalling (Kohlstedt *et al*, 2006). Despite the apparently contradictory findings of these two studies, it is possible that more than one mechanism is involved.

Dimerisation can be mediated via non-covalent interactions involving the reactive side groups of the peptide backbone, mainly through the hydrophobic effect (Jones *et al*, 1995), and through the glycan residues of glycoproteins, as with follicle-stimulating hormone (Ulloa-Aguirre *et al*, 1999) and human bradykinin B2 receptor (Michineau *et al*, 2006). Strong covalent interactions also occur through inter-chain disulphide bond formation, such as the

homodimer formation of endothelin converting enzyme 1 (ECE-1), a type II membrane protein, with similar functional properties to ACE (Shimada *et al*, 1996). There is evidence for the involvement of both non-covalent and disulphide-mediated dimer formation in a number of proteins, where there appears to be dependence of the formation of one type of interaction on the formation of the second. For example, the MAM domain of the membrane protein meprin forms disulphide-mediated dimers that stabilise the molecule and allow for the formation of non-covalent interactions (Marchand *et al*, 1996) via glycans (Ishmael *et al*, 2006). A similar mechanism is involved in the homodimerisation of a number of G-protein coupled receptors (GPCRs) such as the human B2-R (Michineau *et al*, 2006) and glycoprotein VI (GPVI) (Arthur *et al*, 2007).

Thus, it is possible that the formation of ACE homodimers on the cell surface occurs via both non-covalent and covalent interactions, the latter involving inter-chain disulphide interactions.

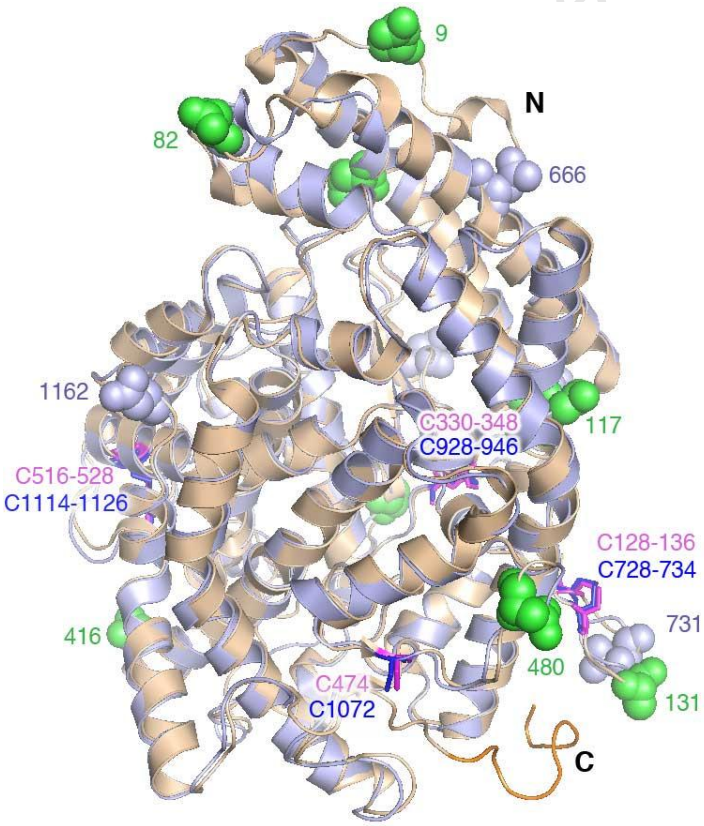

Figure 5.1. Bonded and non-bonded cysteine residues in ACE. Overlay of Ndom (*light orange*) and tACE (*blue-grey*) crystal structures with cysteine residues shown in magenta (*N domain*) and blue (*C domain*). The three intra-chain disulphide bridges are indicated, in pink (*N domain*) and blue (*C domain*). The linker region at the C-terminal end of the N domain (*orange*) and glycans (*green spheres*) are shown.

The N and C domains of sACE each contain seven cysteine residues that form three intra-chain disulphide bridges with a high degree of structural homology between each domain (Figure 5.1). According to the crystal structures of each domain, two of these disulphide bridges are buried within the structure, whereas the third (N domain: C126-C138, C domain: C728-734) lies within a flexible loop on the surface. The final cysteine (N domain: C474, C domain: C1072) is present in the reduced form (Sturrock *et al*, 1996) and lies on the surface of the structure, proximal to the C terminal region of each domain. This group may be involved in the formation of inter-chain disulphide bonds responsible for dimer formation. Furthermore, these interactions may be important in cellular processes such as signalling and shedding.

Thus, the aim of this study was to determine the role of the free thiols in each domain of sACE.

This included the following objectives:

1. To investigate the role of free thiols by site-directed mutagenesis and Western blotting.
2. To determine the role of each domain in disulphide-mediated dimerisation.
3. To determine the effect of removal of free thiols on shedding and ACE conformation.

5.2 RESULTS

5.2.1 Detecting mechanisms of ACE dimer formation

Based on the observations that ACE dimerisation may be the result of non-covalent interactions in the N domain (Kost *et al*, 2003) and/or covalent interactions in the C domain (Kohlstedt *et al*, 2006), native PAGE and western blotting analysis was performed on total cell lysate from CHO cells expressing sACE (Figure 5.2) (Methods in Chapter 2, Sections 2.2.7.2 & 2.2.8). The resolution of sACE was determined under native conditions in the presence of the reducing agent β-ME, which would disrupt any covalent disulphide-mediated interactions. In addition, samples were resolved in the presence of SDS to detect non-covalent interactions that would be susceptible to addition of this solvent. Under native conditions sACE in CHO cell lysate resolves at >260kDa, corresponding to a dimeric form. Addition of β-ME results in the appearance of a second band, resolving at approximately 190kDa, the expected size of an ACE monomer, with the majority of ACE detected as the higher MW form. In the presence of SDS, ACE resolves predominately as the 190kDa form with a second higher MW form and a faint higher MW band is still visible. From these results, it appears that sACE resolves predominantly as a higher MW form that is susceptible to SDS and are thus most likely forms aggregates mediated by non-covalent interactions. A smaller population is susceptible to β-ME suggesting the involvement of disulphide bridges.

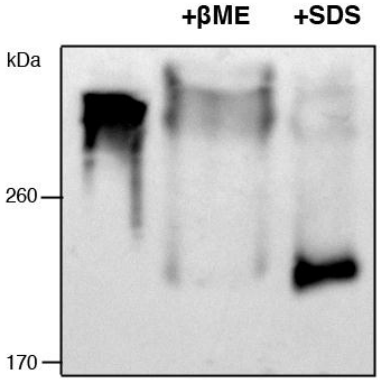

Figure 5.2. Dimerisation of sACE. Total cell lysate from CHO cells expressing full-length sACE was separated by 7% native PAGE under non-reducing, reducing (+βME) and denaturing (+SDS) conditions. sACE was detected by western blotting using the N domain-specific mAb 1D8.

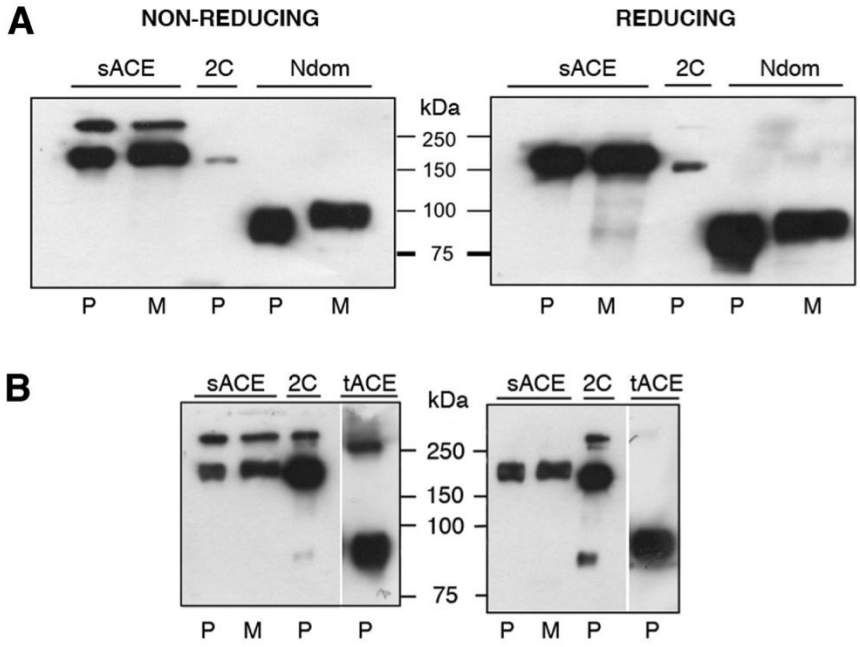

Figure 5.3. Covalent dimerisation of ACE isoforms. A. Western blotting analysis using the N domain-specific mAb 4G6 and B. with the C domain-specific antibody 1D8 in the absence (*left*) and presence (*right*) of β-ME. Purified protein (P) and concentrated medium (M) harvested from CHO-ACE cells were used as sources of ACE. sACE: somatic ACE, Ndom: soluble N domain construct, 2C: CCdom-ACE chimera, tACE: soluble tACE-Δ36NJ.

5.2.2 The role of each domain in disulphide-mediated dimerisation

Analysis of ACE single domain constructs was performed to determine the role of each domain in disulphide-mediated dimerisation. Purified sACE, tACE-Δ36NJ and Ndom as well as the two domain CCdom-ACE chimera were used as sources of ACE (for a description of these constructs refer to Chapter 2, Section 2.1.1). Medium harvested from CHO cells expressing soluble sACE and Ndom was included. Samples were separated by SDS-PAGE under non-reducing and reducing conditions and western blotting analysis was performed (Figure 5.3) (Methods in Chapter 2, Section 2.2.8). Under reducing conditions, sACE resolved as a 190kDa band in both purified and medium samples, detected with both mAbs. A higher MW form was observed under non-reducing conditions for both purified sACE and medium samples (approx. 350kDa), corresponding to a dimeric form. The loss of this higher MW form in the presence of reducing agent indicates that it is formed by a disulphide-mediated interaction. The CCdom-ACE chimera resolved at a similar size as sACE with a similarly sized higher MW form. An additional band resolving at approximately 75kDa, similar to the mobility of tACE, is most likely a product of limited proteolysis in the linker region, separating the two domains (Woodman *et al*, 2005). Under non-reducing conditions

tACE runs as two bands, one at 75kDa and the other at approximately 250kDa. The latter disappears in the presence of reducing agent. The formation of a dimeric, or from the size, an oligomeric, disulphide-mediated dimer would explain the presence of this higher MW form. Ndom resolved as a 90kDa band, larger than tACE, since this domain is more extensively glycosylated than the C domain. No higher MW forms were observed under non-reducing conditions. From these results, it appears that sACE is able to form a disulphide-mediated dimer via residues in the C domain.

5.2.3 Homo-dimerisation of purified sACE

To confirm that the higher MW bands observed by non-reducing western blotting correspond to ACE homodimers and not heterodimeric forms, purified sACE was separated by 2D-PAGE (Methods in Chapter 2, Section 2.2.7.1). Protein was separated in the first dimension by SDS-PAGE under non-reducing conditions. A band corresponding to the ACE monomer was observed at approximately 190kDa. Two higher MW bands could be observed, consistent with previous immunoblotting of crosslinked sACE cell lysate (Figure 5.4). Electrophoresis was then performed in the second dimension in the presence of β-ME. The two higher MW bands co-migrated with the monomer, indicating that these are indeed ACE, most likely homodimers in two conformations. Alternatively, a higher MW form could be a heterodimer formed between ACE and another protein. However, in the second dimension, both higher MW bands resolved at the same size as the monomeric form.

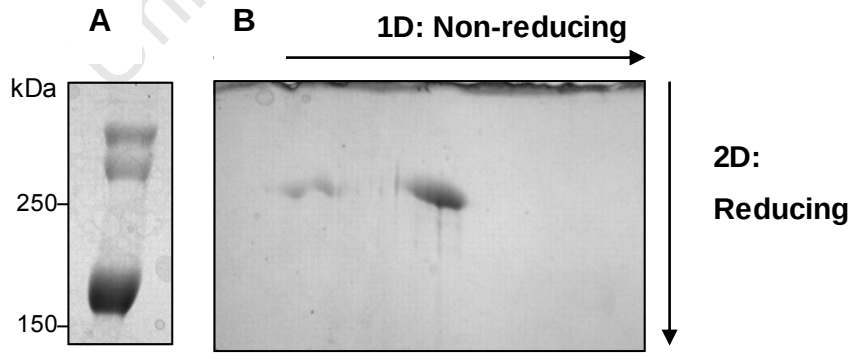

Figure 5.4. Two-dimensional electrophoresis of purified sACE. A. sACE was separated by non-reducing 7% SDS-PAGE and then B. separated by reducing SDS-PAGE in the second dimension in the presence of β-ME. Protein was visualised by Coomassie Blue staining.

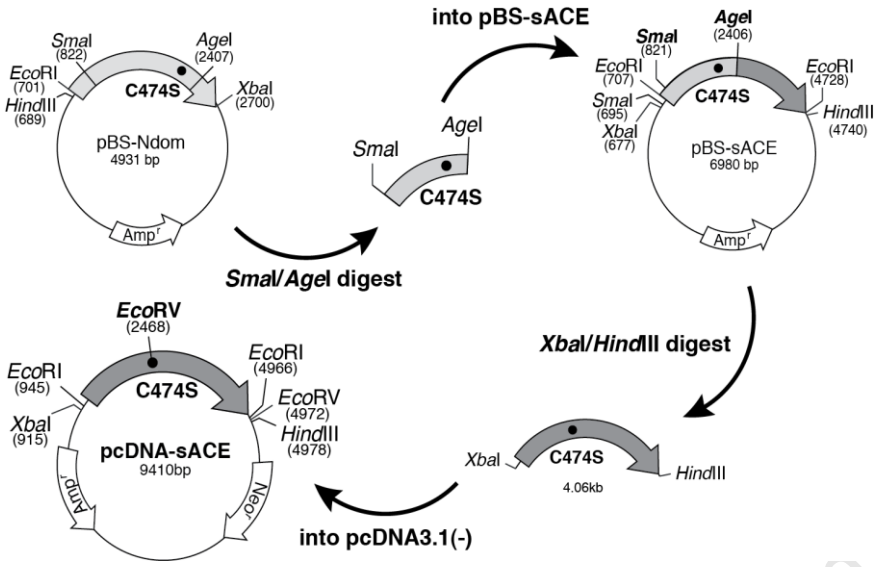

Figure 5.5. Subcloning of C474S into pcDNA. A 1.5kb N domain fragment containing C474S (*top, middle*) was excised from pBS-Ndom (*top, left)* by *Sma*I/*Age*I digestion. This fragment was introduced into pBS-sACE, generating pBS-sACE-C474S (*top, right)*. *Xba*I/*Hind*III digestion removed sACE cDNA (4.06kb) containing C474S (*bottom, right)*, which was introduced into pcDNA3.1(-) producing pcDNA-sACE-C474S (*bottom, left*).

5.2.4 Mutagenesis and expression of free thiol mutants

5.2.4.1 Removal of free thiols by site-directed mutagenesis and introduction of mutants into a mammalian expression vector

The free thiols in the N domain (C474) and the C domain (C1072) were mutated to serine residues by site-directed mutagenesis using pBS-Ndom and pBS-sACE, respectively, as templates (Methods in Chapter 2, Section 2.1.2). Mutagenesis was confirmed by nucleotide sequencing of the entire Ndom and sACE genes using primers complementary to pBS and internal primers complementary to the ACE gene. No spurious mutations were detected in the C474S and C1072S constructs. Three full-length sACE constructs were produced by subcloning the two mutants into the mammalian expression vector, pcDNA3.1(-) (Methods in Chapter 2, Section 2.1.3.) They contain a single free thiol in the C domain (C474S), a single free thiol in the N domain (C1072S) and lack both free thiols (CC/SS).

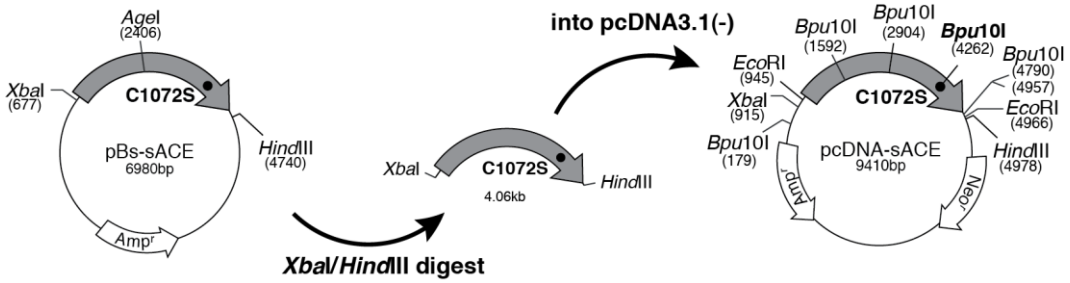

Figure 5.6. Subcloning of C1072S into pcDNA. The 4.06kb sACE cDNA insert containing C1072S (*middle*) was excised from pBS-sACE (*left)* by *Xba*I/*Hind*III digestion and introduced into pcDNA3.1(-), generating pcDNA-sACE-C1072S (*right)*.

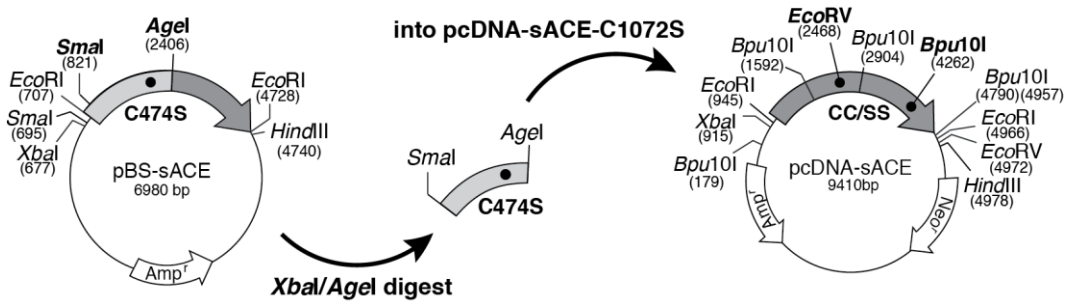

Figure 5.7. Construction of CC/SS in pcDNA. The 1.5kb N domain fragment containing C474S (*middle*) was excised from pBS-sACE-C474S (*left)* by *Sma*I/*Age*I digestion and introduced into pcDNA-sACE-C1072S, generating pcDNA-sACE-CC/SS (*right)*.

Due to the lack of compatible sites between pBS-Ndom and pcDNA-sACE, an intermediary step was used to clone C474S from Ndom into sACE (Figure 5.5). An N-terminal portion of Ndom containing C474S was excised from pBS-Ndom-C474S with *Sma*I and *Age*I and inserted into pBS-sACE. The entire sACE cDNA was then cloned from pBS into pcDNA3.1(-) via a *Xba*I/*Hind*III digestion. pBs-sACE contains two *Sma*I sites, one in the multiple cloning site and a second in the sACE gene, thus the 5' region of the sACE cDNA could potentially be removed during subcloning. An *Eco*RI digest of pcDNA-sACE-C474S confirmed that this region was intact since the *Eco*RI site that is flanked by the two *Sma*I sites was still present (Figure 5.8). pcDNA-sACE-C1072S was constructed by excising C1072S from pBS-sACE using *Xba*I/*Hind*III sites (Figure 5.6). The CC/SS mutant was generated by cloning an *Xba*I/*Age*I N domain fragment from pBS-sACE-C474S into pcDNA-sACE-C1072S (Figure 5.7). The size and orientation of the genes and the presence of the mutations in pcDNA was confirmed by restriction enzyme digestion (Figure 5.8).

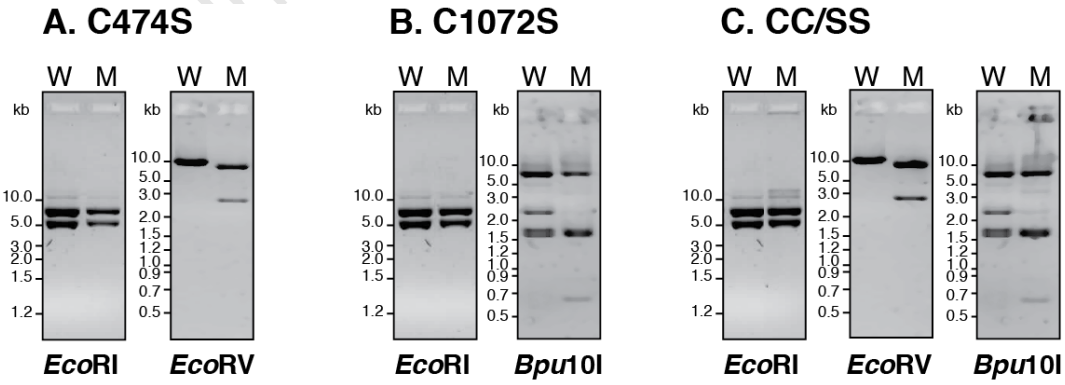

Figure 5.8. Restriction enzyme digestion of pcDNA constructs. pcDNA-sACE-C474S (*A*), pcDNA-sACE-C1072S (*B*) and pcDNA-sACE-CC/SS (*C*) were digested with restriction enzymes to confirm the presence and correct size of the ACE cDNA (*Eco*RI) and the presence of C474S (*Eco*RV) or C1072S (*Bpu*10I) and separated by 1% agarose gel electrophoresis. W: wt pcDNA-sACE, M: mutant pcDNA-sACE.

5.2.4.2 Expression of mutants in CHO cells

Wt sACE, sACE-C474S, sACE-C1072S and sACE-CC/SS were stably transfected into CHO cells (Methods in Chapter 2, Section 2.2.1). To overcome the problems encountered with determining ACE shedding and mAb binding due to low expression of sACE mutants (Chapter 4), a FACS-based cell sorting method was introduced to generate high expressing cell lines. FACS cell sorting was performed on the four cell lines, yielding an average of 100 mU/ml ACE activity in cell lysate. This represented a 4–fold increase in expression compared to transfections carried out without FACS sorting. The level of ACE expression was fairly consistent between cell lines, although the amount of ACE detected in the medium differed (Table 5.1).

Table 5.1 ACE activity of wt and mutant sACE transfected into CHO cells. Activity in cell lysate and culture fluid after overnight incubation in 2% FCS was determined (Chapter 2, Section 2.2.2).

	CELLS	**MEDIUM**
	mU/ml	mU/ml
wt sACE	92.19 ± 0.62	5.25 ± 0.03
sACE-C474S	184.15 ± 19.63	8.36 ± 0.23
sACE-C1072S	99.01 ± 9.40	17.30 ± 0.06
sACE-CC/SS	200.84 ± 3.84	14.99 ± 0.23

5.2.5 Effect of free thiol mutants on dimerisation of sACE

5.2.5.1 Dimerisation in total cell lysate

Western blot analysis of total cell lysate from cells expressing wt sACE, sACE-C474S, sACE-C1072S and sACE-CC/SS was performed to determine the effect of the mutations on covalent dimerisation (Methods in Chapter 2, Section 2.2.8). Samples were separated by SDS-PAGE under non-reducing and reducing conditions to detect disulphide-mediated dimer formation. Wt and mutant sACE resolved as a single 190kDa band under both non-reducing and reducing conditions in repeated experiments and no dimer band could be detected. In some experiments, a faint higher MW form could be detected for wt sACE in the absence of reducing agent, but this was not observed for the mutants.

To further investigate the dimerisation of sACE in cells, mutant cell lines were incubated with the membrane-impermeable amide crosslinker, BS^3. This would potentially covalently link ACE dimers that consist of more transient protein-protein interactions, catching them in the act (Figure 5.9A). In the presence of crosslinker, sACE resolved as two bands, of approximately 190kDa and 350kDa with the higher MW form present as 5-10% of the lower. These bands correlate to monomeric and dimeric forms of ACE. Densitometric determination

of the percentage dimer formed shows a significant increase in the formation of crosslinked dimer for the two single mutants sACE-C474S and sACE-C1072S, but not for sACE-CC/SS.

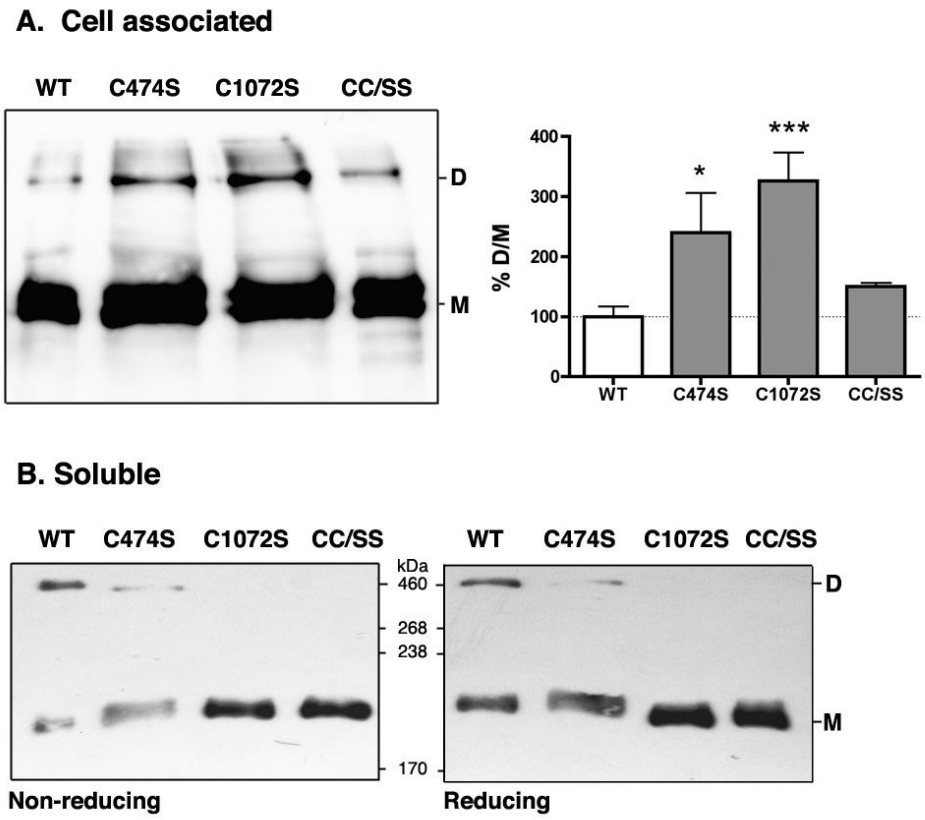

Figure 5.9. Dimerisation of sACE mutants. A. Total cell lysate from CHO cells incubated in the presence of BS^3, a representative Western blot (*left*) and densitometry (*right*), mean±SD of three experiments. B. Harvested and concentrated medium visualised by SDS-PAGE and Western blotting in the absence and presence of β-ME. sACE was detected using the N domain-specific mAb 1D8. D: sACE dimer, M: sACE monomer.

5.2.5.2 Dimerisation in culture medium

Since disulphide-mediated dimers were detected in concentrated medium samples from sACE and Ndom (Section 5.2.2), western blot analysis was performed on concentrated medium harvested from cells expressing wt sACE and all three mutants (Figure 5.9B). Under non-reducing conditions, wt sACE and sACE-C474S resolved as two forms of approximately 190kDa and 400kDa corresponding to the ACE monomers and dimers. The higher MW form was not detected with sACE-C1072S and sACE-CC/SS.

In the presence of the reducing agent β-ME, these bands lowered in intensity (by approx. 2-fold) but did not disappear completely. It is unclear whether these aggregates were shed in the dimeric form or formed *in situ* as the result of concentrating the medium and why they

would be resistant to reduction. The dimerisation of the sACE-C474S mutant that only had a free thiol in the C domain suggests that disulphide-mediated dimerisation occurs via the free thiol in the C domain.

5.2.6 Effect of mutants on ACE shedding

5.2.6.1 Basal shedding

Previous findings indicated that regions of ACE might be involved in both dimerisation and shedding and that there might be an association between these two events (Chapter 4) (Kost *et al*, 2003). Thus, the effect that removing the free thiols had on ACE shedding was determined (Methods in Chapter 2, Section 2.2.4). The amount of ACE shed was calculated from the ACE activity in cell lysate and medium. Basal shedding of wt sACE for this high expressing cell line was 3% of total ACE, which was consistent with previous results (Woodman *et al*, 2000; Woodman *et al*, 2005) (Figure 5.10). The removal of the free thiol in the N domain (sACE-C474S) had no effect on shedding whereas the lack of a thiol at the C domain (sACE-C1072S) resulted in a 3-fold increase in shedding. Interestingly, the loss of both thiols showed increased shedding from wt (sACE-CC/SS), but not as markedly as when a thiol is present in the N domain. Further investigations of the role of the free thiols in shedding were conducted using the CC/SS mutant as this would allow for the determination of the effect of the complete loss of free thiols.

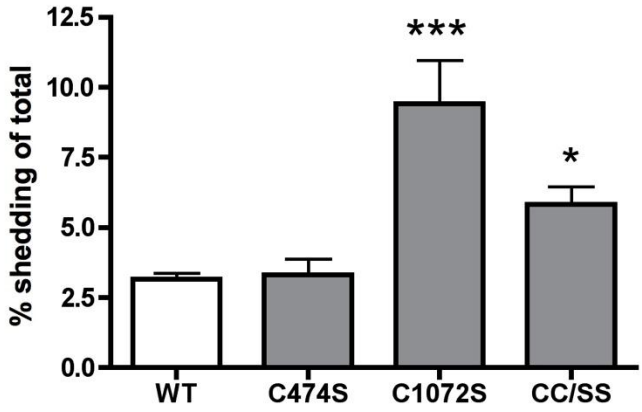

Figure 5.10. Constitutive shedding of sACE mutants. Cells were incubated overnight in minimal medium and shedding was determined as described in chapter 2. Data represented is the mean±SD of 3 experiments performed in duplicate.

5.2.6.2 Induction and inhibition of shedding

Shedding of sACE-CC/SS in the presence of the phorbol ester PDBu, the serine protease inhibitor DCI and the hydroxamate-based metalloprotease inhibitor TAPI-1 was determined (Figure 5.11) (Methods in Chapter 2, Section 2.2.4.1). sACE and sACE-CC/SS shedding was stimulated in the presence of PDBu by 1.5- and 2-fold respectively. A dramatic 5.5-fold increase in shedding was observed for sACE-CC/SS and wt sACE in the presence of DCI. This is consistent with previous work and likely due to a stimulation in the burst of shedding from the cell surface (Schwager *et al*, 1999). sACE-CC/SS shedding was significantly increased compared to wt in the presence of DCI. The shedding of both wt and sACE-CC/SS was inhibited significantly by TAPI-1. The similar response of sACE-CC/SS to PDBu and TAPI-1 indicate that removal of the free thiols has no significant effect on proteolytic processing of ACE. However, the increase in DCI induced shedding observed suggests that there may be a pool of cell surface sACE-CC/SS that is more susceptible to cleavage than wt sACE.

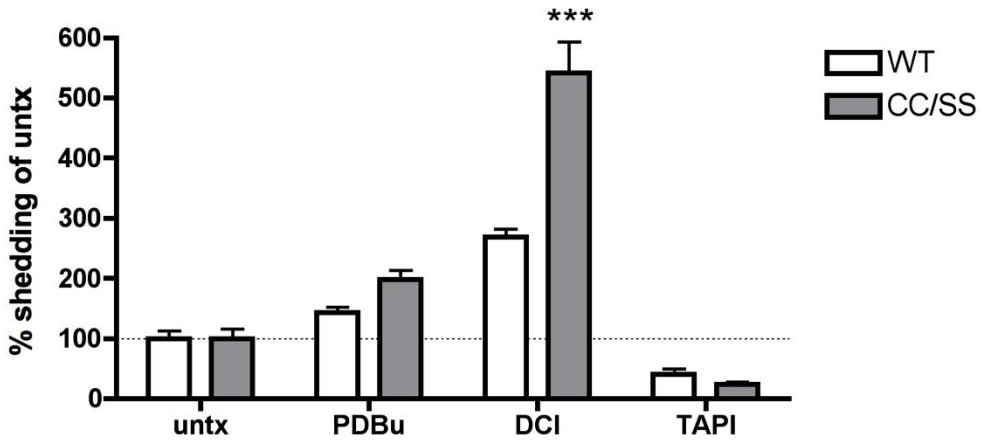

Figure 5.11. Induction and inhibition of shedding. CHO cells expressing wt (*white bars*) and sACE-CC/SS (*grey bars*) were incubated for four hours in minimal medium containing 1μM PDBu, 200μM DCI and 10μM TAPI. The percentage ACE shed was determined as described in chapter 2. Data is represented as the ratio of total percentage shed/untreated (*untx*) and is the mean±SD of two experiments performed in duplicate.

5.2.6.3 mAb induced shedding

Since mAbs 9B9 and 3G8 were shown to inhibit dimerisation and alter shedding and their epitopes have been implicated in dimerisation (Kost *et al*, 2003), their effect on shedding of sACE-CC/SS was investigated (Figure 5.12) (Methods in Chapter 2, Section 2.2.4.2). Cells were incubated in the presence of IgG and the N domain-specific mAbs 9B9, 3G8, 3A5 and i2H5 and shedding determined. Shedding of wt sACE showed mAb i2H5 has no effect on

shedding whereas mAbs 9B9 and 3A5 induced shedding by approximately 1.5- and 2-fold respectively, consistent with previous findings (Balyasnikova *et al*, 2002; Kost *et al*, 2003). mAb 3G8 had no effect on shedding of wt and sACE-CC/SS. Shedding of sACE-CC/SS followed the same trend as wt, being induced by mAbs 9B9 and 3A5 by approximately 1.5- and 2-fold respectively. This indicates that removal of the free thiols does not affect mAb induced shedding.

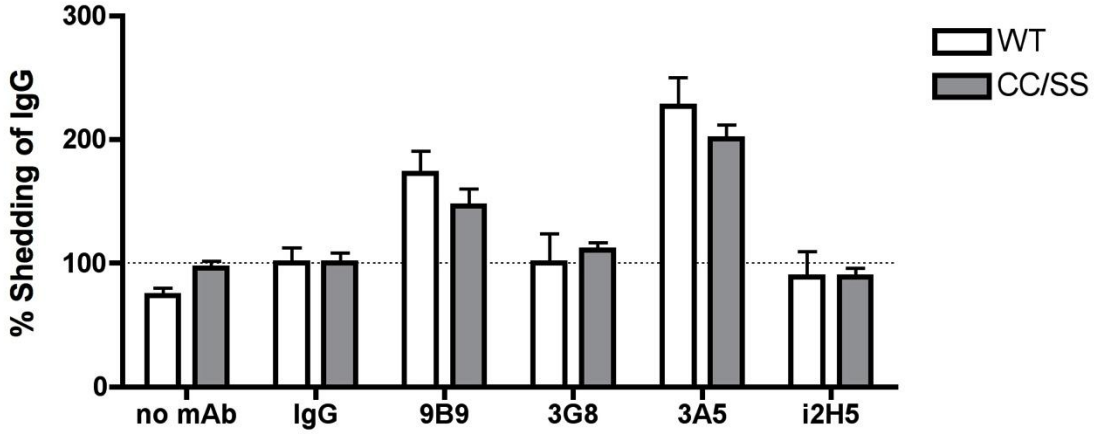

Figure 5.12. mAb induced shedding. CHO cells expressing wt (*white bars*) and sACE-CC/SS (*grey bars*) were incubated for four hours in minimal medium containing 10μg/ml mAbs to ACE. The percentage ACE shed was determined as described in chapter 2. Data is represented as the ratio of total percentage shed/IgG control and is the mean±SD of three experiments performed in duplicate.

5.2.7 Conformational changes induced by the free thiol mutants

The panel of 8 N domain-specific and 8 C domain-specific mAb to ACE were used to develop a conformational footprint of each mutant (Chapter 1, Section 1.4). Plate precipitation assays of wt and mutant sACE were conducted with total cell lysate (Section 5.2.71.) and concentrated medium (Section 5.2.7.2) collected from each cell line (Methods in Chapter 2, Section 2.2.5). To assess the effect of these mutations on mAb binding of sACE on the cell surface, an ELISA assay was performed on CHO cells expressing wt sACE and sACE-CC/SS (Section 5.2.7.3) (Chapter 2, Section 2.2.6).

The unbound cysteine in the N domain (C474) lies proximal to the mAb 5F1 epitope (which is within a distinct region). C1072 in the C domain lies within the mAb 1B3 epitope and in close proximity to the epitopes of mAb 1B8 and 3F10 (Chapter 1, Section).

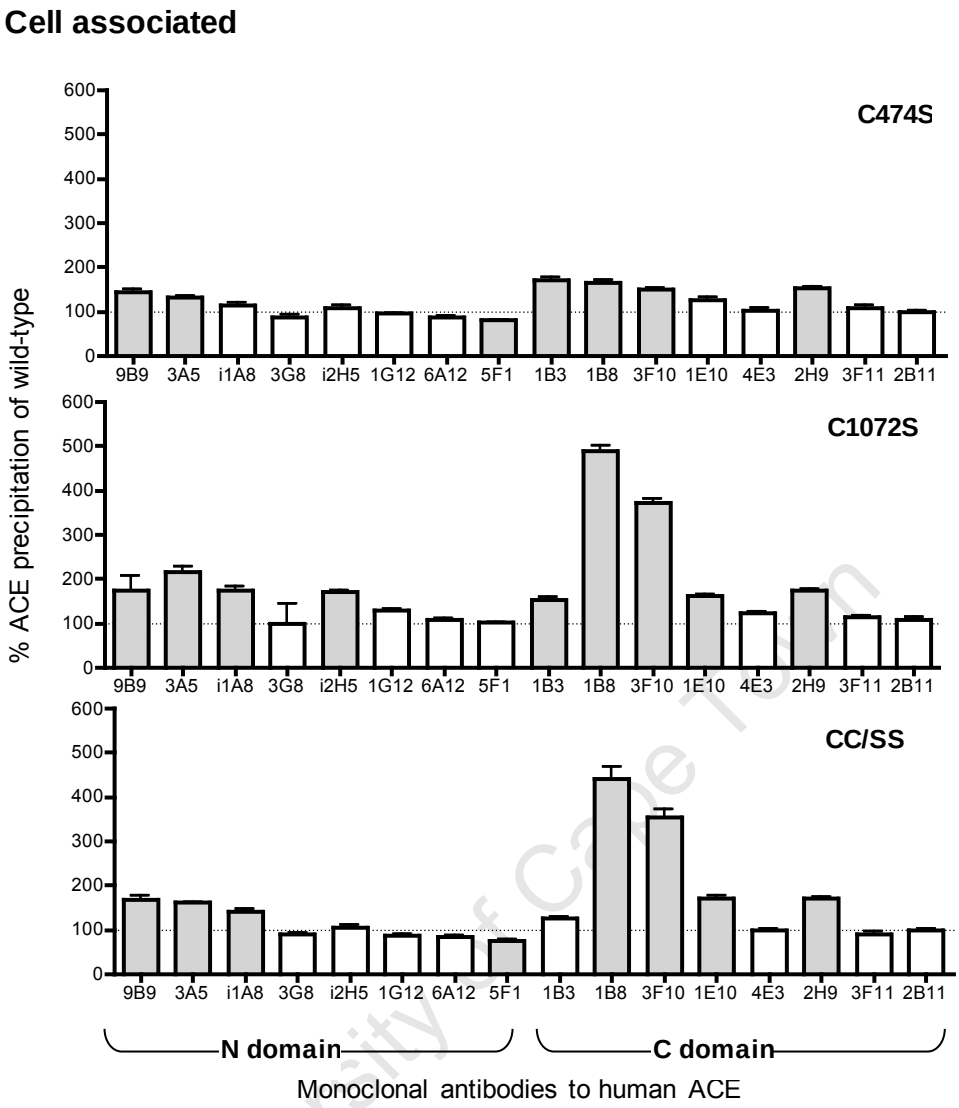

Figure 5.13. Plate precipitation assay of cell associated sACE. Total cell lysate from CHO cells expressing wt and mutant sACE was precipitated by a panel of domain-specific mAbs as described in chapter 2. Data is the mean±SD of two experiments performed in duplicate, shown as the percentage ACE precipitated as a ratio of wt, after normalising to IgG control. Changes in binding are indicated (*grey bars*).

5.2.7.1 Plate precipitation assay of total cell lysate

Similar trends were observed between the three mutants with respect to binding of mAbs to cell associated sACE (Figure 5.13). There is a slight decrease in binding of mAb 5F1 with sACE-C474S and sACE-CC/SS, which suggests that C474 is not a critical residue in the epitope but may play a role in mAb 5F1:ACE interaction. An increase in affinity for N domain-specific mAbs 9B9, 3A5 and i1A8 in the N-terminal antigenic region to all three mutants suggests an arrangement of the N domain resulting in exposure of this region. C domain-specific mAbs 1B3, 1B8 and 3F10, in the C-terminal antigenic region show an increased affinity for all three mutants, sACE-C1072S and sACE-CC/SS in particular. Since C1072 lies within this region, this could be explained by the mutation itself or due to

rearrangement of the domains resulting in exposure of the juxtamembrane stalk. Increased affinity of C domain-specific mAbs 1E10 and 2H9, which lie in the N-terminal antigenic region that is shielded by the N domain (Naperova *et al*, 2008a), for sACE-C0172S and sACE-CC/SS indicate some degree of arrangement of both domains exposing these epitopes. Interestingly, an increased affinity of mAb i2H5 in the C-terminal antigenic region of the N domain for sACE-C1072S suggests the same effect.

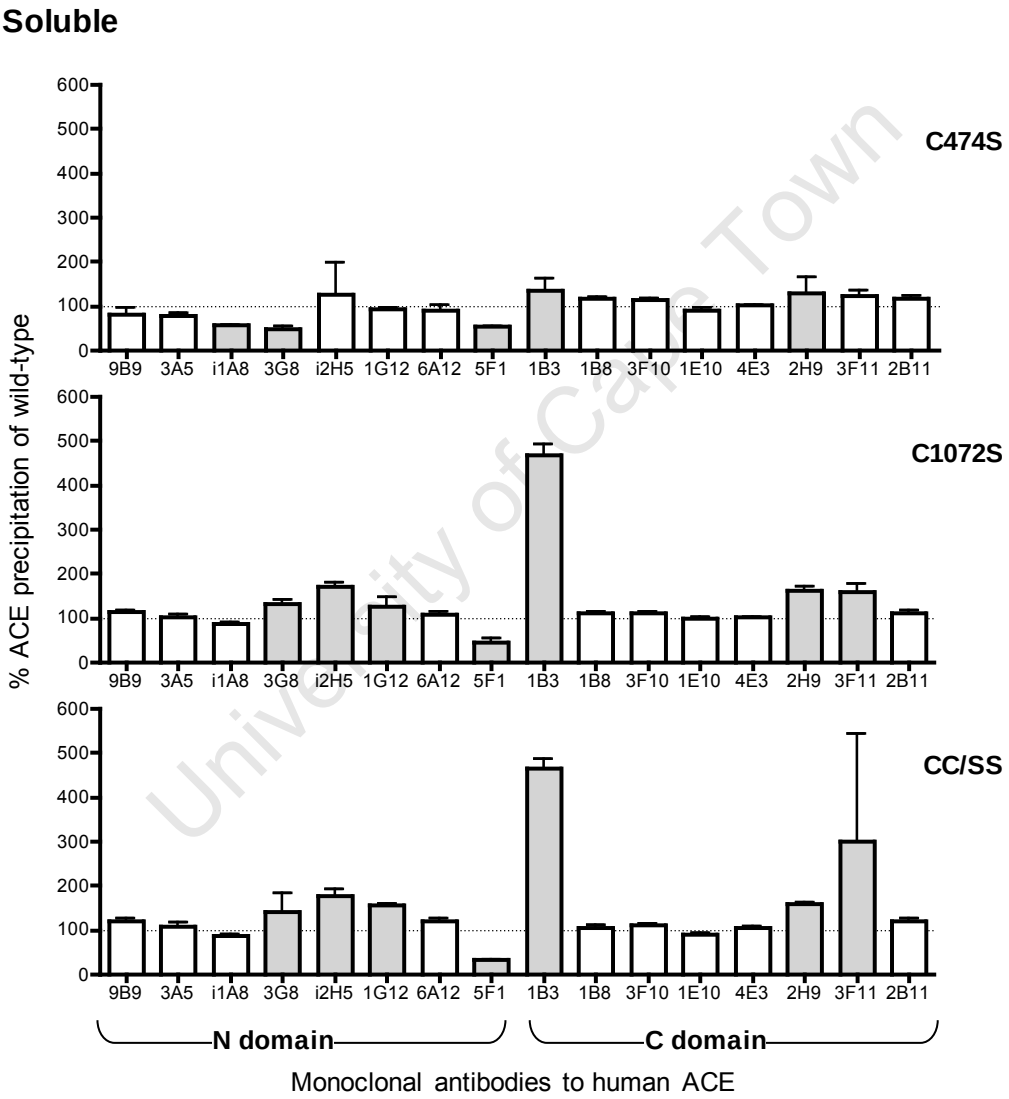

Figure 5.14. Plate precipitation assay of soluble sACE. Medium harvested from CHO cells expressing wt and mutant sACE was concentrated and precipitated by a panel of domain-specific mAbs as described in chapter 2. Data is the mean±SD of two experiments performed in duplicate, shown as the percentage ACE precipitated as a ratio of wt, after normalising to IgG control. Changes in binding are indicated (*grey bars*).

5.2.7.2 Plate precipitation assay of medium

With soluble sACE, the trends are similar for all three mutants (Figure 5.14). There is a distinct loss of affinity of mAb 5F1. For sACE-C474S and sACE-CC/SS this could be due to removal of the N domain thiol, however the loss of affinity for sACE-C1072S suggests that some other mechanism may be causing occlusion of this epitope. Interestingly, there is a loss of affinity of N domain-specific mAbs i1A8 and 3G8 for sACE-C474S and an increase in affinity for sACE-C1072S, suggesting an alteration in this region as a result of the mutations. Here the noticeable increase in affinity of mAb 1B3 for sACE-C1072S and sACE-CC/SS, and sACE-C474S to some extent, is explained by the loss of the transmembrane domain upon cleavage secretion, which exposes this epitope (Balyasnikova *et al*, 2005b). The increase in affinity of the N domain-specific mAb 1G12 and the C domain-specific mAbs 2H9 and 3F11 for sACE-C1072S and sACE-CC/SS suggests that there has been some degree of inter-domain movement, exposing these epitopes.

5.2.7.3 Cell ELISA

A cell-based ELISA assay was performed to obtain a conformational fingerprint of ACE expressed on live cells (Figure 5.15). There was no significant change in binding of the N domain-specific mAbs to sACE-CC/SS whereas significant decreases in affinity for the C domain-specific mAbs 1E10, 4E3, 2H9 and 3F11 were observed (36.65 ± 10.80%, 58.44 ± 4.87%, 41.90 ± 4.27% and 47.06 ± 15.53% compared to wt, respectively). These mAbs lie within the same N-terminal antigenic region, which is occluded by the N domain (Naperova *et al*, 2008a).

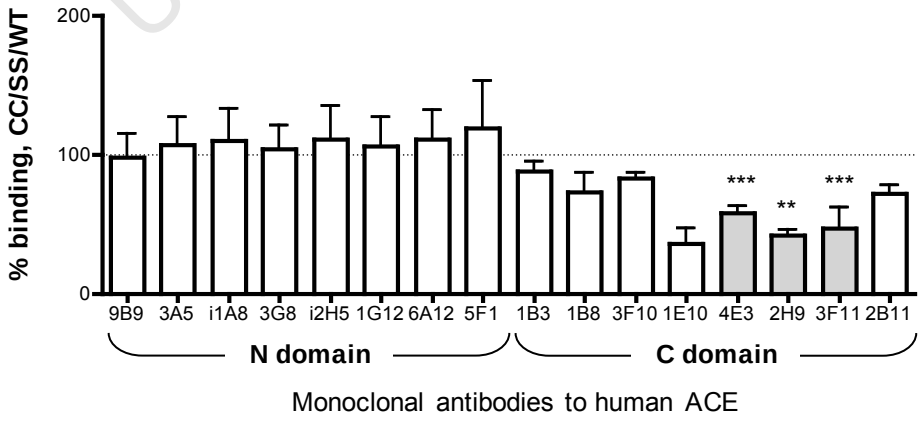

Figure 5.15. Binding of mAbs to membrane-bound sACE. A cell-based ELISA assay was performed on CHO cells expressing wt and mutant sACE as described in chapter 2. The panel of 16 domain-specific mAbs were used and data is the mean±SD of three (N domain mAbs) or two (C domain mAbs) experiments performed in duplicate and is shown as the ratio of binding to CC/SS of wt, normalised against IgG control.

5.3 DISCUSSION

Protein-protein interactions and particularly dimerisation are important regulatory processes. The formation of homo- or hetero-dimers occurs upon ligand binding to receptors to relay messages across the cell membrane, to activate and regulate enzymes. Dimerisation improves protein stability and alters access to active sites.

Recently, two studies reported that sACE has the ability to form dimers (Kost *et al*, 2003, Kohlstedt 2006) and that this may play an important role in processing and signalling. Kost *et al* (2003) showed that interactions via the N domain, most likely mediated by carbohydrates, enable dimer formation of sACE and the N domain in reverse micelles. Whereas Kohlstedt *et al* (2006) indicated that in porcine aortic endothelial cells overexpressing sACE dimerisation was mediated by interactions in the C domain. Homodimerisation was inhibited in reverse micelles by the addition of the N domain-specific mAbs 9B9 and 3G8, which affect shedding of sACE from CHO cells, implicating regions within these epitopes in dimerisation and shedding, as discussed in Chapter 4. The induction of dimerisation by ACE inhibitors was shown to initiate intracellular signalling (Kohlstedt 2006).

In this study, the role of disulphide interactions in dimerisation of sACE transfected into CHO cells was investigated. The relationship between dimerisation and shedding using mutants lacking the free thiol in each domain or both domains was explored.

ACE dimers were detected with purified protein and in culture fluid when sufficient protein was present, but were not consistently detected in total cell lysate (Figure 5.9). This may have been due to the means of sample preparation or possibly the condition of the cells when lysed causing insufficient formation of disulphide-linked dimers.

The results from this study suggest that sACE dimers comprise both non-covalent and covalent interactions. Most noticeably, the predominance of a high MW form under native, non-reducing conditions indicates that sACE has the propensity to form aggregates (Figure 5.2). A large percentage of this aggregate resolved at a 190kDa band in the presence of SDS, indicating that the higher MW form is largely held together by non-covalent interactions. A small percentage persisted as the higher MW form, which was susceptible to reduction. Furthermore, roughly 10% of total purified sACE was visualised as a disulphide-linked dimer under reducing conditions (Figure 5.3). This covalently linked dimer persisted in culture medium from CHO cells expressing wt sACE, which suggests that the protein is shed in this state (Figures 5.3 and 5.9B). The involvement of non-covalent interactions is also

indicated after addition of a crosslinker to cells where visible dimer was formed (Figure 5.9A). The bands observed seemed not to be accounted for solely by disulphide-mediated interactions since these higher MW forms were present, and increased, with removal of the free thiols.

The formation of disulphide-mediated sACE dimers appears to involve the C domain sulphydryl, C1072. This is suggested by several observations: firstly, the appearance of covalent dimers in sACE and tACE but not the N domain isoform in non-reducing gels of purified protein and culture medium from CHO cells expressing these isoforms (Figure 5.3). Secondly, the lack of dimer formation in culture medium of mutants lacking the free thiol at 1072 (sACE-C1072S) or both sites (sACE-CC/SS) while an intact C1072 (sACE-C474S) was able to mediate dimerisation (Figure 5.9). Thirdly, the conformational fingerprint of sACE upon removal of the C domain sulphydryl is more noticeably altered compared to the N domain thiol (Figures 5.13 & 5.14). In particular, three antigenic regions become exposed, evidenced by increased affinity for mAbs within these regions. These are the the N-terminal region of the N domain, containing mAbs 9B9, 3G8 and i1A8; the regions of the N and C domains shown to overlap, containing N domain-specific mAbs i2H5, 6A12, 1G12 and C domain-specific mAbs 1E10, 4E3, 2H9 and 3F11 and lastly, the C-terminal region of the C domain, containing mAbs 1B3, 1B8 and 3F10.

By removing the C domain thiol, and thus the ability of ACE to form a covalent dimer, the two domains may adopt an "extended" conformation (Figure 5.16), allowing access of these mAbs.

It is unclear why there would be preference of formation of disulphide-mediated dimers via the C domain, since there is a high degree of structural homology between the N and C domains. This may be due to conformational constraints where the C domain free thiol is more accessible and the N domain thiol is occluded by either the linker region or the C domain. Since the C domain is tethered to the membrane by the juxtamembrane stalk this may restrain it and increase the likelihood of protein-protein interaction. The presence of carbohydrates may also obstruct disulphide-mediated dimerisation, which would require that molecules be in close proximity. The N domain is more extensively glycosylated than the C domain and the glycosylation sequon N480, unique in the N domain, proximal to C474 is present in the glycosylated form in the truncated N domain (Anthony *et al*, 2010) (Figure 5.1).

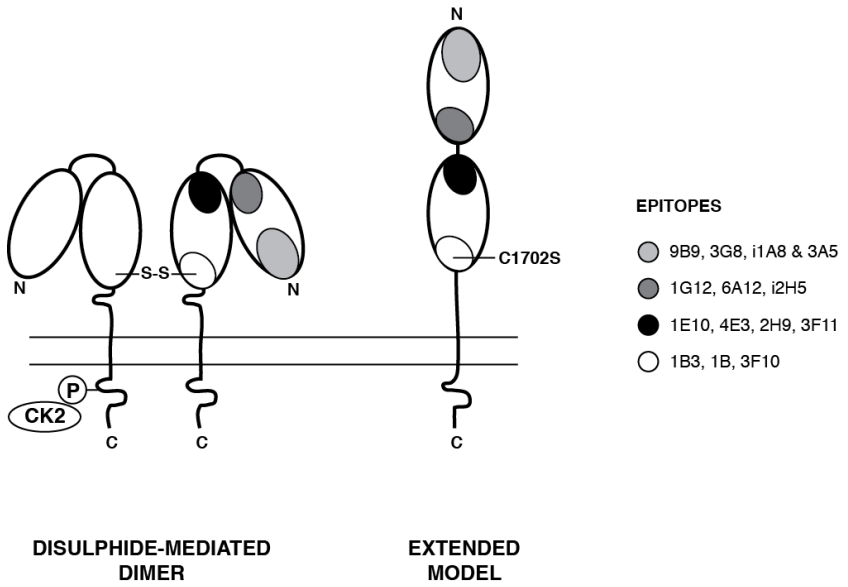

Figure 5.16. Cartoon of sACE disulphide-mediated dimer. Disulphide-mediated sACE dimers are depicted in the "compact" conformation, formed via the C domain free thiol (*left*). With removal of this sulphydryl sACE could adopt an "extended" conformation (*right*), allowing better access of mAbs and the secretase. CK2 phosphorylation may be induced by disulphide-mediated dimerisation, affecting conformation and shedding.

Kost *et al* (2003) demonstrated a link between dimerisation of sACE and cleavage secretion where mAbs 9B9 and 3G8 that affect shedding of sACE from CHO cells were shown to inhibit dimerisation of sACE in reverse micelles. As discussed in Chapter 4, the overlapping region of the epitopes for these mAbs does indeed appear to play a role in dimerisation and shedding. The presence of mAbs 9B9 and 3G8 were shown to have no effect on ACE inhibitor induced dimerisation in porcine aortic endothelial cells overexpressing sACE (Kohlstedt *et al*, 2006) and the authors point out that this mechanism may be distinct from dimerisation involving the CRD described by Kost *et al* (Danilov *et al*, 2006; Fleming & Kohlstedt, 2006).

Interestingly, the loss of the C domain thiol (C1072) that appears to be involved in disulphide-mediated dimerisation results in a highly significant increase in shedding whereas the presence of this group alone in the C474S mutant has no effect (Figure 5.10). This suggests that shedding is impaired by covalently linked dimerisation via the C domain in CHO cells, but not necessarily inhibited since disulphide-mediated dimers were observed in culture medium. This may be due to steric hinderance of the secretase by the dimer and might be an important regulatory mechanism in cleavage-secretion. This is corroborated by the increased affinity of mAbs 1B3, 1B8 and 3F10 for cell-associated sACE-C1072S, suggesting that the juxtamembrane stalk is exposed (Figure 5.13). Increased affinity for mAb 1B3 has been associated with an increased shedding efficiency (Balyasnikova *et al*, 2005b). Furthermore

Kohlstedt *et al* (2006) showed that dimerisation via the C domain induced an intracellular signalling cascade, mediated by phosphorylation on S1270 by CK2 (Chapter 1, Section 1.3.5). Interestingly, a mutant, S1270A, lacking the ability to be phosphorylated was retained in the membrane and significantly reduced shedding (Kohlstedt *et al*, 2002). The significant increase in shedding observed upon removal of the C domain thiol may be related to this mechanism (Figures 5.10 & 5.16).

Removal of both thiols affected the DCI-stimulated release of sACE from CHO cells but not PDBu stimulated shedding (Figure 5.11). It has been proposed that the sharp increase in shedding induced by DCI is due to the release of a pool of ACE on the cell surface (Schwager *et al*, 1999). Thus, the loss of both thiols, and potentially the ability of ACE to form disulphide-mediated dimers, appears to affect the pool of membrane bound protein, suggesting that dimerisation occurs on the cell surface. The presence of mAbs 9B9 and 3G8 had no significant effect on shedding when both thiols were removed (sACE-CC/SS), suggesting that the mechanism, which causes an increase in shedding with the loss of the C domain thiol, is not the same as that induced in the presence of mAbs (Figure 5.12).

The ability to consistently observe disulphide-mediated dimers in total cell lysate limited the conclusions that could be drawn directly regarding disulphide-linked dimerisation and shedding. It is interesting to note that removal of the thiol from each domain individually increased the formation of dimers in the presence of crosslinker, with the loss of the C domain thiol having the greatest effect. This may be an indication of the interplay between different mechanisms of dimerisation, where loss of the ability to form disulphide-mediated dimers has enabled the formation of non-covalent interactions. Albeit if the hypothesis that disulphide-mediated dimerisation occurs via the C domain holds, this does not explain why removal of the N domain thiol (sACE-C474S) increased dimer formation and why the removal of both (sACE-CC/SS) had no effect at all. The possibility that the high MW form observed after crosslinking is an ACE heterodimer can also not be ruled out, although there is some evidence to suggest that it is in fact a homodimer. First, Kohlstedt *et al* (2006) showed that sACE forms a homodimer using a split-ubiquitin assay. Second, bands at consistently the same position were observed with sACE samples from total cell lysate and medium, as well as purified ACE. Third, 2-D PAGE of purified sACE showed that the higher MW forms observed under non-denaturing conditions resolved with sACE under reducing conditions (Figure 5.4).

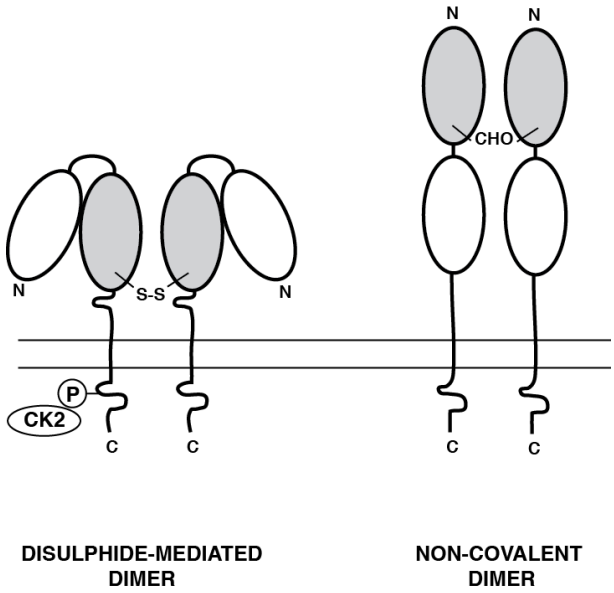

Figure 5.17. Cartoon of sACE dimers. Disulphide-mediated sACE dimers are depicted in the "compact" conformation, formed via the C domain free thiol (*left*) and non-covalent dimers in the "extended" conformation, formed via carbohydrate interaction. CK2 phosphorylation may be induced by disulphide-mediated dimerisation, affecting conformation and shedding

In conclusion, the generation of mutants lacking free thiols in one or both domains has indicated that ACE dimerisation involves two possible mechanisms, via non-covalent interactions in the N domain, possibly through the proposed carbohydrate recognition domain (Kost *et al*, 2000; Kost *et al*, 2003), and via disulphide-mediated interactions through the free thiol in the C domain (Figure 5.17). The latter appears to play a role in cleavage secretion of ACE and is most likely the mechanism involved in ACE inhibitor initiated signalling (Figure 5.16) (Kohlstedt *et al*, 2006).

However, further investigation into the relationship between dimerisation, shedding and intracellular signalling is required. The role of non-covalent interactions, particularly via glycans, in dimerisation needs to be further explored. The minimal glycosylation requirements for expression of the N domain (Anthony *et al*, 2010) and tACE (Gordon *et al*, 2003) have been determined and the panel of mutations generated from these studies would be a useful springboard for further investigations. The design and expression of tagged sACE constructs could be a viable system for determining homodimerisation, as used successfully to investigate homodimerisation of the human B2-R (Michineau *et al*, 2006) and its heterodimerisation with ACE (Chen *et al*, 2006). The relationship between non-covalent and covalent interactions in dimerisation could also be investigated in this way. Finally, the role of covalent dimerisation in ACE inhibitor initiated signalling could be investigated using the mutants produced in this study.

CHAPTER 6: A novel ACE substitution: the role of the N domain in shedding of sACE

6.1 INTRODUCTION

In addition to expression on the surface of endothelial cells in a number of tissues, ACE is found in biological fluids including plasma and seminal fluid as the result of cleavage-secretion of membrane-bound ACE (Ching *et al*, 1983; Hooper *et al*, 1997; Wei *et al*, 1991b). Cleavage has been shown to occur in the juxtamembrane stalk region between R1203 and S1204 (Ramchandran *et al*, 1994; Ehlers *et al*, 1996; Woodman *et al*, 2000).

Levels of plasma ACE remain fairly stable in healthy individuals, but are elevated with certain clinical symptoms including Gaucher's disease and granulomatous diseases such as sarcoidosis (Lieberman, 1975; Lieberman & Beutler, 1976; Silverstein *et al*, 1976). Two novel ACE substitutions that are associated with increased plasma ACE have been recently described. Firstly, the P1199L mutation in studies of unrelated individuals in Germany (Linnebank *et al*, 2003), Holland (Kramers *et al*, 2001, Eyries *et al*, 2001) and the USA (Semmler *et al*, 2006) was shown to be responsible for elevated plasma ACE. Expression of recombinant P1199L sACE in COS-7, CHO and HMEC-1 cells (Eyries *et al*, 2001) showed that this mutation caused increased cleavage-secretion of ACE, most likely through a local conformational change in the juxtamembrane region allowing better access of the secretase. The second study described the W1197Stop transition in a family of African-Americans that introduced a premature stop codon into the stalk region resulting in the expression of exclusively soluble sACE in cells carrying the mutation (Nesterovich *et al*, 2009). In both these cases, no adverse clinical symptoms were associated with the increased levels of plasma ACE.

The role of soluble plasma ACE remains unclear; however, it has been shown that membrane-bound sACE is critical for AngII production in the vascular endothelium since soluble ACE is not sufficient to restore blood pressure in null ACE mice (Kessler *et al*, 2007).

A novel ACE substitution has recently come to light that seems to be associated with adverse clinical symptoms (Prof. S. Danilov, personal communication). It is present in a family of individuals where the affected members suffer from intermittent nausea, vomiting, fatigue and depression. This was discovered through the youngest member affected, a 17-year male. During routine clinical tests conducted to find the underlying cause of the condition, it was

discovered that the patient had dramatically elevated levels of plasma ACE (367U/L vs normal range of 12-68U/L).

A number of known causes for elevated plasma ACE, including Gaucher's disease, histoplasmosis and sarcoidosis (Leiberman *et al*, 1975; Leiberman & Beutler, 1976; Silverstein *et al*, 1976) were investigated and ruled out. The CARD15/NOD2 gene was sequenced and a P723L substitution was discovered. Substitutions of this gene have been associated with Blau syndrome (Miceli-Richard *et al*, 2001), Crohn's diease and early onset sarcoidosis (Kambe *et al*, 2005). However the only family members to have this mutation were the index patient and the mother, who did not present with any of the clinical symptoms. Thus, this was ruled out as a potential cause. Therefore the most likely explanation for the elevated plasma ACE was a novel ACE substitution. Sequencing of the entire ACE gene of the index patient found a single base pair substitution at position 1480 converting the codon TAT to GAT, which converts a Tyr to Asp at position 465 in the ACE protein. The patient was heterozygous for the substitution and this transition was found in only affected members of the family, who also had elevated plasma ACE (Prof. S. Danilov, personal communication).

Within the secondary structure of sACE, Y465 lies in the C terminal portion of the N domain on helix α-21 in proximity to C474, within 10Å of the linker region, close to the epitope of mAb 5F1 (refer to Chapter 1, Section 1.4). The aromatic side chain of Y465 forms a predominant protuberance from the cell surface, which could be involved in intra-chain interactions or protein-protein interactions. The transition to the acidic Asp results in the loss of this protuberance from the surface structure (Figure 6.1). The altered surface structure induced by the Y465D mutation may result in conformation changes that alter ACE expression or processing that result in elevated plasma ACE.

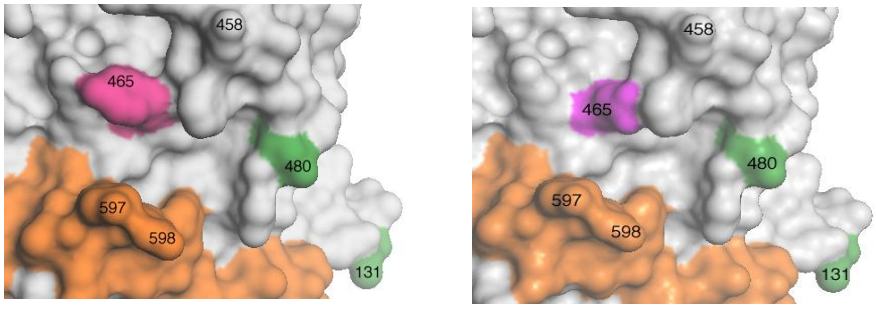

Figure 6.1. Change in surface structure with Y465D substitution. Surface representation of the crystal structure of the N domain indicating Y465 (*left, pink*) and D465 (*right, magenta*), the linker region (*orange*) and glycosylation sites (*green*).

A likely cause of the symptoms experienced by affected family members is elevated levels of substance P, a peptide involved in pain and chronic inflammation associated with nausea, vomiting, depression and fatigue (Harrison *et al*, 2001). This could be the result of increased production of substance P through aberrant signalling or of insufficient breakdown. The major enzymes involved in degradation of substance P are neprilysin (NEP) and sACE (Skidgel *et al*, 1984; Ehlers & Riordan, 1991a). Considering the novel ACE substitution in affected individuals, there may be a correlation between the role of ACE in substance P catalysis and the symptoms observed. Interestingly, plasma samples from the same individuals were shown to have elevated substance P levels (Prof. S. Danilov, personal communication).

Thus the aim of this study was to investigate the mechanism responsible for increased soluble ACE in affected individuals using a model system in CHO cells.
This involved the following objectives:

1. To generate the Tyr 465 to Asp in sACE by site-directed mutagenesis, express the Y465D mutant in CHO cells and determine its effect on the rate of ectodomain shedding.
2. Assess what effect this mutation has on the conformation of ACE by mAb binding.
3. Investigate the effect of this mutation on the hydrolysis of physiological substrates.

6.2 RESULTS

6.2.1 Expression of sACE-Y465D in CHO cells

sACE-Y465D cDNA, a generous gift from Prof S. Danilov (refer to Chapter 2, Section 2.1.2), was stably transfected into CHO cells. Soluble wt sACE (pcDNA-sACE-sol) expressed in CHO cells was used as a source of ACE for protein purification (for details refer to Chapter 2, Section 2.1.1)

High-expressing sACE-Y465D CHO stable cell lines were generated by FACS-based cell sorting (refer to Chapter 2, Section 2.2.1 for methods). The level of expression was determined by ACE activity assays of culture medium and total cell lysate (refer to Chapter 2, Section 2.2.2 for methods). The sACE-Y465D cell line had comparable levels of cell associated ACE activity compared to wt sACE (Figure 6.2A). However, activity in culture medium from CHO cells expressing sACE-Y465D was significantly increased compared to wt, indicating that this mutant has an effect on ACE shedding (Figure 6.2B). Thus, the Y465D mutation did not appear to have affected sACE expression in CHO cells, but appeared to influence proteolytic processing from the cell surface.

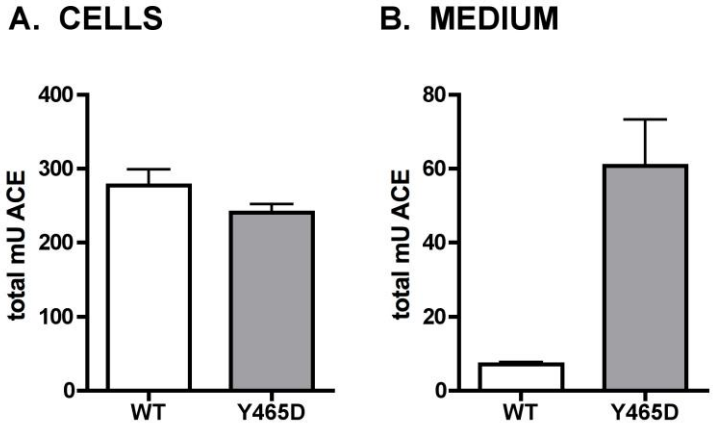

Figure 6.2. ACE activity in CHO cell lysate and culture medium. The ACE activity in total cell lysate (*A*) and culture medium (*B*) from CHO cell expressing wild-type sACE and sACE-Y465D was determined using ZFHL as a substrate. Data is shown as the total mU in each sample and is the mean±SD of four experiments (wt) or three experiments (sACE-Y465D) performed in triplicate.

6.2.2 Protein expression and processing of membrane-bound and soluble sACE-Y465D

Western blot analysis was performed on total cell lysate and culture medium from CHO cells expressing wt sACE and sACE-Y465D to further examine the effect of the mutation on sACE expression and processing (for methods refer to Chapter 2, Section 2.2.8). The cell associated wt and sACE-Y465D resolved at approximately 190kDa (Figure 6.3A). A higher MW form

>300kDa was observed for both wt and the mutant consistent with a disulphide-mediated ACE dimer, since this form is not observed in the presence of reducing agent (refer to Chapter 5). Densitometric analysis of cell lysate indicated a 5-fold increase in the ratio of dimer to monomer with sACE-Y465D (Figure 6.3B). However, these data were not reproducible and the increase in dimer could not be confirmed. The amount of soluble sACE in harvested medium assessed by an activity assay was insufficient to perform western blotting analysis. Thus, culture medium from CHO cells expressing wt sACE was concentrated to obtain sufficient protein for western blotting. sACE-Y465D resolved as band similar in size to the wt and cell associated sACE, of approximately 190kDa. In both cell associated and soluble forms, the mutant resolves slightly higher than the wt, which could be the result of alterations in post-translational processing such as glycosylation or phosphorylation that might alter its migration through the gel. These results suggest that the mutation has no aberrant effect on sACE expression and processing to the cell membrane. In addition, the elevated plasma ACE levels observed in individuals expressing the Y465D substitution are more likely to be the result of changes in the cleavage-secretion of sACE-Y465D than the result of increased protein expression.

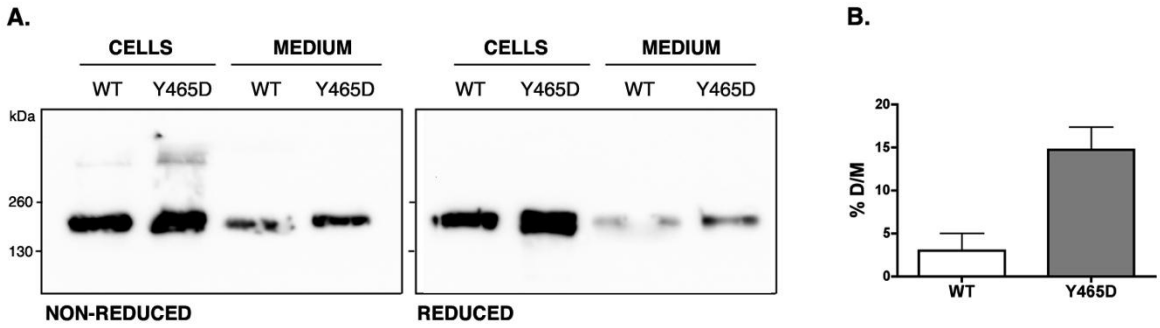

Figure 6.3. Protein expression of sACE-Y465D in CHO cells. A. Western blot analysis was performed on total cell lysate and concentrated medium from CHO cells transfected with wt and sACE-Y465D. Samples were separated by 6% SDS-PAGE in the presence (*right*) or absence (*left*) of β-ME. Immunoloblotting was performed and ACE was detected with the C domain-specific mAb 1D8. B. Densitometric analysis of cell lysate separated by Western blot, calculated as the percentage dimer of monomer (D/M). Data is the mean±SD of samples prepared in duplicate.

6.2.3 Purification of sACE-Y465D

Purified sACE-Y465D was prepared for further biochemical analysis. CHO cells expressing full-length sACE-Y465D were used as a source of soluble ACE in cell culture medium for protein purification. sACE-Y465D was purified by lisinopril-sepharose affinity

chromatography, as described (Chapter 2, Section 2.2.3). Sufficient yields were obtained for further experiments (3.2mg/L) and protein resolved as a ~190kDa band with SDS-PAGE under reducing conditions (Figure 6.4). Faint bands of ~80kDa and ~90kDa were observed with wt sACE and sACE-Y465D, consistent with the N and C domain products generated from limited proteolysis of sACE (Sturrock *et al*, 1997). There was a negligible amount of proteolysis evident as faint bands migrating slightly faster than sACE. Since these were present as a small percentage of the total protein, these samples were considered suitable for further experimentation.

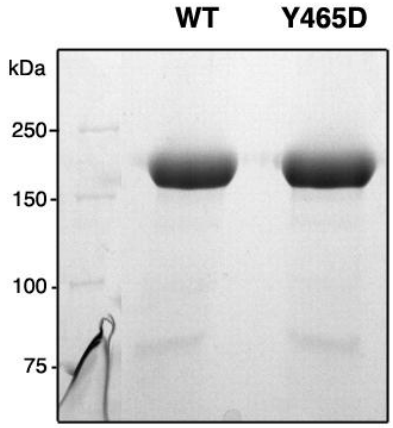

Figure 6.4. Protein purification of sACE-Y465D. Soluble sACE-Y465D was purified from CHO cell culture medium by lisinopril-sepharose affinity chromatography. 15µg-20µg protein was separated on a 6% SDS-PAGE and visualised by Coomassie Blue staining. Purified sACE (refer to Chapter 3, Section 3.2.4.2) was included as a molecular weight control.

6.2.4 Shedding of sACE-Y465D

Since Y465D did not alter enzyme activity (Section 6.2.1) or protein expression (Section 6.2.2) in CHO cells, it seemed that the elevated levels of soluble ACE in vivo and in vitro could be explained by changes in the cleavage-secretion of sACE. This could be the result of either aberrant shedding or conformational changes in sACE that improve accessibility of the sheddase.

6.2.4.1 Basal shedding

ACE activity in culture medium from CHO cells expressing sACE-Y465D was noticeably increased compared to wt sACE (Figure 6.2). Basal shedding was calculated from activity assays of culture fluid and total cell lysate from CHO cells expressing wt and sACE-Y465D (Figure 6.5) (for methods refer to Chapter 2, Section 2.2.4). There was an 8-fold increase in shedding of sACE-Y465D compared to wt (813.47% ± 97.35%, $p < 0.001$ of wt).

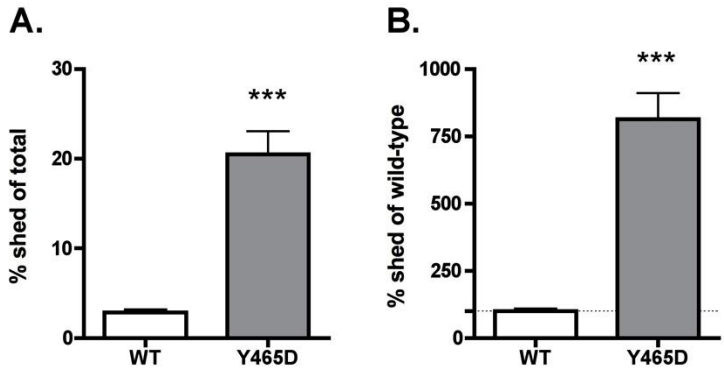

Figure 6.5. Basal shedding of sACE-Y465D in CHO cells. Shedding of wild-type sACE (*white*) and sACE-Y465D (*grey*) was calculated as the percentage ACE activity in culture medium of total activity in cell lysate and medium after incubation in minimal medium for 4 hours. A. Percentage shed of total ACE activity and B. Percentage total shed of wild-type. Data is the mean±SD of three experiments performed in triplicate.

6.2.4.2 Induction and inhibition of shedding

The effect of stimulation of shedding by the phorbol ester, PDBu, and the serine protease inhibitor, DCI, as well as inhibition by the hydroxymate-based metalloprotease inhibitor, TAPI-1, was determined (Figure 6.6) (refer to methods in Chapter 2, Section 2.2.4.1). PDBu induced basal shedding of wt sACE by approximately 1.5-fold and DCI caused an increase in shedding (140.77% ± 8.15%, $p < 0.05$ and 238% ± 11.29%, $p < 0.001$ of untreated, respectively) (Figure 6.6). Shedding was significantly inhibited in the presence of TAPI-1 (32.77% ± 2.08% of untreated, $p < 0.01$). A similar trend was observed for sACE-Y465D, where a 4-fold induction of shedding in the presence of PDBu and a 5-fold increase in the presence of DCI was observed (PDBu: 434.00% ± 16.26%, $p < 0.001$; DCI: 527.42% ± 14.57%, $p < 0.001$ of untreated). There was a significant inhibition of shedding in the presence of TAPI-1 (27.04% ± 3.30%, $p < 0.05$ of untreated). The induction of shedding by PDBu and DCI was significantly increased with the mutant compared to wt. These results suggest that cleavage-secretion of sACE-Y465D occurs via the same mechanism as native sACE and that an aberrant shedding mechanism is not likely the cause of its increased shedding.

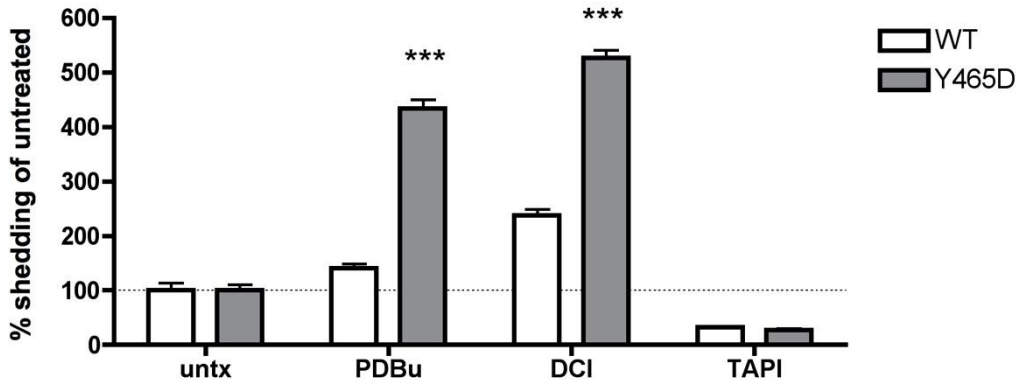

Figure 6.6. Stimulation and inhibition of shedding of sACE-Y465D. CHO cells expressing wt (*white*) and sACE-Y465D (*grey*) were incubated in minimal medium containing PDBu, DCI or TAPI-1 for four hours. Shedding was calculated as described in Figure 6.5. Data is the mean±SD of two experiments performed in duplicate, expressed as % of untreated (*untx*).

6.2.4.3 mAb induced shedding

Induction of shedding by mAbs 9B9 and 3A5 to ACE as well as inhibition by mAb 3G8 has been reported previously (Balyasnikova *et al*, 2002). This has been attributed to localised conformational changes, which either improve or reduce access of the secretase by altering the conformation of ACE upon mAb binding. The effect of the Y465D mutation on mAb induced shedding was determined to investigate whether similar effects are observed (Figure 6.7) (for methods refer to Chapter 2, Section 2.2.4.2).

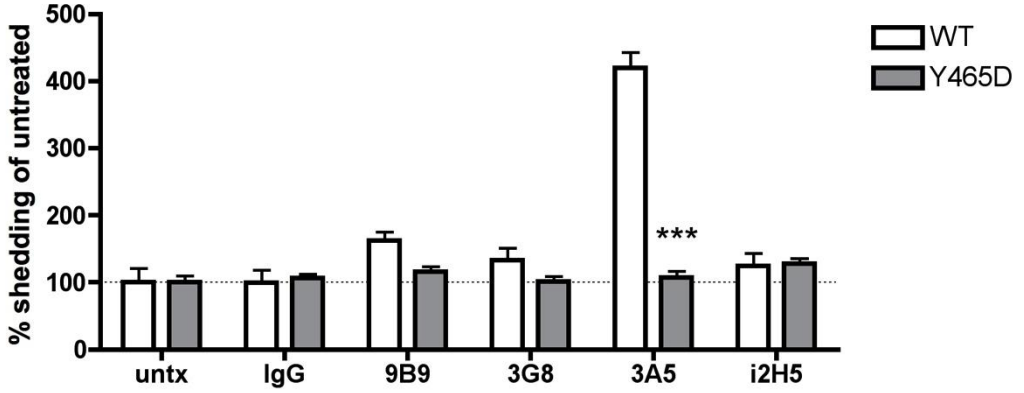

Figure 6.7. mAb induced shedding of sACE-Y465D. CHO cells expressing wt (*white*) and sACE-Y465D (*grey*) were incubated in the presence of mAbs to ACE in minimal medium for four hours. Shedding was calculated as described in Figure 6.5. Data is the mean±SD of two experiments performed in duplicate.

A 2.7-fold induction of shedding by mAb 9B9 and 4.1-fold induction by mAb 3A5 was observed for wt (162.39% ± 12.95%, $p < 0.05$ and 420.21% ± 23.25%, $p < 0.001$ of untreated,

respectively) whereas no inhibition of shedding by mAb 3G8 was observed. There was no significant change in mAb induced ACE shedding with sACE-Y465D for all the mAbs tested, except mAb 3A5 where the induction of shedding observed with wt returns to basal levels and a slight but not significant increase in shedding was observed in the presence of mAb 9B9.

6.2.4.4 Effect of substance P on shedding

In addition to the elevated plasma ACE levels observed in individuals with the Y465D substitution, increased levels of substance P were detected. Substance P is a substrate for sACE (Jaspard *et al*, 1993) but its interaction with ACE and involvement in ACE expression and regulation is unknown. To determine whether substance P plays a role in ACE cleavage-secretion, shedding was determined after incubation of cells in the presence of substance P for four hours (refer to methods in Chapter 2, Section 2.2.4.3). No significant difference in shedding of sACE-Y465D compared to wt was observed (Figure 6.8). In addition there was no observable difference in ACE activity in cell lysate in the presence of substance P. This suggests that substance P does not have a direct effect on ACE expression and proteolytic processing of sACE Y465D.

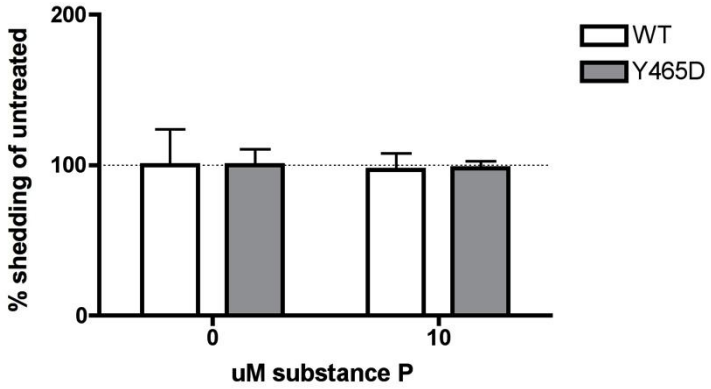

Figure 6.8. Effect of substance P on shedding of sACE-Y465D. CHO cells expressing wt (*white*) and sACE-Y465D (*grey*) were incubated in the presence of 10μM substance P in minimal medium for four hours. Shedding was calculated as described in Figure 6.5. Data is the mean±SD of two experiments performed in triplicate.

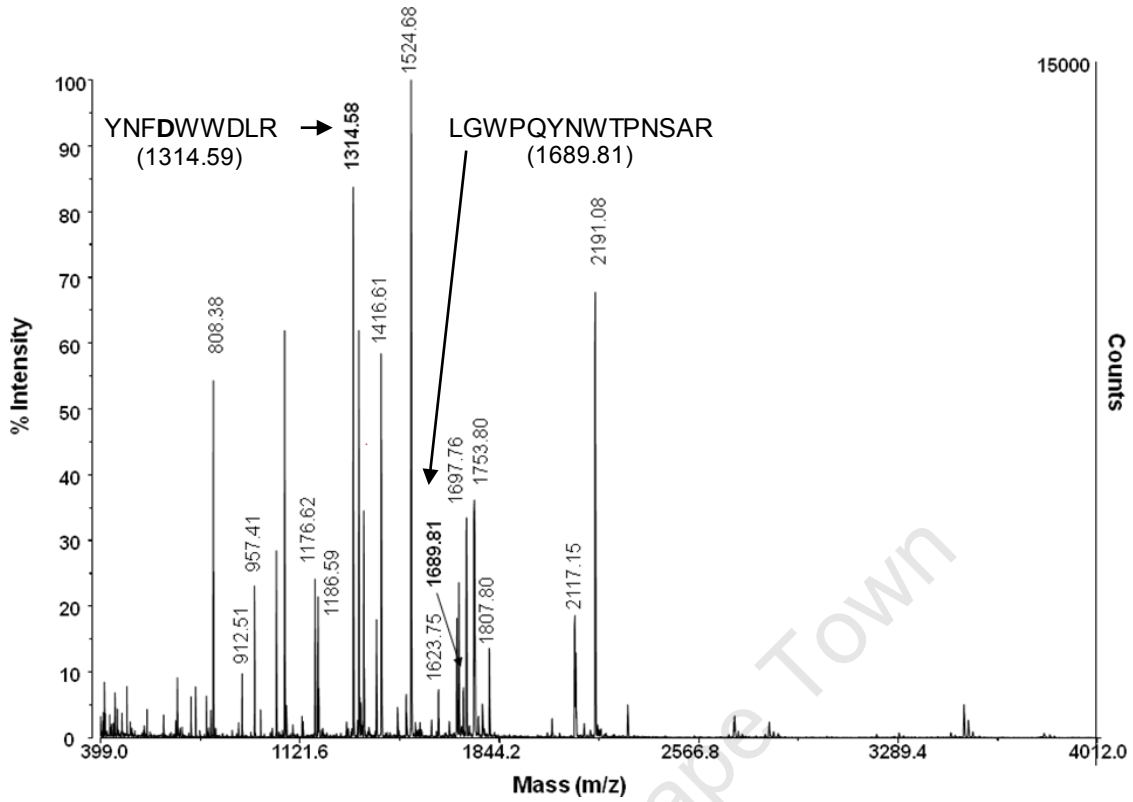

Figure 6.9. MALDI TOF/TOF spectrum of sACE-Y465D after tryptic digest. An in gel tryptic digest was performed on sACE-Y465D and subjected to MALDI TOF/TOF. Masses corresponding to predicted ACE peptides are labelled. The masses corresponding to peptide containing Y465D and the C-terminal cleavage peptide are indicated in bold, labelled with the peptide sequence, and expected masses are indicated in brackets.

6.2.4.5 Cleavage site determination

A possible explanation for the 8-fold increase in shedding observed for sACE-Y465D is that the mutation has altered the interaction of the secretase with ACE causing aberrant shedding, most likely at a novel cleavage site. To test this hypothesis, the cleavage site of sACE-Y465D was determined by MALDI MS/MS (Figure 6.9. & Table 6.1) (for methods refer to Chapter 2, Section 2.2.10). A tryptic digest of purified soluble ACE revealed a fragment (*m/z* 1689.81, expected *m/z* 1689.81), which corresponds to the C-terminal cleaved peptide (L1190-R1203). The peptide, containing Y465D (Y459-R467) was identified as an *m/z* 1314.58 fragment (expected *m/z* 1314.59), confirming the presence of the mutation in the protein sequence. Thus, the Y465D transition does not alter the cleavage site of the ACE secretase and these results strongly suggest that cleavage occurs by the same mechanism as wt sACE.

Table 6.1. MALDI MS/MS analysis of sACE-Y465D after tryptic digest. Masses (*m/z*) corresponding to ACE peptides, the peptide containing Y465D (*underlined*) and the C-terminal peptide are indicated (*bold*)

Residue no	**Expected mass** [MH]+	**Observed mass** [MH]+	**Peptide sequence** identified by MS/MS
53-71	2190.70	2191.08	
133-151	2121.03	2121.04	
188-199	1416.61	1416.61	
327-340	1753.76	1753.80	
433-446	1724.92	1724.91	
447-453	808.41	808.38	
459-467	**1314.59**	**1314.58**	**YNF<u>D</u>WWDLR**
518-532	1807.81	1807.80	
623-629	957.43	957.41	
751-762	1623.76	1623.75	
776-785	1176.64	1176.62	
798-811	1697.77	1697.76	
812-828	2117.15	2117.15	
1055-1065	1524.69	1524.68	
1068-1077	1186.60	1186.59	
1174-1180	912.53	912.51	
1190-1203	**1689.81**	**1689.81**	**LGWPQYNWTPNSAR**

6.2.5 Conformational changes induced by the Y465D mutation

The possibility of conformational changes induced by the Y465 transition was investigated using a plate precipitation assay and cell-based ELISA. The same panel of domain-specific mAbs were used as that used to investigate changes in conformation in Chapters 3, 4 and 5.

6.2.5.1 Binding of mAbs to cell-associated and soluble sACE-Y465D

Plate precipitation assay of total cell lysate (cell associated) and concentrated cell culture medium (soluble) from cells expressing wt sACE and sACE-Y465D revealed the following trends (Figure 6.10) (refer to Chapter 2, Section 2.2.5 for methods). There is a marked decrease in precipitation of both cell-associated and soluble sACE-Y465D by mAb 5F1, which indicates or suggests that Y465 is important for mAb 5F1:ACE interaction or that this epitope is occluded with sACE-Y465D. With cell-associated sACE-Y465D, precipitation by the N domain-specific mAbs; 9B9, 3G8, i1A8 and 3A5; in the N-terminal antigenic region is increased. C-terminal N domain epitopes, namely mAbs 1G12 and 6A12, appear to be occluded with sACE-Y465D, as evidenced by the decreased affinity of these mAbs for the mutant. However, N-terminal C domain epitopes appear to be exposed since there is an increased affinity of mAbs 1E10 and 2H9 for the mutant. A marked increase in precipitation of sACE-Y465D by C domain-specific mAbs to the C-terminal region indicates that there has been rearrangement of the juxtamembrane stalk allowing access to the cleavage site, as was observed for P1199L (Eyries *et al*, 2001).

Soluble sACE-Y465D does not exhibit as marked changes in affinity for the ACE mAbs compared to the cell-associated form, indicative of domain rearrangement upon shedding. Greater exposure of the cleavage site due to domain rearrangement is compounded by the increased affinity of mAb 1B3 for the mutant.

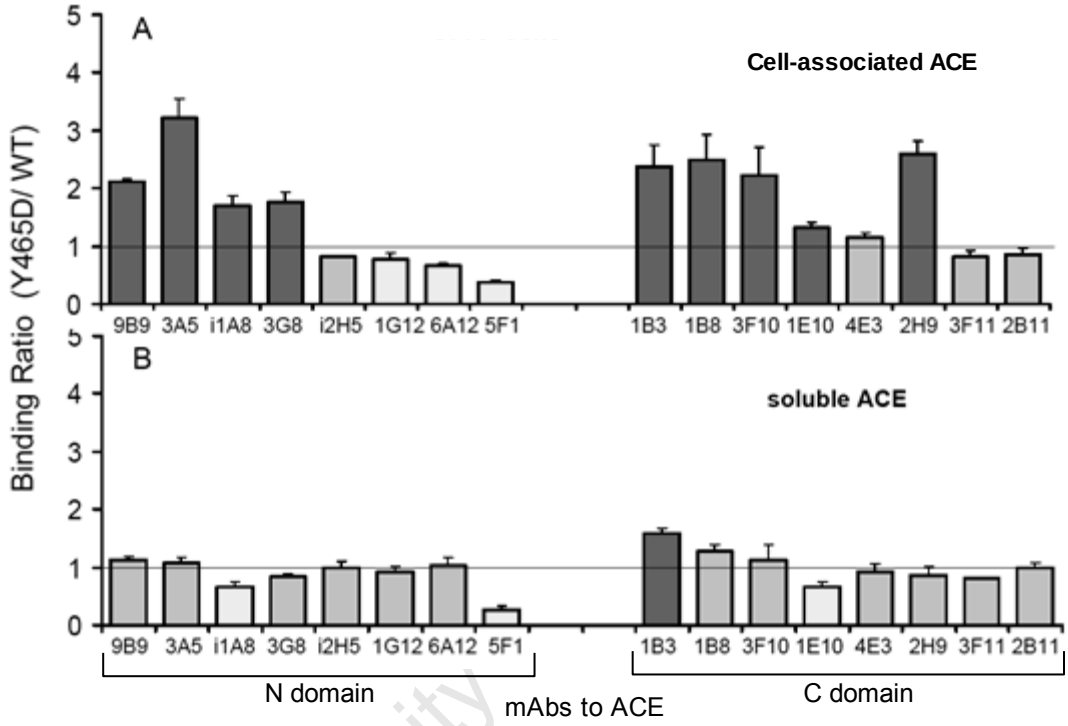

Figure 6.10. Precipitation of sACE-Y465D by ACE mAbs. A plate precipitation assay was performed with total cell lysate (*top*) and culture medium (*bottom*) from cells expressing wt sACE and sACE-Y465D using the panel of domain-specific mAbs. Data is shown as the ratio of binding of sACE-Y465D to wt, normalised to control (IgG) and is indicated as a noticeable increase in binding (*black*), decrease in binding (*light grey*) and no change in binding (*dark grey*) compared to wt.

6.2.5.2 Binding of mAbs to membrane-bound sACE-Y465D

An ELISA assay was performed on CHO cells to determine the binding affinity of the panel of domain-specific mAbs for membrane-bound sACE-Y465D compared to wt sACE (Figure 6.11) (for methods refer to Chapter 2, Section 2.2.6). As seen with the plate precipitation assay, there was a significantly decreased affinity of mAb 5F1 for membrane-bound sACE-Y465D (50.51% ± 6.49% of wt, $p < 0.001$), supporting the observation that Y465 is important for mAb 5F1 binding or that this epitope is occluded. The N domain-specific mAb 3A5 showed significantly increased affinity for the mutant (141.58% ± 6.98% of wt, $p < 0.001$) whereas mAbs to other epitopes in the N-terminal region did not. This may be due to decreased accessibility of these epitopes when sACE is tethered to the membrane.

Similarly to cell-associated sACE-Y465D, the membrane-bound form showed significantly increased affinity for the C domain-specific mAbs 1B3, 1E10 and 2H9, (324.33% ± 23.16%, 295.17% ± 18.01% and 179.66% ± 6.68% of wt respectively, $p < 0.001$) suggesting movement of the N domain to expose these epitopes. The striking increase in binding of mAb 1B3 to membrane-bound sACE-Y465D observed with the cell-associated and soluble forms, substantiates the rearrangement of the juxtamembrane region, exposing this epitope.

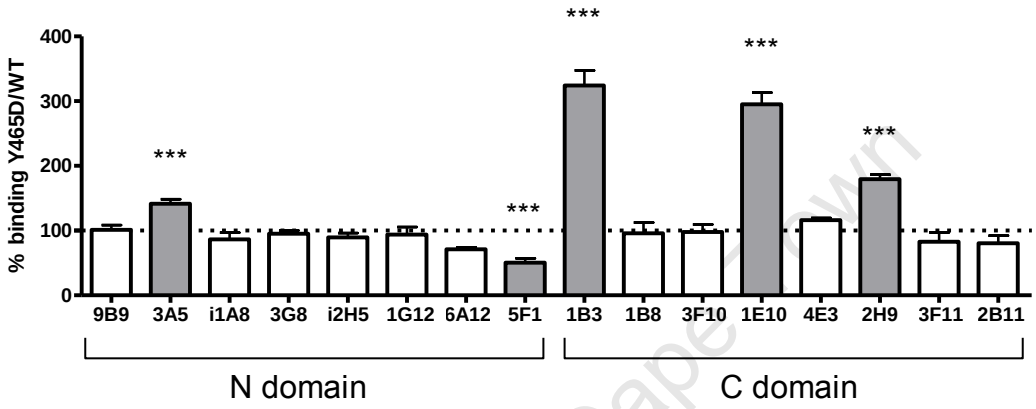

Figure 6.11. Binding of ACE mAbs to membrane-bound sACE-Y465D. A cell ELISA assay was performed on cells expressing wt sACE and sACE-Y465D using the panel of domain-specific mAbs. Data is shown as the ratio of binding of sACE-Y465D to wt, normalised to control (IgG) and is the mean±SD of two experiments (N domain mAbs) or three experiments (C domain mAbs) performed in duplicate. mAbs showing significant changes in binding compared to wild-type are indicated (*grey bars*).

6.2.6 Kinetic characterisation of sACE-Y465D

The hydrolysis of the physiological ACE substrates, angiotensin I (angI) and substance P (subsP), by wt sACE and sACE-Y465D was determined to evaluate whether the Y465D substitution had any effect. HPLC was performed to visualise the hydrolysis products, which may be altered by the mutation, particularly as sACE is known to digest subsP at multiple sites (Yokosawa *et al*, 1983; Skidgel *et al*, 1984). The rate of hydrolysis was determined using fluorogenic assays since this was the routine approach for determining enzyme activity in our hands and would require less substrate (for methods refer to Chapter 2, Section 2.2.12).

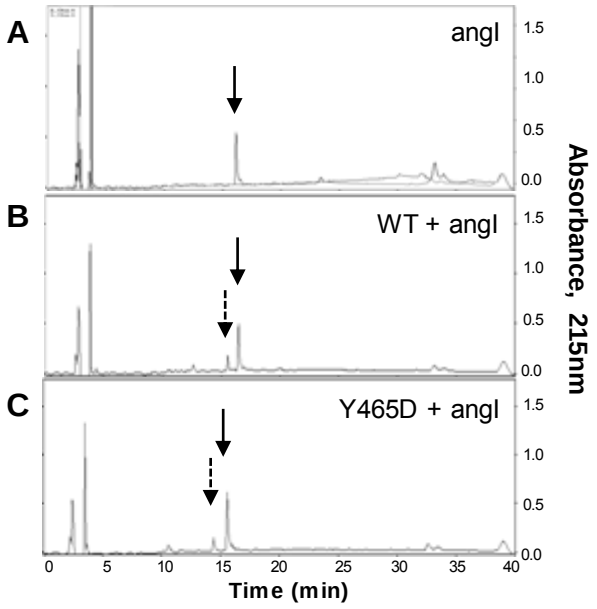

Figure 6.12. Hydrolysis of angiotensin I by wt and sACE-Y465D. HPLC profile of undigested angI (*A*) and angI incubated with wt sACE (*B*) or sACE-Y465D (*C*) for 1 hour in 50mM HEPES, 0.3M NaCl, 10μM $ZnSO_4$. Samples were separated over a 14-70% ACN gradient, absorbance at 215nm is shown. Peaks corresponding to angI substrate (*solid arrow*) and angII product (*dashed arrow*) are indicated.

6.2.6.1 Hydrolysis of angiotensin I

AngI digestion by wt sACE and sACE-Y465D was visualised by HPLC (refer to Appendix A.3 for peptide sequence and Chapter 2, Section 2.2.12.1 for methods). Undigested angI eluted at approximately 16 minutes at λ = 215nm in a control run (Figure 6.12A). After an hour digestion with wt sACE, a second peak was observed at 215nm that eluted at approximately 15 minutes (Figure 6.12B), consistent with angII product. The same profile was observed after digestion with sACE-Y465D (Figure 6.12C).

Michaelis-Menten kinetics were determined using a fluorogenic assay based on the protocol used for the synthetic substrate ZFHL (for methods refer to Chapter 2, Section 2.2.2). To overcome the potential derivitisation of the N-terminal primary amine by the fluorophore, leading to increased background fluorescence, a modified form of angI with an acetylated N-terminal group (acetyl-angI) was used. Thereby, a fluorogenic assay was established using the same conditions as ZFHL-based assay where hydrolysis of acetyl-angI was determined from a standard curve of the fluorescence of the product HL (refer to Appendix A.2.2) and detected using the fluorophore *o*-phthaldialdehyde (Figure 6.13 & Table 6.2) (refer to Chapter 2, Section 2.2.12.2 for methods).

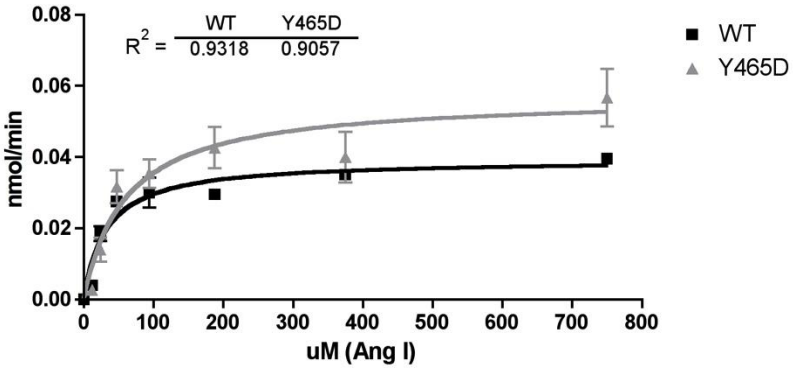

Figure 6.13. Michaelis-Menten curve of angiotensin I hydrolysis by wt and sACE-Y465D. 5nM ACE was incubated with increasing concentrations of angI for 15min at 37°C in 50mM HEPES, 0.3M NaCl, 10μM $ZnSO_4$. Hydrolysis products were detected with *o*-pthaldialdehyde as described (Chapter 2, Section 2.2.12.2). Data shown is a representative curve (mean±SD) of three experiments performed in duplicate (wt, *black*) and two experiments performed in triplicate (sACE-Y465D, *grey*). A Michaelis-Menten curve was generated using the in-built analysis software in GraphPad Prism.

Rate constants were determined from Michaelis-Menten curves to compare the rate of hydrolysis of acetyl-angI by sACE-Y465D to wt sACE. The mutation resulted in a ~1.5-fold decrease in affinity for angI, according to the K_m, with a 1.5-fold increase in turnover (k_{cat}). The overall catalytic efficiency of sACE-Y465D was unchanged compared to wt (k_{cat}/K_m). This indicates that the mutant does not have a remarkable effect on ACE activity with respect to this physiological substrate.

Table 6.2. Kinetics of hydrolysis of acetyl-angI by wt sACE and sACE-Y465D. Rate constants were determined from the Michaelis-Menten curve (Figure 6.13)

	WT	**Y465D**
K_m (μM)	33.46 ± 2.77	57.92 ± 2.82
k_{cat} (s^{-1})	3.25 ± 0.31	5.11 ± 0.54
k_{cat}/K_m ($\mu M^{-1}. s^{-1}$)	0.097 ± 0.003	0.089 ± 0.014

6.2.6.2 Hydrolysis of substance P

Digestion products of subsP by wt sACE and sACE-Y465D were separated by HPLC and absorbance recorded at λ = 215nm (refer to Chapter 2, Section 2.2.12.1 for methods and Appendix A.3 for peptide sequence). Undigested subsP eluted at 17 minutes (Figure 6.14A) and after 1 hour digestion with sACE, three peaks that eluted at approximately 12, 15 and 17 minutes, were observed (Figure 6.14B). The appearance of multiple peaks is consistent with previous HPLC of subsP hydrolysed by sACE (Yokosawa *et al*, 1983; Skidgel *et al*, 1984). A

similar profile was observed after digestion with sACE-Y465D (Figure 6.14C) and it appears that the mutant does not affect the ability of the enzyme to cleave substance P.

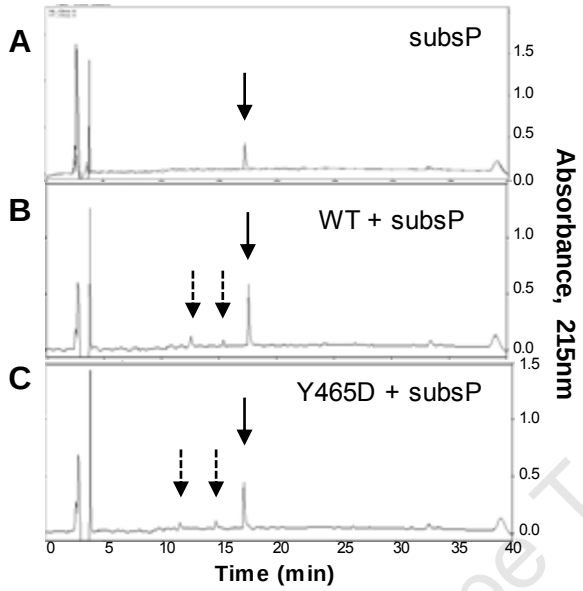

Figure 6.14. Hydrolysis of substance P by wt and sACE-Y465D. HPLC profile of undigested subsP (*A*) and subsP incubated with wt sACE (*B*) or sACE-Y465D (*C*) for 1 hour in 50mM HEPES, 0.3M NaCl, 10μM $ZnSO_4$. Samples were separated over a 14-70% ACN gradient, absorbance at 215nm is shown. Peaks corresponding to subsP substrate (*solid arrow*) and products (*dashed arrows*) are indicated.

A fluorogenic assay was established to determine the rate of hydrolysis of substance P by sACE and the mutant sACE-Y465D (for methods refer to Chapter 2, Section 2.2.12.1). The derivitising agent fluorescamine was used to detect the product. This compound reacts with primary amines to form a highly fluorescent fluorophore (Udenfriend *et al*, 1972). In the case of subsP, high baseline fluorescence, proportional to the concentration of substrate present was observed, which was used to adjust readings (refer to Appendix A.2.3). Rate constants of subsP hydrolysis by sACE-Y465D were determined from Michaelis-Menten curves (Figure 6.15 and Table 6.3).

Table 6.3. Kinetics of hydrolysis of substance P by wt sACE and sACE-Y465D. Rate constants were determined from the Michaelis-Menten curve (Figure 6.15)

	WT	**Y465D**
K_m (μM)	89.36 ± 14.27	87.78 ± 46.42
k_{cat} (s^{-1})	5.48 ± 0.27	8.44 ± 0.82
k_{cat}/K_m ($\mu M^{-1}. s^{-1}$)	0.062 ± 0.013	0.115 ± 0.070

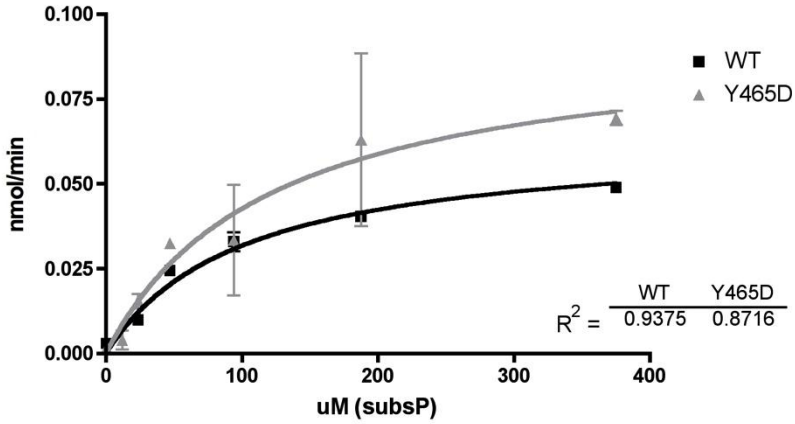

Figure 6.15. Michaelis-Menten curve of substance P hydrolysis by wt and sACE-Y465D. 5nM ACE was incubated with increasing concentrations of subsP for 15min at 37°C in 50mM HEPES, 0.3M NaCl, 10µM $ZnSO_4$. Hydrolysis products were detected with fluorescamine as described (Chapter 2, Section 2.2.12.2). Data shown is a representative curve (mean±SD) of two experiments performed in duplicate and triplicate (wt sACE, *black*; sACE-Y465D, *grey*). A Michaelis-Menten curve was generated using the in-built analysis software in GraphPad Prism.

The mutation did not appear to affect the affinity of ACE for subsP as the K_m values were similar. There was 1.5-fold increase in the turnover of subsP by the mutant and the overall catalytic efficiency increased 1.8-fold. However, there was a degree of experimental error, evident from the rate constants, most likely introduced due to difficulty in handling the fluorescamine solution. Therefore, these results suggest that the mutation does not affect the hydrolysis of subsP by sACE.

6.3 DISCUSSION

A novel sACE mutation has recently emerged in a family where certain members presented with chronic nausea, fatigue and vomiting (Prof. S. Danilov, personal communication). Elevated plasma ACE levels were observed in affected individuals within the family and sequencing of the ACE gene in the primary patient revealed a single base pair mutation at nucleotide position 1480, causing a Tyr to Asp transition at residue 465 (Figure 6.1).

The increase in plasma ACE observed in affected individuals could be explained in the following ways. First, it might be due to altered expression of sACE in cells, leading to a higher amount of ACE released into the plasma, as observed with the recently described W1197Stop substitution. This mutation introduces a premature stop codon in the stalk region, resulting in the expression of an active soluble form of sACE (Nesterovich *et al*, 2009). Second, an increased rate of shedding caused by changes in the affinity/access of the ACE secretase or changes in the shedding mechanism itself could result in increased plasma ACE, as observed with the P1199L substitution (Kramers *et al*, 2001; Eyries *et al*, 2001).

To investigate the cause of the increased levels of soluble ACE, the biochemical effects of the Y465D substitution on ACE expression and processing were characterised. The substitution was introduced into sACE cDNA by site-directed mutagenesis and the mutant expressed in CHO cells. The effect of this mutation on ACE expression, shedding, conformation and substrate hydrolysis was investigated.

The Y465D mutation had no observable effects on protein expression in CHO cells. Equivalent levels of enzyme were detected in cell lysate using an ACE activity assay (Figure 6.2) and western blotting (Figure 6.3). However, levels of ACE were significantly increased in culture medium from CHO cells (Figure 6.2). This was consistent with the observed increase in plasma ACE in affected individuals and suggested that transfection of sACE-Y465D into cultured cells was an effective model system to characterise the biochemical effects of this substitution. Since protein expression did not appear to be affected by the mutation, the increased plasma ACE levels observed with affected individuals could be explained by an increased rate of shedding of ACE from the cell surface.

Indeed, the Y465D mutation led to a dramatic increase in basal shedding of sACE from CHO cells (8-fold) (Figure 6.5). The profile of sACE-Y465D shedding in the presence of PDBu, DCI and TAPI-1 showed the same trend as wt (Figure 6.6) indicating that the same mechanism and moreover, the same sheddases might be involved. The cleavage site within the stalk region of sACE-Y465D was shown to lie between residues R1203 and S1204

(Figure 6.9, Table 6.1), as previously observed for wt sACE (Woodman *et al*, 2000). This suggests that the increased basal shedding observed is not due to changes in the mechanism of shedding and that the same sheddase is involved. This also supports the hypothesis that altered access of the secretase to the cleavage site might have led to increased shedding.

A significantly greater induction of sACE-Y465D shedding compared to wt sACE was observed in the presence of PDBu and DCI. This may be the result of altered signalling pathways and thus increased expression of the secretase. The DCI-induced response could be the result of an increase in the pool of membrane-bound ACE. However, without observable changes in ACE expression, this seems unlikely. sACE shedding is less efficient compared to tACE, which has been proposed to be the result of occlusion by the N domain of a recognition motif in the C domain (Beldent *et al*, 1995; Woodman *et al*, 2005). Regardless of the concentration of membrane-associated sACE, the rate-limiting step for cleavage would then be the access of the secretase to the scissile bond. Therefore, it seems that increased PDBu or DCI-induced shedding may be due to a greater efficiency of shedding rather than increased levels of the sheddase or ACE.

Increased binding of mAb 3A5 to cell-associated and membrane-bound sACE-Y465D was observed (Figures 6.10 & 6.11). Moreover, shedding of the mutant was not induced by mAb 3A5, or mAb 9B9 to some extent (Figure 6.7). These mAbs bind to the antigenic region of the N domain that appears to be involved in regulation of ACE shedding, most likely due to steric hinderance of a recognition motif on the C domain or juxtamembrane region (Balyasnikova *et al*, 2002). These results suggest that sACE-Y465 has adopted the conformation typically imposed by binding of mAbs 3A5 and 9B9 and thus has adjusted the basal levels of shedding by allowing better access of the secretase. This is supported by the increased affinity of C domain-specific mAbs 1E10 and 2H9 for both cell-associated and membrane-bound sACE-Y465D (Figures 6.10 & 6.11). It appears that sACE has assumed a conformation similar to the "extended" model proposed by Corradi *et al* (2006) and observed in the EM structure (Chen *et al*, 2010) (refer to Chapter 1, Section 1.2.5 & Figure 1.5), reducing the occlusion of the N domain by the C domain. Interestingly, mAb 3A5 induces a 4.5-fold increase in shedding (Figure 6.7), whereas shedding of sACE-Y465D is 8-fold more efficient than wt. This suggests that besides the unmasking of the C domain, another effect may be involved. The striking increase in affinity for the C domain-specific mAb 1B3 (Figures 6.10 & 6.11), which is an indicator of re-arrangement of the juxtamembrane region

(Danilov *et al*, 2005), suggests that greater accessibility of the cleavage site may also be a factor.

These results indicate a novel mechanism in the regulation of ACE shedding where a mutation in the N domain results in rearrangement of the domains, exposing the cleavage site and a potential cleavage recognition domain. It is possible that Y465 is involved in this mechanism through interactions with residues in the linker region. In the N domain crystal structure Y465 is 10-12Å from the peptide backbone of the linker region. Considering the flexibility of the linker region, it is possible that some interaction of the amino acid side chains with proximal residues in the N domain could occur. Interaction of Y465 and residues in the linker region could facilitate positioning of sACE in a conformation closer to the "compact" model proposed by Corradi *et al* (2006) (refer to Chapter 1, Section 1.2.5 & Figure 1.5), with the N and C domains in close proximity. The introduction of an acidic Asp group at position 465 could potentially disrupt this interaction, allowing for movement of the N domain, leading to the "extended" conformation of sACE. There was a consistent loss of affinity for the N domain-specific mAb 5F1 with cell-associated and soluble sACE-Y465D in the precipitation assay as well as membrane-bound sACE-Y465D (Figures 6.10 & 6.11). It is possible that Y465 is necessary for mAb 5F1 binding, or that the mutation has resulted in conformational changes that have altered access of this region. Interestingly, Y465D lies within the dimer interface observed in the most recently solved crystal structure of the N domain (Anthony *et al*, 2010), which suggests that Y465D may be involved in protein-protein interactions, such as dimerisation, that regulate shedding.

This is the first endogenous ACE mutation described where increased plasma ACE levels are associated with deleterious effects. The increased rate of shedding observed with sACE-Y465D does not directly explain the clinical symptoms observed with affected individuals. Elevated levels of soluble ACE and substance P were observed in plasma of the index patient as well as affected family members suggesting that these may play a role. This is surprising considering that substance P is a substrate for ACE and it would be expected that the increased levels of ACE would result in increased hydrolysis of substance P. A recent study of migraineurs showed a similar phenomenon (Fusayasu *et al*, 2007), but the authors fail to explain this observation.

There is no evidence to suggest that elevated plasma ACE is detrimental, despite this being a good marker for sarcoidosis (Lieberman *et al*, 1975; Rømer, 1984; Danilov *et al*, 2010), or produces the symptoms described. It may be possible that Y465D has increased the

sensitivity of ACE to endogenous substrates or inhibitors that has led to alterations in expression or processing. Alternatively, the mutation could have altered the kinetic parameters of ACE with regards to some substrates thereby disrupting important physiological pathways. The most likely candidate is substance P, a substrate for sACE as well as being associated with similar clinical symptoms. The first possibility seems unlikely since there was no change in the level of expression of sACE-Y465D in both the absence and presence of substance P. Furthermore, this substrate had no effect on basal shedding of sACE-Y465D (Figure 6.8). This leaves aberrant degradation of substance P by sACE-Y465D as a possible explanation. However, it appeared that the kinetic parameters of angI hydrolysis were not affected by Y465D, indicating that this mutation has had little effect on ACE activity (Figures 6.12 & 6.13, Table 6.2). Similarly, the rate of substance P hydrolysis was unchanged and similar peak profiles compared to wt were obtained by HPLC (Figures 6.14 & 6.15, Table 6.3). Thus, altered hydrolysis of substance P by ACE is not likely the cause of elevated levels or the symptoms described.

It appears that the mechanism involved may be due to an indirect effect of ACE on substance P, potentially mediated by other substrates or enzymes.

For the benefit of this family, it is imperative that the underlying mechanism is elucidated. This would entail investigating other candidate genes for substitution that may assist in this phenotype, which include the NEP gene, genes related to substance P production. Whole genome sequencing of the index patient and 2 affected family members is currently being conducted.

In conclusion, a novel ACE substitution has been described which does not affect ACE expression but results in aberrant shedding from the surface of CHO and HEK cells. This is attributed to the conformational rearrangement of the N domain, most probably exposing a recognition motif on the C domain as well as the stalk region, which allows better binding and access of the ACE secretase. This substitution has been described in family were it seems to result in chronic clinical symptoms that may be the result of elevated substance P. This is the first ACE substitution to be described that is associated with adverse effects.

CHAPTER 7: Conclusions and Future Directions

Increased understanding of the structure-function of biological molecules has led to the development of interactomes, or protein-protein interaction networks, which, in terms of proteomics, describe the cross-talk between components of different pathways. Predictions of protein-protein interactions have made use of complexes of solved protein structures and their interaction surfaces. Furthermore, mapping of the interaction regions or "hotspots" on proteins gives insight into particular biological reactions and allows for modelling of unknown protein structures.

With the identification of novel physiological substrates of ACE, it has become increasingly evident that this enzyme acts outside of its classic role as a regulator of the cardiovascular system. Its action on the Aβ peptide implicates it in Alzheimer's disease (Oba *et al*, 2005) and on AcSDKP with stem cell haematopoiesis (Azizi *et al*, 2006). The cross-talk of ACE between these pathways is most likely regulated by specific interactions, which need to be better appreciated. Moreover, the development of domain-specific inhibitors necessitates clearer definition of the sACE interactome and the role of each domain in these interactions. One approach is to harness the structural knowledge of ACE and investigate the surface topology of each domain towards pinpointing regions involved in protein-protein interactions and biological processes.

Thus, the overall aims of this work were to identify regions of sACE involved in protein-protein interactions and to determine their role in processes such as dimerisation, shedding and inter-domain movement. Particular regions and residues were identified using site-directed mutagenesis and a panel of domain-specific anti-ACE mAbs, where several aspects were investigated. These included the effect of an engineered disulphide bridge on inter-domain movement (Chapter 3); determining the role of each domain in dimerisation and shedding through fine epitope mapping of three N domain-specific mAbs (Chapter 4). Furthermore, the role of the free cysteine in each domain was investigated (Chapter 5) and finally, the biochemical effects of a novel mutation, Y465D, on shedding were determined (Chapter 6).

The interaction of the two domains has been demonstrated in several ways. First, it has been suggested by the negative cooperativity of the domains with respect to substrate hydrolysis (Andujar-Sanchez *et al*, 2004). Second, the occlusion of domain-specific mAb epitopes by each domain (Balyasnikova *et al*, 2007; Naperova *et al*, 2008a) and the identification of

regions of the N domain implicated in shedding indicate interplay between the two domains (Balyasnikova *et al*, 2002). Third, the inefficient rate of shedding of sACE compared to tACE implicates the N domain in shedding regulation (Woodman *et al*, 2005). These findings indicate that domain interaction is an important regulatory mechanism in post-translation processing of ACE, such as in ectodomain shedding and dimerisation.

Much of what is known regarding ACE ectodomain shedding is the result of work with the tACE isoform, used to determine the basis of secretase recognition and binding. It is generally agreed that a recognition domain in the C domain or juxtamembrane stalk is responsible for interaction while the role of the N domain in sACE shedding is unclear. Steric hinderance of a C-domain recognition motif by the N domain is purported to be the reason for inefficient shedding of sACE compared to tACE (Woodman *et al*, 2005). Indeed, the N domain mutations produced in this study had a significant effect on shedding, namely those in the overlapping portion of the epitopes of mAbs 9B9 and 3G8 (Q18H, L19E and Q22A) and the Y465D mutation proximal to the linker region. With Y465D in particular, a dramatic increase in shedding was concomitant with an altered conformational footprint, determined using the panel of domain-specific anti-ACE mAbs, that exposed epitopes associated with shedding (mAb 3A5) and domain interaction (mAbs 1E10 and 2H9) (Balyasnikova *et al*, 2002; Naperova *et al*, 2008a). Moreover, the increased shedding induced by mutations such as Y465D and CC/SS were associated with increased affinity of mAbs to the C-terminal antigenic region of the C domain (containing the epitopes of mAbs 1B3, 1B8 and 3F10). These results support the hypothesis that the conformation of the N and C domains in sACE are largely responsible for its poor efficiency with respect to ectodomain shedding when compared to the single domain tACE. A similar mechanism was attributed the increased shedding observed upon binding of N domain-specfic mAbs 3A5 and 9B9 (Balyasnikova *et al*, 2002). Under physiological conditions, specific protein-protein interactions, such as dimerisation or binding of a co-factor, could trigger this conformational change that might be an important regulatory mechanism for sACE shedding.

The role of dimerisation in the regulation of shedding has been alluded to in previous studies, where mAbs 9B9 and 3G8 that inhibit dimerisation in reverse micelles, altered shedding of sACE from CHO cells (Kost *et al*, 2003). However, a direct link between these two events has not been established. This work sought to define the role of residues in an overlapping region of the epitopes of the N domain-specfic mAbs 9B9 and 3G8 and the free thiols in each domain in dimerisation and shedding and towards establishing the relationship between these

mechanisms. These studies indicated that ACE dimerisation occurs via two mechanisms, though covalent interaction of the C domain free thiol and non-covalent interactions in the N domain. Disulphide-linked dimerisation via the C domain may be associated with the ACE inhibitor induced dimer activation of CK2 phosphorylation and intracellular signalling (Kohlstedt *et al*, 2006). Moreover, this mechanism has been associated with negative regulation of shedding (Kohlstedt *et al*, 2002) and could be the link between the two processes, particularly since removal of the C domain thiol had a significant effect on sACE shedding. It is unclear what role dimerisation of the N domain plays, although residues in the N terminal antigenic region, particularly Q22, affected both dimerisation and shedding. A future direction would be to determine the role of the N domain glycans in dimerisation, which would be assisted by the set of minimally glycosylated N domain mutants that have been generated (Anthony *et al*, 2010). However, further investigations into dimerisation would benefit from a means to differentiate between non-covalent and covalent interactions and from a robust approach to detecting native dimers on the cell surface. Non-covalent dimers of human B2K-R were successfully characterised by co-immunoprecipitation of V5- and myc-tagged receptors (Michineau *et al*, 2006). This is a reliable and standard technique for detecting protein-protein interactions in their native state, if the proper controls are in place to rule out non-specific interactions. Difficulties arise when the protein complex is in low abundance or proteins interact indirectly, via a co-factor for example (Phizicky & Fields, 1995). An alternative approach would be to use fluorescence resonance energy transfer (FRET) or bioluminescence resonance energy transfer (BRET) fusion proteins, as was used to detect human ACE/B2K-R heterodimers (Chen *et al*, 2006). These techniques are highly advantageous in that they can monitor protein-protein interactions in live cells and detect interactions within 100Å (Rebois *et al*, 2008). However, this requires the correct combination and position of donor and acceptor tags to maximise energy transfer, careful implementation of a number of controls to eliminate artefacts (Pfleger *et al*, 2006) and potentially complicated and expensive instrumentation. In addition, there may likely be a decrease in signal due to the formation of ACE-donor and ACE-acceptor homodimers.

The linker region confers flexibility of movement between the domains and, according to the sACE model proposed by Corradi *et al* (2006), allows the enzyme to adopt conformations ranging between two extreme "compact" and "extended" poses. The recent cryo-EM structure of sACE attests to the "extended" pose as a native conformation, albeit in solution (Chen *et al*, 2010). The conformational footprint of the mutants described in these studies

confirms that certain regions are involved in domain interaction, particularly those that affect shedding. These include the epitopes of the N domain-specific mAbs 1G12, 6A12 and 3A5 and the C domain-specific mAbs 1E10, 4E3 and 2H9. From the changes in binding it seems that with increased shedding efficiency and the exposure of certain epitopes, sACE adopts a pose closer to the "extended" conformation that would allow access of mAbs 3A5, 9B9, 3G8, 6A12 and 1G12 on the N domain and rearrangement of the juxtamembrane region, exposing the epitopes of mAbs 1B3, 1B8 and 3F10. This is in agreement with the Corradi *et al* (2006) models. However, this requires further confirmation from a high resolution structure of sACE has been resolved, which is hampered by the difficulty in obtaining viable crystals. Engineering a disulphide into the linker region was a viable approach towards limiting inter-domain movement, although this study has shown that the positioning of the bridge is vital. The most likely mutation to succeed would be one that introduces a link between the two domains downstream of the linker region. However, without knowing where the two domains interact it is difficult to engineer disulphide bridges. The conformational footprint of the mutants has given clues as to which epitopes are affected and these may be a stepping stone towards determining inter-domain interaction. Intramolecular FRET may be useful here, where fluorescent tags could be attached to candidate regions in order to determine whether the two domains interact. A means to identify key residues might be to define the epitopes even further. The most viable approach would be to co-crystalise the single domain isoform and an anti-ACE mAb fragment, as has been performed with other proteins (Leonard *et al*, 2008; Newman *et al*, 2009; Teplyakov *et al*, 2009). Considering the advance in x-ray crystallography and the development of viable candidates for crystallisation, this may be a viable approach. Alternatives to obtaining structural data such as cryo-EM and small-angle x-ray scattering (SAXS) could be pursued, both of which have the advantage of not requiring crystals for analysis. However, the resolution with both these techniques is low compared to x-ray crystallography (50-250Å for SAXS, 5-10Å for cryo-EM at best).

In summary, this is the first set of studies exploring the functions of the free thiols; to identify residues in the N domain that play a role in shedding and dimerisation and to attempt to engineer disulphides in the linker region towards stabilising ACE. These studies have given insight into the role of inter-domain interaction(s) of ACE and post-translational processing - specifically shedding and dimerisation.

APPENDIX

A.1. MUTAGENESIS AND SUBCLONING

A.1.1. Primers for site-directed mutagenesis

Table A.1. Primers for site-directed mutagenesis (SDM) of Ndom or sACE. The forward primer is indicated, both the forward and the reverse complementary primer was used in each reaction. Restriction enzyme (RE) sites altered are underlined and nucleotides changed are indicated in bold.

		RE Site	Tm
H600C	5′-GGGCTGGCC**G**GAGTACCAGTGG**TGC**CCGCCGTTGCCTGAC-3′	+ *Bsa*XI	89.3°C
P3A	5′-CTGGCGTTGGAC**G**C**A**GG**A**CTGCAGCCCGGC-3′	- *Sma*I	79.1°C
G4E	5′-CCCTGGCGTTGGA**T**CCCG**AA**CTGCAGCCCGGC-3′	+ *Bam*HI	80.5°C
Q6A	5′-CTGGCGTTGGACCCTGGGCTG**GCA**CCCGGCAACTTTTC-3′	- *Pst*I	80.2°C
Q18H	5′-GCTGACGAGGCCGG**A**GC**T**CA**T**CTCTTCGCGCAGAGC-3′	+ *Sac*I	81.8°C
L19E	5′-CGAGGCCGGGGC**C**CAG**GAG**TTCGCGCAGAGC-3′	+ *Apa*I	78.6°C
Q22A	5′-CGCAGCTCTTCGCG**GC**GAG**T**TA**T**AACTCCAGCGCC-3′	+ *Psi*I	76.6°C
N25Q	5′-GCAGAGCTAC**C**A**A**TCCAGCGC**T**GAACAGGTGCTG-3′	+ *Eco47*III	76.9°C
Q30V	5′-CAACTCCAGCGCCGAA**GT**GGT**C**CTGTTCCAGAGCGTGG-3′	- *Alw*NI	81.7°C
I79V	5′-GGAGCTGTATGAACCG**G**TCTGGCAGAACTTCAC-3′	+ *Age*I	80.4°C
R340A	5′-CTTGGGACTTCTACAAC**GCT**AA**G**GACTTCAGGATCAAGCAGTG-3′	+ *Bpu*10I	78.8°C
D374A	5′-CAGTACTAC**A**TACAAGG**C**TCTGCCCGTCTCCC-3′	- *Pst*I	81.1°C
C474S	5′-GTATCAGGGGAT**A**T**C**TCCTCCTGTTACC-3′	+ EcoRV	70.8°C
C1072S	5′-GAAGTACCA**A**GGCCTC**A**GCCC**A**CCAGTGCCC-3′	+ *Bpu*10I	76.5°C

A.1.2. Internal sequencing primers

A set of internal primers to ACE were used for nucleotide sequencing. They comprise both forward and reverse complementary primers designed to enable sequencing of the entire N domain and sACE genes in pBS.

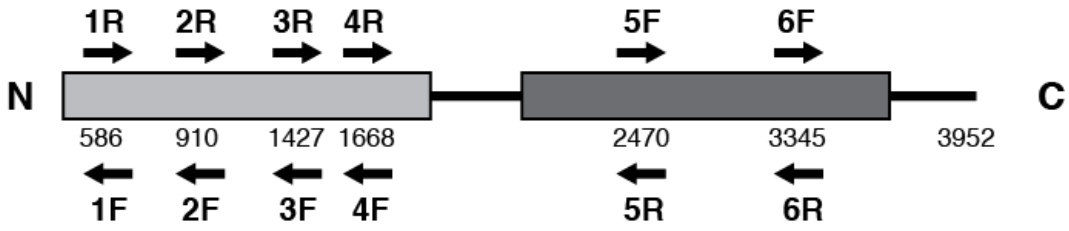

Figure A.1. Schematic representation of sACE gene. Forward primers are indicated above gene and reverse primers below. The nucleotide position of the beginning of the forward primer is indicated.

A.1.3. Bacterial Cell Lines And Culturing

E.*coli* JM109 cells (endA1 glnV44 thi-1 relA1 gyrA96 recA1 mcrB$^+$ Δ(lac-proAB) e14- [F' traD36 proAB$^+$ lacI^q lacZΔM15] hsdR17($r_K^-m_K^+$)) were used for plasmid DNA expression. Bacterial cells were cultured in Luria Broth (LB) growth medium (10g tryptone, 5g yeast extract, 10g NaCl in 1L dH_2O) and plated on LB agar plates (Luria broth with 1.5% w/v agar) containing 100µg/ml ampicillin for selection of cells containing recombinant DNA.

Competent cells were prepared using the $CaCl_2$ method (Sambrook & Russell, 2001). Overnight bacterial mini-cultures grown in LB in the absence of antibiotic were inoculated into a larger volume (1/100 dilution) and grown until OD_{600} ~ 0.5. Cells were pelleted at 5000rpm at 4°C and resuspended in cold 100mM $MgCl_2$. After a 30 minute incubation on ice, cells were re-pelleted at 5000rpm at 4°C and then resuspended in cold 100mM $CaCl_2$ with 15% glycerol. Competent cells were aliquoted and stored at -80°C until use.

For transformation into competent *E.coli* JM109 cells, 50-100ng plasmid DNA was mixed with cells and incubated on ice for 30 minutes. DNA uptake occurred by heat-shock at 42°C for 45 seconds followed by 2 minutes on ice. Cells were then diluted 1/10 in LB without antibiotic and grown at 37°C for 1 hour. Cells were pelleted by centrifugation, resuspended in 100µl LB, plated onto LA plates containing antibiotic and grown overnight at 37°C.

A.1.4. DNA isolation

Small-scale DNA isolation was performed to screen colonies for positive clones after mutagenesis using a STET buffer based protocol. A single colony from plated culture of cells transformed with plasmid DNA was inoculated into Luria broth and grown at 37°C overnight. Cells were pelleted by centrifugation and resuspended in STET buffer [200mM sucrose, 50mM Tris-HCl (pH 8), 50mM EDTA (pH 8), 5%w/v Triton X-100] containing 1mg/ml lysozyme. Cells were lysed by boiling and protein precipitated by centrifugation. The protein pellet was removed and DNA precipitated with 25% isopropanol by centrifugation and dried on a SpeedyVac (Savant, USA). DNA was re-suspended in dH_2O with 100µg/ml RNaseA.

A.1.5. Restriction enzyme digestion

A 20µl digestion cocktail containing 100-300ng DNA, 1X restriction enzyme buffer, 0.5U restriction enzyme (Fermentas, USA) in dH_2O was incubated at 37°C for 1 hour. Double restriction enzyme mixes calculated using the online DoubleDigest^{TM} Tool (www.fermentas.com, Fermentas, USA) in the same reaction volume. Reactions were

stopped with 1/6 volume 6X loading dye (0.025g Bromophenol Blue, 0.025g Xylene Cyanol, 30% glycerol) and separated by agarose gel electrophoresis.

A.1.6. DNA ligation

Vector and insert DNA were mixed (3:1 ratio) with 1X ligation buffer and 1U T4 DNA ligase (Fermentas, USA) in dH_2O and placed at 4°C for 48 hours. Aliquots of the reaction were transformed into competent E.*coli* JM109 cells and plated onto LB agar plates containing 100µg/ml ampicillin.

A.1.7. cDNA synthesis

Synthesis of cDNA from total RNA was performed using the Advantage® RT-for-PCR kit (Clonetech Laboratories, USA) according to the manufacturer's instructions. Briefly, 1ug total RNA was incubated with 1.5µM oligo$(dT)_{18}$ primer at 70°C for 2 minutes, then quenched on ice. A cocktail containing 1X reaction buffer, 500µM dNTPs, 0.5µl recombinant RNase inhibitor and 10U recombinant Moloney-Murine Leukemia Virus (MMLV) reverse transcriptase was added and the mixture incubated at 42°C for 1 hour followed by a denaturation step at 95°C for 5 minutes.

A.1.8. PCR protocols

A.1.8.1. Site-directed mutagenesis with Pfu DNA polymerase

A 50µl cocktail in nf dH_2O:

- 1 x *Pfu* Polymerase Buffer*
- 400µM dNTP mix
- 200nM Forward primer
- 200nM Reverse primer
- 5% DMSO
- 2-6mM $MgCl_2$
- 25-50ng Template DNA
- 2U *Pfu* DNA Polymerase

Reaction parameters:

- 94°C, 5 minutes

16 cycles of:

- 94°C, 30 seconds
- Tm of primer, 30 seconds
- 75°C, 10 minutes

Followed by:

- 75°C, 15 minutes

* 20mM Tris-HCl (pH 8.8), 10mM KCl, 10mM $(NH_4)_2SO_4$, 2mM $MgSO_4$, 0.1% Triton X-100, 100µg/ml BSA

A.1.8.2. Site-directed mutagenesis with HiFiTM DNA polymerase

A 50µl reaction cocktail of:

- 1x HiFi Fidelity buffer (2mM Mg^{+})
- 300µM dNTP mix
- 300nM Forward primer
- 300nM Reverse primer
- 0-4mM $MgCl_2$
- 20ng Template DNA
- 1U HiFi^{TM} DNA polymerase

in nuclease-free dH_2O

Reaction parameters:

- 94°C, 2 minutes

20 cycles of:

- 98°C, 20 seconds
- Tm of primer, 15 seconds
- 68°C, 30s/kb template DNA

Followed by:

- 68°C, 5 minutes

A.1.8.3. RT-PCR

cDNA synthesis from total RNA extracted from CHO cells was performed using the following protocol:

A 50µl reaction cocktail of:

- 1x HiFi Fidelity buffer (2mM Mg^{+})
- 300µM dNTP mix
- 300nM Forward primer*
- 300nM Reverse primer
- 10µl cDNA
- 1U HiFi^{TM} DNA polymerase

in nuclease-free dH_2O

Reaction parameters:

- 94°C, 2 minutes

20 cycles of:

- 94°C, 20 seconds
- 72°C, 30 seconds
- 68°C, 15 seconds

Followed by:

- 68°C, 2 minutes

*or G3PDH mix (containing 300nM forward and reverse primers)

A.2. PROTEIN EXPRESSION AND CHARACTERISATION

A.2.1. Bradford Protein Concentration Determination

Protein concentration of full-length sACE was determined using the IgG curve and for single domain ACE (Ndom and tACE), the albumin curve was used. The curves were determine by linear regression analysis using GraphPad Prism 4.0 software.

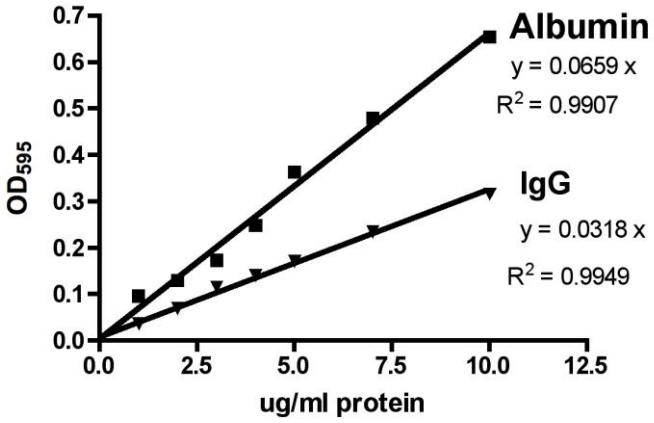

Figure A.2. Standard curve of absorbance over increasing protein concentration.

Protein concentration was determined using the following equation:

$$\mu g/ml = \frac{OD595 \times dilution}{slope}$$

A.2.2. HL Standard Curve

A 5mM HL (Sigma, USA) stock solution in dH_2O was prepared and diluted into a 0.5mM working stock solution in 1X potassium phosphate buffer. 30µl aliquots of HL in increasing concentrations, prepared by diluting in 1X potassium phosphate buffer, were placed in a 96-well plate in triplicate and assayed for fluorescence as described (Chapter 2, Section 2.2.2), beginning with the addition of 0.4M NaOH. The curve was determine by linear regression analysis using GraphPad Prism 4.0 software.

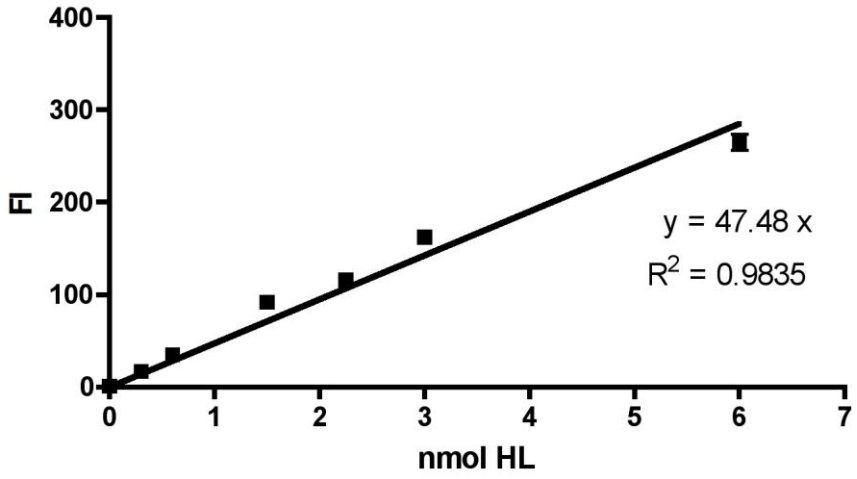

Figure A.3. Standard curve of fluorescence over increasing HL concentrations.

ACE activity was calculated as follows:

$$mU\ ACE = \frac{FI\ \times\ dilution\ \times\ initial\ volume\ (\mu l)}{slope\ \times\ sample\ volume\ (\mu l)\ \times\ time\ (min)} = nM\ HL/min$$

A.2.3. Baseline fluorescence of substance P

Dilutions of subsP in 50mM HEPES buffer (containing 300mM NaCl, 10µM $ZnSO_4$) were aliquoted into 96-well plates in triplicate. Derivitisation was performed by the addition of 2mg/ml fluorescamine and assayed as described in Chapter 2, Section 2.2.12.2.

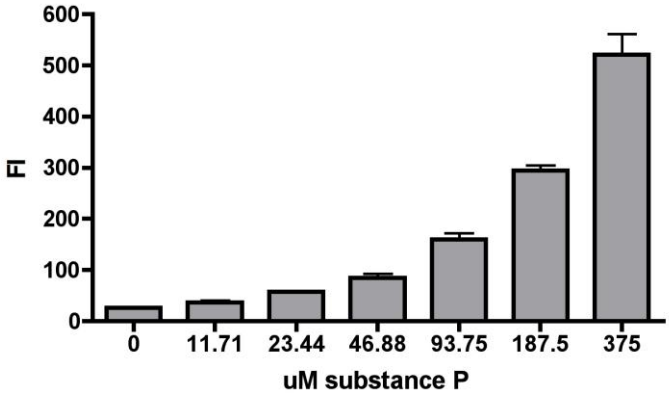

Figure A.4. Baseline fluorescence of substance P after derivatisation with fluorescamine. Data is mean±SD of triplicate samples.

A.2.4. Complete hydrolysis of substance P

Increasing concentrations of subsP were incubated with 10nM ACE at 37°C overnight to allow for complete hydrolysis. A fluorogenic assay to determine fluorescence of product was determined in triplicate as described (Chapter 2, Section2.2.12.2), beginning with the addition of 1M HCl. The curve was determine by linear regression analysis using GraphPad Prism 4.0 software.

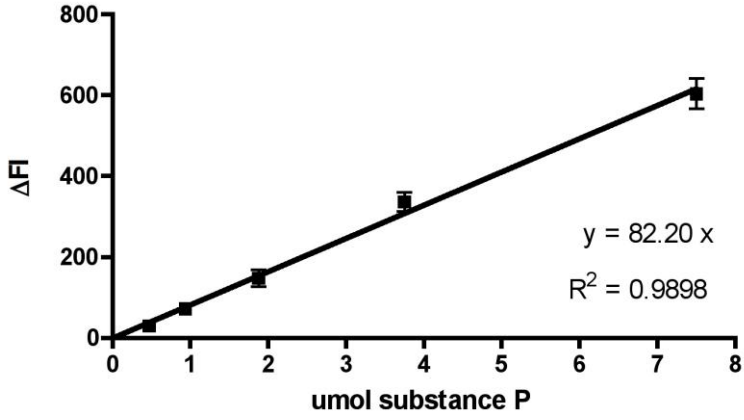

Figure A.5. Standard curve of complete hydrolysis of substance P.

A.2.5. Synthetic peptides

A.2.5.1 Preparation of ZFHL

A 20mM ZFHL stock was prepared by dissolving 110g powder (MW = 549.63 g/mol) in 1ml 0.28M NaOH (with heating), with dropwise addition of 9ml dH_2O, aliquoted and stored at -20°C until use. A 1mM working stock was prepared by dilution in 4ml 5X potassium phosphate buffer (pH 8.3), 2ml 3M NaCl, 13ml dH_2O and 20µl 10mM $ZnSO_4$, filter sterilised and stored at 4°C.

A.2.6. Endogenous peptides

A.2.6.1 Preparation of endogenous substrates

AngI, acetyl-angI and subsP were received in powder form. A 1mM stock of subsP (MW = 1347.63 g/mol) and 10mM stocks of angI (MW = 1296.50 g/mol) and acetyl-angI (MW = 1338.53 g/mol) were prepared by dissolving the appropriate weight in dH_2O. Solutions were aliquoted and stored at -20°C until use.

A.2.6.2. Sequence of peptides

Cleavage site indicated by arrow, with relevant references indicated.

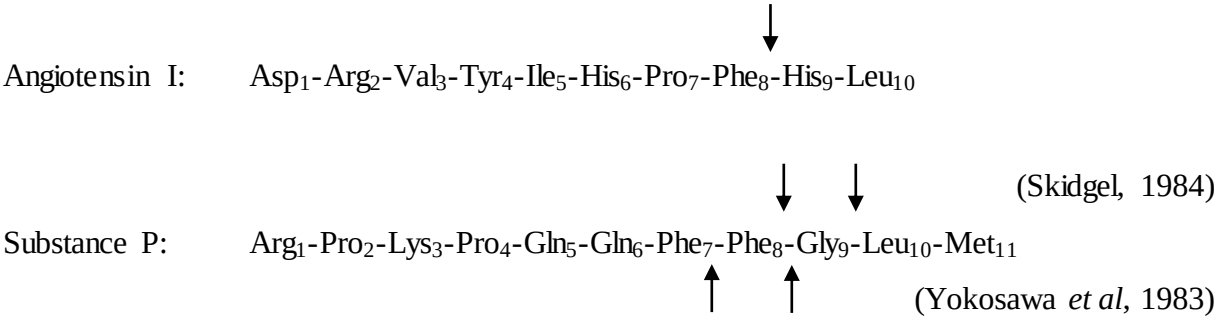

REFERENCES

AbdAlla, S. *et al*. (1999). Involvement of the amino terminus of the B(2) receptor in agonist-induced receptor dimerization. *J Biol Chem*, 274(37): 26079-84.

Alfalah, M. *et al*. (2001). A point mutation in the juxtamembrane stalk of human angiotensin I-converting enzyme invokes the action of a distinct secretase. *J Biol Chem*, 276(24): 21105-9.

Allinson, T.M.J. *et al*. (2004). The role of ADAM10 and ADAM17 in the ectodomain shedding of angiotensin converting enzyme and the amyloid precursor protein. *Eur J Biochem*, 271(12): 2539-47.

Andújar-Sánchez, M. Cámara-Artigas, A. & Jara-Pérez, V. (2004). A calorimetric study of the binding of lisinopril, enalaprilat and captopril to angiotensin-converting enzyme. *Biophys Chem*, 111(2): 183-9.

Anthony, C.S. *et al*. (2010). The N domain of human angiotensin-I converting enzyme: the role of N-glycosylation and the crystal structure in complex with an N domain specific phosphinic inhibitor RXP407. *J Biol Chem*. 286(46): 35685-93.

Anthony, L.C., Dombkowski, A.A. & Burgess, R.R. (2002). Using disulfide bond engineering to study conformational changes in the beta'260-309 coiled-coil region of Escherichia coli RNA polymerase during sigma(70) binding. *J Bacteriol*, 184(10): 2634-41.

Arndt, J.W. *et al*. (2002). Crystal structure of a novel carboxypeptidase from the hyperthermophilic archaeon Pyrococcus furiosus. *Structure*, 10(2): 215-24.

Arthur, J.F. *et al*. (2007). Ligand binding rapidly induces disulfide-dependent dimerization of glycoprotein VI on the platelet plasma membrane. *J Biol Chem*, 282(42): 30434-41.

Azizi, M. *et al*. (1996). Acute angiotensin-converting enzyme inhibition increases the plasma level of the natural stem cell regulator N-acetyl-seryl-aspartyl-lysyl-proline. *J Clin Inves*, 97(3): 839-44.

Baloria, U. *et al*. (2011). *In silico* proteomic characterization of human epidermal growth factor receptor 2 (HER-2) for the mapping of high affinity antigenic determinants against breast cancer. *Amino Acids*. Jan 13. [Epub ahead of print]

Balyasnikova, I.V. *et al*. (2002). Epitope-specific antibody-induced cleavage of angiotensin-converting enzyme from the cell surface. *Biochem J*, 362: 585-95.

Balyasnikova, I.V. *et al.* (2003). Monoclonal antibodies to denatured human ACE (CD 143), broad species specificity, reactivity on paraffin sections, and detection of subtle conformational changes in the C-terminal domain of ACE. *Tissue Antigens*, 61(1): 49-62.

Balyasnikova, I.V. *et al.* (2005a). Localization of an N-domain region of angiotensin-converting enzyme involved in the regulation of ectodomain shedding using monoclonal antibodies. *J Proteome Res*, 4(2): 258-67.

Balyasnikova, I.V. *et al.* (2005b). Monoclonal antibodies 1B3 and 5C8 as probes for monitoring the integrity of the C-terminal end of soluble angiotensin-converting enzyme. *Hybridoma*, 24(1): 14-26.

Balyasnikova, I.V. *et al.* (2007). Monoclonal Antibodies 1G12 and 6A12 to the N-domain of human angiotensin-converting enzyme: fine epitope mapping and antibody-based detection of ACE inhibitors in human blood. *J Proteome Res*, 6(4): 1580-94.

Balyasnikova, I.V. *et al.* (2008). Epitope mapping of mAbs to denatured human testicular ACE (CD143). *Tissue Antigens*, 72(4): 354-68.

Batista, E.C. *et al.* (2011). ACE activity is modulated by the enzyme α-galactosidase A. *J Mol Med,* 89(1): 65-74.

Bause, E. (1983). Structural requirements of N-glycosylation of proteins. Studies with proline peptides as conformational probes. *Biochem J*, 209(2): 331-6.

Beldent, V. *et al.* (1995). Cell surface localization of proteolysis of human endothelial angiotensin I-converting enzyme. Effect of the amino-terminal domain in the solubilization process. *J Biol Chem*, 270(48): 28962-9.

Bernstein, K.E. *et al.* (1988). The isolation of angiotensin-converting enzyme cDNA. *J Biol Chem*, 263(23): 11021-4.

Binevski, P. V *et al.* (2003). Evidence for the negative cooperativity of the two active sites within bovine somatic angiotensin-converting enzyme. *FEBS Letters*, 550(1-3): 84-8.

Bosenberg, M.W., Pandiella, A. & Massagué, J. (1992). The cytoplasmic carboxy-terminal amino acid specifies cleavage of membrane TGF alpha into soluble growth factor. *Cell*, 71(7): 1157-65.

Böttcher, A. *et al.* (2006). Angiotensin-converting enzyme signalling in human preadipocytes and adipocytes. *Centr Eur J Biol*, 1(2): 203-220.

Brentjens, J.R. *et al.* (1986). Gametes contain angiotensin converting enzyme (kininase II). *Experientia*, 42(4): 399-402.

Brown, C.K. *et al.* (2001). Structure of neurolysin reveals a deep channel that limits substrate access. *Proc Natl Acad Sci USA*, 98(6): 3127-32.

Bryan, P.N. (2000). Protein engineering of subtilisin. *Biochim Biophys Acta*, 1543(2): 203-222.

Bull, H.G., Thornberry, N.A. & Cordes, E.H. (1985). Purification of angiotensin-converting enzyme from rabbit lung and human plasma by affinity chromatography. *J Biol Chem*, 260(5): 2963-72.

Bünning, P., Holmquist, B. & Riordan, J.F. (1983). Substrate specificity and kinetic characteristics of angiotensin converting enzyme. *Biochemistry*, 22(1): 103-10.

Butters, T.D. *et al.* (1999). Effects of N-butyldeoxynojirimycin and the Lec3.2.8.1 mutant phenotype on N-glycan processing in Chinese hamster ovary cells: application to glycoprotein crystallization. *Protein Sci*, 8(8): 1696-701.

Caporaso, G.L. *et al.* (1992). Protein phosphorylation regulates secretion of Alzheimer beta/A4 amyloid precursor protein. *Proc Natl Acad Sci USA*, 89(7): 3055-9.

Casarini, D.E. *et al.* (2001). Angiotensin converting enzymes from human urine of mild hypertensive untreated patients resemble the N-terminal fragment of human angiotensin I-converting enzyme. *Int J Biochem & Cell Biology*, 33(1): 75-85.

Chattopadhyay, S. *et al.* (2005). Calmodulin binds to the cytoplasmic domain of angiotensin-converting enzyme and regulates its phosphorylation and cleavage secretion. *J Biol Chem*, 280(40): 33847-55.

Chattopadhyay, S. *et al.* (2008). A small region in the angiotensin-converting enzyme distal ectodomain is required for cleavage-secretion of the protein at the plasma membrane. *Biochemistry*, 47(32): 8335-41.

Chen, Z. *et al.* (2006). Human ACE and bradykinin B2 receptors form a complex at the plasma membrane. *FASEB J*, 20(13): 2261-70.

Chen, H. *et al.* (2010). Porcine pulmonary angiotensin I-converting enzyme-biochemical characterization and spatial arrangement of the N- and C-domains by three-dimensional electron microscopic reconstruction. *Micron*, 41(6): 674-85.

Ching, S.F., Hayes, L.W. & Slakey, L.L. (1983). Angiotensin-converting enzyme in cultured endothelial cells. Synthesis, degradation, and transfer to culture medium. *Arteriosclerosis*, 3(6): 581-8.

Chubb, A.J. *et al.* (2004). Deletion of the cytoplasmic domain increases basal shedding of angiotensin-converting enzyme. *Biochem Biophys Res Commun*, 314(4): 971-5.

Cianfriglia, M. *et al.* (2002). Monoclonal antibodies as a tool for structure-function studies of the MDR1-P-glycoprotein. *Curr Prot Pep Sci*, 3(5): 513-30.

Claffey, K.P., Senger, D.R. & Spiegelman, B.M. (1995). Structural requirements for dimerization, glycosylation, secretion, and biological function of VPF/VEGF. *Biochim Biophys Acta*, 1246(1): 1-9.

Corradi, H.R. *et al.* (2006). Crystal structure of the N domain of human somatic angiotensin I-converting enzyme provides a structural basis for domain-specific inhibitor design. *J Mol Biol*, 357(3): 964-74.

Corradi, H.R. *et al.* (2007). The structure of testis angiotensin-converting enzyme in complex with the C domain-specific inhibitor RXPA380. *Biochemistry*, 46(18): 5473-8.

Cushman, D.W. *et al.* (1977). Design of potent competitive inhibitors of angiotensin-converting enzyme. Carboxyalkanoyl and mercaptoalkanoyl amino acids. *Biochemistry*, 16(25): 5484-91.

Danilov, S.M. Allikmets, Sakharov, *et al.* (1987). Monoclonal antibody to human lung angiotensin-converting enzyme. *Biotech Appl Biochem*, 9(4): 319-22.

Danilov, S.M. *et al.* (1994). Structure-function analysis of angiotensin I-converting enzyme using monoclonal antibodies. Selective inhibition of the amino-terminal active site. *J Biol Chem*, 269(43): 26806-14.

Danilov, S.M. *et al.* (1996). Development of enzyme-linked immunoassays for human angiotensin I converting enzyme suitable for large-scale studies. *J Hypertens*, 14(6): 719-27.

Danilov, S.M. *et al.* (2003). Angiotensin-converting enzyme (CD143) is abundantly expressed by dendritic cells and discriminates human monocyte-derived dendritic cells from acute myeloid leukemia-derived dendritic cells. *Exp Hematol*, 31(12): 1301-9.

Danilov, S.M. *et al.* (2005). Detection of mutated angiotensin I-converting enzyme by serum/plasma analysis using a pair of monoclonal antibodies. *Clin Chem*, 51(6): 1040-3.

Danilov, S.M., Kost, O.A. & Sturrock, E.D. (2006). The Missing Link : ACE Dimerization and Shedding. *Mol Pharmacol*. http://molpharm.aspetjournals.org/content/ 69/5/1725/reply

Danilov, S.M. *et al.* (2007). Fine epitope mapping of monoclonal antibody 5F1 reveals anticatalytic activity toward the N domain of human angiotensin-converting enzyme. *Biochemistry*, 46(31): 9019-31.

Danilov, S.M. *et al.* (2008). Simultaneous determination of ACE activity with 2 substrates provides information on the status of somatic ACE and allows detection of inhibitors in human blood. *J Cardvasc Pharm*, 52(1): 90-103.

Danilov, S.M. *et al.* (2010a). Conformational Fingerprinting of the Angiotensin I-Converting Enzyme (ACE). 1. Application in Sarcoidosis. *J Proteome Res*, 9(11): 5782-93.

Danilov, S.M. *et al.* (2010b). Angiotensin I-converting enzyme Gln1069Arg mutation impairs trafficking to the cell surface resulting in selective denaturation of the C-domain. *PloS One*, 5(5): e10438.

Das, M. *et al.* (2007). Design of disulfide-linked thioredoxin dimers and multimers through analysis of crystal contacts. *J Mol Biol*, 372(5): 1278-92.

Datta, S. *et al.* (2008). A disulfide-stabilized conformer of methionine synthase reveals an unexpected role for the histidine ligand of the cobalamin cofactor. *Proc Natl Acad Sci USA*, 105(11): 4115-20.

Deddish, P A *et al.* (1994). Naturally occurring active N-domain of human angiotensin I-converting enzyme. *Proc Natl Acad Sci USA*, 91(16): 7807-11.

Dykewicz, M.S. (2004). Cough and angioedema from angiotensin-converting enzyme inhibitors: new insights into mechanisms and management. *Curr Opin Alergy Clin Immun*, 4(4): 267-70.

Edwards, D.R., Handsley, M.M. & Pennington, C.J. (2008). The ADAM metalloproteinases. *Mol Aspects Med*, 29(5): 258-89.

Ehlers, M.R. *et al.* (1989). Molecular cloning of human testicular angiotensin-converting enzyme: the testis isozyme is identical to the C-terminal half of endothelial angiotensin-converting enzyme. *Proc Natl Acad Sci USA*, 86(20): 7741-5.

Ehlers, M.R., Chen, Y.N. & Riordan, J.F. (1991). Purification and characterization of recombinant human testis angiotensin-converting enzyme expressed in Chinese hamster ovary cells. *Protein Expres Purif*, 2(1): 1-9.

Ehlers, M.R. & Riordan, J.F. (1991a). Angiotensin-converting enzyme: zinc- and inhibitor-binding stoichiometries of the somatic and testis isozymes. *Biochemistry*, 30(29): 7118-26.

Ehlers, M.R. & Riordan, J.F. (1991b). Membrane proteins with soluble counterparts: role of proteolysis in the release of transmembrane proteins. *Biochemistry*, 30(42): 10065-74.

Ehlers, M.R., Chen, Y.N. & Riordan, J.F. (1992). The unique N-terminal sequence of testis angiotensin-converting enzyme is heavily O-glycosylated and unessential for activity or stability. *Biochem Biophys Res Commun*, 183(1): 199-205.

Ehlers, M.R., Scholle, R R & Riordan, J.F. (1995). Proteolytic release of human angiotensin-converting enzyme expressed in Chinese hamster ovary cells is enhanced by phorbol ester. *Biochem Biophys Res Commun*, 206(2): 541-7.

Ehlers, M.R. *et al.* (1996). Proteolytic release of membrane-bound angiotensin-converting enzyme: role of the juxtamembrane stalk sequence. *Biochemistry*, 35(29): 9549-59.

El-Dorry, H.A. *et al.* (1982). Molecular and catalytic properties of rabbit testicular dipeptidyl carboxypeptidase. *J Biol Chem*, 257(23): 14128-33.

Ellgaard, L. & Ruddock, L.W. (2005). The human protein disulphide isomerase family: substrate interactions and functional properties. *EMBO Reports*, 6(1): 28-32.

Erdös, E.G. *et al.* (1985). Neutral metalloendopeptidase in human male genital tract. Comparison to angiotensin I-converting enzyme. *Lab Inves*, 52(4): 437-47.

Eyries, M. *et al.* (2001). Increased shedding of angiotensin-converting enzyme by a mutation identified in the stalk region. *J Biol Chem*, 276(8): 5525-32.

Ferguson, K.M. *et al.* (2003). EGF activates its receptor by removing interactions that autoinhibit ectodomain dimerization. *Mol Cell*, 11(2): 507-17.

Fleming, I. (2006). Signaling by the angiotensin-converting enzyme. *Circ Res,* 98(7): 887-96.

Fleming, I. & Kohlstedt, K. (2006). Authors' response. *Mol Pharmacol*. http://molpharm.aspetjournals.org/content/69/5/1725/reply

Friedland, J. & Silverstein, E. (1976). A sensitive fluorimetric assay for serum angiotensin-converting enzyme. *Am J Clin Path*, 66(2): 416-24.

Fusayasu, E. *et al.* (2007). Increased plasma substance P and CGRP levels, and high ACE activity in migraineurs during headache-free periods. *Pain*, 128(3): 209-14.

Gahmberg, C.G. & Tolvanen, M. (1996). Why mammalian cell surface proteins are glycoproteins. *Trends Biochem Sci*, 21(8): 308-11.

Garton, K.J., Gough, P.J. & Raines, E.W. (2006). Emerging roles for ectodomain shedding in the regulation of inflammatory responses. *J Leukocyte Biol,* 79(6): 1105-16.

Gearing, A.J. *et al.* (1994). Processing of tumour necrosis factor-alpha precursor by metalloproteinases. *Nature*, 370(6490): 555-7.

Georgiadis, D. *et al.* (2003). Roles of the two active sites of somatic angiotensin-converting enzyme in the cleavage of angiotensin I and bradykinin: insights from selective inhibitors. *Circ Res*, 93(2): 148-54.

Gething, M.J. (1999). Role and regulation of the ER chaperone BiP. *Semin Cell Dev Biol*, 10(5): 465-72.

Gordon, K. *et al.* (2003). Deglycosylation, processing and crystallization of human testis angiotensin-converting enzyme. *Biochem J*, 371: 437-42.

Gordon, K. *et al.* (2010). Fine epitope mapping of monoclonal antibodies 9B9 and 3G8 to the N domain of angiotensin-converting enzyme (CD143) defines a region involved in regulating angiotensin-converting enzyme dimerization and shedding. *Tissue Antigens*, 75(2): 136-50.

Haass, C. & Selkoe, Dennis, J. (2007). Soluble protein oligomers in neurodegeneration: lessons from the Alzheimer's amyloid beta-peptide. *Nature Rev. Mol Cell Biol*, 8(2): 101-12.

Hagaman, J.R. *et al.* (1998). Angiotensin-converting enzyme and male fertility. *Proc Natl Acad Sci USA*, 95(5): 2552-7.

Han, Z. *et al.* (2009). Enhancing thermostability of a Rhizomucor miehei lipase by engineering a disulfide bond and displaying on the yeast cell surface. *Appl Microbiol Biot*, 85(1): 117-26.

Harrison, R.L. & Jarvis, D.L. (2006). Protein N-glycosylation in the baculovirus-insect cell expression system and engineering of insect cells to produce "mammalianized" recombinant glycoproteins. *Adv Vir Res*, 68: 159-91.

Harrison, S. & Geppetti, P. (2001). Substance P. *Int J Biochem & Cell Biology*, 33(6): 555-76.

Hayashida, K. *et al.* (2010). Molecular and cellular mechanisms of ectodomain shedding. *Anat Rec (Hoboken)*, 293(6): 925-37.

He, F. *et al.* (2010). Complementary monoclonal antibody-based dot ELISA for universal detection of H5 avian influenza virus. *BMC Microbiology*, 10:330.

Helenius, A. & Aebi, M. (2001). Intracellular Functions of N-Linked Glycans. *Science*, 291(5512): 2364-2369.

Hooper, N.M. (1991). Angiotensin converting enzyme: implications from molecular biology for its physiological functions. *Int J Biochem*, 23(7-8): 641-7.

Hooper, N.M., Karran, E.H. & Turner, A.J. (1997). Membrane protein secretases. *Biochem J*, 321: 265-79.

Howard, T.E. *et al.* (1990). Transcription of testicular angiotensin-converting enzyme (ACE) is initiated within the 12th intron of the somatic ACE gene. *Mol Cell Biol*, 10(8): 4294-302.

Hubert, C. *et al.* (1991). Structure of the angiotensin I-converting enzyme gene. Two alternate promoters correspond to evolutionary steps of a duplicated gene. *J Biol Chem*, 266(23): 15377-83.

Hunziker, W. *et al.* (1986). The sucrase-isomaltase complex: primary structure, membrane-orientation, and evolution of a stalked, intrinsic brush border protein. *Cell*, 46(2): 227-34.

Iacob, R.E. *et al.* (2008). Structural elucidation of critical residues involved in binding of human monoclonal antibodies to hepatitis C virus E2 envelope glycoprotein. *Biochim Biophys Acta*, 1784(3): 530-42.

Imperiali, B. & O'Connor, S.E. (1999). Effect of N-linked glycosylation on glycopeptide and glycoprotein structure. *Curr Opin Chem Biol*, 3(6): 643-9.

Ishmael, S.S. *et al.* (2006). Protease domain glycans affect oligomerization, disulfide bond formation, and stability of the meprin A metalloprotease homo-oligomer. *J Biol Chem*, 281(49): 37404-15.

Jaggi, R. *et al.* (1997). The two opposing activities of adenylyl transferase reside in distinct homologous domains, with intramolecular signal transduction. *EMBO J*, 16(18): 5562-71.

Janin, J., Bahadur, R.P. & Chakrabarti, P. (2008). Protein-protein interaction and quaternary structure. *Q Rev Biophys*, 41(2): 133-80.

Jaspard, E,. Wei, L. & Alhenc-Gelas, F, (1993). Differences in the properties and enzymatic specificities of the two active sites of angiotensin I-converting enzyme (kininase II). Studies with bradykinin and other natural peptides. *J Biol Chem*, 268(13): 9496-503.

Jones, S. & Thornton, J.M. (1995). Protein-protein interactions: a review of protein dimer structures. *Prog Biophys Mol Biol*, 63(1): 31-65.

Kambe, N., Nishikomori, R. & Kanazawa, N. (2005). The cytosolic pattern-recognition receptor Nod2 and inflammatory granulomatous disorders. *J Dermatol Sci*, 39(2): 71-80.

Kasturi, L., Chen, H. & Shakin-Eshleman, S.H. (1997). Regulation of N-linked core glycosylation: use of a site-directed mutagenesis approach to identify Asn-Xaa-Ser/Thr sequons that are poor oligosaccharide acceptors. *Biochem J*, 323: 415-9.

Kasturi, S. *et al.* (1994). Role of glycosylation in the biosynthesis and activity of rabbit testicular angiotensin-converting enzyme. *Biochemistry*, 33(20): 6228-34.

Kessler, S.P. *et al.* (2007). Vascular expression of germinal ACE fails to maintain normal blood pressure in ACE-/- mice. *FASEB J*, 21(1): 156-66.

Kim, E. *et al.* (2000). Cross-linking constraints on F-actin structure. *J Mol Biol*, 299(2): 421-9.

Kim, H.M. *et al.* (2003). Crystal structure of Drosophila angiotensin I-converting enzyme bound to captopril and lisinopril1. *FEBS Letters*, 538(1-3): 65-70.

Kobata, A. (1992). Structures and functions of the sugar chains of glycoproteins. *Eur J Biochem*, 209(2): 483-501.

Kohlstedt, K. *et al.* (2002). CK2 phosphorylates the angiotensin-converting enzyme and regulates its retention in the endothelial cell plasma membrane. *Circ Res*, 91(8): 749-56.

Kohlstedt, K. *et al.* (2004). Angiotensin-converting enzyme is involved in outside-in signaling in endothelial cells. *Circ Res*, 94(1): 60-7.

Kohlstedt, K., Busse, R. & Fleming, I. 2005. Signaling via the angiotensin-converting enzyme enhances the expression of cyclooxygenase-2 in endothelial cells. *Hypertension*, 45(1): 126-32.

Kohlstedt, K. *et al.* (2006). Angiotensin-converting enzyme (ACE) dimerization is the initial step in the ACE inhibitor-induced ACE signaling cascade in endothelial cells. *Mol Pharmacol*, 69(5): 1725-32.

Kohlstedt, K. *et al.* (2009). Angiotensin-converting enzyme (ACE) inhibitors modulate cellular retinol-binding protein 1 and adiponectin expression in adipocytes via the ACE-dependent signaling cascade. *Mol Pharmacol*, 75(3): 685-92.

Kohlstedt, K. *et al.* (2010). Adipocyte-derived lipids increase angiotensin-converting enzyme (ACE) expression and modulate macrophage phenotype. *Bas Res Card,* 106(2):205-15.

Kondoh, G. *et al.* 2005. Angiotensin-converting enzyme is a GPI-anchored protein releasing factor crucial for fertilization. *Nature Med*, 11(2): 160-6.

Kost, O A *et al.* (1998). Carbohydrates regulate the dimerization of angiotensin-converting enzyme. *Biochem Mol Biol Int*, 44(3): 535-42.

Kost, O A *et al.* (2000). New feature of angiotensin-converting enzyme: carbohydrate-recognizing domain. *J Mol Recog*, 13(6): 360-9.

Kost, Olga A *et al.* (2003). Epitope-dependent blocking of the angiotensin-converting enzyme dimerization by monoclonal antibodies to the N-terminal domain of ACE: possible link of ACE dimerization and shedding from the cell surface. *Biochemistry*, 42(23): 6965-76.

Kramers, C. *et al.* (2001). Point mutation in the stalk of angiotensin-converting enzyme causes a dramatic increase in serum angiotensin-converting enzyme but no cardiovascular disease. *Circulation*, 104(11): 1236-40.

Kriegler, M. *et al.* (1988). A novel form of TNF/cachectin is a cell surface cytotoxic transmembrane protein: ramifications for the complex physiology of TNF. *Cell*, 53(1): 45-53.

Kröger, W.L. *et al.* (2009). Investigating the domain specificity of phosphinic inhibitors RXPA380 and RXP407 in angiotensin-converting enzyme. *Biochemistry*, 48(35): 8405-12.

Kumar, R.S. *et al.* (1989). Structure of testicular angiotensin-converting enzyme. A segmental mosaic isozyme. *J Biol Chem*, 264(28): 16754-8.

Ladner, R.C. (2007). Mapping the Epitopes of Antibodies. *Biotechnol Genet Eng Rev*, 24: 1-30.

Lattion, A.L. *et al.* (1989). The testicular transcript of the angiotensin I-converting enzyme encodes for the ancestral, non-duplicated form of the enzyme. *FEBS Letters*, 252(1-2): 99-104.

Leisle, L. *et al.* 2005. Angiotensin-converting enzyme as a GPIase: a critical reevaluation. *Nature Med*, 11(11): 1139-40.

Leonard, P. *et al.* (2008). Crystal structure of vascular endothelial growth factor-B in complex with a neutralising antibody Fab fragment. *J Mol Biol*, 384(5): 1203-17.

Lieberman, J. (1975). Elevation of serum angiotensin-converting-enzyme (ACE) level in sarcoidosis. *Am J Med*, 59(3): 365-72.

Lieberman, J. & Beutler, E. (1976). Elevation of serum angiotensin-converting enzyme in Gaucher's disease. *N Engl J Med*, 294(26): 1442-4.

Linnebank, M *et al.* (2003). Hereditary elevation of angiotensin converting enzyme suggesting neurosarcoidosis. *Neurology*, 61(12): 1819-20.

Lis, H. & Sharon, N. (1993). Protein glycosylation. Structural and functional aspects. *Eur J Biochem*, 218(1): 1-27.

Ma, B. *et al.* (2003). Protein-protein interactions: structurally conserved residues distinguish between binding sites and exposed protein surfaces. *Proc Natl Acad Sci USA*, 100(10): 5772-7.

Mantei, N. *et al.* (1988). Complete primary structure of human and rabbit lactase-phlorizin hydrolase: implications for biosynthesis, membrane anchoring and evolution of the enzyme. *EMBO J*, 7(9): 2705-13.

Marchand, P., Volkmann, M. & Bond, J.S. (1996). Cysteine mutations in the MAM domain result in monomeric meprin and alter stability and activity of the proteinase. *J Biol Chem*, 271(39): 24236-41.

Marcic, B. *et al.* (1999). Enhancement of bradykinin and resensitization of its B2 receptor. *Hypertension*, 33(3): 835-43.

Marcic, B. *et al.* (2000). Replacement of the transmembrane anchor in angiotensin I-converting enzyme (ACE) with a glycosylphosphatidylinositol tail affects activation of the B2 bradykinin receptor by ACE inhibitors. *J Biol Chem*, 275(21): 16110-8.

Marianayagam, N.J., Sunde, M. & Matthews, J.M. (2004). The power of two: protein dimerization in biology. *Trends Biochem Sci*, 29(11): 618-25.

McPherson, A. (1982). *Preparation and analysis of protein crystals.*, New York: John Wiley & Sons.

Mellquist, J.L. *et al.* (1998). The amino acid following an asn-X-Ser/Thr sequon is an important determinant of N-linked core glycosylation efficiency. *Biochemistry*, 37(19): 6833-7.

Menz, B. *et al.* (2008). Structural analysis of the adenovirus type 2 E3/19K protein using mutagenesis and a panel of conformation-sensitive monoclonal antibodies. *Mol Immunol*, 46(1): 16-26.

Miceli-Richard, C. *et al.* (2001). CARD15 mutations in Blau syndrome. *Nature Genetics*, 29(1): 19-20.

Michineau, S., Alhenc-Gelas, F. & Rajerison, R.M. (2006). Human bradykinin B2 receptor sialylation and N-glycosylation participate with disulfide bonding in surface receptor dimerization. *Biochemistry*, 45(8): 2699-707.

Minshall, R.D., Erdös, E.G. & Vogel, S.M. (1997). Angiotensin I-converting enzyme inhibitors potentiate bradykinin's inotropic effects independently of blocking its inactivation. *Am J Card*, 80(3A), 132A-136A.

Mogi, M., Iwai, M. & Horiuchi, M. (2009). New insights into the regulation of angiotensin receptors. *Curr Opin Neph Hyper*, 18(2): 138-43.

Munro, S. & Pelham, H.R. (1987). A C-terminal signal prevents secretion of luminal ER proteins. *Cell*, 48(5): 899-907.

Naim, H.Y. (1992). Angiotensin-converting enzyme of the human small intestine. Subunit and quaternary structure, biosynthesis and membrane association. *Biochem J*, 286: 451-7.

Naperova, I.A. *et al.* (2008a). Mapping of conformational mAb epitopes to the C domain of human angiotensin I-converting enzyme. *J Proteome Res*, 7(8): 3396-411.

Naperova, I.A. *et al.* (2008b). [Characteristics of monoclonal antibody binding with the C domain of human angiotensin converting enzyme]. *Bioorg Khim*, 34(3): 358-64.

Natesh, R. *et al.* (2003). Crystal structure of the human angiotensin-converting enzyme-lisinopril complex. *Nature*, 421(6922): 551-4.

Nchinda, A.T. *et al.* (2006). Synthesis and molecular modeling of a lisinopril-tryptophan analogue inhibitor of angiotensin I-converting enzyme. *Bioorg Med Chem Lett*, 16(17): 4616-9.

Nchinda, A.T. *et al.* (2006). Synthesis of novel keto-ACE analogues as domain-selective angiotensin I-converting enzyme inhibitors. *Bioorg Med Chem Lett*, 16(17): 4612-5.

Nesterovitch, A.B. *et al.* (2009). Angiotensin I-converting enzyme mutation (Trp1197Stop) causes a dramatic increase in blood ACE. *PloS One*, 4(12): e8282.

Newman, J. *et al.* (2009). Crystallization and preliminary X-ray analysis of the complexes between a Fab and two forms of human insulin-like growth factor II. *Acta Crystallogr Sect F Struct Biol Cryst Commun.*, 65: 945-8.

Nikolaeva, M.A. *et al.* (2006). Testicular isoform of angiotensin I-converting enzyme (ACE, CD143) on the surface of human spermatozoa: revelation and quantification using monoclonal antibodies. *Am J Repr Immunol*, 55(1): 54-68.

Nooren, I.M.A. & Thornton, J.M. (2003). Diversity of protein-protein interactions. *EMBO J*, 22(14): 3486-92.

Nybroe, O., Linnemann, D. & Bock, E. (1989). Heterogeneity of soluble neural cell adhesion molecule. *J Neurochem*, 53(5): 1372-8.

Oba, R. *et al.* 2005. The N-terminal active centre of human angiotensin-converting enzyme degrades Alzheimer amyloid beta-peptide. *Eur J Neuroscience*, 21(3): 733-40.

Oppong, S Y & Hooper, N M, (1993). Characterization of a secretase activity which releases angiotensin-converting enzyme from the membrane. *Biochem J*, 292: 597-603.

Orlova, A. *et al.* (2001). Probing the structure of F-actin: cross-links constrain atomic models and modify actin dynamics. *J Mol Biol*, 312(1): 95-106.

O'Neill, H.G. *et al.* (2008). The role of glycosylation and domain interactions in the thermal stability of human angiotensin-converting enzyme. *Biol Chem*, 389(9): 1153-61.

Palmert, M.R. *et al.* (1989). The beta-amyloid protein precursor of Alzheimer disease has soluble derivatives found in human brain and cerebrospinal fluid. *Proc Natl Acad Sci USA*, 86(16): 6338-42.

Pandiella, A. *et al.* (1992). Cleavage of membrane-anchored growth factors involves distinct protease activities regulated through common mechanisms. *J Biol Chem*, 267(33): 24028-33.

Pang, S. *et al.* (2001). Roles of the juxtamembrane and extracellular domains of angiotensin-converting enzyme in ectodomain shedding. *Biochem J*, 358: 185-92.

Parkin, E.T. *et al.* (2002). Structure-activity relationship of hydroxamate-based inhibitors on the secretases that cleave the amyloid precursor protein, angiotensin converting enzyme, CD23, and pro-tumor necrosis factor-alpha. *Biochemistry*, 41(15): 4972-81.

Parkin, E.T. *et al.* (2003). The ectodomain shedding of angiotensin-converting enzyme is independent of its localisation in lipid rafts. *J Cell Sci,* 116(15): 3079-87.

Parvathy, S. *et al.* (1997). Angiotensin-converting enzyme secretase is inhibited by zinc metalloprotease inhibitors and requires its substrate to be inserted in a lipid bilayer. *Biochem J*, 327(6): 37-43.

Parvathy, S. *et al.* (1998a). The secretases that cleave angiotensin converting enzyme and the amyloid precursor protein are distinct from tumour necrosis factor-alpha convertase. *FEBS Letters*, 431(1): 63-5.

Parvathy, S. *et al.* (1998b). Alzheimer's amyloid precursor protein alpha-secretase is inhibited by hydroxamic acid-based zinc metalloprotease inhibitors: similarities to the angiotensin converting enzyme secretase. *Biochemistry*, 37(6): 1680-5.

Pecher, P. & Arnold, U. (2009). The effect of additional disulfide bonds on the stability and folding of ribonuclease A. *Biophys Chem*, 141(1): 21-8.

Pfleger, K.D.G., Seeber, R.M. & Eidne, K.A. (2006). Bioluminescence resonance energy transfer (BRET) for the real-time detection of protein-protein interactions. *Nature Protocols*, 1(1): 337-45.

Phizicky, E.M. & Fields, S. (1995). Protein-Protein Interactions: Methods for Detection and Analysis. *Microbiol Rev*, 59(1): 94-123.

Pornillos, O. *et al.* (2010). Disulfide bond stabilization of the hexameric capsomer of human immunodeficiency virus. *J Mol Biol*, 401(5): 985-95.

Porteu, F. *et al.* (1991). Human neutrophil elastase releases a ligand-binding fragment from the 75-kDa tumor necrosis factor (TNF) receptor. Comparison with the proteolytic activity responsible for shedding of TNF receptors from stimulated neutrophils. *J Biol Chem*, 266(28): 18846-53.

Ramchandran, R. *et al.* (1994). Regulated cleavage-secretion of the membrane-bound angiotensin-converting enzyme. *J Biol Chem*, 269(3): 2125-30.

Ramchandran, R. & Sen, I, (1995). Cleavage processing of angiotensin-converting enzyme by a membrane-associated metalloprotease. *Biochemistry*, 34(39): 12645-52.

Rawlings, N.D. & Barrett, A.J. (1993). Evolutionary families of peptidases. *Biochem J*, 290: 205-18.

Ray, K. *et al.* (2004). Crystal structure of human thimet oligopeptidase provides insight into substrate recognition, regulation, and localization. *J Biol Chem*, 279(19): 20480-9.

Rebois, R.V. *et al.* (2008). Combining protein complementation assays with resonance energy transfer to detect multipartner protein complexes in living cells. *Methods*, 45(3): 214-8.

Ripka, J.E. *et al.* (1993). N-glycosylation of forms of angiotensin converting enzyme from four mammalian species. *Biochem Biophys Res Commun*, 196(2): 503-8.

Roitsch, T. & Lehle, L. (1989). Structural requirements for protein N-glycosylation. Influence of acceptor peptides on cotranslational glycosylation of yeast invertase and site-directed mutagenesis around a sequon sequence. *Eur J Biochem*, 181(2): 525-9.

Rømer, F.K. (1984). Clinical and biochemical aspects of sarcoidosis. With special reference to angiotensin-converting enzyme (ACE). *Acta Med Scand. Suppl*, 690: 3-96.

Ronin, C. *et al.* (1981). Synthetic substrates for thyroid oligosaccharide transferase. Effects of peptide chain length and modifications in the Asn-Xaa-Thr-region. *Eur J Biochem*, 118(1): 159-64.

Sadhukhan, R, Sen, G C & Sen, I, (1996). Synthesis and cleavage- secretion of enzymatically active rabbit angiotensin-converting enzyme in Pichia pastoris. *J Biol Chem*, 271(31): 18310-3.

Sadhukhan, R *et al.* (1998). The distal ectodomain of angiotensin-converting enzyme regulates its cleavage-secretion from the cell surface. *Proc Natl Acad Sci USA*, 95(1): 138-43.

Sadhukhan, R *et al.* (1999). Unaltered cleavage and secretion of angiotensin-converting enzyme in tumor necrosis factor-alpha-converting enzyme-deficient mice. *J Biol Chem*, 274(15): 10511-6.

Sambrook, J. & Russell, D.W. (2001). *Molecular Cloning*. Third Edition, New York: Cold Spring Harbor Laboratory Press.

Santhamma, Kizhakkekara R & Sen, I, (2000). Specific cellular proteins associate with angiotensin-converting enzyme and regulate its intracellular transport and cleavage-secretion. *J Biol Chem*, 275(30): 23253-8.

Santhamma, Kizhakkekara R *et al.* (2004). Role of tyrosine phosphorylation in the regulation of cleavage secretion of angiotensin-converting enzyme. *J Biol Chem*, 279(38): 40227-36.

Scheuermann, S. *et al.* (2001). Homodimerization of amyloid precursor protein and its implication in the amyloidogenic pathway of Alzheimer's disease. *J Biol Chem*, 276(36): 33923-9.

Schwager, S.L. *et al.* (1998). Phorbol ester-induced juxtamembrane cleavage of angiotensin-converting enzyme is not inhibited by a stalk containing intrachain disulfides. *Biochemistry*, 37(44): 15449-56.

Schwager, S.L. *et al.* (1999). Modulation of juxtamembrane cleavage ("shedding") of angiotensin-converting enzyme by stalk glycosylation: evidence for an alternative shedding protease. *Biochemistry*, 38(32): 10388-97.

Schwager, S.L., Carmona, A.K. & Sturrock, E.D. (2006). A high-throughput fluorimetric assay for angiotensin I-converting enzyme. *Nature Protocols*, 1(4): 1961-4.

Sears, P. & Wong, C.H. (1998). Enzyme action in glycoprotein synthesis. *Cell Mol Life Sci*, 54(3): 223-52.

Semmler, A. *et al.* (2006). Hereditary hyper-ACE-emia due to the Pro1199Leu mutation of somatic ACE as a potential pitfall in diagnosis: a first family outside Europe. *Clin Chem Lab Med*, 44(9): 1088-9.

Shen, X.Z. *et al.* (2007). Mice with enhanced macrophage angiotensin-converting enzyme are resistant to melanoma. *Am J Path*, 170(6): 2122-34.

Shimada, K. *et al.* (1996). Rat endothelin-converting enzyme-1 forms a dimer through Cys412 with a similar catalytic mechanism and a distinct substrate binding mechanism compared with neutral endopeptidase-24.11. *Biochem J*, 315: 863-7.

Siadat, O.R. *et al.* (2006). The effect of engineered disulfide bonds on the stability of Drosophila melanogaster acetylcholinesterase. *BMC Biochemistry*, 7: 12.

Silverstein, E. *et al.* (1976). Elevation of angiotensin-converting enzyme in granulomatous lymph nodes and serum in sarcoidosis: clinical and possible pathogenic significance. *Ann NY Acad Sci*, 278: 498-513.

Skidgel, R A *et al.* (1984). Hydrolysis of substance p and neurotensin by converting enzyme and neutral endopeptidase. *Peptides*, 5(4): 769-76.

Skirgello, O.E. *et al.* 2005. Kinetic probes for inter-domain co-operation in human somatic angiotensin-converting enzyme. *Biochem J*, 391: 641-7.

Skirgello, O.E. *et al.* (2006). Inhibitory antibodies to human angiotensin-converting enzyme: fine epitope mapping and mechanism of action. *Biochemistry*, 45(15): 4831-47.

Soffer, R.L. & Sonnenblick, E.H. (1978). Physiologic, biochemical, and immunologic aspects of angiotensin-converting enzyme. *Prog Cardiovasc Dis*, 21(3): 167-75.

Soubrier, F *et al.* (1988). Two putative active centers in human angiotensin I-converting enzyme revealed by molecular cloning. *Proc Natl Acad Sci USA*, 85(24): 9386-90.

Strittmatter, S.M. & Snyder, S.H. (1984). Angiotensin-converting enzyme in the male rat reproductive system: autoradiographic visualization with [3H]captopril. *Endocrinology*, 115(6): 2332-41.

Sturrock, E.D. *et al.* (1996). Assignment of free and disulfide-bonded cysteine residues in testis angiotensin-converting enzyme: functional implications. *Biochemistry*, 35(29): 9560-6.

Sturrock, E.D., Danilov, S.M. & Riordan, J.F. (1997). Limited proteolysis of human kidney angiotensin-converting enzyme and generation of catalytically active N- and C-terminal domains. *Biochem Biophys Res Commun*, 236(1): 16-9.

Sun, X. *et al.* (2008). Interaction of angiotensin-converting enzyme (ACE) with membrane-bound carboxypeptidase M (CPM) - a new function of ACE. *Biol Chem*, 389(12): 1477-85.

Sun, X. *et al.* (2010). Signal transduction in CHO cells stably transfected with domain-selective forms of murine ACE. *Biol Chem*, 391(2-3): 235-44.

Takeda, S. *et al.* (2006). Crystal structures of VAP1 reveal ADAMs' MDC domain architecture and its unique C-shaped scaffold. *EMBO J*, 25(11): 2388-96.

Teplyakov, A. *et al.* (2009). Epitope mapping of anti-interleukin-13 neutralizing antibody CNTO607. *J Mol Biol*, 389(1): 115-23.

Tomiya, N. *et al.* (2004). Comparing N-glycan processing in mammalian cell lines to native and engineered lepidopteran insect cell lines. *Glycoconjugate J*, 21(6): 343-60.

Towler, P. *et al.* (2004). ACE2 X-ray structures reveal a large hinge-bending motion important for inhibitor binding and catalysis. *J Biol Chem*, 279(17): 17996-8007.

Udenfriend, S. *et al.* (1972). Fluorescamine : A Reagent for Assay of Amino Acids, Peptides, Proteins and Primary Amines in the Picomole Range. *Science*, 178(4063): 871-872.

Ulloa-Aguirre, A. *et al.* (1999). Role of glycosylation in function of follicle-stimulating hormone. *Endocrine*, 11(3): 205-15.

Voronov, S. *et al.* (2002). Temperature-induced selective death of the C-domain within angiotensin-converting enzyme molecule. *FEBS Letters*, 522(1-3): 77-82.

Watermeyer, J.M. *et al.* (2006). Structure of testis ACE glycosylation mutants and evidence for conserved domain movement. *Biochemistry*, 45(42): 12654-63.

Watermeyer, J.M. *et al.* (2008). Probing the basis of domain-dependent inhibition using novel ketone inhibitors of Angiotensin-converting enzyme. *Biochemistry*, 47(22): 5942-50.

Watermeyer, J.M. *et al.* (2010). Characterization of domain-selective inhibitor binding in angiotensin-converting enzyme using a novel derivative of lisinopril. *Biochem J*, 428(1): 67-74.

Wei, L *et al.* (1991a). The two homologous domains of human angiotensin I-converting enzyme are both catalytically active. *J Biol Chem*, 266(14): 9002-8.

Wei, Lei *et al.* (1991b). Expression and Characterization of Recombinant Human Angiotensin I-converting Enzyme. *Biochemistry*, 266(9): 5540-5546.

Wei, L *et al.* (1992). The two homologous domains of human angiotensin I-converting enzyme interact differently with competitive inhibitors. *J Biol Chem*, 267(19): 13398-405.

Weidemann, A. *et al.* (1989). Identification, biogenesis, and localization of precursors of Alzheimer's disease A4 amyloid protein. *Cell*, 57(1): 115-26.

Wilson, I.B., Gavel, Y. & von Heijne, G. (1991). Amino acid distributions around O-linked glycosylation sites. *Biochem J*, 275: 529-34.

Woodman, Z.L. *et al.* (2000). Shedding of somatic angiotensin-converting enzyme is inefficient compared with testis ACE despite cleavage at identical stalk sites. *Biochem J*, 347: 711-8.

Woodman, Z.L. *et al.* 2005. The N domain of somatic angiotensin-converting enzyme negatively regulates ectodomain shedding and catalytic activity. *Biochem J*, 389: 739-44.

Woodman, Z.L. *et al.* (2006). Homologous substitution of ACE C-domain regions with N-domain sequences: effect on processing, shedding, and catalytic properties. *Biol Chem*, 387(8): 1043-51.

Wyss, D.F. & Wagner, G. (1996). The structural role of sugars in glycoproteins. *Curr Opin Biot*, 7(4): 409-16.

Yokosawa, H. *et al.* (1983). A new feature of angiotensin-converting enzyme in the brain: hydrolysis of substance P. *Biochem Biophys Res Commun*, 116(2): 735-42.

Yotsumoto, H., Sato, S. & Shibuya, M. (1984). Localization of angiotensin converting enzyme (dipeptidyl carboxypeptidase) in swine sperm by immunofluorescence. *Life Sci*, 35(12): 1257-61.

Yu, X.C. *et al.* (1997). Identification of N-linked glycosylation sites in human testis angiotensin-converting enzyme and expression of an active deglycosylated form. *J Biol Chem*, 272(6): 3511-9.